Design of Communication and Wireless Power Transmission Strategies for Robotic Exoskeleton

Konstantinos Drosos

Submitted in accordance with the requirements for the degree of

Doctor of Philosophy

The University of Leeds

School of Mechanical Engineering

Institute of Design, Robotics and Optimisation

September 2019

Acknowledgements

It is a pleasure to thank those people who made this research possible. Firstly, it is my pleasure to have Prof. Abbas Dehghani-Sanij as a head supervisor, who provided the appropriate knowledge and guidance during my research and especially during my work on this report. In addition, Prof. Dehghani helped me to overcome all the challenges that faced and provided the guidance that led to the successful conduction of this report. Without his guidance and persistent help, this research would not have been possible. I would also like to say special thanks to my co-supervisors, Dr. Lotfi Mhamdi and Dr. Nutapong Somjit, who helped during my research and provided useful ideas and recommendations about this report. Their knowledge, help and motivation were vital. It was a pleasure to work along with them and learn new things that helped me to complete this report. Finally, I would also like to acknowledge that Mr Maciej Napora, Mr Arman Fazeli, Mr Sina Firouzy, Mr Pourshid Jan Fani, Mr. Thomas Magil and Mr. Mohd Alias were very supportive at various stages of the project.

Konstantinos Drosos

The candidate confirms that the work submitted is his own and that appropriate credit has been given where reference has been made to the work of others.

Abstract

Exoskeletons have become an attractive field of research over the past decades. These devices have great potential to enhance or assist individuals by combining human intelligence and machine power. Exoskeletons are used in industry to increase the efficiency and decrease the work–related injuries. Search and rescue operations is another field in which exoskeletons are used considering the fact that in most cases time is essential for saving human lives. For example, when victims are trapped in structural collapse due to natural disasters, such as earthquakes, exoskeletons are deployed to move debris, evacuate people and transfer them to a safe place to receive medical care.

The preliminary requirements for the communication strategy of the exoskeletal device are specified. Evaluation of the most advanced communication protocols is presented along with any previous related work. EtherCAT is found to be the most suitable candidate. Virtual and physical EtherCAT network models –designed to test and validate the theoretical approach– are being introduced in this work. Moreover, a simulation study is conducted, from which the communication cycle time of the protocol is derived, providing satisfactory results that match the theoretical approach of having a minimum cycle time of 33.68μs. A frame size optimisation algorithm for a novel design of EtherCAT protocol for full–body robotic exoskeleton is proposed. The theoretical and simulation approaches are validated experimentally using different kind of sensors to record and analyse the protocol performance under different conditions.

Power sources and systems that can be used to provide the needed power are also specified. The current state and challenges of the energy harvesting and wireless power transmission (WPT) technologies are evaluated. WPT is found to be the most reliable solution, since the energy harvesting technologies can only provide the energy for the on–board electronics. The simulation model of the proposed WPT system shows that the developed magnetic resonant coupling technique can transmit up to 1.8 kW of electric power with a transfer efficiency of approximately 92%.

This research presents a novel design methodology for using an array of coils in combination with the magnetic resonant coupling technique to deliver the required amount of power the exoskeleton needs to perform certain tasks. The analysis of this methodology demonstrates that by placing receiver coils at the sole of the exoskeleton and transmitter coils under the floor, the device can be charged when entering the coverage area.

Contents

List of Figures

List of Tables

Nomenclature

AFC	Alkaline Fuel Cell
BiSS	Bidirectional Serial Synchronous
BLEEX	Berkeley Lower Extremity Exoskeleton
CAN	Controller Area Network
CPU	Central Processing Unit
CSMA/CD	Carrer–Sense–Mulptiple–Access with Collision Detection
DOF	Degrees Of Freedom
DYN	Dynamic segment
ECU	Electronic Control Unit
EMF	Electromotive Force
FMMU	Fieldbus Memory Management Unit
FRF	Floor Reaction Force
GRF	Ground Reaction Force
GUI	Graphical User Interface
HAL	Hybrid Assistive Limb
HAL–UL	Hybrid Assistive Limb – Upper–Limb
HEPU	Hydraulic–Electric Power Unit
HULC	Human Universal Load Carrier

I2C	Inter–Integrated Circuit (communication protocol)
IC	Internal Combustion engine
LAN	Local Area Network
LIN	Local Interconnect Network
LSB	Least Significant Bit
LVDT	Linear Variable Differential Transformer
MCFC	Molten Carbonate Fuel Cell
MSB	Most Significant Bit
OSI	Open System Interconnection
PCB	Printed Circuit Board
PV cell	Photovoltaic cell
PVDF	Polyvinylidineuoride
PZT	Piezoelectric
RIOM	Remote Input/Output Module
RTR	Remote Transit Request
SGA	Strain Gauge Amplifier
SIOM	Supervisory Input/Output Module
SOFC	Solid Oxide Fuel Cell
SPI	Serial Peripheral Interface
SSI	Serial Synchronous Interface
ST	Static segment
SUBAR	Sogang-University's-Biomedical-Assistive-Robot
TDMA	Time Division Multiple Access
UAV	Unmanned Air Vehicle

UGV	Unmanned Ground Vehicle
USART	Universal Synchronous/Asynchronous Receiver/Transmitter
UUV	Unmanned Underwater Vehicle
WPT	Wireless Power Transmission
ZT	figure of merit
A	cross–sectional area
ΔT	difference between hot and cold temperatures
ϵ	ratio of the strain
μ	efficiency of thermoelectric device
ρ	resistivity of the material
GM_{max}	encoder's mask
GM_{ST}	encoder's submask
h_D	datagram header
h_e	Ethernet header
h_{ECAT}	EtherCAT header
h_{wkc}	working counter
K	gauge factor
L_{frame}	length of EtherCAT frame
l	length of the strain gauge
n_{slaves}	number of slaves in EtherCAT simulation model
p	average payload per slave
R	resistance of the strain gauge
SF	Scaling Factor
s_M	set of tasks used for EtherCAT simulation

s_n	random task in EtherCAT telegram
$T_{ambient}$	environmental temperature
T_{body}	temperature of the human body
T_c	cold temperature
T_{cable}	delay caused by physical medium
T_{cycle}	EtherCAT network period used in simulations
T_{ecat}	communication cycle time of EtherCAT simulation model
T_{frame}	time of EtherCAT frame
T_h	hot temperature
$T_{networkPeriod}$	time at which EtherCAT simulation model configured to operate
T_{slave}	delay in the hardware of the slave
T_x	period at which each s_n is transmitted
T_M	execution time of each s_M task
$t_{forwardDelay}$	forward delay of EtherCAT slave device
t_n	time instant at which s_n is transmitted

Chapter 1

Introduction

1.1 Background

A robotic exoskeleton is a device which has the potential to enhance the physical capabilities of a human being or to assist individuals with disabilities and allow them to perform every–day tasks. The first attempts to develop and build a robotic exoskeleton could be traced back to the 1960s. The "Man Amplifier" by Cornell Aeronautical [2] Laboratory is one of the very first attempts to design and develop an exoskeleton. The device was developed in such a way that it would consist of a structural exoskeleton with appropriate articulated joints, which would be compatible with the portions of human body. Mizen of Cornell Aeronautical Laboratory designed a non–powered, full–scale exoskeletal structure, which its movements and –in general– kinematics were compliant with the ranges of motion of the human body. Additionally, the device was adjustable in order to be worn by different people or subjects [2, 3]. Another attempt to build an exoskeletal device similar to Man Amplifier is coming from General Electric (GE) and the governmental institutions of US. This attempt resulted in a prototype with the name "Hardiman I" [4]. The exoskeletal system was a master–slave device, which consisted of two complete 'skeletons'. While the Hardiman was a set of overlapping exoskeletons worn by a human operator. An inner structure operating as the 'master' device used to record the rotational movement of the joints of the human body and an outer structure operating as the 'slave' device used to carry the working load. The project was not successful, since it did not meet the initial objectives. Any attempts to use the full exoskeleton resulted in a violent, uncontrolled motion, and as a result, the exoskeleton was never turned on with a person inside [4–6].

Starting from 1970s, there are no reported attempts to design and build a full–body exoskeletal device, until 2000, where *Kazerooni* and his research group were involved in researching the design and implementation of the first load–carrying, field–operational and energetically autonomous lower–extremity exoskeleton. The exoskeleton was designed and built at Berkeley is commonly referred to as BLEEX (Berkeley Lower Extremity Exoskeleton) [7–12]. Following their initial design, Berkeley Bionics designed the ExoHiker and ExoClimber in 2005 [13], and HULC (Human Universal Load Carrier) in 2008, with the support of the US Department of Defence. HULC was a structure able to carry up to 90 kg of payload without impeding wearer's moves and was also able to decrease metabolic cost of the user [14,15]. In addition, the license of the technology that was employed in HULC is owned by the Lockheed Martin company (located in Maryland, US), so that it could be used for further field–ready military development.

Using the support from DARPA's *Exoskeletons for Human Performance Augmentation* financial programme in 2005, *Jacobsen* et al. of Sarcos released a full–body, load–bearing enhancive exoskeleton, named XOS. [16]. The device was initially designed to be used in logistics in order to help the military personnel when performing repetitive tasks, such as heavy lifting of military equipment. The device was able to carry a load that can weigh up to 90 kg. The second generation of XOS, named XOS–2, was presented in 2010. The new exoskeletal device was revealed once Sarcos became part of Raytheon company. A fully–operating tethered XOS–2 version was expected to enter into military service by 2015 [17–19]. Another interesting development is PERCRO's Body Extender which was revealed in 2010 and funded by the Italian Ministry of Defence. It is a full–body exoskeleton which uses electric actuators powered via a tethered source. The body extender (BE) is an advanced wearable robot expressly conceived for augmenting the human strength for the handling of heavy materials (up to 100 kg) in unstructured environments [20–22].

Apart from the full–body exoskeletons, other researchers have developed different classes of exoskeletal devices. Such exoskeletons compromise devices that are able to assist human muscular system and provide assisting torque to the joints. *Yamamoto* et al. of Kanagawa Institute of Technology developed a standalone wearable power assisting suit which gives nurses the 'extra muscle' they need to lift patients from a bed and avoid back injuries [23–26]. *Pratt* et al. developed the RoboKnee, an exoskeleton for enhancing strength, endurance and speed during walking. The RoboKnee allows the wearer to climb stairs and perform knee bends while carrying a significant load in a backpack [27]. *Kong* et al. of Sogang University of South Korea developed in 2005 a lightweight wearable exoskeleton (of approx. 3 kg) which is connected to a smart caster walker and is able to provide assistance for elderly and patients, during walking, sitting down and standing up. The device has been named as EXPOS [28,29]. Furthermore, an advanced version of EXPOS has been developed in 2008, named SUBAR (Sogang-University's-Biomedical-Assistive-Robot). In the case of SUBAR, the mechanical impedance has been increased significantly as the gear reduction ratio is augmented for higher torque production and, in general, for more power assistance [30–32]. *Sankai*, *Kawamoto* et al. of Sankai Laboratory at University of Tsukuba developed a lower extremities assistive exoskeleton named Hybrid Assistive Limb (HAL). This device is capable of sensing the electrical signals in the muscles and translate them into the desired locomotion of the human operator. Significant work took place in order to reduce the overall weight of the device to 21 kg. Combining the human's body strength and the exoskeleton's power, HAL–5 has been able to lift up to 80 kg, about twice of the capacity of the user on its own. However, the high metabolic cost of the wearer when lifting heavy loads could result in quick tiredness which could make the device unreliable for situations where the user is required to carry heavy objects for longer [33–42]. Following the initial design, the researchers' of University of Tsukuba, have developed several other advanced versions of HAL. An advanced, more sophisticated version has been built, where the controller was able to reproduce walking patterns triggered by user intention for walking support of paraplegics [43]. In addition, a single–legged version of HAL has been developed in order to be used as an assistive device providing walking motion support to hemiplegic patients that suffer from any disease, such as strokes, and paralyses [44,45] as well as for patients that suffer from poliomyelitis [46]. Apart from the single legged exoskeletons, the researchers have been developing the upper limb type HAL (HAL-UL) to assist the arm movement during a meal, for people with upper limb paralysis [47,48]. A full–body exoskeleton version of HAL has been developed in order to be used for bathing care assistance. The updated version of HAL used a new method that mainly uses the caregiver's upper limb to support the weight of the care–receiver [49,50]. As a result of these efforts, HAL for Medical Use - Lower Limb Model by *Sankai's* and *Kawamoto's* spin–off company Cyberdyne Inc. was certified as conforming with the requirements of Medical Device Directives in the European Union [51].

Power systems have become an interesting area of research when designing and building full–body exoskeletal devices. The only attempt to build an on–board power unit was from Kazerooni et. al., where they have developed a hybrid hydraulic–electric power unit. An internal combustion engine has been used as a main unit to produce power, due to the high density of energy that can be produced from gasoline. This hybrid solution was capable of constantly providing pressure, hydraulic and electric power, which are used for the locomotion and the on–board computer, respectively. A prototype has been used for the BLEEX exoskeleton providing a 2.3 kW of hydraulic power and 220 W of electric power at 15 VDC [52]. There are no other reported attempts to use an on–board power supply for full–body exoskeletons. The devices that have been examined previously, such as HAL, XOS–2, PERCRO's body extender etc., are all featuring tethered solutions to deliver the required amount of both hydraulic and electric power, where the exoskeletons are connected either on external electric power sources or, simply, on a wall socket when the energy requirements are not that high.

At the time of writing this report, the exoskeleton technology has matured and is moving into series production. The nature of the exoskeleton as a complex mechatronic device poses many challenges. As it is described in later chapters, the exoskeleton must employ numerous distributed–electronic devices, which need to be connected into a network. An efficient method is needed to reduce wiring complexity and weight. At the same time, a reliable and efficient solution is needed to deliver the amount of energy required by the hydraulics and on–board electronics. The literature on exoskeletons and power systems provides limited information on this topic. However, it is worth noting that a communication system is an adequate solution along with a safe power system. This has been a well–known problem which incentivised progress in the automotive and industrial automation sectors. The need to reduce the amount of wiring and complexity of distributed–electronic systems led to the development of important communication technologies that are widely adopted standards nowadays. Finally, the increasing demand for energy and environmental concerns are driving forces toward renewable energy sources and wireless power transmission (WPT) technologies.

1.2 Motivation for Research

The ageing population in the world is increasing, it is estimated that by 2050 it will nearly double. This represents a problem because part of the elderly population has difficulties performing every–day ordinary tasks, due to common conditions such as stroke, spinal injury, muscle weakness and others. There has been interest in researching for ways to help improve the lives of these people by restoring natural motion control. The advantages of using wearable robots are many [53]. However, the technology that is available at the moment is not enough to provide a reliable solution. This is the beginning of an era which aims to bring a substitute to the wheelchair in the future [54].

Enhancive exoskeletons like BLEEX, Sarcos XOS and PERCRO's Body Extender, after initial phase of development were licensed to military companies and their details became confidential. A few details of Sarcos XOS were presented in the media but no further information was revealed to the public, apart from the patents that have been used [17, 55]. Moreover, the researchers of BLEEX have developed their own unique Exoskeleton Communication Architecture that realises the serial ring topology and is specially designed for the Exoskeleton [56]. That specific communication architecture has not yet been applied to other exoskeletons, precisely there are no reported attempts to develop a communication protocol/architecture that is based on the BLEEX's architecture. Understanding of allowable and required properties of the interaction between a full–body exoskeleton and the user upper extremities is therefore limited as well as the need for efficient and reliable communication between the sensors/electronics and the processor. To the best of author's knowledge, the communication strategies of enhancive, load–bearing exoskeletons has not yet been investigated. Also, since an exoskeleton encloses a human, safety of operation is paramount. Requirements and guidelines for the inherently safe design, protective measures, and information for use of personal care robots are specified in [57], although information on solutions providing safe operation of enhancive exoskeletons are limited.

Taking into consideration the urgency and expected benefits of exoskeletal devices to the society, as well as the newly developed and advanced communication protocols, the author's motivation is coming from an endeavour of building an exoskeleton as part of a project at the University of Leeds. Although, decades have passed since the first exoskeletons were built, the current developments still have many challenges to overcome to achieve an operational device. Aside from a detailed description of the communication system of BLEEX, it was found that the literature offers very limited information on the communication systems used in exoskeletons. In addition, the author's research interest is motivated by the importance of developing a communication protocol and especially EtherCAT. Apart from that, EtherCAT seems to be the most suitable candidate for such exoskeletal devices and the author's research interest is motivated by the importance of developing further this protocol, since there are no other reported attempts to use this protocol, other than PERCRO's exoskeleton. Lastly, the importance of having a reliable power source to meet the power requirements of an exoskeletal devices has motivated the author to research for novel solutions that are capable to deliver the energy wirelessly, without limiting the movements of the exoskeleton by using complex wiring connected to external power sources.

1.3 Aims and Objectives

1.3.1 Aims

The aims of this research are:

- To determine the most suitable communication strategy for exoskeletons, including its implementation and evaluation. In addition, implement a basic prototype to successfully transfer data between modules, based on the selected protocol. Thus, implementing a communication system of an enhancive modular exoskeleton helping to transfer signals across the processors and electronic devices;
- To research for the potential energy harvesting and wireless power transmission strategies that can be used to supply the power needed by the on–board electronics to operate.

1.3.2 Objectives

The following objectives have been set for this research in order to achieve the above aims.

- Acquire basic understanding on the main aspects and requirements of exoskeletons, with focus on the communication and power systems;
- Survey potential communication strategies for the entire robot, assess/evaluate the main technical specifications and determine which communication systems are suitable for the exoskeleton;
- Choose sensors and electronics for a novel single joint prototype, which is intended to be a base for further development and serve as a platform for proving the successful operation of the communication network architecture. Develop electronics and software for the platform;
- Construct communication–oriented model of the device and simulate the proposed communication strategy for the exoskeleton, on the level of the entire device, to gain insight into communication related issues. Evaluate the performance and assess its stability, efficiency, reliability and robustness;
- Implement an experimental setup to assess the feasibility of the proposed communication protocol. Validate the theoretical and simulation approaches;

- Compare and contrast different power systems and energy harvesting methods;
- Assess the main technical specifications of potential power sources and technologies that can be used for exoskeletons and determine which technology is the most suitable candidate;
- Identify challenges of using energy harvesting and wireless power transmission solutions to design and implement a novel and hybrid power system
- Simulate and propose a novel solution of using wireless power transmission technologies for the final structure of the exoskeleton.

1.4 Scope of the Research

The scope of the individual project is limited to the:

- evaluation of potential communication strategies against requirements;
- development of a novel communication strategy to minimise the communication's cycle time and transmit data efficiently;
- development of electronics interfacing with sensors and executing proposed algorithm to reduce the frame size of the protocol;
- validation and verification of the proposed algorithm and simulation model on a prototype;
- critical analysis of proposed wireless power transmission (WPT) technology that can be used to establish a novel solution to transmit wirelessly the required energy to the robotic exoskeleton .

1.5 Contribution of the Research

The research will contribute to the power enhancing field of research in exoskeletons with the focus on the potential communication strategies and the suitable power sources that can be used by the exoskeletons.
The contributions are summarised as follows:

- Development of a design methodology for a novel high–level communication strategy for the enhancive full–body exoskeleton in which frame is modular;
- Suggestions for a greater spectrum of communication protocols to be used by exoskeletons;

- Evaluation of the wireless power transmission technologies and the safety concerns that arise by using such solution in human wearable robots;

- Demonstrating by comparison to FEA results that wireless power transmission is a feasible solution to deliver the required amount of electric power to the exoskeleton.

1.6 Outline of the Thesis

This thesis is divided and organised into two main sections and eight chapters in total. Each chapter is summarised as follows:

- **Chapter 1**: This chapter covers the background, author's motivation and the aims and objectives. In addition, the chapter outlines the scope and the contributions of this research.
- **Chapter 2**: Literature review on the human body biomechanics, the anatomy and history of robotic exoskeletons are presented in this chapter. The current state and challenges in the robotic exoskeletons field are outlined. Then classification of exoskeleton, methods of actuation and control strategies are explained in detail. The importance of using a real–time network to establish the on–board communications is outlined along with the review of the BLEEX's communication architecture. Moreover, a review of the power unit used for BLEEX is discussed thoroughly. The chapter concludes by presenting the gaps in the body of knowledge in the field of communications and power systems for full–body exoskeletons.
- **Section I - Communications**
  - **Chapter 3**: The chapter starts by introducing the preliminary requirements that should be addressed in order to select the most appropriate communication candidate that will be used for this project. The widely adopted communication protocols are discussed in detail and previous related work is presented. The specifications of each protocol, by means of hardware availability, maximum frame–size and available topologies, are evaluated thoroughly and a scoring system has been used to summarise the characteristics of each protocol and choose the most suitable solution that will meet the needs of this research.
  - **Chapter 4**: This chapter presents a simulation study of EtherCAT communication protocol. The concept of data transmission in real–time Ethernet protocol is explained in detail. Three different simulation models are

discussed, and the results of the simulations are presented. A theoretical approach is outlined in order to estimate the communication cycle time of the final design and is compared with the results obtained from the simulations. The chapter concludes by introducing an algorithm that can be used to reduce the size of the frame that is transmitted in the network and by proposing a design methodology for the real–time communication system that will be used on the actual exoskeleton device.

  – **Chapter 5**: The chapter introduces the mechanical design of the single–joint prototype that will be used for the experiments. The locations of the sensors that are used in this project are also presented in this design. Included, also, a discussion of the sampling rate and the bandwidth of motion that derived from the motion capture study conducted at University of Leeds. The sensors that are used for the experimental setup and their nature of operation are discussed in detail to devise a plan for the software development that follows. Finally, the electronic components, EtherCAT terminals and plan for the software implementation are presented at the end of this chapter.

  – **Chapter 6**: This chapter includes a presentation and thorough discussion of the experimental work and results obtained. The hardware and software implementations of the LVDT, loadcell and encoder sensors are presented and the challenges faced during the implementation are highlighted. The chapter concludes by presenting a critical evaluation of the control strategy developed by the controls' engineer of this project.

- **Section II - Power Systems**

  – **Chapter 7**: This chapter presents the potential power sources that are suitable for exoskeletons. Such power sources include non–rechargeable batteries, internal combustion engines, electrochemical fuel cells and tethered solution. The advantages and disadvantages of using each solution are highlighted. Moreover, energy harvesting and wireless power transmission technologies are reviewed for their suitability for this project and evaluated in terms of their specifications and the amount of energy they can provide. Moreover, this chapter discusses the limitations, challenges and safety concerns.

  – **Chapter 8**: This chapter deals with the simulation approach of a wireless power transfer system. The human gait is examined to provide an estimation of the time that the human foot is in contact with the ground and the variation of the foot angle during normal walking. The results from this analysis are then used to design and simulate the antennas that are used for the wireless power transmission system. In addition, the electromagnetic field distribution and the power flow are examined by means of simulations. The last part of this chapter looks on the efficiency of power transfer and the frequency of operation of the wireless technology. The chapter concludes by proposing a design of a wireless power transmission system that can be used to deliver uninterrupted power to the exoskeleton.

- **Chapter 9**: The final chapter summarises the research work reported in this thesis, highlights the main contributions and outlines the recommendations for future work.

Chapter 2

Literature Review

2.1 Introduction

As the exoskeleton is a machine intended for use around the human body it is, first, necessary to understand the basic structure of the human. Therefore, human motions relevant to this research are presented, including gait analysis.

Moreover, a presentation of the history of the exoskeletons robots is included. This is discussed from the perspective of communication strategies and challenges that was faced during the design process of an exoskeletal device.

The anatomy of a robotic exoskeleton will be discussed briefly and will serve as an introductory platform for the exoskeleton classifications section. Some key developments in enhancive exoskeletons will be presented. An overview of other exoskeleton classifications will serve to enhance the properties of the enhancive exoskeletons.

Furthermore, actuation methods within the exoskeleton research are also highlighted. Special focus has been put on the challenges and solutions on the actuation systems, along with the control strategies that can be used on human wearable robots. Actuation sensing and control signals make the important elements of a communication system in an exoskeleton.

The emphasis is put on the communication systems and protocols that have been used in the exoskeletons which have been mentioned in Chapter 1. Despite the fact that there are several exoskeletons of different types that have been developed by other researchers and engineers in the past, there is limited literature on the communication and power systems used for these devices. As mentioned in Chapter 1, exoskeletons can be of different type, such as enhancive, assistive, rehabilitative exoskeletons and many more. In addition, the exoskeletons that have been introduced previously are used either for upper/lower body or for a specific part of the human body and there is no need for a real–time communication system or a power supply that can provide high amounts of energy to operate the device. Most of the exoskeletons studied in the introduction of this report are using low–level communication protocols, such as SPI, I2C, CAN and USART. Furthermore, tethered power systems or on–board batteries have been used for most of the exoskeletons examined previously. The only reported attempt to use a real–time communication architecture and a stand–alone on–board power supply is coming from Kazerooni et. al [8] who developed BLEEX. Thus, special attention has been paid to the analysis of the communication and power system architecture of BLEEX, by examining the specific protocol that is used to transmit all the data to the potential nodes of this specific exoskeleton and by reviewing the power system used for supplying the required amount of hydraulic and electric power.

2.2 Human Body Biomechanics

For the purpose of governance of an exoskelton, the human body–exoskeleton system is treated as a cybernetic system. Two objects are coupled and mutually affect each other through power and information exchange. The exoskeleton is a machine that can be described in engineering terms but the other object, that is human body, is far more complex than any human creation. In order to describe and quantify human locomotion for the engineering purpose, a new domain applying mechanistic paradigm called biomechanics emerged on the brink of medical discipline of physiology [56]. Drawing from the domain, input–output pairs in the human body–exoskeleton system can be identified and a proper human–machine interface in form of measurement system and robot's structure can be designed.

The human body is capable of numerous manoeuvres in the environment using both lower and the upper extremities as well as the core. Among all of those, the task of walking is the most basic [58], [56]. To realise this aspect of human locomotion the lower–body part of the exoskeleton couples with the user for the purpose of gait augmentation or restoration. Thus, an understanding of the gait process is of a paramount importance in the designing of an exoskeleton. During walking, the majority of human segments displacement occurs in the sagittal plane. The main joints involved in walking are the hip, knee and the ankle, which is built of the talocrural (flexion–extension) and the subtalar joint (inversion–eversion). In Figure 2.1 cycle of normal gait is depicted. Most generally operation of a leg in normal gait in healthy person can be divided into two phases with different functions: stance phase (approx. 62% of the gait cycle duration) and swing phase (approx. 38%).

In order to realise control, the exoskeleton system, has to follow or aid the legs for each of the functions. Moreover, it can be observed that equivalent kinematic chain to human legs changes its configuration [58], [56]. During swing of any of the legs an open kinematic chain is formed, whereas during so called double support phase a closed kinematic chain is formed (total approx. 24%). The situation directly affects dynamics of the system. It is then beneficial to recognise which leg is in contact with the ground. A biological parameter suitable for that is the Ground Reaction Force (GRF, also called Floor Reaction Force – FRF). During the stance phase the centre of GRF shifts from a heel to toes [58, 59], (see Figure 2.2), so not only binary information about contact with the ground can be retrieved but also periods of the gait cycle can be recognised. Constructors of exoskeletons have developed several sensors for GRF measurement. For example, in Figure 2.3 a GRF sensor used in HAL–3 is depicted.

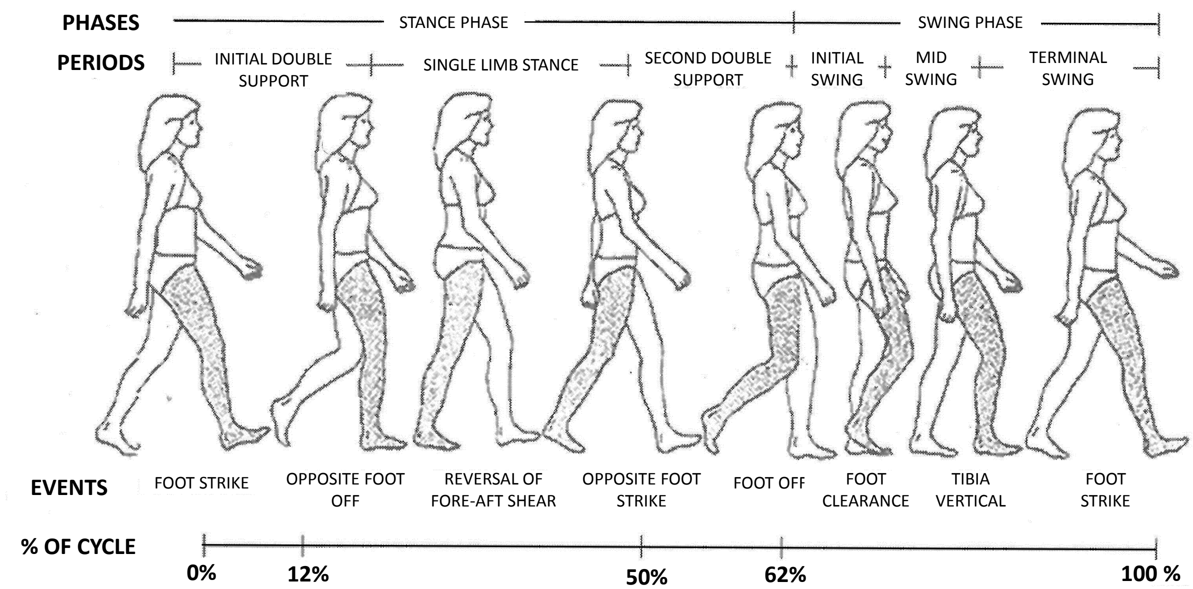

Figure 2.1: Normal gait cycle [58]

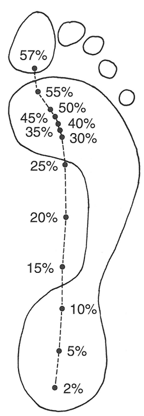

Figure 2.2: Ground Reaction Force centre during walking [56]

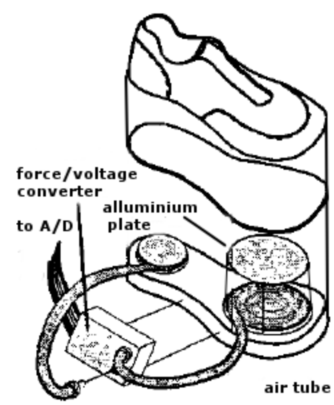

Figure 2.3: GRF sensor of HAL–3 [38]

The Figures 2.4a and 2.4b show similar sensors that are used in BLEEX. The highest levels of GRF occur at the heel and the ball of the foot, that is where measuring elements are placed.

In contrast to the lower extremities, usually the upper extremities are involved in a much diverse range of tasks requiring interaction with numerous objects, tools and living organisms [56]. They are also given greater manoeuvrability. For this reason, it is more advisable to analyse their biomechanics in terms of the task they are intended

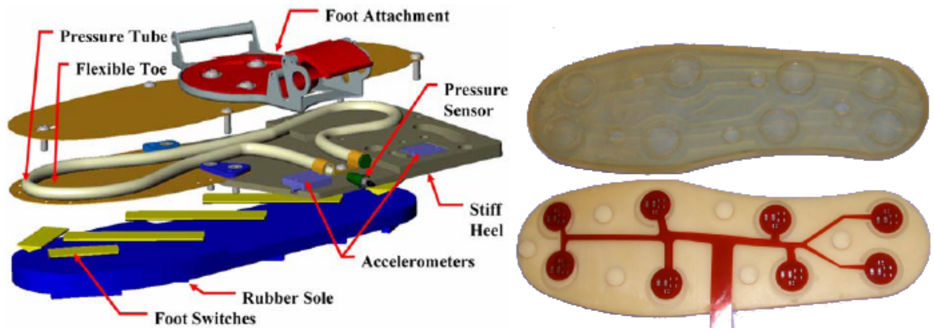

(a) (b)

Figure 2.4: Two version of GRF sensor of BLEEX: a) with switches and tube [9], b) with MEMS sensors [60]

to perform. Nonetheless, movement in each joint in the body is caused by forces acting on nearby bones [56].

2.3 Anatomy of Robotic Exoskeletons

An exoskeleton in biology can be considered to be an extension of the human body, for example a creature such as a crab has an outer exoskeleton to protect its internal organs, also the full metal body armour that is worn by knights can be considered an exoskeleton because it provides protection to the user. In the case of humans, the links and joints of an exoskeleton should match those of the body. The exoskeleton uses the motions of the user as information to provide additional torque and power, this way the strength is enhanced for the person and the intelligence enhanced for the robot [61]. Nowadays scientists and researchers refer to the exoskeleton as a “supersuit” to enhance human capabilities. In military operations this would be a serious advantage since the soldier could run faster, jump higher and carry more weapons [62]. Alternatively these devices are important because they can provide assistance to individuals with disabilities. Table 2.1 [62] shows a comparison between the biological exoskeleton and the exoskeleton technology.

Clearly there are similarities in biological and technological exoskeletons. Nonetheless, there are currently many difficulties to equal the biological model as this document will discuss later. The design of an exoskeleton for the human body should be anthropomorphic and ergonomic in both shape and function. Besides, it should be length adjustable for the different sizes of people, as well as it should be comfortable and manoeuvrable without reductions in natural agility [62].

Table 2.1: Comparison between biological and technological exoskeleton

Function	**Biological Exoskeleton**	**Exoskeleton Technology**	**Application**
Support	Supporting the body of the invertebrates	Supporting physically disabled patient or walking assistance	Rehabilitation robotics or power amplifier
Enhancement	Enhancing the power of animals	Strengthening the human operator	Assistance equipment
Protection	Protecting the animal's body	Protecting the human operator	Automatic armour for soldier, rescue devices or safe manipulation of hazardous materials

2.4 History of Exoskeletons

The first reported work on exoskeletons was done in 1948 by Professor Bernstein, a Russian bio–mechanic, whose work was a prosthetic concept to aid those with injuries from war, though it was never executed [62]. During the decade of 1960's the US Defence department showed interest in developing a suit that would give more strength to their soldiers. They soon established that a suit similar to the human body in terms of joints with fewer degrees of freedom should accomplish most tasks. From 1960 to 1971 General Electric worked on a prototype named Hardyman [61]. This model was purely a master–slave system that duplicated the motions of the individual wearing it. Authors found that duplicating these motions was not the correct way to go, and there were many difficulties in sensing the desired locomotion from the human operator [15]. Furthermore the device was powered by a tethered source of hydraulic pumps which were very large and heavy, which was inconvenient [62].

In 1971 a Yugoslavian professor developed the first anthropomorphic exoskeleton to restore motion to paraplegics [63]. Similarly, in 1990 a German company developed the "Gehhilfe" system to assist disabled individuals to walk again [64]. During all this time in the 20th century scientists and engineers wondered about artificial intelligence (AI) and what it could actually do. Some claimed that AI was dead. Others proposed that to address the difficulties in AI perhaps the human intelligence could be combined with machines [62].

By the end of the 20th century numerous concepts of exoskeletons began to appear from researchers from the USA, Japan, Germany and other countries, with breakthrough advancements in the fields of electrical and mechanical engineering. Nevertheless, there were still many aspects to improve in the areas of intelligence and control algorithms [62].

2.5 Current State and Challenges

The aging population in the world is increasing, it is estimated that by 2050 it will nearly double [65]. This represents a problem because part of the elderly population has difficulties to perform every-day ordinary tasks, due to common conditions such as stroke, spinal injury, muscle weakness and others. There has been interest in researching on ways to help improve the lives of these people by restoring natural motion control. The advantages of using wearable robots are many [53], however the technology that is available at the moment is not enough to provide a reliable solution. This is the beginning of an era which aims to bring a substitute to the wheelchair in the future [54]. The most recent exoskeletons have been possible thanks to the new technologies available over the past five years, mainly new rare earth magnet brushless motors, the reliability of microprocessors and the small size of power drives. Overall the technologies that have been developed in the past 10 years have contributed to making possible exoskeletons as of today [54].

Current technology has not yet reached the stage of providing the perfect exoskeleton. This one should not make the user carry unbearable weight and movements should be natural without sudden motion changes [61]. An additional problem lies in the fact that the focus has been too much on the hardware, but the simpler and smaller the better, the focus now should be on software and control, so that the users can have a seamless experience. According to researchers the objective should be basic motions, those that allow the person to perform basic tasks; more complicated locomotion will come in the future, but for now is to reach a viable solution [54].

2.6 Classification of Exoskeletons

2.6.1 Upper Extremity Exoskeletons

Upper extremity exoskeletons have been considered for a wide range of applications such as rehabilitation devices, for strength augmentation, and even as haptic devices for teleoperation. On [66] Kiguchi et al. improve their previously developed exoskeleton with the aim to assist elder or handicapped persons. The exoskeleton has a specially designed mechanism to recreate the motion of the shoulder using a fuzzy–neuro controller with the electrical signals picked up from the muscles of the wearer.

Other researchers have been working on exoskeletons to help those with brain stroke, this is damage on the brain and results in loss of movement in parts of the body. Researchers at the University of California have developed an upper limb two arm exoskeleton that offers 95% of the same movements as natural arms would [67]. Based on a theory of neural science which states that mirror movement is a natural way for the brain to control the arms, the patient is then put into the exoskeleton, and with the healthy part of his upper body controls the exoskeleton that is able to move the paraplegic part. In this manner, the brain restores and repairs itself, allowing eventually the patient to show improvement and begins to gain back mobility [54]. Upper extremity exoskeletons are not only for helping disabled people, they have also proven to be useful to assist users while handling loads for example in warehouses or factories, and these are usually hung from the roof. The person handles a large payload but only feels a small fraction of it and with this the user can make judgments and perform the desired motions [15].

2.6.2 Lower Extremity Exoskeletons

In terms of lower extremity, BLEEX (Berkley Lower Extremity Exoskeleton), conceived at UC Berkley, is the state of the art. It was introduced in 2004 and it has an anthropomorphic design. The exoskeletal device designed to enable the user to carry large loads up to 34 kg. In addition, the user had the ability to squat, manoeuvre and swing from side–to–side while wearing the exoskeleton. Some of its potential applications are for soldiers, rescuers and other emergency personnel allowing them to carry much larger payloads such as weapons, food, rescue equipment without the fatigue this work might imply [7].

2.6.3 Full–Body Exoskeletons

Full–body exoskeletons combine both previously mentioned types into one device. The Hybrid Assistive Limb (HAL) was developed at the University of Tsukuba, which is a full–body exoskeleton for both assisting and power augmenting purposes. This device is capable of sensing the electrical signals in the muscles and translate them into the desired locomotion of the human operator. Constant work has been able to reduce weight to 21 kg, and the device is capable of supporting itself so the wearer does not feel it. Combining the user's power and the exoskeleton's power HAL-5 has been able to lift up to 80 kg. However, this causes the wearer to become tired quickly when lifting heavy loads [68]. Another interesting development is the XOS–2 from Raytheon Sarcos [69], this full–body exoskeleton uses hydraulic actuators powered via a tethered source offering great strength augmentation whilst remaining manoeuvrable for the user.

2.6.4 Main Categories of Exoskeletons Based on Application

The following list will classify the aforementioned types of exoskeletons into three main categories based on their application and functionality.

- Enhancive Exoskeletons designed with the purpose of augmenting human strength. The main functionality of such exoskeletons is to allow humans to carry loads and perform every day tasks without putting any unwanted effort on the human body. Such exoskeletons are the Sarcos XOS-2 (Fig. 2.5a), PERCRO's Body Extender (Fig. 2.5b) and BLEEX (Fig. 2.5c).

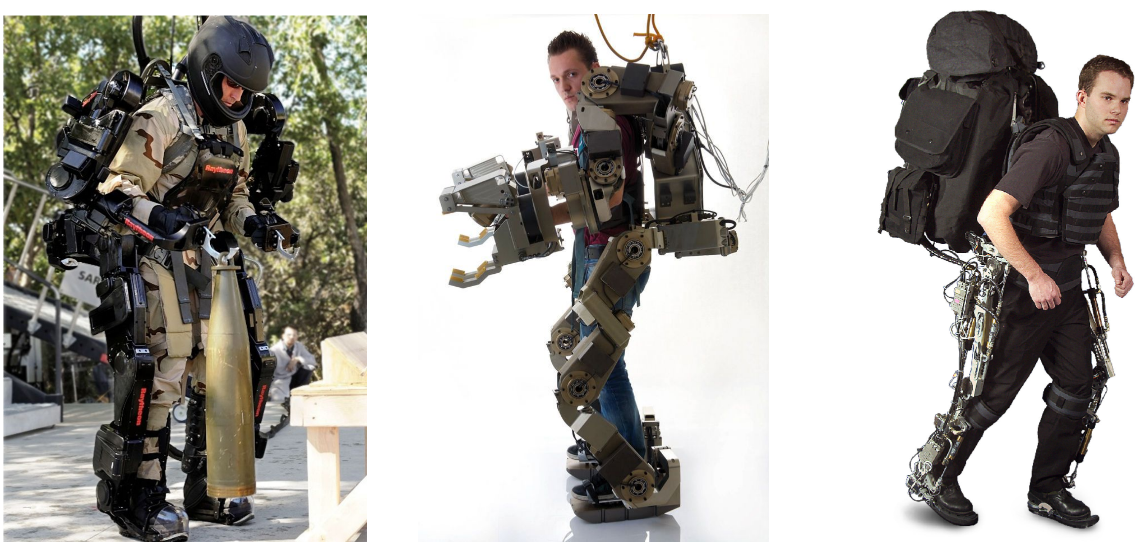

(a) (b) (c)

Figure 2.5: Known enhancive exoskeletons: a) Sarcos XOS-2 [70], b) PERCRO Body–Extender [22], c) BLEEX [10]

- Assistive Exoskeletons designed with the purpose to assist elder or handicapped persons where muscles functionality has been affected by any kind of accident or disease. Such exoskeleton is known as HAL.

- Rehabilitative Exoskeletons designed with the purpose to assist people on the rehabilitation process due to, for example, neural damage that caused from a stroke. They allow users to perform certain activities that will help to recover specific human functions, such as walking or arm movement.

2.7 Actuators for Exoskeletons

There are many actuators used in the field of exoskeletons such as series elastic actuators (cable transmission) and pneumatic muscle actuators. However, only the two main types of actuators are discussed here. These two main types have been studied thoroughly, since they have been considered to be used for the exoskeleton examined in this report.

2.7.1 Hydraulic Actuation

These types of actuators are a feasible choice for exoskeletons because they present high torque-weight ratio. Example of exoskeletons that adopted these actuators are BLEEX and Sarcos XOS–2. The objective of these devices is mainly to enhance capabilities of soldiers. Based on clinical gait analysis, they know that the required torques in the lower limbs are significant.

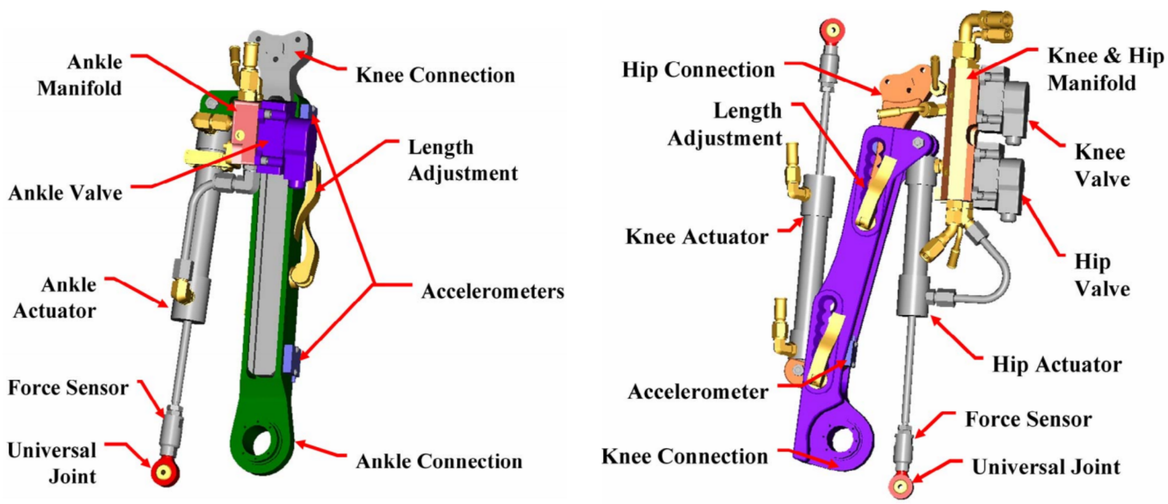

(a) (b)

Figure 2.6: BLEEX hydraulic actuation systems: a) ankle actuation, b) hip and knee actuation [9]

BLEEX uses linear hydraulic actuators (depicted in Figure 2.6a and 2.6b), these receive power from a specially designed hydraulic–electrical power unit which is a large part of the weight of the exoskeleton. On the other hand, Sarcos XOS–2 uses rotary hydraulic actuators placed on each joint and it is powered by a tethered source [53].

2.7.2 Electric Actuation

In the development of the exoskeleton BLEEX, electrical motor actuators were also considered taking into account the clinical gait analysis (Figure 2.7). It was demonstrated that electric motors were more efficient during walking than hydraulic actuators, although the location in the joints of the motors may represent some drawbacks, as well as bigger size and weight compared to hydraulics for the same purpose. Nevertheless, if the requirements of the exoskeleton do not entail assisting in power or carrying heavy loads, then electric motors are more suitable because by lowering the torque requirements, the size and weight of the actuators also decreases. This is of importance for a rehabilitation device [53].

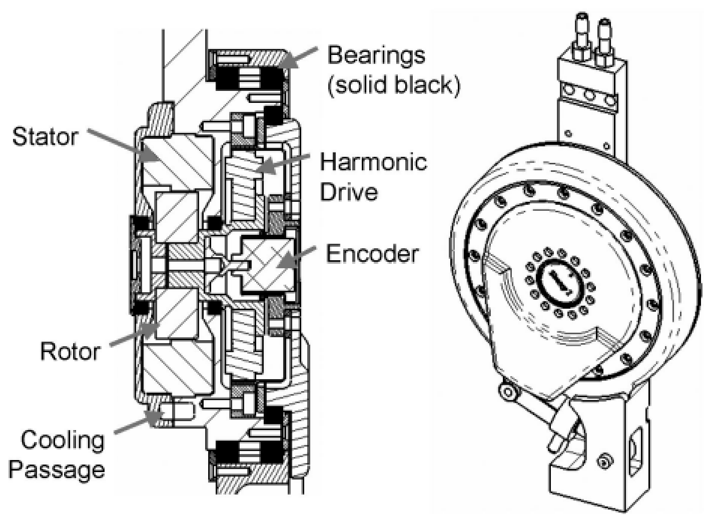

Figure 2.7: Electrical actuation system of the BLEEX exoskeletal device [10]

In the case of the HAL exoskeleton, which is intended for both assistive and power augmenting, the researchers make use of computer controlled electro–driven joints called power units to follow the user's motions. The device has a specially designed mechanism to switch back–drivability of the joints to be able to keep loads steady when lifting them [49].

The PERCRO Body Extenders actuation system shown in Figure 2.8 includes electric rotary motors which are designed to provide up to 500 Nm constant toque (800 Nm stall torque) with a total weight of 6 kg per unit [20]. The device is built to allow for dual direction drive using a pantograph mechanism. The actuation system of the BE is meant to be modular therefore it is replicated throughout the exoskeleton.

Figure 2.8: Electrical actuation system of the PERCRO exoskeletal device [20]

2.8 Control Strategies

Control algorithms denote the behaviour of the exoskeleton, since the device is worn by humans and the user is part of the control loop so this is very different than traditional robotics control. Thus it is essential to determine the intention of motion. Different control algorithms are based on different ways of measuring this interaction of the wearer with the device [53, 62].

For a good control, human and machine must work together. The exoskeleton receives information from the user and from sensing the environment. The human can intuitively and dynamically execute the work, but it is not easy to implement this type of control. The exoskeletons are capable of assisting the user under dynamic situations. These situations are unpredictable and out of the reach of control, which can lead to unwanted situations where the dynamics of the environment may change and cause an accident. Therefore, the system needs to be monitored continuously without failure of delivering control signal, otherwise it would end in the system failing. For this reason the control of an exoskeleton system needs to be in real–time. One of the most important factors that affect control in this application is the delay in the LAN (local area network), which connects all modules of the system for data exchange [62].

2.8.1 Signals Measured From the Human Body

This approach measures the signals from the human body that reflect intention of motion directly. For this purpose, there are two types of signals used, from the surface of the skin and electroencephalogram [53].

The exoskeleton HAL has been developed in the University of Tsukuba since 1992. The researchers of this exoekeleton created a new concept which is a new multidisciplinary term that incorporates cybernetics, mechatronics, informatics and integrates neuroscience [68].

The control algorithm is one of the most important parts of the system. The cybernic control system is a hybrid as it uses the so called "cybernic voluntary control" and a "cybernic autonomous control". The voluntary control supports the user's actions by sensing the electrical signals that are travelling from the brain to the muscles, this way providing extra torque through the actuators [71]. HAL can accurately detect the voluntary motions and assist the user to walk or stand up. However, when it comes to a handicapped person the voluntary control is not as accurate. The case is even worse when the person has gait disability, because the signals from the brain to the muscles arrive partially or do not arrive at all, this is where the autonomous control has its function [68].

Since a handicapped person's brain signals to the muscles cannot be used to implement a control, another approach is used. Although the brain can think of walking, there is still no technology available that can sense the human intention from the brain, but sometimes the intention can be determined from looking at the motions of the body. In this scenario if a person wants to walk, their centre of gravity changes and therefore an intention of walking can be noticed. The reverse change in the centre of gravity can be used to predict a desire to stop walking [53]. This is achieved by placing floor reaction force sensors embedded on the sole of the foot, this way being able to provide correct measurements of the change in the centre of gravity [72]. Hence, the aim is to sense the changes in the centre of gravity and perform a natural and comfortable walking pattern for the user, making it possible for the patients with paraplegia to be able to walk.

2.8.2 Measurements Only From the Exoskeleton

The exoskeleton BLEEX takes measurements directly from the device. The exoskeleton can be efficient because it combines the intelligence of a human operator and the strength of the machine. The control algorithm is intended to allow the exoskeleton to follow the motions of the user with the least force interaction between the two. The controller of BLEEX does not make use of force sensors or electrical signal sensing; instead the only information collected is from the exoskeleton itself. This control approach is different than any other control used before in robotics [8].

The principle here is that the exoskeleton must follow the motions of the wearer very fast. For this the exoskeleton needs to be highly sensible to external forces and torques especially by the ones coming from the user. Nevertheless, this principle goes against classical control theory where the system must have minimal sensitivity to ensure robustness [8].

One of the important issues that can be considered with relation to the concept of control is that the exoskeleton could react to an external force (e.g. being pushed) just as if it were the user applying a force, then the exoskeleton could impose movements that are not desired. In order to deal with such an issue, it is important that the wearer quickly reacts creating a stable situation for both the exoskeleton and himself [8].

2.9 Communication Systems

2.9.1 Definition of a Communication Protocol

In its most basic form, a communication protocol is a defined set of rules that allow for two or more entities in a communication system to exchange information [73].

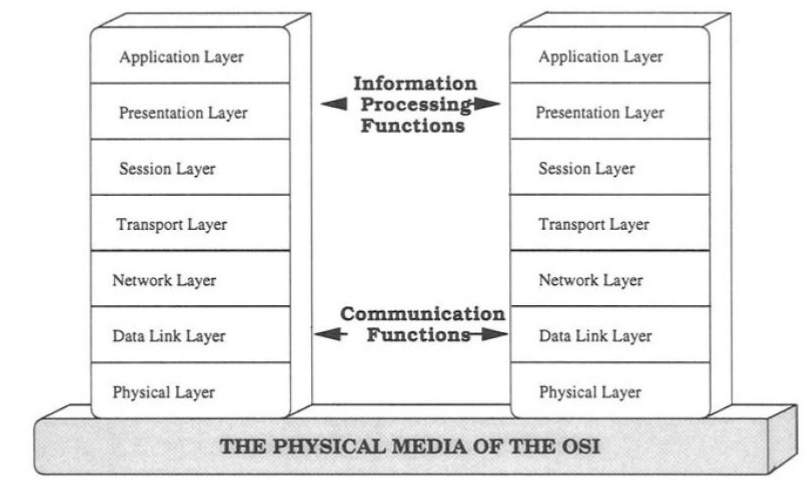

Figure 2.9: The OSI reference model [73]

The rules must be clearly defined as a standard to avoid any ambiguities. In the decade of the '80s, the International Organisation for Standardisation (ISO) initiated a program to formalise protocol models. Since protocols can be complex, the solution provided by ISO was a division of these into a model of layers called the Open Systems Interconnection (OSI). Reference Model depicted in Figure 2.9. This Reference Model made protocols easier to be understood, tested and modified. Each layer performs a well–known function and has a well–established interface between the layer directly below and above, making the implementation of each layer independent from the rest [73].

2.9.2 Review of BLEEX Communication Architecture

This section discusses the communication network for control used in BLEEX exoskeleton based on [8] and [74]. BLEEX exoskeleton consists of 16 accelerometers, 10 encoders, 8–foot sensors, 6 force sensors, 1 load cell, 1 inclinometer and 6 hydraulic servo valves. According to the authors, the control electronics responsible for handling the signals from these components would require more than 200 wires. For this reason a high–speed serial communication using a ring topology network was proposed to transfer large amount of data with low latency. This implementation allowed to transfer all necessary data with only 24 wires [8, 74].

The sampling period of the control algorithm is an important factor that affects the performance. In this protocol the stations are connected circularly by serial point–to–point links. This protocol enables multiple stations to send data packets without creating congestion in the network. The protocol is optimised for hard real–time transmission. Real–time Ring topologies have been used in the industry [8, 74].

The BLEEX communication architecture consists of the so called ExoBrain, which is composed of three boards: ExoCPU, ExoPCI and Supervisory I/O Modules (SIOMs). All the control algorithm computations are processed in the ExoCPU. The ExoPCI serves as an interface for the SIOMs to make use of the parallel bus interface of the CPU. Lastly there are Remote I/O Modules (RIOMs) located on different parts of the exoskeleton. In Figure 2.10 the connection scheme of the different modules is shown [74]. RIOMs 0-2 are located in the right leg, RIOMs 3-4 on the right side of the back, RIOMs 5-7 on the left leg, RIOMs 8-9 left side of the back. The modules from the right side of the exoskeleton are connected to SIOM-0 and on the left side to SIOM-1, the third SIOM is used to communicate with a GUI (graphical user interface) in LabVIEW to change parameters of the exoskeleton [8, 74].

The control sequence of the ExoBrain is: a) The ExoCPU performs the computation of the control algorithm, b) then new control actuation data is sent via parallel interface to the ExoPCI, which converts the parallel interface data into serial, c) then transfers the control actuation data to the SIOMs, d) the SIOMs then transfer the data to the RIOMs to execute the commands, e) immediately they return the new sensor data to the SIOMs, f) which then transfers it to the ExoPCI, g) which then transforms the

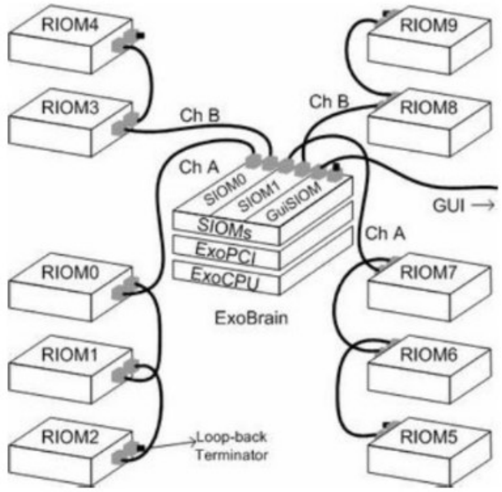

Figure 2.10: Communication scheme of BLEEX [74]

new sensor data into parallel data for the ExoCPU to compute once again [8, 74]. As mentioned before the RIOMs are located throughout the exoskeleton. Their purpose is to acquire data using 16–bit A/D converters from the six sensors assigned to each module, while at the same time they handle one actuator.

The goal of this communication scheme is to achieve fast, real–time data transfer between modules with the least amount of latency. The sample time of the control–loop is a determining factor for the entire system and thus for the communication. Arbitrarily, the authors chose a control–loop frequency of 10 kHz as a target, which is one loop every 100 μs. The goal was to make the communication time 20 μs and the remaining time is to be used for computation by the ExoCPU. One full communication cycle is regarded to be the time it takes from the transfer of actuator data to the reception of new sensor data. Figure 2.11 shows a representation of the desired communication time compared with the control loop time [74].

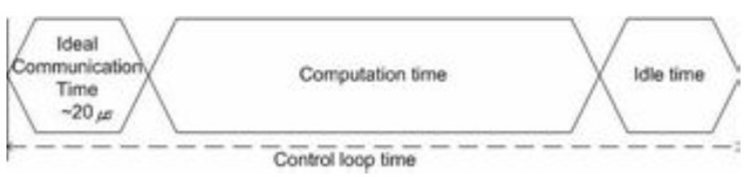

Figure 2.11: Comparison of communication time and the control–loop time [74]

2.9.3 Analysis of Operation of BLEEX's Communication Protocol

Data packets are the way data is sent in communication networks. These contain actuator data or sensor data. In this application the sensor or the actuator information occupies 16-bits while 8 other bits are added to the protocol to denote a type of packet (2-bits), address (3-bits) and error detection (3-bits). This configuration allows up to 7 RIOMs per each SIOM. The data packet is depicted in Figure 2.12 [74].

Figure 2.12: Data packet [74]

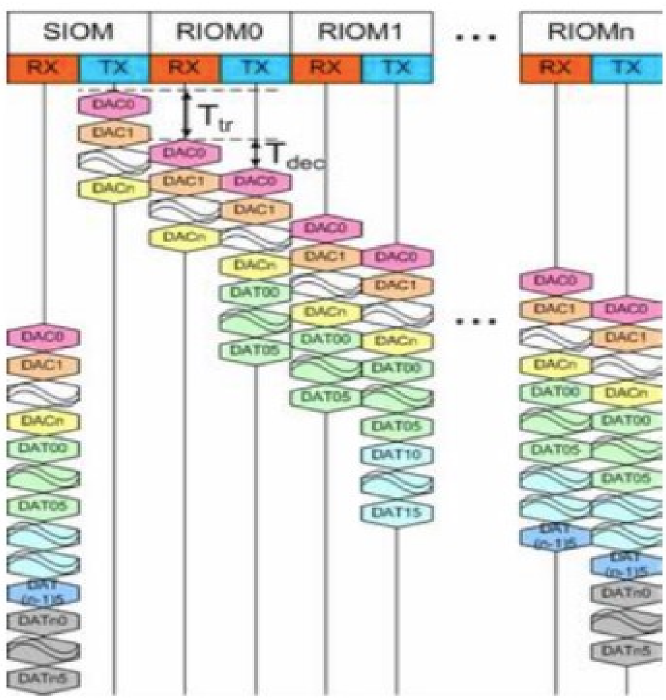

Figure 2.13: Data transfer sequence

Each RIOM makes a packet of data for each sensor, so 6 packets in total, and since each RIOM is in charge of one actuator, it receives one packet of data for that purpose. The actuator data for all RIOMs on the ring is transferred from the SIOM to the first RIOM on the ring, this one receives it and adds to this message the new sensor data, in order for the output to be the same message as well as the new sensor data of that

RIOM. This sequence continues until the last RIOM on the ring and returns all this message to the SIOM. This is depicted on Figure 2.13 [74].

According to the tests performed, the total communication time is 16.49 μs which satisfies the goal of 20 μs. Overall, this communication scheme is satisfactory for the exoskeleton BLEEX. As explained before, the conventional control in parallel would have resulted in more than 200 wires present in the system.

2.9.3.1 Concept of Real–Time Systems

Real–time systems are those that must execute a required task within a very limited time frame. The failure of executing an action within the specified time can lead to a failure of the entire system, which could result in a dangerous situation [75]. Nowadays many complex systems such as industrial automated plants, robotics and automotive control, rely partially or totally on computers.

The environment plays an important role in such systems because it influences directly the reaction of the system. The real–time system must be prepared for unexpected situations and still be able to deliver the required action within the specified time frame. A real–time system is often misinterpreted as a system that must be fast. There is no logic in designing a real–time computing system for a device without being aware of the specific timing characteristics of the device. There are three classes of real–time tasks according to the consequences of a missing a deadline [75]:

- **Hard:** A real–time task is considered to be hard if there is a strong time deadline, that is, if the failure of accomplishing the task leads to the entire system failing or if it causes damage in the physical world or to humans.
- **Firm:** There is a slight tolerance if the system misses a deadline. The system cannot make use of this delayed signal, but it does not end in a dangerous situation.
- **Soft:** The system can continue to operate though the degradation of the operation will be noticeable.

2.10 Power Systems

An increasing demand for energy has been reported over the past years for power–hungry applications such as exoskeletons. Conventional power sources such as fossil–fuel and environmental concerns are driving forces toward renewable and wireless power transmission energy sources. Moreover, gas, oil and coal energy sources are being depleted quickly and their reserves are becoming insufficient and intended for future use. In addition, due to greenhouse gas emissions these energy sources are not environmentally friendly. Thus, renewable energy sources are becoming more essential over the years.

A full–body enhancive exoskeleton may requires both hydraulic and electric power to ensure the energetic autonomy of the robot. The hydraulic power is used for locomotion and the electric power is used by the on–board electronics, such as microprocessor, sensors and other peripheral devices. Furthermore, the power source that will be used by the robot should be lightweight and do not pose a risk on operator's health. Most of the human scale robots examined in Chapter 1, are powered by tethers or battery systems that are increasing the overall weight of the robot. Thus, there is a great need for developing a compact and portable power system that will be capable of meeting both mechanical and electrical energy requirements of the robot. The only reported attempt to develop and build a lightweight and reliable on–board power supply, has been presented by Kazerooni et. al in [1], where they have used an internal combustion engine on the backpack carried by the exoskeleton. Their system is presented briefly below. Finally, Chapter 7 contains a detailed discussion of the power sources available for exoskeletons.

2.10.1 Review of BLEEX Hydraulic–Electric Power Unit

The hydraulic–electric power unit (HEPU) used to provide sufficient amount of hydraulic and electric energy o BLEEX is using an internal combustion engine as its prime mover [1]. In their research, Kazerooni et al. have examined several different HEPU systems to identify the most suitable candidate that will meet the power requirements of BLEEX. HEPUs such as Honda GX31, GXH50 and FUJI BT50SA have been reviewed. However, they were note capable of providing the sufficient amount of hydraulic and electrical power. Thus, their design for the on–board power supply has been selected based on the ZDZ80. A HEPU system with integrated noise deadening measures was realised with a ZDZ80 two–stroke engine. The prototype design of power unit of BLEEX is depicted in Figure 2.14. The overall weight of the HEPU is 27 kg and has been mounted at the back of the exoskeleton device. It uses a compact two–stroke opposed twin cylinder internal combustion engine capable of all–angle operation in order to provide hydraulic and electric power.

The main schematic layout of the HEPU unit is depicted in Figure 2.15 and its main architecture is summarised on the following:

a. The alternator used for generation of electric power is driven by a single shaft;
b. Hydraulic power is generated by the gear pump that is driven by the single shaft;
c. Air circulation is undertaken by the cooling fan that is also driven by the single shaft;
d. The hydraulic fluid pressure is regulated by a hydraulic solenoid valve by directing the hydraulic flow from the gear pump to either an accumulator or to the hydraulic reservoir;
e. The pressurised nitrogen gas is separated from the hydraulic fluids by a piston that can be found in the accumulator;
f. The reservoir of the nitrogen gas is made of carbon fibre and is attached to the gas side of the accumulator;
g. The pressure of the hydraulic fluid is measured by the pressure transducer;
h. The filter and the solenoid valve are accommodated by a manifold that is designed for this purpose;
i. Actuators of the robot are using hydraulic fluid to operate. Approximately 38% of this fluid is used to cool the internal combustion engine;
j. The heat generated from the hydraulic fluid is removed by the heat exchanger before it reaches the hydraulic reservoir where it is mixed with the rest of the fluid.

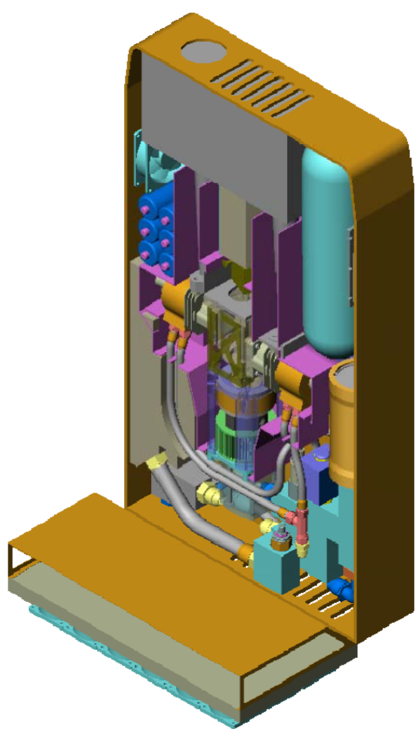

Figure 2.14: Hydraulic–electric power unit of BLEEX exoskeleton [1]

From the experiments conducted with the HEPU it was demonstrated that it is capable of producing 6 kW of shaft power at 8200 rpm and is used as the prime mover of this unit. According to the power requirements, BLEEX needs 2.3 kW of hydraulic power for the actuators and for the cooling system. It has been found from the experimental results, that the HEPU unit can deliver adequate amount of hydraulic power when operating at 6300 rpm with a shaft power of 3.06 kW. The overall output hydraulic power has been measured at 2.3 kW [1].

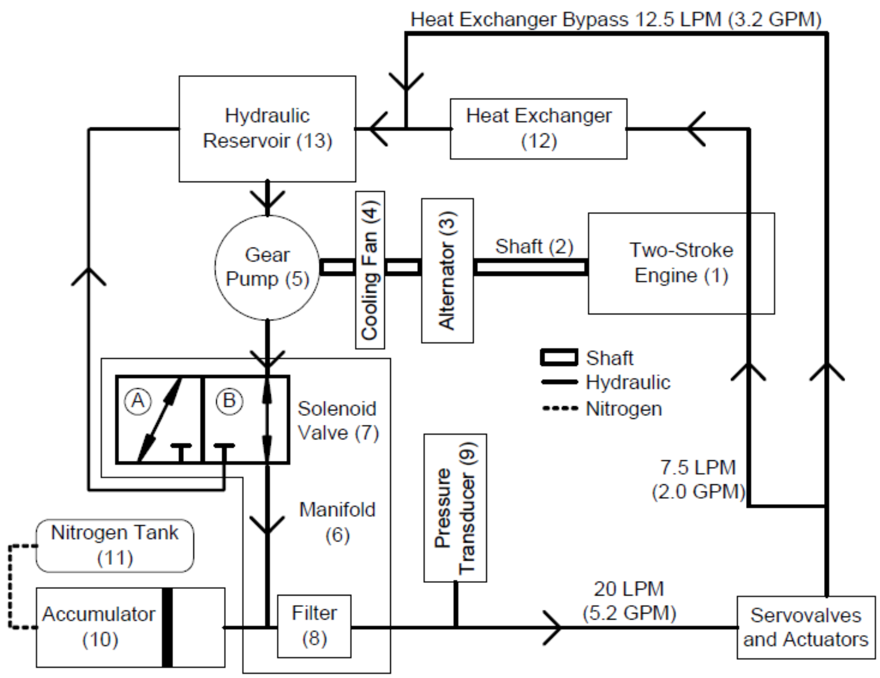

Figure 2.15: Hydraulic–electric power unit schematic layout of BLEEX exoskeleton [1]

On the other side of the spectrum, the HEPU used for BLEEX can generate electric power that used by the on–board electronics, such as the cooling fan, sensors, microcontrollers and many more. It has been estimated that the power budget of the electronics of BLEEX is approximately 230 W, with 65 W for the communication system, sensors and microcontrollers and 100 W for the motors used by the cooling fans. The remaining 65 W are used by the peripheral devices and losses. A three phase, 12–pole frameless, brushless DC motor is used as an electric power alternator. The three phases are converted into single phase with two separate 15 VDC bus voltages. The first bus voltage is used to deliver power to the solenoid valves, ignition for the engine and the cooling fans. The other bus voltage to deliver power to the HEPU controller, to throttle the servos, charge the on–board batteries and electronics [1].

Taking everything into account, it seems that the on–board HEPU of BLEEX is one of the most advanced, efficient and reliable power systems that ever designed for exoskeletons. Their design for the power system is using an internal combustion engine that can deliver adequate amount of hydraulic and electric power with a maximum of 2.3 kW and 230 W, respectively. In addition, Kazerooni et al. used a sophisticated cooling system for the power unit where the hydraulic fluids from the actuators used to cool the engine.

2.11 Gaps in the Body of Knowledge in This Field

Although there are many exoskeletons used in the past for assisting, enhancing and rehabilitating purposes, there is very limited literature on the architectures that used to establish the on–board communications of the exoskeletons. Most of the exoskeletons presented in Chapter 1 have used low–level communication protocols that cannot provide real–time characteristics. In addition, most of these devices are either for upper or lower body and have been used for recovering specific human functionalities during the rehabilitation process or deployed on the battlefield and used by the military services. It is also worth noting that several exoskeletons that are used for military purposes were funded by the defence industry and became confidential. To the best of author's knowledge, there are no reported attempts to use a real–time communication architecture to establish the on–board communications for a full–body enhancive exoskeleton. The only attempt is coming from Kazerooni et al. in [8] who developed a network architecture based on PCI protocol that can provide real–time monitoring and controlling characteristics.

On the other hand, based on the background research, it has been found that most of the exoskeletal devices, such as XOS-2, PERCRO's body–extender and HAL, are using tethered solutions or rechargeable batteries to supply power to the on–board electronics and components. The only attempt to use a standalone power supply has been reported by BLEEX's researchers [52], who developed an internal combustion engine that can provide the full amount of hydraulic and electric power that is required for the actuation and the on–board electronics. Apart from BLEEX, there are no other reported attempts to build an autonomous full–body enhancive exoskeleton. Finally, there are many challenges and concerns that need to be addressed when dealing with high amount of electrical and hydraulic power since exoskeletons are devices that will be worn by humans. The limitations and safety risks of using different types of power supplies have been examined thoroughly in this report and presented in Chapter 7.

2.12 Summary and Conclusions for the Literature Review

According to the literature review, the exoskeleton system can be recognised as a multidisciplinary device with anthropomorphic form that matches the joints of the human body. Therefore, it can be worn to work in conjunction with the user to provide enhancements by combining human intelligence and machine power. It is important to note that the human operator plays an important role because he/she is part of the unconventional control system providing vital information. However, currently there are many limitations as the technology is not yet at the correct state to provide the perfect exoskeleton.

Nonetheless, there has been significant progress made thanks to the advancements in technology from the past 10 years. Exoskeletons can be classified in very different ways depending on the section of the body that they assist, the actuators involved, and the type of assistance or enhancements provided, as well as the control strategies used, which depends directly on the method of measurement of motion intention.

A communication architecture has been analysed from one of the state–of–the–art exoskeletons, BLEEX. It is clear that the requirements of such complex device need an implementation of a hard real–time communication technology. The computation time of a control loop and sample time are determining factors that leave a small margin for data transfer time. In such scenario, the time it takes for the information to be transferred in the network must be substantially smaller than the time it takes to compute the control algorithm.

Finally, the HEPU used to supply the required amount of hydraulic and electric power that BLEEX needs to operate has been reviews and analysed briefly to identify any potential gaps that such implementation can introduce to the power systems that can be used for exoskeletons. The chapter concludes by introducing the gaps in the body of knowledge in this field which will be examined thoroughly in the following sections.

Section I - Communications

Chapter 3

Potential Communication Protocols Suitable for the Exoskeleton

3.1 Introduction

In this section the contributions from this PhD to the exoskeleton project are presented. This includes the research, analysis and evaluation of the most advanced industrial real–time communication protocols. The purpose of these are to aid in the selection of the communication system that will be used for the exoskeletal device, based on the specifications that each potential communication strategy is able to provide.

The first section of this chapter begins by defining the requirements for the potential communication strategy to be used. First, the widely adopted communication protocols are analysed and previous related work is outlined. This is followed by outlining the specifications of each protocol, which includes the evaluation of the available hardware, the message size, potential network topologies and, finally, the bit–rate. This chapter concludes with a summary of the evaluations and outlines the reasons for choosing EtherCAT as the best communication protocol for this project.

3.2 Preliminary Requirements

The idea of this project as a whole is to develop a modular full–body robotic exoskeleton. The modularity means that any extremity could be easily detached or exchanged for another that has a different end–tool or function.

Based on the literature review, it is reasonable to think that each module (e.g. arms, legs) of the exoskeleton must be operated by a remote–control unit, which will be in charge of handling a few sensors and perhaps more than one actuator. Moreover, it is reasonable to think that there will be a more powerful central processing unit (CPU) where the control algorithm for the entire exoskeleton will be computed. According to this, there will be several electronic units that need to communicate with the main CPU. It can be appreciated from the literature, that this type of system has been implemented with success in other exoskeletons such as BLEEX.

The purpose of this project is to research communication protocols to find the one that best suits the exoskeleton needs. The following preliminary requirements must be considered:

- Since the exoskeleton is intended to be modular, the communication network must allow connection of multiple stations.
- It is important that the protocol is a widely used standard so that the hardware can be easily interfaced and expanded.
- Since the system will be dealing with a person who is the wearer, any failure while functioning may cause damage to the physical surrounding environment or to the individual wearing it. For this reason the communication protocol must be in hard real–time.
- The frequency of the control algorithm is a deterministic factor. The communication protocol must be capable of transferring all data in a fraction of the control–loop time.

3.3 Widely Adopted Communication Protocols

The literature offers very little insight on the communication systems that have been used in previous exoskeletons. The literature mainly concentrates on other aspects such as the control and actuation systems. For this reason it is necessary to consider the available communication systems. Throughout history, the automotive industry has been responsible for numerous technological innovations including real–time distributed systems [76]. In early stages of auto-mobiles, every new function was implemented in a dedicated electronic control unit (ECU), which is a microcontroller connected to a set of sensors and actuators using point–to–point connections. Rapidly, this approach proved to be unsatisfactory because some information needed to be distributed over several ECUs and the amount of wiring was a main issue due to its heavy weight. Therefore, the automotive industry was motivated to create a solution to this problem. The solution was to use multiplexed communications over a shared medium with a defined set of rules (protocols) for communication. The automotive industry has created standards such as LIN (local interconnect network) for low cost, CAN (controller area network) for mid-range and FlexRay for high-end applications [77].

Industrially, in certain contexts such as in factories or automated plants, communication systems are widely adopted to reduce the complexity and amount of wiring. In the past, distributed control systems were used in manufacturing plants, where each device in the field had a direct connection to the main computer. This required kilometres of wiring, mistakes during setup were easily made and users had to go to each field device to modify parameters. To solve these issues and replace centralised parallel wiring, fieldbus control systems were considered as a solution. Fieldbus controlled systems aim to have a single physical medium where all field devices are connected, thus reducing wiring costs, complexity and mistakes during installation. Nowadays, fieldbus technology has different standards such as Fieldbus Foundation, Profibus, Modbus, Hart, along with others [78]. In [79] Profibus is highlighted as one of the most widely adopted and dominant fieldbuses. Furthermore, the advantages of Ethernet are underlined, which justify the development of real–time Ethernet for use as an Ethernet fieldbus. It becomes apparent that these applications have the same aspect in common, to reduce the amount of wiring in the connection of remote units with each other or with one or several CPUs, sharing a single transmission medium. Therefore, it is reasonable to think that the exoskeleton, in terms of electronics, can be seen as an automation problem similar to that of the automotive and industrial automation fields.

3.3.1 CAN Protocol

The Controller Area Network (CAN) was developed by the German automotive system supplier Bosh in 1985 for automotive applications with the purpose of providing robust serial communication. Prior to CAN, automotive manufacturers connected the electronic components in a point-to-point configuration, resulting in bulky wire harnesses that were very expensive and added weight to the vehicle [80]. After its introduction CAN became very popular in automotive/truck applications, as well as industrial applications. CAN also proved to be adequate for military vehicles, industrial machinery, medical systems, marine control and navigation [81].

To allow interoperability between different products of different manufacturers, the International Standards Organisation (ISO), created the Network Reference Model. Most network applications follow this layer model. CAN implements the lowest two layers, physical layer and data–link layer. CAN is a message–based protocol, which means that all nodes in the system receive every message sent on the bus and each one decides whether to keep the message and process it or to discard it. This method simplifies the encoding within the network and speeds the transmission traffic. An important feature of CAN is the ability of one node to request information from other nodes. This is defined as Remote Transit Request (RTR), where nodes can communicate with each other [81]. Figure 3.1 [82] shows the details of a CAN system, where the nodes include a CAN transceiver and a controller, all connected to the same physical medium which is a pair–wire bus. The bus transmits the signal in differential voltage, providing CAN with robust noise immunity.

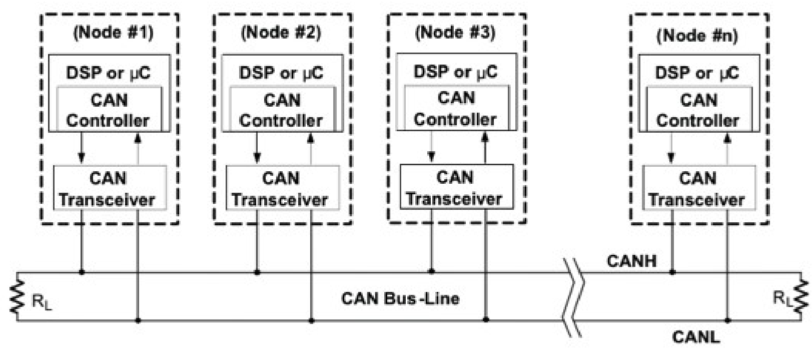

Figure 3.1: Details of CAN bus [82]

CAN is a career–sense–multiple–access protocol with collision–detection (CSMA/CS), which means that all nodes have the same opportunity to send a message when the bus is inactive, when this happens, the message with the highest priority is able to gain bus access, and the other nodes have to wait and send their message after this transmission. This priority scheme makes of CAN a very attractive protocol for real–time systems [82]. This feature also means that components can easily be removed or added in the system without having to reprogram other nodes. The new nodes will simply begin to receive messages and based on the message ID it will choose to discard or make use of it [81]. In conclusion, CAN is an inexpensive protocol to implement, optimised for systems that require reliable transmission of relatively small amounts of information with high reliability and in rugged environments.

3.3.1.1 Previous Related Work With CAN

A dual CAN network for control distribution of a mobile humanoid robot was implemented in [83]. One of the reasons that Cha et al. used CAN was for its noise immunity, which is critical for a robot of this nature. The robot can perform some ordinary every–day tasks such as taking food out of an oven and deliver it to a person. In [84], the work acknowledged CAN as an event–triggered system, which means that whenever a value from one of the sensors in the network changes, a signal will be sent to the bus. This event–triggered functionality has been well–accepted for controlling robots and coordinating manufacturing processes. In [85] the researchers proposed CAN where 14 local controllers could communicate with the main controller in a 22 degree of freedom humanoid robot. The researchers carried out a simulation to acquire the real response time of the messages and the results showed that the response time satisfied their timing requirements.

3.3.2 LIN Protocol

During the 1980s, serial communication hardware such as the UART (Universal Asynchronous Receiver Transmitters) was becoming increasingly popular in consumer electronic products, which in turn increases availability and reduces costs. As the automotive industry evolved, it was equally benefiting from this technology. Communication technologies using UART hardware began to emerge, sharing common characteristics but were often incompatible. With the goal to create an industry–standard, a consortium was founded by leading automotive and semiconductor manufacturers. At this point LIN (Local Interconnect Network) became a standard promising low–cost UART–based communication [86].

LIN is a bus system which uses a single–master/multiple–slave configuration. The master requests data from a slave by sending an identifier; based on this identifier, the slaves choose to process the message and respond or to dismiss it. All this is done on a single wire that operates at vehicle battery voltage. For example, a sensor is a slave connected to the network, this sensor is constantly measuring an analogue value regardless of the LIN communication. Only in response to a periodical request from the master that the sensor will send the data. A LIN slave typically consists of a microcontroller in charge of the protocol and a LIN transceiver which serves as an interface between the physical layer and the controller [87]. The protocol is intended for simple electronic tasks in automobiles such as operating car seats, door locks, sun roofs, rain sensors and mirrors [88].

3.3.2.1 Previous Related Work With LIN

LIN is one of the dominant communication protocols dedicated for low–cost applications in the automotive industry. Its wide adoption is a key factor for considering this protocol for the exoskeleton project. Despite the lack of evidence that LIN has been used in exoskeleton or robotics fields before, it is worth keeping in mind that the exoskeleton device can be considered to be an automation problem similar to that of the automotive field.

3.3.3 FlexRay Protocol

A consortium founded by BMW, Bosch, DaimlerChrysler and Philips in the year 2000, is responsible for developing the FlexRay protocol for the next generation of automobiles [89]. Currently, automobiles are in need of providing better performance and safety. Therefore, the demand in the amount, speed and reliability of the data transferred between ECUs is increasing. There is a growing need for synchronisation between ECUs, which is more than the existing CAN protocol is able to provide. As a solution to meet these new challenges, the FlexRay standard has been developed. FlexRay is designed to overcome present and future challenges. However, it is not likely to replace the two dominant automobile buses, CAN and LIN. FlexRay will be used for high–end applications, CAN for general applications and LIN for low–cost applications [90].

FlexRay uses an unshielded twisted pair wire as transmission medium, which supports bus topology, star and a combination of the two. It also allows for double channel to increase bit rate and to enable fault tolerance. One of the most important features that FlexRay was designed for is time–determinism. All nodes in the network are synchronised at the same clock, and everything occurs according to a schedule. For that specific reason, FlexRay uses Time Division Multiple Access (TDMA). Since all nodes are synchronised and each node waits for its turn to write on the bus. All the messages fall into the "FlexRay communication cycle". The cycle is divided into small practical units referred to as "macroticks", about 1 μs long and all nodes are synchronised to this macrotick [90].

Figure 3.2 represents the sequence of FlexRay communication cycles (a) and a detailed view of each cycle (b). The blue section is referred to as the static segment (ST) and it is divided into slots. When each slot occurs in time, the reserved ECU can transmit its data into that slot and once the designated time passes it is the turn of another ECU to write. The dynamic segment (DYN) allows for ECUs to write sporadic data prioritised based on the order with which it is written. While an ECU is writing on the bus, all others have access to read the message and decide to process or dismiss each specific message/event [90].

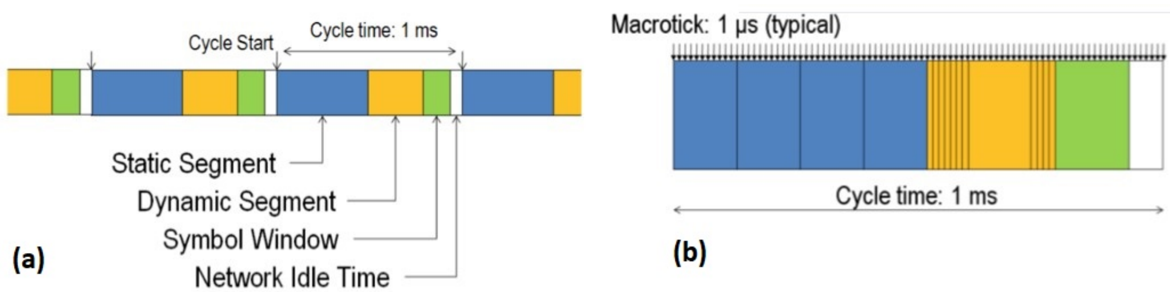

Figure 3.2: FlexRay communication cycles (CC) (left), Detailed Cycle (right) [90]

An interesting application that is possible with this protocol is the ability to do in–cycle control. In Figure 3.3, the example presents 4 ECUs transmitting data of the wheel position in their respective time frame. Since the wheel positions occur before the static segment ends, ECU number 5 is able to read, process and write the control signal on the bus during the same cycle. Thus, allowing for very high–speed control in the FlexRay network [90].

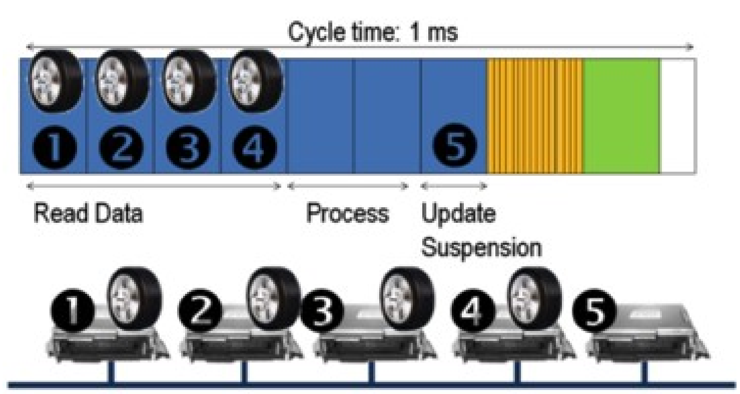

Figure 3.3: In–cycle control example [90]

3.3.3.1 Previous Related Work With FlexRay

In [76] the authors mentioned that FlexRay is considered the potential successor of CAN, and that the increasing usage of FlexRay in vehicles will result in decreasing costs of its hardware, thus the rapid adoption would place FlexRay as a standard network for automation and control systems. According to the authors, around 20% of CAN nodes are used in non–automotive applications, such as embedded networks and industrial control systems, which can be partially replaced by FlexRay nodes. Furthermore, this percentage might be increased due to the new features brought by FlexRay.

Additionally, Froschauer et al. in [76] highlighted the potential of FlexRay outside of the automotive field by giving two example applications. The first was a scenario of an autonomous renewable supply network, which consists of components like renewable generators, energy storages and energy consumers. The energy consumption is managed based on priority and all the nodes could easily be connected using FlexRay. The second example was a modular robot system, where FlexRay could be used as a master–less communication system to maintain synchronisation of a robot assembly line. In [89] the researchers designed a FlexRay protocol using Verilog HDL and it was integrated with a sound localisation system used in robotics applications. The sound from four microphones located in the robot's head was processed and transmitted to a host PC via FlexRay to determine the source of the sound.

3.3.4 Profibus DP Protocol

Profibus (Process Field Bus, Decentralised Peripherals) originated in a development done by the German Federal Ministry of Research and Technology in cooperation with automation manufacturers in 1989. Since then, Profibus has advanced into a widely implemented fieldbus system used in machine and production plant automation. Profibus promises a safe investment thanks to the use of open standards instead of proprietary solutions. Industrially it is the most accepted international networking standard being almost universal in Europe and also widely used in USA [91].

Different versions of the standard exist, such as Profibus PA/DP/FMS. Profibus DP (decentralised peripherals) means that peripherals are relocated and distributed in the network. On this version, the standard works on a Master/Slave configuration and these are the two types of devices connected in the network.

The protocol is address–based, which means that all devices connected to the network can hear the message, but in order for a device to recognise the message and respond, it must have a unique address. The address is assigned physically with switches in every peripheral. The only way that a slave could send data is if the master makes a request. The master requests data in a cyclic fashion (*slave 1, slave 2,...,slave n*). Profibus also allows the use of multiple masters, where all masters can read data from all slaves. However, in the case of sending data to a slave, only one master can control the bus at a given time. Once a master is finished, it grants permission to another master to occupy the bus. This permission from master–to–master is referred to as token–passing principle and it is depicted in Figure 3.4 [92], where a network of two masters interact with three slaves using the token–passing principle.

The transmission medium is a shielded–twisted pair of cables, although fibre optic or wireless can also be used. The topology is generally bus and can also be implemented in a tree configuration with the use of repeaters. The message that could be transmitted on Profibus has a size of 256 bytes, of which 244 are the actual data and 12 bytes are the overhead [92].

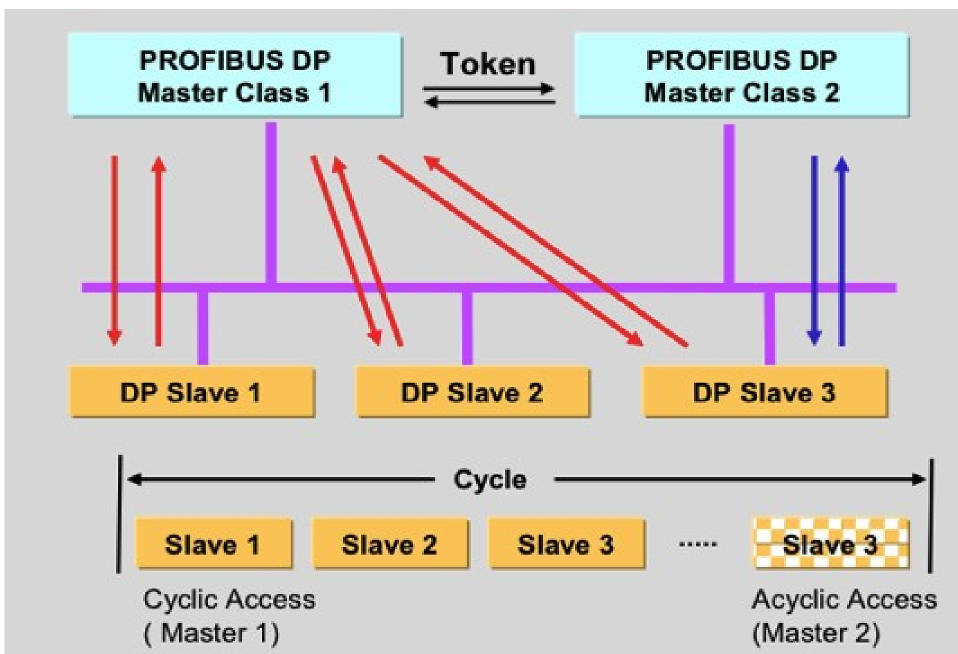

Figure 3.4: Profibus network with multiple masters [92]

3.3.4.1 Previous Related Work With Profibus DP

On [93] the researchers recognised that the synchronised control of multiple motors is increasing in many industrial fields. To carry out this type of control, real–time data communication is necessary. The key is to perform synchronised control of the speed and torque of the multi–motor system. The setup comprised a Profibus network with a single master and multiple intelligent slaves, each executing fuzzy logic control algorithms. On [94] the researchers made use of Profibus as a real–time solution to monitor and control the running parameters of motors in an automated enterprise. Profibus was integrated with LabVIEW software, and thanks to its interactive graphical interphase, users were able to view and modify parameters easily.

3.3.5 EtherCAT Protocol

EtherCAT is an industrial Ethernet technology specially designed to support real–time applications. EtherCAT was developed by Beckhoff Automation and it was released in 2003. Today it is an open standard managed by the EtherCAT Technology group. The main focus in the design of the protocol was short cycle times. It is noteworthy that EtherCAT is capable of processing 1000 distributed I/Os in 30 μs [95].

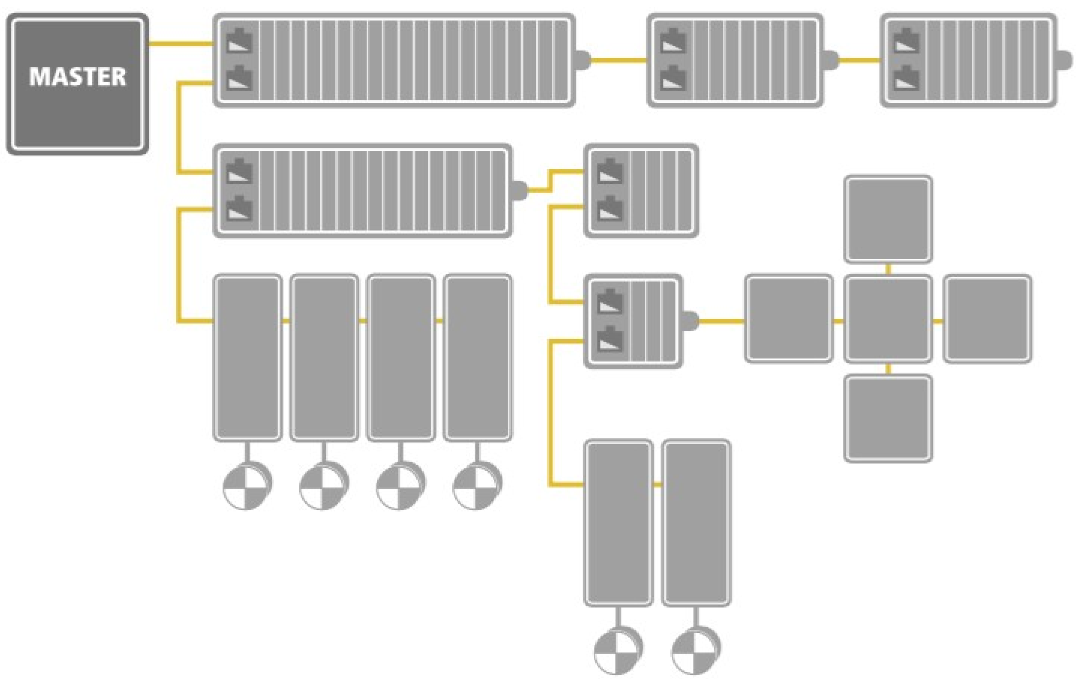

Figure 3.5: EtherCAT combined topology, daisy–chain and tree [96]

The protocol is Master–Slave based. The key of operation in EtherCAT is the "Ethernet on the fly". In conventional Ethernet, data packets are sent from the master to each slave, the slave reads the data and sends it back to the master. This process is repeated until all devices are updated. The total time is the sum of the time it takes to do all these iterations. On the other hand, on EtherCAT, a data frame is sent from the master to the first slave in the network, the slave reads the data that is addressed to it as it passes through and writes any response data. The only delay is due to the propagation delay in the hardware, which is in the order of nanoseconds. This packet continues to travel through all slaves in the network in the order in which they are physically connected until it reaches the last node. Then the fully updated frame is returned to the master for processing [95].

The physical medium accounts for robust noise immunity by using a twisted pair of cables along with a standard RJ–45 Ethernet connector. The topology on EtherCAT is flexible, allowing for daisy–chain, tree, star or a combination of these. Figure 3.5 shows the flexibility of topologies [96].

3.3.5.1 Previous Related Work With EtherCAT

The Body Extender is a full–body robotic exoskeleton for human power augmentation developed by PERCRO laboratory. The system has anthropomorphic form composed of legs, arms and a trunk with a total of 22 actuated degrees of freedom. Each joint is operated by an electric motor coupled to an incremental encoder.

In terms of electronics, the exoskeleton accounts for a Central Control Unit (master) in charge of managing the global state of the entire system, which is connected to a number of distributed Local Control Units (slaves) by means of EtherCAT communication. This communication system was used by the authors with the purpose of reducing wiring complexity and latency [21, 97].

Furthermore, the researchers on [98], has developed a lightweight ankle exoskeleton based on previous research results, which show that the metabolic cost of walking can be reduced by means of an ankle exoskeleton. The exoskeleton is to be worn in pairs, one for each leg. The design includes an electric motor linked to a ball–screw mechanism for linear motion. The exoskeleton has a distributed control system using EtherCAT. The master CPU was connected to two EtherCAT slaves which controlled each motor and received angular position signals from incremental encoders.

The table on the next page represents the comparison between all the aforementioned protocols, where technical and other specifications are included, so that a quick comparison and evaluation could be done between the most appropriate candidates.

Feature	Profibus DP	CAN	LIN	EtherCAT	FlexRay
Family	Fieldbus	Fieldbus/Automotive	Automotive	Ethernet/Robotics/Control	Automotive
Common Applications	Large industrial automated processes, PLCs and remote I/Os	Automotive, military vehicles, industrial machinery, medical systems, elevator control	Peripherals in automobiles: doors, mirrors, seat controls, wipers, rain sensors, climate control, sun roof Usually a sub-network	Large industrial automated processes, robotics, machine tools, packing machines, power plants	High-end automotive applications: drive-by-wire, steer-by-wire, brake-by-wire
Layer	Layers 1 and 2 (physical and data link)	Layers 1 and 2 (physical and data link)	Layers 1 and 2 (physical and data link)	Ethernet based: all layers, from bit sensor to enterprise and operations	Layers 1 and 2 (physical and data link)
Topology	Bus Tree (with repeaters)	Bus	Bus	Bus Tree Daisy-chain Allows combination	Bus Star Hybrid (bus and star)
Principle of operation	Master-Slave model. Allows multiple masters. One master controls the bus at any time. Masters can exchange data. Messages are address-based, all devices have an address. Slave sends data only upon request from the master.	All messages are broadcast. Any node is allowed to broadcast a message. Each message has an ID that determines the source and content. Each node decides to process or ignore each message. The bus is occupied based on priority.	Master-Slave model. Only one master per network. The master requests data from the slave, the message contains an identifier, the slave responds immediately.	Master-Slave model. The key of operation is 'Ethernet on the fly'. Master sends a message that passes through all nodes in the network. As the message passes through data is collected and written. At the final node the message is returned to the master.	Based on a time fixed (1-5ms) 'FlexRay communication cycle'. All nodes are synchronised to the same clock. There is a time schedule and each node waits for its turn to write on the bus while all other nodes can read. The exact point in time is known in the cycle.
Transmission medium	Shielded-twisted pair cables (9-Pin Sub D connector) Fiber optic Wireless	Single twisted pair wire terminated on each end	Single wire	Single twisted pair wire within conventional RJ45 Ethernet connector	Unshielded-twisted pair wire Supports single and dual channel using two pairs of wire
Bit rate/distance	1000m – 187.5 Kbps 400m – 500 Kbps 200m – 1.5 Mbps 100m – 3.6-12 Mbps	500m – 125 Kbps 200m – 250 Kbps 100m – 500 Kbps 40m – 1Mbps	40m - ~ 20 Kbps	100 Mbps, no more than 100m between nodes	10 Mbps, no more than 24m between nodes
Number of stations	126 available (out of 128 addresses)	Not specified Usually up to 64 nodes	60 available(out of 64) Usually 2-16 slaves	65535 stations	22 - Bus 64 - Star and Hybrid
Data size	0-244 bytes	0-8 bytes	0-8 bytes	Up to 1500 bytes per frame telegram	0-254 bytes
Noise immunity	Very Good	Good	-	Good	Good
Cost	Slightly higher cost than some other field buses	Inexpensive	Very Inexpensive	Reasonable cost considering large networks	Relatively expensive compared to other automotive protocols
Advantages	Optimised for I/O applications Redundant Universal in Europe Suitable for large amounts of data and large applications	Designed for reliability in sending many short messages Inexpensive to implement Simpler than other protocols Easy integration of new nodes	Inexpensive to implement with low cost microcontrollers Simple protocol	Can operate at all layers due to large data capabilities Supports combination of networks	Time-determinism is guaranteed Fault tolerant with dual channel Allows very high-speed control rates, ability to do control calculation within the same cycle
Disadvantages	High overhead to message ratio	Size of data can be a limiting factor depending on the application	Size of data and network can be limiting factors depending on the application Slow bit rate For operations in the order of hundredths of milliseconds	Complex protocol (Ethernet based)	Any new node has to be strictly configured with specific network parameters before integration

3.4 Evaluation of the Protocols' Specifications

This section focuses on evaluating the potential communication protocols. The criteria are hardware availability, topology, message size and bit–rate. A scoring scheme has been adopted to quantify the features of each protocol. The protocols are evaluated on each of the four aspects, specifically for the exoskeleton application. The protocols are ranked from best to worst performance and the best will receive the highest score (5), decreasing by one unit for each protocol falling each place in the ranking.

The nature of application that is investigated in this project, requires a communication strategy that will be able to provide hard real–time communications between the nodes that are connected on the network. Thus, high transmission rates are required to achieve the real–time requirements. In addition, since the exoskeleton is modular, it is essential for the selected communication protocol to support several different topologies or even a combination in order to avoid wiring complexity. Moreover, the exoskeletal devices employ many nodes/terminals where different types of sensors are attached and able to transmit on the bus the data that have been collected. Therefore, the increased number of nodes will, also, increment the number of bytes that are transmitted on the network, thus the size of the frame for each network should also be carefully considered. Lastly, the hardware that will be used to interface each protocol is another important factor. The hardware will be evaluated for its availability, the overall weight and the complexity of implementation.

3.4.1 Hardware Evaluation

It is important to discover how the protocols could be implemented in terms of hardware. It is known that National Instruments (NI) and Beckhoff Automation hardware along with LabVIEW and TwinCAT softwares, respectively, makes a solid platform for engineering prototyping. NI hardware offers off–the–shelf solutions along with a high–level graphical interface language, which minimises configuration, making this option suitable for fast prototyping. Beckhoff's hardware offers a more advanced solution for the implementation of EtherCAT, which could fit the project needs.

3.4.1.1 EtherCAT Hardware

NI offers the CompactRIO platform, which has controllers for processing and reconfigurable chassis with FPGA that allow the connection of swappable I/O modules, making this platform a potential solution for the exoskeleton. Furthermore, it is the most compact and lightweight hardware platform from NI. Since the EtherCAT protocol is master–slave based, NI provides diverse solutions for the master which include the following hardware: cRIO-9024/33/68/82 and PXI-8840.

For slave modules the solution provided is to make use of the NI 9144 (NI EtherCAT slave). To implement this, a master controller may be daisy chained to multiple NI 9144 slave modules. It is worth noting that both master and slave modules from the compact RIO family offer expansion slots where C series I/O modules can be inserted. These modules add functionality such as analogue and digital inputs and outputs. Furthermore there are compatible third–party modules available for other specific functionalities.

Table 3.1: CPU idle time test for cRIO-9033/82

	cRIO-9033		**cRIO-9082**	
Scan Frequency	**Data Payload**			
	9 bytes	**553 bytes**	**9 bytes**	**553 bytes**
2 kHz	64.95%	41.95%	85.9%	64.41%
1 kHz	79.6%	67.95%	92.46%	81.32%

NI demonstrates the efficiency of their hardware by making benchmark tests to several setups, which only differ on the Master. The test consists of transmitting a set of payloads of different sizes and frequencies to determine which setup allows for more CPU idle time. This is of absolute importance since the CPU idle time is the time left for the CPU to compute algorithms. The results on Table 3.1 show the performance for the cRIO-9082/9033 at different payloads and scanning frequencies. The results show that when 553 bytes of data are transmitted at 2 kHz (8.848 Mbps), the cRIO-9033 allows for 41.95% of CPU idle time, and the cRIO-9082 allows for 64.41% of CPU idle time. A possible setup could be a cRIO-9033 or cRIO-9082 connected in daisy chain topology with multiple NI 9144 slave modules.

Figure 3.6: cRIO-9082 (left) and cRIO-9033 (right)

From the benchmark test in Table 3.1, it is clear that the cRIO-9082 has higher CPU performance. Moreover the device offers twice as many expansion slots as the cRIO-9033. As depicted in Figure 3.6, this feature may be important depending on whether the researchers of this project choose to have peripherals (sensors, actuators) connected to the master or not. Furthermore, there are several trade–offs. The cRIO-9082 is 72% heavier and bulkier occupying 87% more volume. Additionally, the cRIO-9033 consumes 87.5% more power than the other device. Another important aspect is that the operating temperature range on the cRIO-9033 is much wider as it can function as low as -40 °C. Finally the cRIO-9082 is 66% more expensive than the counterpart.

The NI-9144 EtherCAT slave modules can be connected in a daisy chain configuration form the master to form the EtherCAT network. The slave modules allow for on–board analysis to then send the results to the master. Figure 3.7 shows the NI 9144 EtherCAT slave device.

Figure 3.7: NI 9144 EtherCAT slave module

The fact that the NI 9144 EtherCAT slave modules have a pre–defined set of slots can be inconvenient. Some nodes in the exoskeleton may require further expansion, while others may require fewer peripherals connected to it. For this reason, it is desirable that the slave nodes are as compact as possible. The wide adoption of EtherCAT as an industrial communication protocol means that there are other manufacturers that support it, therefore resulting in high interoperability. Beckhoff Automation is the developer of the EtherCAT protocol and offers a great number of solutions that could be applied to this project. Therefore, another solution could be to implement the entire EtherCAT system with Beckhoff Automation hardware.

Beckhoff Automation offers a range of embedded PCs capable of operating as fieldbus masters. The embedded PCs use Microsoft Windows to run Beckhoff Automation software called TwinCAT, which has support for high–level programming such as MATLAB/Simulink. This feature is valuable for the project as MATLAB/Simulink is a well–known software used in engineering that can also be a solution for creating the control algorithms of the exoskeleton.

The Beckhoff Automation CX embedded PC line offers various options which include the CX2030/CX5130 depicted in Figure 3.8. These CPUs are similar in terms of technical specifications to the NI cRIO-9082/9033 controllers. For the slave nodes, Beckhoff Automation offers EtherCAT bus couplers. The bus couplers are only the slave connection and functionality have to be added by clicking in place EtherCAT terminals.

Figure 3.8: CX2030 (left) and CX5130 (right) embedded PCs

The EtherCAT terminals are available in a variety of functions such as digital and analogue I/O. The couplers can be expanded with up to 65,534 terminals. Figure 3.9 shows an EtherCAT coupler and an EtherCAT terminal being added. To assemble an entire network, a number of couplers with attached terminals are the slaves and these can be daisy chained with either a Beckhoff Automation or an NI master. Beckhoff Automation provides a solution for acquiring data from the SSI encoders. The EL5002 EtherCAT terminal allows for direct connection for two SSI encoders. A combination of different EtherCAT terminals can be integrated with an EtherCAT coupler (EK1100) resulting in a very flexible and compact modular system.

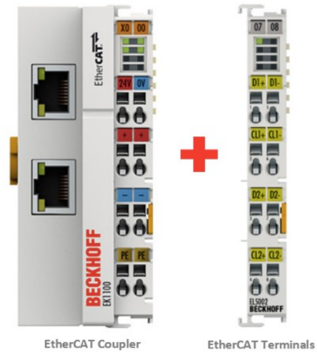

Figure 3.9: EtherCAT coupler EK1100 and EtherCAT terminals ELxxxx

It is important to point out that these devices make for a very compact and lightweight solution. Since the coupler is almost unlimited in the number of terminals it can support, new terminals can be mounted on the rail of the previous terminal. Hence, the size of a node will be determined by this factor, unlike the NI hardware, where the chassis comes with pre–defined number of slots occupying a larger volume.

3.4.1.2 Profibus DP Hardware

Similar to EtherCAT, NI hardware can be used for the CPU/master device to take full advantage of the LabVIEW software. A compactRIO Profibus master/slave module depicted in Figure 3.10, can be directly inserted into one of the slots of the cRIO-9082/9033 controllers. Furthermore the NI compactRIO slave module is compatible with compactRIO reconfigurable chassis such as NI cRIO-911x, very similar to the NI 9144 EtherCAT slave module.

Figure 3.10: Profibus interface module for NI compactRIO

An entire Profibus network can be built from NI hardware integrating these modules with the compactRIO platform. However, the datasheet from the manufacturer [99] states that since Profibus modules require 2.5W of power, two slots should be left empty in the controller or chassis. This can prove to be a disadvantage because there will be unused slots occupying space and adding unnecessary weight to the system.

Nevertheless, there are also other options that can be implemented as slaves for Profibus. Beckhoff Automation offers a series of Bus couplers that serve as Profibus slaves and functionality, such as digital/analogue I/O, is added to these devices by connecting in place Bus terminals KLXXXX. The BK3100 is a standard Profibus Bus coupler which can be extended in a modular fashion similar to the EtherCAT couplers and terminals from Figure 3.9.

This setup also supports the SSI inputs for the encoders in the exoskeleton. The KL5001 is a Bus terminal that can be mounted in the rails of the Bus coupler, and can receive direct connection from a single SSI encoder. The Bus coupler can support up to 64 Bus terminals. It is important to highlight that with Profibus, the Bus terminal only supports input for one encoder, whereas the EtherCAT terminal supports two inputs for encoders. The Profibus network can be completed by connecting these bus couplers to the NI master (cRIO-9033/9082) or the embedded PC from Beckhoff Automation (CX5010/5020).

3.4.1.3 FlexRay Hardware

NI currently does not offer any FlexRay solution in the CompactRIO platform [90]. Nevertheless, NI offers a solution for implementing the FlexRay protocol in their PXI platform. Similar to the compactRIO platform, on PXI, modules and controllers can be inserted into a chassis for modularity and customisability achieving similar results as with compactRIO. Figure 3.11 shows the PXI system.

Figure 3.11: PXI system

The problem with the PXI platform is the large size and weight of the entire system, as it is designed to be used in laboratories. This was the main reason why the compactRIO platform was considered, since it is smaller and more light–weight. In theory, a FlexRay network could be built from this platform. However, it can prove to be inconvenient for the exoskeleton application due to the large size and weight. Other options have been explored, but since the FlexRay protocol is relatively new and, at the moment, dominated by the automotive industry, it is difficult to find off–the–shelf solutions that can be convenient for the exoskeleton. The work done in [89] demonstrates that the protocol can be implemented by means of FPGAs using Verilog HDL code. This solution requires a great deal of work to program the protocol. On [100] the researchers discusse that FlexRay is already at a stage where it allows for implementation on silicon using the CIC-310 standalone FlexRay communication controller [101] as one of the options. This standalone controller would require to be coupled with a microcontroller to operate.

3.4.1.4 CAN Hardware

A CAN network can be created using NI hardware. The NI-9862 is a CAN C series module [102] which can be inserted in the slots of any cRIO controller (cRIO-9082/9033) or cRIO reconfigurable chassis (cRIO-911x), providing CAN capabilities to the hardware. Another approach to implement CAN is to use a transceiver device [82,103]. This is a silicon chip operated with a microcontroller. Hence, creating a CAN node. This implementation would require electronic and software design. These custom–designed nodes could be connected in a network with the NI CPU (cRIO-9033/9082) that has a CAN C series module. Under this configuration, nodes operate with equal rights, but the NI CPU would be in charge of computing the control algorithms.

3.4.1.5 LIN Hardware

Similar to CAN, NI offers the NI-9866 LIN C series module which can be directly inserted into compactRIO hardware. An entire network can be built with this module and compactRIO hardware. LIN is a master/slave-based protocol and this module allows for both master and slave operation. Similar to CAN, LIN slaves can also be implemented by means of a transceiver device [104] coupled to a microcontroller, creating custom designed slaves that can be connected to the NI master (cRIO-9033/9082).

3.4.1.6 Hardware Overall Score

The following table (Table 3.2) provides the final score for the hardware evaluation.

Table 3.2: Hardware Score

Protocol	Score	Comment
EtherCAT	5	Has the greatest range of possibilities for hardware implementation. NI hardware is very robust, flexible and expandable, in addition, Beckhoff Automation hardware for the master and slaves is very robust, expandable, compact and light weight. Reasonable cost considering large networks.
Profibus	4	There are a good number of options from NI and Beckhoff Automation, very robust and compact. With NI, there is a need of 2.5 W of power for the Profibus C series module, this means that two slots must be left empty. With Beckhoff Automation the SSI encoder terminals only offer one input per device. Slightly higher cost than some other field buses.
CAN	3	Good option to implement with NI hardware, but can be bulky. Furthermore there was no third–party hardware found that was as robust and expandable as Profibus or EtherCAT. Inexpensive hardware since it can be implemented with simple microcontrollers.
LIN	3	Good option to implement with NI hardware, but can be bulky. Moreover, there was no third–party hardware found that was as robust and expandable as Profibus or EtherCAT. Very inexpensive since it can be implemented using simple microcontrollers.
FlexRay	2	Possible to implement with NI hardware but with very large and heavy hardware not suitable for this application. Other options are more complex and include coding the protocol on FPGA or making use of available silicon solutions to interface with microcontrollers. Relatively expensive hardware compared to other solutions for automotive applications.

3.4.2 Message Size Evaluation

The message size of the protocols is an important factor to consider, because regardless of the bit–rate, the messages define how many communication cycles are needed to fully update the CPU with sensor values to compute a control algorithm. Accordingly, it is convenient to have the least amount of communication cycles for a more reliable set of data. In section 2.9.2 the communication system of the exoskeleton BLEEX was discussed, where the researchers highlight how all sensor and actuator data is updated in a single communication cycle.

To provide a score for the message size, it is important to have an initial approximation of how many nodes are needed in the exoskeleton and where these could be located. This provides an idea of how many sensors will be connected to each node and consequently, how much data will each node must send to perform a full update of the sensor readings. Table 3.3 provides a list of the nodes along with the sensors and data that each one will handle, complemented by Figure 3.12, which shows the location of the nodes on the prototype frame of the exoskeleton.

It is necessary to consider the “wrapped in 8 bit messages” format because in the protocols data is transferred in bytes. Out of the potential 13 nodes, it is clear that the node located in the back must handle the highest amount of data (17 bytes), while the nodes located at the lower back have to handle the least amount of data (6 bytes). Since this is an initial approximation, it is expected that each node will have to handle

Table 3.3: List of Nodes With Corresponding Data

Node	**Serves**	**Signals**	**Bits**	**Wrapped in 8-bit messages**
Shank x 2	Foot, ankle	Angular displacement: Ankle_FlexExt, Ankle_AbdAdd, Angular acceleration: Ankle_top, Sole, Shank, Ground reaction force: Sole, Actuator_out: Ankle_FlexExt, Actuator_in: Ankle_FlexExt	90	120 (15 bytes)
Thigh x 2	Knee, part of hip	Angular displacement: Knee_FlexExt, Hip_FlexExt, Angular acceleration: Thigh, HipGimbal_Bottom, Actuator_out: Knee_FlexExt, Hip_FlexEx, Actuator_in: Knee_FlexExt, Hip_FlexEx	90	128 (16 bytes)
Lower back x 2	Part of hip	Angular displacement: Hip_AbdAdd, Hip_InvEv, Angular acceleration: HipGimbal_Top	38	48 (6 bytes)
Shoulder x 2	Shoulder	Angular displacement: Shoulder_AbdAdd, Shoulder_FlexExt, Shoulder_InvEv, Angular acceleration: ShoulderGimbal_Bottom,ShoulderGimbal_Top, Actuator_out: Shoulder_FlexExt, Actuator_in: Shoulder_FlexExt	83	112 (14 bytes)
Arm x 2	Arm, elbow	Angular displacement: Elbow_FlexExt, Angular acceleration: Arm,Actuator_out: Elbow_FlexExt, Actuator_in: Elbow_FlexExt	45	64 (8 bytes)
Forearm x 2	Forearm, Hand	Angular acceleration: Forearm, Force: Hand	108	112 (14 bytes)
Back x 1	Back	Angular acceleration: Back, Inclination: Back, Force: Back	132	136 (17 bytes)
Total			1040	1304 (163 bytes)

more data in the future as more peripherals are added.

3.4.2.1 Message Size Score

Having this information, it is possible to provide a score for each protocol. Since each node (shown in Figure 3.12) has a minimum amount of data to transfer, it is ideal that all the data can fit in a single message to perform a full update on a single communication cycle. To quantify this analysis, there should be a consideration of the node which handles the highest amount of data. In this case, 17 bytes would be ideally transferred by any node in the network within a single message. This data will occupy a portion of the message of the protocol. Hence, the percentage of space left is the criteria for the score. This is calculated with equation 3.1.

$$Freespace = 1 - (\frac{RequiredSize}{MessageSize}) \tag{3.1}$$

In EtherCAT the messages are sent in a different way. There is only a single EtherCAT frame of maximum 1,498 bytes in size, which passes through all the nodes in the

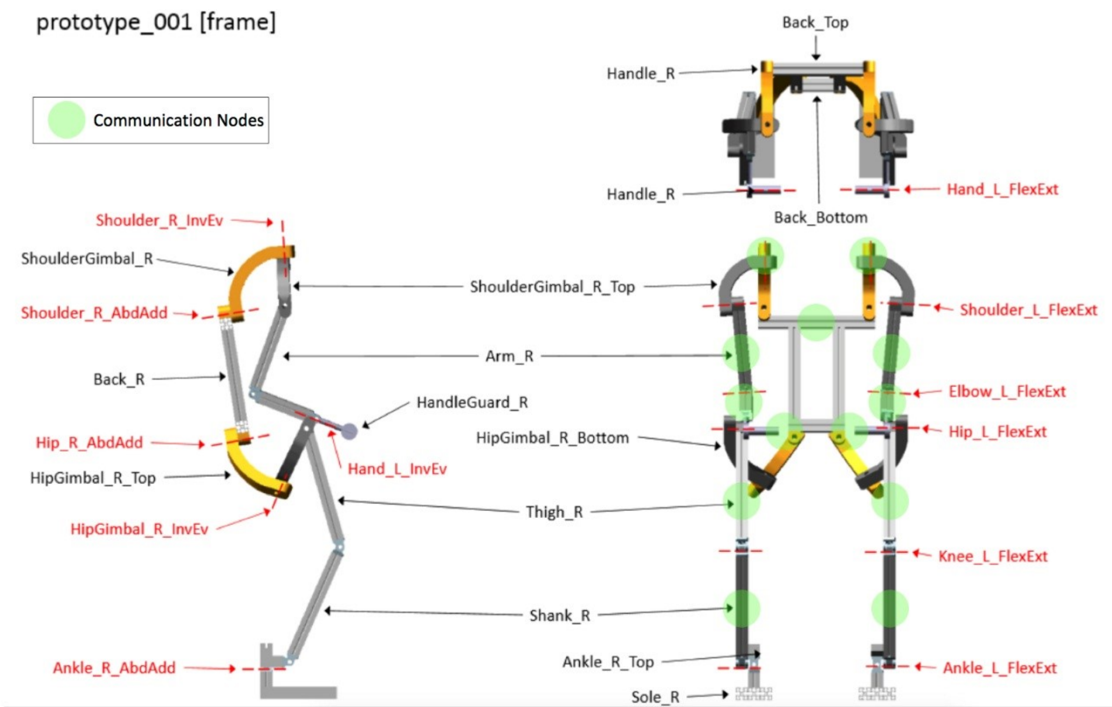

Figure 3.12: Potential node locations on the exoskeleton prototype

network. The data from all the nodes should be able to fit in this EtherCAT frame to update the entire system in a single communication cycle. Table 3.4 provides a summary of the final message size scores.

Table 3.4: Message Size Score

Protocol	Maximum Message Size	Free Space Left in Message	Score
FlexRay	254 bytes	93.3%	5
Profibus	244 bytes	93%	4
EtherCAT	1498 bytes	89.1%	3
CAN	8 bytes	-112%	2
LIN	8 bytes	-112%	2

3.4.3 Topology Evaluation

The initial exoskeleton prototype will consist of 13 nodes located throughout the device. Therefore it is necessary to consider which protocol allows for a more optimum physical connection between all these nodes and the main CPU. The possible topologies for the protocols are analysed in order to provide a score. The ideal topology should be one that minimises the use of physical wiring and networking components, should not limit the features of the protocol, and should allow for easy expansion in the future.

3.4.3.1 EtherCAT Topologies

EtherCAT supports bus, tree, daisy-chain topologies, and it even allows for a combination of these. This is important because it means that the protocol has a highly customisable topology that can be set up in many configurations.

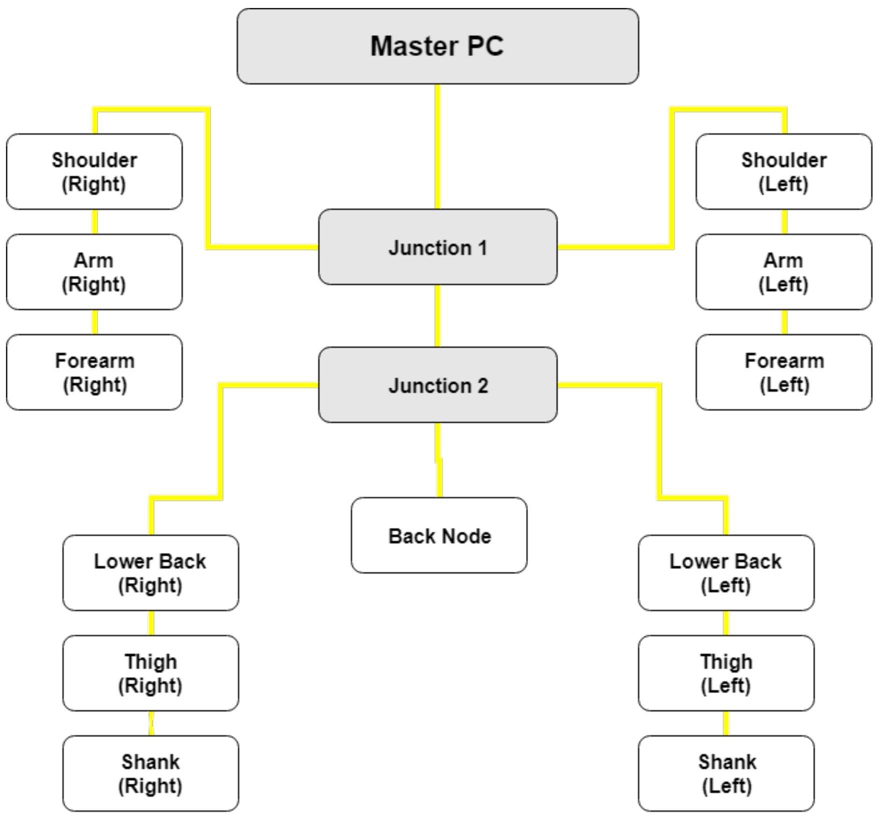

Figure 3.13: Potential topology implementation with EtherCAT

Since it is ideal that the exoskeleton uses the least amount of wiring, a star topology in combination with daisy–chain topology is considered as a potential implementation with EtherCAT. Figure 3.13 shows this potential topology implementation, where the "N" blocks are each of the nodes and the "Junction" block is a CU1128 EtherCAT junction module by Beckhoff Automation [105]. As illustrated in the figure, the EtherCAT network initiates in the main CPU, the physical wiring first passes through a node which can be the Back node from Table 3.3, p. 57. Once the network passes the first node, it is divided into a tree topology by the CU1128 EtherCAT junction module. Its purpose is to allow for several branches at a given point. The branches that come out of this junction module correspond to daisy–chained modules for the upper and lower extremities of the exoskeleton.

3.4.3.2 Profibus DP Topologies

For Profibus the main topology used is bus. Nonetheless, the protocol allows for star/tree topologies to be combined with bus topology by making use of repeaters [106]. Repeaters in Profibus can be used to extend the number of participants or to extend the maximum length of the physical layer. In this case a repeater [107] is considered as a suitable device to expand the topology capabilities of Profibus. As shown in Figure 3.14, the manufacturer of the repeater shows how the device is used to expand the Profibus network. It can be seen that some connections that come out of the repeater have their own bus with connected devices. This can be implemented in the exoskeleton in a similar way to the previously proposed EtherCAT topology from Figure 3.13.

A disadvantage using this repeater is that there would be a module from a third manufacturer integrated into the system, and this could make configuration and programming the network more difficult.

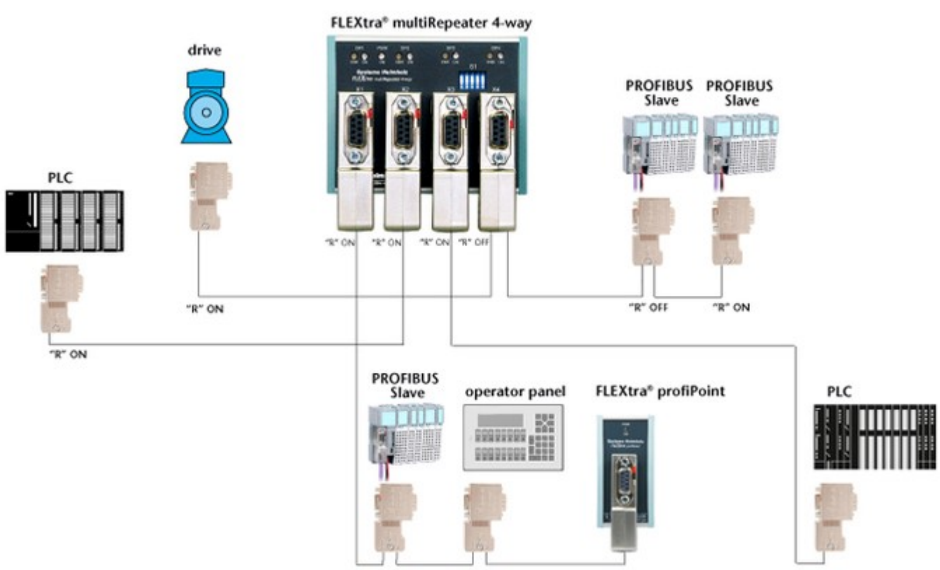

Figure 3.14: Example of Profibus topology with a repeater

3.4.3.3 CAN Topologies

CAN is a protocol based on the bus topology. The content in [108], gives no indication that the bus topology can be modified or combined with any other, nor does the content in [82, 109]. To implement a bus topology in the exoskeleton, the device must have physical wiring that is close enough to all nodes so these can connect to the bus. The section of wire connected from a node to the bus is known as stub, as shown in Figure 3.15. The standard recommends that for a CAN network working at 1 Mbps the maximum stub length for a node should not exceed 0.3 m.

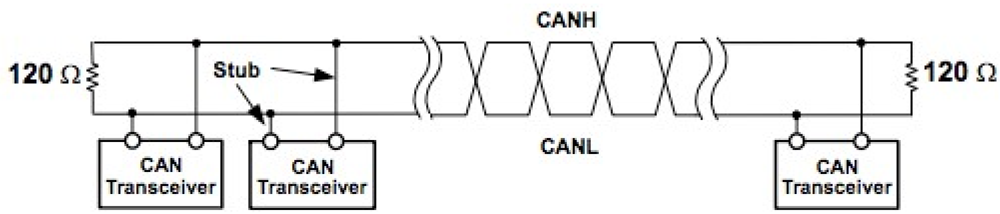

Figure 3.15: CAN bus network and stub length

3.4.3.4 LIN Topologies

According to the LIN specification package [88], this protocol is master/slave based implementing bus topology. The implementation on an exoskeleton should be very similar to that of CAN with the benefit that LIN only makes use of a single wire as transmission medium, this would significantly decrease the amount of cable needed.

3.4.3.5 FlexRay Topologies

The FlexRay protocol is capable of supporting bus, star and a combination of these topologies. The topologies can be either single or dual channel for enhanced speed and functionality. First it is important to understand how bus and star networks work independently. Figure 3.16 shows a dual bus network (a) and its equivalent in active star topology (b). It can be noticed that in both examples, nodes B and D are connected only to channels B and A respectively.

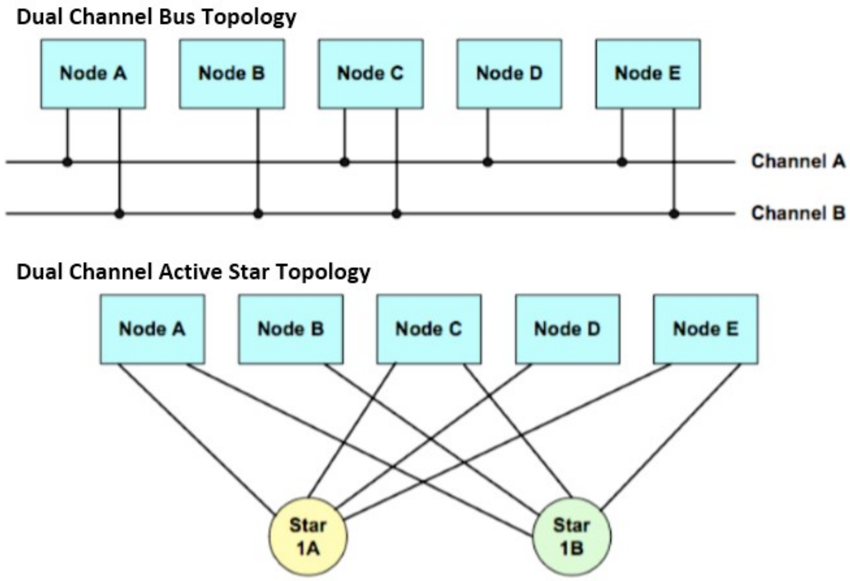

Figure 3.16: FlexRay dual–channel bus and equivalent active star topology

A more optimum implementation for the exoskeleton could be to take advantage of the possibility to combine bus and active star topologies. Figure 3.17 shows an example of a hybrid between these two topologies using a single channel. From this example it can be seen that an active star can be attached either to a single node or to a bus composed of various nodes. For example, if node A wanted to transmit data to node B in the network, node A would first transfer the data to active star 1A, then active star 1A would transfer the data to node B. This means that the branches are physically electrically decoupled from each other by the active star [110].

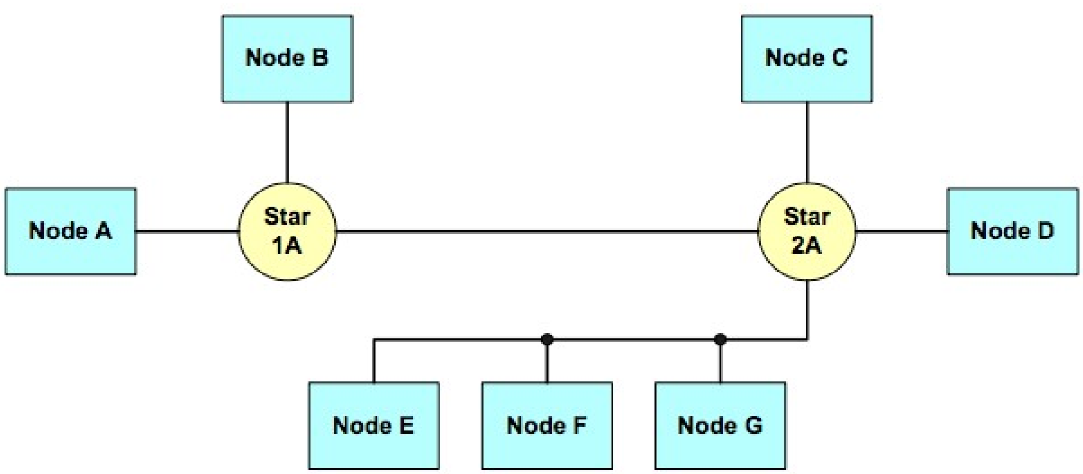

Figure 3.17: FlexRay single channel hybrid example

Extending this idea, a network similar to that proposed previously with EtherCAT and Profibus can be achieved with a single active star attached to four buses. The ELMOS-E981.56 [111] is a silicon device that serves as a FlexRay active star coupler providing support for 4 branches for coupling 4 buses. As mentioned in section 3.4.1.3, the implementation for this communication protocol must be made with custom designed ECUs.

3.4.3.6 Topologies Score

Having understood the basic topology concepts of all the protocols, it is important to make a simple analysis. The exoskeleton frame is a complex mechanical piece. It is the support for every part including sensors, actuators, nodes and wires. Regardless of the topology chosen, the physical wiring is subject to the path provided by the mechanical frame, so that the wire can be secured to the exoskeleton. For a topology analysis, a simple node layout is proposed in Figure 3.18. Each green circle represents a node, equally spaced by distance ‘a’, and the grey area behind the nodes represents the exoskeleton frames. All nodes must be connected, and the only path is through the exoskeleton frame.

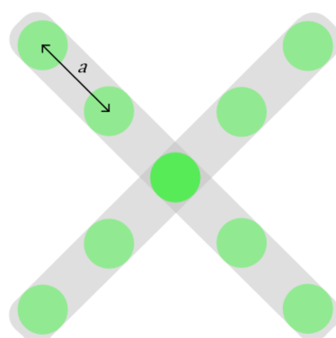

Figure 3.18: Simple node layout

It is known that CAN and LIN only support bus topology. For this reason, a reasonable wiring path is presented in 3.19a. It should be noticed how the wiring starts at the top left corner and ends at the top right, having to go inside and back out at the bottom to reach all nodes. An important aspect to consider is that LIN utilises a single wire, as opposed to CAN which uses a pair of twisted wires, leading to doubling the amount of wire in CAN. This configuration assumes that there is no stub length for either CAN or LIN.

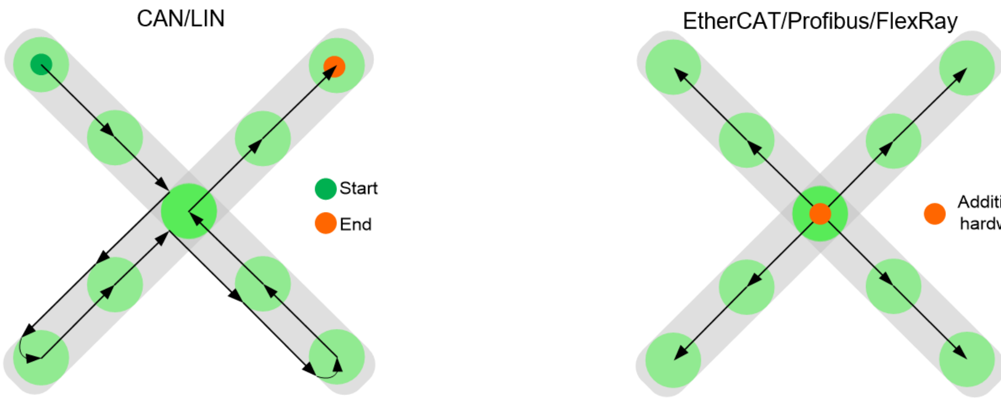

(a) (b)

Figure 3.19: Wiring analysis for a) CAN/LIN and b) EtherCAT/Profibus/FlexRay

As mentioned earlier, EtherCAT, Profibus, and FlexRay can support combined network topology with the use of an additional piece of hardware. A reasonable wiring path is presented in Figure 3.19b. It should be noticed how all the wires are distributed to each path from the centre, and there is no need for the wire to return.

Table 3.5 presents a summary of how many length units would be required to physically wire these topologies, taking into consideration that LIN uses only a single wire and the rest of the protocols use a twisted pair of wires. The table also includes the score which is ranked based on the wiring efficiency.

Table 3.5: Summary of Required Wire Length and Score

Protocol	**Length Units**	**Score**	**Comment**
LIN	12 α	5	Offers reduced length of wire with no additional hardware
EtherCAT	16 α	3	Length of wiring is low, but the need for additional hardware reduces the score by one unit
Profibus	16 α	3	
FlexRay	16 α	3	
CAN	24 α	3	Highest length of wire

3.4.4 Bit–Rate Evaluation

The criteria for evaluating the different communication protocols in this aspect, is based on the data requirements presented in Table 3.3. The table contains the sensors and actuators that could potentially be implemented in the first prototype of the exoskeleton. It must be realised that at this stage there is room for modifications and some of the components mentioned in the table might not be used or might change. Table 3.6 briefly summarises this information. It can be noted that the total number of bits required for a single update on the entire system is 1040, but the data must be "wrapped in 8 bit messages", for a total 1304 bits.

Table 3.6: Summary of Data Requirements

Component Data	**Quantity**	**Total bits**	**Total bits wrapped in 8-bit messages**
Angular displacement	20	260	320
Angular acceleration	23	252	336
Actuator torque out	10	100	160
Actuator torque in	10	100	160
Back inclination	1	24	24
Ground reaction force on soles	2	16	16
Force on back and hands	3	288	288
Total	67	1040	1304

From the motion capture study it has been found that the system could have a sampling frequency of 2 kHz. This criterion is based on the work done in [112], where the author explains that in the exoskeleton (BLEEX) the researchers use a factor of 20 to 40 times higher than the natural frequency for normal walking, this yields a sampling frequency of 2 kHz that can satisfy their requirements. Based on this previous work and the total number of bits (in 8-bit messages) required for a single system update, the total bits per second (bps) required under these conditions is 2,608,000 bps (2.6 Mbps). This result is obtained with equation 3.2. Having this requirement, the protocols can be given a score based on their capability to fulfil this need.

$$BitRate = SampleFrequency \times TotalBits \tag{3.2}$$

The efficiency of a protocol to fulfil the data rate requirement can be analysed in the form of a ratio as shown in equation 3.3. Table 3.7 summarises the results, which are presented in the form of percentage of occupied bus load.

$$BitRateRatio = \frac{RequiredBitRate}{ProtocolBitRate} \tag{3.3}$$

Table 3.7: Bit-Rate Ratio and Score

Protocol	**Bit Rate**	**% of Occupied Bus Load**	**Score**
EtherCAT	100 Mbps	2.6%	5
Profibus DP	12 Mbps	21.6%	4
FlexRay	10 Mbps	26%	3
CAN	1 Mbps	260%	2
LIN	20 kbps	1300%	1

3.4.5 Final Scores of the Protocols

The scores that have been discussed in the previous sections for each specific protocol are summarised in table 3.8 that follows. This table has been used to compare the specifications and other aspects of the potential communication candidates that can be used for this project and finally choose the most appropriate protocol that can satisfy the communication requirements for this project.

Table 3.8: Summary of the Final Scores

Protocol	**Hardware Score**	**Message Score**	**Topology Score**	**Bit-Rate Score**	**Total Score**
EtherCAT	5	3	3	5	**16**
Profibus DP	4	4	3	4	**15**
FlexRay	2	5	3	3	**13**
LIN	3	2	5	1	**11**
CAN	3	2	3	2	**10**

3.5 Summary

The first chapter of this section looked at the preliminary requirements for the potential communications protocol to be used for the exoskeletal device. Based on these requirements, a thorough research has been conducted on the most advanced communication protocols that are widely adopted in the industry for robotic applications. In addition, previous related work with the potential protocols has been presented and examined.

After the analysis of the potential communication strategies, the protocols have been evaluated in their most significant features with respect to the specific application of the exoskeleton. The results of this analysis show that EtherCAT is the most suitable protocol/candidate for the exoskeleton project followed closely by Profibus DP. The superiority of EtherCAT in terms of bit–rate and the availability of hardware were determining factors that positioned the protocol above the rest. Table 3.8 summarises the scores of the protocols.

Chapter 4

Simulation Models and EtherCAT Network Design

4.1 Introduction

In this chapter the design of the EtherCAT network is presented along with the simulations that have been performed to verify the theoretical approach based on the specifications of the exoskeleton design. The purpose of these is to aid in the analysis and testing of the potential communication strategy to be developed.

In the second section of the chapter, the simulation models along with the simulation approach are discussed briefly. In order to simulate the behaviour of EtherCAT network, the concept of 'data-exchange interval' is presented and will be used later in this chapter to analyse the simulation results. These sections are examined thoroughly in the discussion section along with the evaluation of the simulations results and the topologies that have been employed.

The chapter concludes with the analysis of the frame size optimisation algorithm that can be applied both on the simulated model and the real application, in order to reduce the size of the frame that is transmitted on the network. This concept has not been considered for the simulations, but only for the implementation of the network design.

4.2 Simulation Approach

In order to examine the behaviour of a real–time protocol such us EtherCAT, particular attention should be paid on the concept of industrial Ethernet networks. In general, industrial Ethernet networks are classified into three main categories according to the performance and the protocols that are used to operate.

These categories are the following:

- Standard Ethernet hardware without using any dedicated devices for real–time processing, along with the use of standard TCP/IP software stack. Using such hardware could lead in having limited real–time performance and delays in the communication process.
- Standard Ethernet hardware without using any dedicated devices for real–time processing and without the use of standard TCP/IP software stack.
- Dedicated Ethernet hardware is used for high performance, along with the use of standard TCP/IP software stack. That could lead to having very small communication cycle times in the order of a few microseconds (depending on the number of the devices that are connected on the network).

For the simulation of the EtherCAT performance and behaviour, the Riverbed Modeler software (previously known as OPNET) has been used. Both models –that simulated using this software– have been designed with respect to the specifications of EtherCAT protocol. In real applications, before running any processes on the actual EtherCAT hardware that is used for real–time processing, the hardware is configured in such way from the manufacturer, to automatically set up the protocol in the hardware during the start–up process. Once this initial process completed successfully, then the transmission of the data can take place. Therefore, the simulations will focus, mainly, on the data transmission (in terms of data–exchange, communication cycle time etc.) and the overall behaviour of the protocol. For each simulation model, the master device has been configured in such way to meet the specifications of EtherCAT, thus the user will only need to configure each slave that is connected on the network. Finally, it should be noted that the master devices of the simulation models could not be configured in such way to meet all of the specifications of EtherCAT protocol, due to some practical implementation issues. However, the most critical factors of the protocol, have been configured successfully for the simulations.

4.2.1 Concept of Data Transmission in Real–Time Ethernet

The nature of operation of EtherCAT involves the execution of several active tasks. In general, these tasks are a sequence of instructions that include reading and writing processes on the different slaves connected on the network. Each of these tasks are executed occasionally during the normal operation of the network and, normally, the execution process is taking place on every communication cycle (usually known as the period of the network).

The models that will be used for the simulations are having a set of tasks $s_1, s_2, ..., s_M$. Each of these tasks have specific execution time, $T_1, T_2, ..., T_M$ that is configured from the master of the network. The simulation has been configured in such way for the user to be able to set the network period parameter, known as T_c, which is the time that all the tasks require to be executed successfully. An example of data–exchange is presented in Figure 4.1.

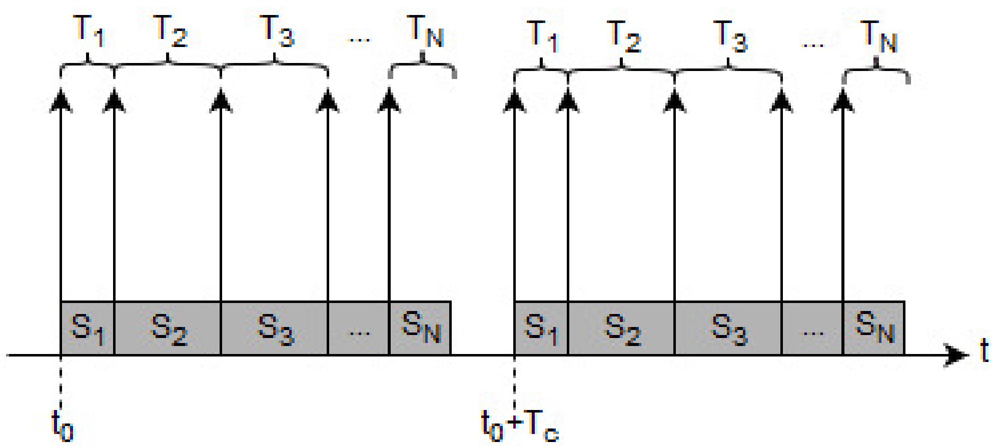

Figure 4.1: Data–exchange example

This example shows when the transmission starts (at t_0) and the arrows show the time at which the master sends the corresponding EtherCAT telegram to the slaves. According to EtherCAT specifications' protocol [96], when the master device starts the transmission, the data are transmitted to the slaves by means of EtherCAT telegrams, where the input data are inserted into the data stream on the fly. The transmission of the EtherCAT telegram for a random task s_n will take place at each time instant t_n, where

$$t_n = t_0 + kT_c + \sum_{x=1}^{n-1} T_x \tag{4.1}$$

where t_n is the time instant at which a random task of the telegram is transmitted,

t_0 is the time at which the transmission of the telegram starts, T_c is the period of the communication cycle and T_x is the period at which a specific task s has been configured to be transmitted in the telegram.

4.2.2 Design of Simulation Models

This part presents the design of the simulation models to be used. The following designs will be discussed in detail in the next section. According to section 3.4.3.1, a combination of topologies has been selected for this project, to meet the specifications of the design of the exoskeletal device. The topologies that used for the simulations are the line and tree topologies.

The simulation models are divided in the following, based on the number of slaves and the topology used:

- Line topology with one master and two slaves (*Master=1* and *Slaves=2*) (Figure 4.2)
- Line topology with one master and thirteen slaves (*Master=1* and *Slaves=13*) (Figure 4.3)
- Tree topology with one master and thirteen slaves (*Master=1* and *Slaves=13*) (Figure 4.4)

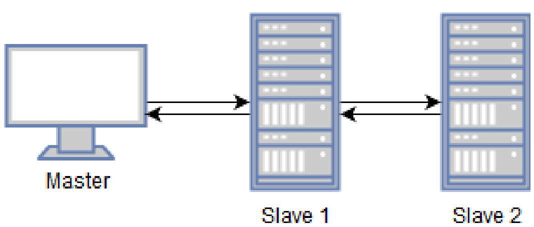

Figure 4.2: Line topology with Master=1 and Slaves=2

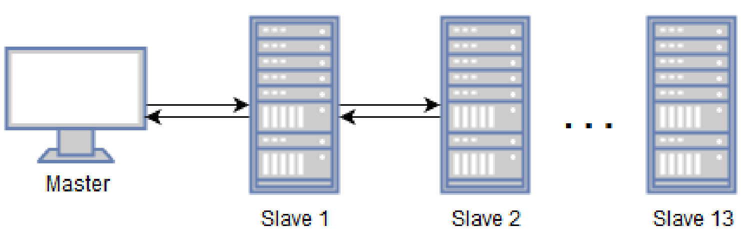

Figure 4.3: Line topology with Master=1 and Slaves=13

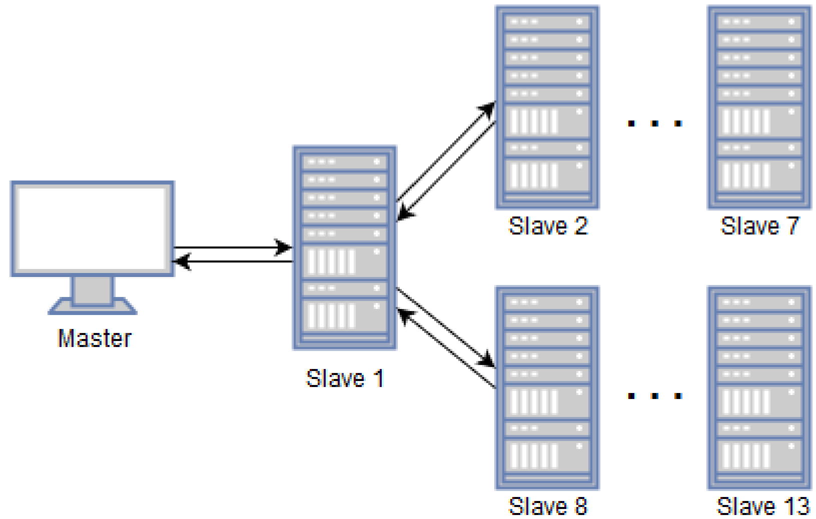

Figure 4.4: Tree topology with Master=1 and Slaves=13

4.3 Discussion

The following section will introduce the analysis of the simulations, where the different models that have been simulated, will be discussed thoroughly and will be discussed in terms of the throughput, communication cycle time and the potential delays which resulted from the lengths of the cables, the junctions and other modules that will add any further delays on the network. Finally, a comparison of the theoretical and simulation approaches will be presented and critically analysed before moving on to the validation of these results by means of experimental work.

4.3.1 Cycle Time Performance Evaluation

Analysis of the cycle time and throughput of the network is introduced in this section as a significant performance indicator for evaluating EtherCAT communication protocol. According to the specifications of the protocol, the performance depends on the architecture and the configuration of the network. Therefore, the simulation approach is taking into account different topologies of the network, by using only one master and adjusting the number of slaves connected on the network.

The outputs of the simulations have been recorded in terms of throughput (measured in bits/s) and used to calculate and evaluate the overall communication cycle time. In detail, the measurements include the time it takes for the EtherCAT telegram to be transmitted from the master to the first slave and the time it takes for the same telegram to be transmitted from the first slave back to the master device during the return path.

The communication cycle time, referred as T_{ecat}, is evaluated as the difference between the instant at which the first transmission starts, t_{s1}, and the instant at which the last transmission stops, t_{e2}.

Finally, before moving on the actual simulation results, it should be mentioned that EtherCAT protocol can physically support many different topologies or even a combination of them (daisy–chain, start, tree etc.). Nevertheless, according to EtherCAT technical specifications [113], in logic terms, there is only a single determined path around all the nodes (master and slaves) that EtherCAT frames go through. The slaves represent an open ring bus, where the master is the source initiates all the frames, transmits them in the networks and receives them at the other end after they have been processed from the related nodes/slaves. Consequently, even by using a logic open ring on the network, EtherCAT protocol guarantees the fast communication between the master and the slaves which, on the other hand, can physically be connected using many different topologies.

4.3.1.1 Line Topology With One Master and Two Slaves

The first simulation model is a simple line topology with one master and two slaves. As described in 4.2.1 section, it is first needed to configure the network period and the number of tasks that will be executed. Thus, $T_{networkPeriod} = 0.0005\ s$ ($500\ \mu s$) and $NumberOfTasks = 1$. In details, it is assumed that only one task will be transmitted from the master to the slaves with the expectation that this task will have an execution time less than the network period. In addition, according to Jasperneite et al. [114], the typical value of the forward delay for a slave device is, usually, $1.35\ \mu s$ and is referred as $t_{forwardDelay}$. The simulation models depicted in Figures 4.2, 4.3 and 4.4 designed with the aid of Reverbed Modeler (previously known as OPNET). The simulation time (within the software) has been configured at 30 minutes for each model in order to obtain a greater range of results that will be used for analysis. Finally, for the output results it has been selected to monitor the bit–rate against the time it takes for the transmitted frame to travel around the whole network. The same configuration has been used for all three simulations examined in this section.

The initial output result that measured from the simulations, is the throughput of the link between the Master and Slave 1. The throughput measured is presented in Figure 4.5. The measurements include the following parameters:

- t_{start1} which is the time it takes for the telegram to be transmitted from the Master to Slave 1 when the transmission starts

- t_{end1} which is the measured time it takes for the transmission from Master to Slave 1 to end
- t_{start2} which is the time it takes for the telegram to be transmitted from the Slave 1 to Master when the transmission starts during the return path
- t_{end2} which is the measured time it takes for the transmission from Slave 1 to Master to end

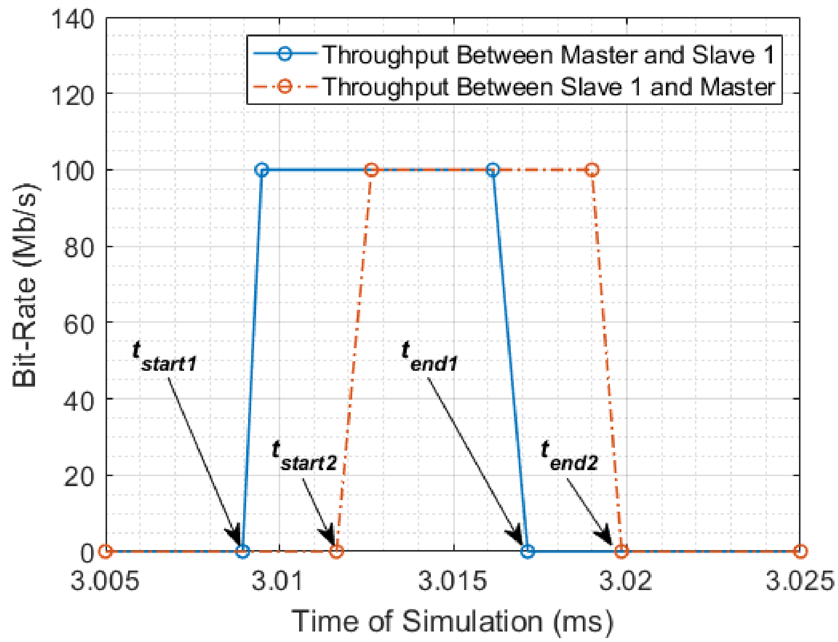

Figure 4.5: Line topology – Measured throughput of one master and two slaves

Table 4.1: Throughput with Two Slaves – Line Topology

$t_{start1}[s]$	$t_{end1}[s]$	$t_{start2}[s]$	$t_{end2}[s]$
0.00300895	0.003017150	0.003011650	0.003019850

The overall communication cycle time is calculated based on two different time measurements obtained from the simulations. The first measurement, t_{start1}, is the time it takes for the whole frame to be transmitted from the Master to Slave 1 which indicates the start of a new transmission on the network. The second measurement, t_{end2}, is obtained once the frame arrived to Slave 1 (after travelling around the whole network and passing through each node) and is ready to be transmitted back to the Master for processing. Thus, based on the numerical values from table 4.1, the communication cycle time of this specific model is

$$T_{ecat} = t_{end2} - t_{start1} = 10.9\ \mu s \tag{4.2}$$

In addition, according to figure 4.5 above, it can be observed that the measured delay $t_{start2} - t_{start1} = 2.7\ \mu s$, which is the obtained time difference between the two throughput "windows", is actually the delay that introduced by the frame when it is transmitted on the slaves ring. That delay can also be calculated by taking into account the number of the slaves connected to the network and the typical value of the forward delay introduced by each slave (as mentioned in [114]). Thus,

$$n_{slaves} \cdot t_{forwardDelay} = 2 \cdot 1.35 = 2.7\ \mu s \tag{4.3}$$

Furthermore, it should be mentioned that the width of the two throughput windows depends on the considered EtherCAT frame size. For the first model, the transmission of the frame takes 8.2 μs, which at the maximum bit rate of 100 Mb/s it provides a telegram of approximately 100 bytes.

4.3.1.2 Line Topology With One Master and Thirteen Slaves

The second simulation model is, again, a simple line topology with one master but this time the number of slaves has changed to thirteen. The network period, $T_{networkPeriod}$, and the number of tasks, $NumberOfTasks$, are the configurations that remained unchanged. The throughput of the simulated model is presented in Figure 4.6 and the output numerical values of this model are depicted in table 4.2.

Table 4.2: Throughput with Thirteen Slaves – Line Topology

$t_{start1}[s]$	$t_{end1}[s]$	$t_{start2}[s]$	$t_{end2}[s]$
0.004254350	0.004271350	0.004268050	0.004287350

Based on the above table 4.2, the communication cycle time of this model will be

$$T_{ecat} = t_{end2} - t_{start1} = 33\ \mu s \tag{4.4}$$

Moreover, according to table 4.2, it can be observed that the measured delay is 17.55 μs. That delay can also be calculated by taking into account the number of the slaves connected on the network and the typical value of the forward delay introduced

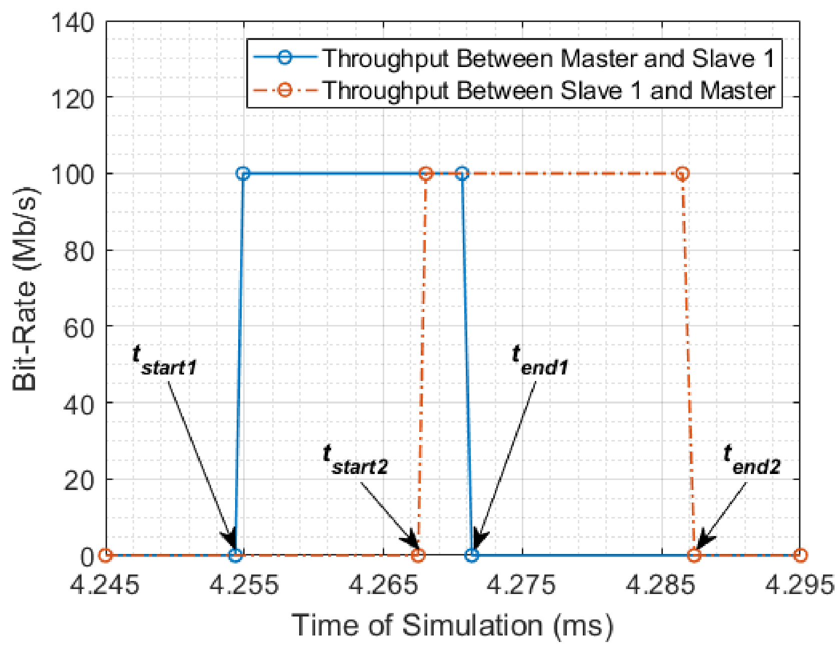

Figure 4.6: Line topology – measured throughput of one master and thirteen slaves

by each slave (as mentioned in [114]). Thus,

$$n_{slaves} \cdot t_{forwardDelay} = 13 \cdot 1.35 = 17.55 \ \mu s \tag{4.5}$$

Finally, it should be mentioned that the width of the two throughput windows depends on the considered EtherCAT frame size. For the second model, the transmission of the frame takes 17 μs, which at the maximum bit rate of 100 Mb/s it provides a telegram of approximately 212 bytes.

4.3.1.3 Tree Topology With One Master and Thirteen Slaves

The final model that has been tested by means of simulation is the binary tree topology presented in Figure 4.4 on page 73. According to the standard, the first slave device located immediately after the master device, has three duplex ports. Such configuration helped to interface the exact topology that can also be used for the real system. Once again, for this final simulation model, the network period, $T_{networkPeriod}$, and the number of tasks, $NumberOfTasks$, are the configurations that remained unchanged. The throughput of the simulated model is presented in Figure 4.7. In addition, the following table 4.3 presents the precise numerical values for the throughput of the model.

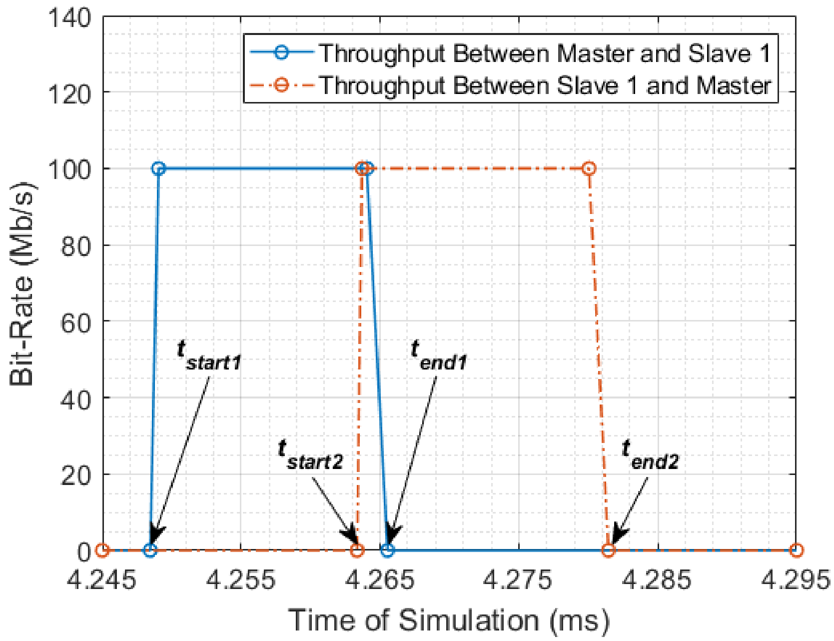

Figure 4.7: Tree topology – Measured throughput of one master and thirteen slaves

Based on the table 4.3 below, the communication cycle time of this model will be

$$T_{ecat} = t_{end2} - t_{start1} = 33\ \mu s \tag{4.6}$$

Table 4.3: Throughput with Thirteen Slaves – Tree Topology

$t_{start1}[s]$	$t_{end1}[s]$	$t_{start2}[s]$	$t_{end2}[s]$
0.004248450	0.004265550	0.004263350	0.004281450

By comparing the output results of line and tree topology with the same number of slaves connected on the network, it can be observed that the throughput is exactly the same for both simulation models. This relies on the concept that in logic terms EtherCAT slaves represent an open ring bus.

4.4 Theoretical Approach

In section 3.4.3.1 the potential topology implementation with EtherCAT has been presented. This topology will also be used for the actual network design, assuming it is the ideal implementation in order to use the least amount of wiring and have the most reliable and efficient operation for the protocol.

Based on the proposed design, it is essential to estimate the communication cycle time which, basically, is the time that it will take for the frame to travel around the network and return back to the master device. For the analysis, the bit–rate, frame size, number of slaves on the network and many other aspects have been considered, in order to provide a more accurate estimation of the communication cycle time. On a later section of this chapter, the theoretical approach is compared with the simulated models to provide an overall evaluation of the both cases.

4.4.1 Estimation of the Communication Cycle Time Based on the Proposed Network Topology

Although the network setup has not been implemented, it is worth presenting a time calculation for the protocol. The communication cycle time for a given EtherCAT network can be estimated. First the structure of the EtherCAT frame is explained. The data of interest (process data) is carried inside a standard IEEE 802.3 Ethernet frame shown in Figure 4.8 [115]. The Ethernet frame has 38 bytes of header, inside is the EtherCAT frame with 2 bytes of header, and inside there are EtherCAT telegrams which take information to one or more slaves and contain 12 bytes of header each.

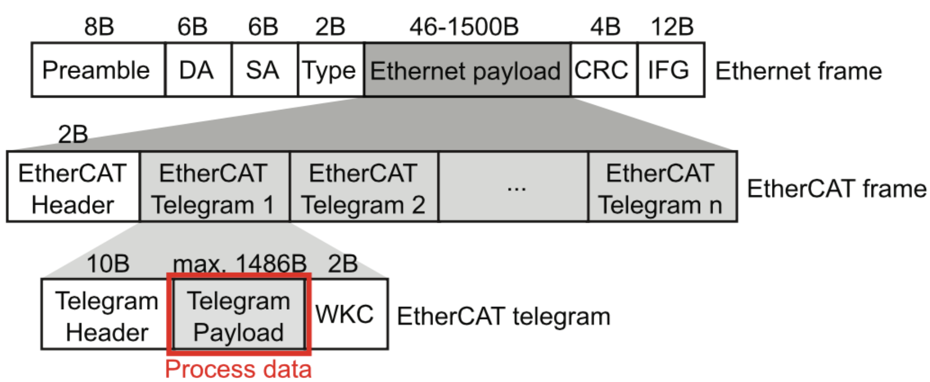

Figure 4.8: Encapsulation of EtherCAT frames

$$T_{cycle} = T_{frame} + T_{network} \tag{4.7}$$

The communication cycle time is influenced by the network topology. Equation 4.7 [116] defines the time for an EtherCAT frame to travel from the master, passing through all slaves and returning on a conventional daisy chain topology.

$$T_{frame} = \frac{8L_{frame}}{bw} \tag{4.8}$$

The time of the frame (T_{frame}) is related to the length of the frame, and can be found with equation 4.8, where bw is the network bandwidth in bits per second (100Mbps).

$$L_{frame} = np + [np + (\frac{np}{1486})(h_E + h_{ECAT} + h_D + h_{wkc})] \tag{4.9}$$

The length of the frame (L_{frame}) is given by equation 4.9. Where n is the number of slaves in the network, p is the average payload per slave (in bytes), h_E is the Ethernet header (38 bytes), h_{ECAT} is the EtherCAT header (2 bytes), h_D is the datagram header (10 bytes) and h_{wkc} is the working counter (2 bytes).

$$T_{network} = 2nT_{cable} + nT_{slave} \tag{4.10}$$

The time of the network ($T_{network}$) relates to the propagation delay in the hardware and the physical medium and can be calculated with equation 4.10. Where T_{cable} is the delay caused by the physical medium (estimated 5 ns/meter), and T_{slave} is the estimated delay in the hardware of the slave, which according to the specifications is 1 μs for an EK1100 EtherCAT coupler.

$$T_{cycle} = T_{frame} + T_{network} + T_{junction} \tag{4.11}$$

Assuming the topology proposed in section 3.4.3.1, the communication cycle time can be calculated by taking into account the Beckhoff Automation junction modules CU118. The purpose of the junction module is to split the network into four branches, each with four daisy–chained slaves. The specifications of the junction devices suggest that there should be 1 μs of delay per port. Taking this consideration, the proposed topology makes use of five ports, this means that an additional 5 μs should be added to the total cycle time (T_{cycle}). Equation 4.11 is the final equation considering the delay added from the junction module. Using this equation and assuming that there are 13 slaves in the network, an average of 13 bytes of payload per slave and one meter of cable between slaves, equation 4.11 yields:

$$T_{cycle} = 13.99\ \mu s + 14.69\ \mu s + 5\ \mu s = 33.68\ \mu s \tag{4.12}$$

According to this analysis, the communication cycle between all slaves and the master should occur in 33.68 μs. This means that in theory 93% of the control loop time (466.32 μs) would be available for the master to compute algorithms.

4.4.2 Comparison of the Simulation Results With the Theoretical Approach

In section 4.4 a theoretical approach presented on how to estimate the communication cycle time base on the proposed network topology described in 3.4.3.1.

By comparing theoretical approach with the simulation results, it can easily be observed that both approaches provide the same numerical results for the network's communication cycle time, which is the key factor that should be considered when designing the architecture of the network. There are slight variations between some elements studied for both theoretical and simulation approach, such as the network delay and the size of the frame. Nevertheless, these variations can be omitted taken into consideration the fact that some of the features of the actual EtherCAT protocol cannot be configured precisely for the simulation models.

The following table 4.4 presents and compares the results for both approaches. The network period ($T_{networkPeriod}$) refers to the time the network needs to execute all the required tasks, communication cycle time (T_{cycle}) defines the time for an EtherCAT frame to travel from the master, passing through all slaves and returning on a conventional daisy chain topology, network delay ($T_{networkDelay}$) relates to the propagation delay in the hardware and the physical medium and the length of the frame (L_{frame}) is referred on the length of the data that are travelling around the network and processed from the related nodes.

Table 4.4: Comparison of Simulation Results With Theoretical Approach

	$T_{networkPeriod}$	T_{cycle}	$T_{networkDelay}$	L_{frame}
Theoretical Approach	500 μs	33.68 μs	14.698 μs	169 bytes
Simulations (Tree Topology)	500 μs	33 μs	17.55 μs	212 bytes

Looking at the above table 4.4, the main differences can be observed on the delay of the network and the size of the frame. As mentioned above, the delay introduced in the network, has a slight variation due to the fact that EtherCAT protocol has features that cannot be configured in the simulation environment, such as the delays that were introduced from the length of the cables that are connecting the nodes. However, this variation can be ignored at the current stage since it is very small and is not affecting the overall performance of the network.

On the other hand, the size of the frame has been estimated at 169 bytes when considering that each node is processing an average payload of 13 bytes. Meanwhile, simulations show that even more data can be processed for the same number of nodes and the same network period. This could be extremely beneficial when designing a real network since there might be some nodes that have to process more data before returning the telegram back to the master device. In many cases, when operating a network with several nodes for different purposes, it is needed to both write to and read from one or more modules. This could lead to having a telegram that carries more data targeting specific slave devices.

4.5 Frame Size Optimisation Algorithm

An interesting approach has been introduced by Knezic et al. in [117] on how to reduce the size of the frame using an optimisation algorithm and increase the overall performance of the protocol. Apart from the research conducted by Knezic et al., there are approaches to increase the performance of EtherCAT protocol. The first approach, introduced by [114] and [118], is to use gigabit Ethernet which is capable to provide higher bit–rate for the protocol and decrease the time of the frame transmission. Another study by [119] and [120] presents a method about reducing the frame times and propagation delays by using conventional switches and EtherCAT couplers and deploy a parallelisation technique.

Taking the aforementioned researches into account, from the study conducted in by Knezic et. al in [117], it has been observed that by physically placing the output terminals before the input terminals on the network, the frame transmission time can be reduced by 50%. However, when having large networks with hundreds or even thousands of nodes, it would not be reliable to physically relocate the nodes on the network in order to have the output terminals at the beginning. The algorithm presented in their research is capable to provide a highly efficient and reliable network for a small network (approx. up to a hundred nodes) where the nature of application and the environmental constraints are not affecting the topology of the network. Therefore, the proposed methodology is based on the symmetric spatial distribution of the slaves in the network and by using logical addressing and appropriate EtherCAT commands.

In EtherCAT protocol, the size of the telegram used for the data–exchange between the master and slaves, can be reduced by 50% by using the logical read/write (LRW) command and exploit the symmetry of the network. As mentioned above, by relocating the nodes on the network by placing the output before the input slaves, the telegram size will be reduced at half. By using this approach, EtherCAT will first write the

Algorithm 1 Frame Size Optimisation Algorithm [117]

```
Set LogAddrI=LogAddrO initial value
for i=1 to n do
    Diff=LogAddrI-LogAddrO
    if Diff>Slave(i).Diff then
        Find i<k≤n for which Diff≤Slave(k).Diff
        if k was not found then
            Find i<k≤n for which min(|Slave(k).Diff|)
        end if
        Swap devices Slave(i) and Slave(k)
    end if
    if Slave(i).Obits≠0 then
        Calculate FMMU parameters for i^th slave
        if Diff>0 then
            LogAddrO=LogAddrI+Slave(i).Obits
        else
            LogAddrO=LogAddrO+Slave(i).Obits
        end if
    end if
    if Slave(i).Ibits≠0 then
        Calculate FMMU parameters for i^th slave
        LogAddrI=LogAddrI+Slave(i).Ibits
    end if
end for
```

related data on the output terminals and then it will read the data from the rest of the input terminals. Therefore, EtherCAT telegram can use the empty space as placeholder to read the data from the input terminals since there are no output data to be written on the rest of the terminals in the network.

The algorithm proposed by Knezic et al. in [117] is presented on page 83. It should be mentioned that this algorithm can also be deployed on this research since the network has a small number of nodes connected to the master and the proposed topology presented in Figure 3.13 (Section 3.4.3.1) is able to take advantage of the algorithm. Briefly, the Algorithm 1 below is divided into two main parts. The first is responsible for rearranging the inputs and the outputs in the network. The second part of the algorithm is responsible for calculating the new logical address of both input and output devices that have been located on a different position than the initial one.
The first part of the algorithm is going through the following steps:

- **Step 1:** Set the logical address for inputs and outputs equal to 0

- **Step 2:** Calculate the difference between the input and output logical addresses (given as *Diff*)

- **Step 3:** Compare the previous calculated difference (given as *Diff*) with the difference of the size (in bits) of the process data for inputs and outputs (given as *Slave(i).Diff*)

- **Step 4:** Check if *Diff* has a greater size than the process data of inputs and outputs

- **Step 5:** In case that the condition in Step 4 is satisfied, then scan the whole network to find that device (at the k^{th} index) where *Diff* is less than the process data of the inputs and outputs

- **Step 6:** In case that the condition in Step 5 is satisfied, then it swaps the device (at the k^{th} index) with the current device (at the i^{th} index)

- **Step 7:** In case that the condition in Step 5 is not satisfied, then it takes the device (at the k^{th} index) with the smallest difference in the process data and swaps it with the current device (at the i^{th} index)

The second part of the algorithm is going through the following steps:

Calculate the New Logical Address of The Output Device/Slave

- **Step 1:** Check if the size of the output process data of the i^{th} slave is not equal to 0

- **Step 2:** If the above condition is satisfied then calculate the FMMU parameters for that specific slave device (FMMU stands for Fieldbus Memory Management Unit)

- **Step 3:** Check if the difference between the input and output logical addresses (*Diff*) calculated in the first part is greater than 0. If the condition is satisfied, then calculate the new logical address of the output device by adding the current logical address of the input device with the size of the output process data of the i^{th} slave. If the condition is not satisfied, then calculate the new logical address of the output device by adding the current logical address of the output device with the size of the output process data of the i^{th} slave

Calculate the New Logical Address of The Input Device/Slave

- **Step 4:** Check if the size of the input process data of the ith slave is not equal to 0

- **Step 5:** If the above condition is satisfied then calculate the FMMU parameters for that specific slave device

- **Step 6:** Calculate the new logical address of the input device by adding the current logical address of the input device with the size of the input process data of the ith slave

4.5.1 Proposed Design Methodology of the Real System for Inclusion of Frame Size Optimisation Algorithm

Prior to moving on the experimental work with EtherCAT protocol, the network should be designed based on the proposed topology introduced in 3.4.3.1 (Figure 3.13) and, also, by taking into account the frame optimisation algorithm presented above and how this algorithm can be deployed on the proposed design. The prototype design of the real network architecture is presented in Figure 4.9, page 86.

According to the prototype in 4.9, the network has been designed in such way to meet the specifications of the exoskeleton project with the least amount of wires and based on the location of the potential nodes on the exoskeletal device. By examining the aforementioned design, it can be seen that the network is divided in the following five subnetworks:

a. Upper–body Subnetwork 1 – Left Side: Nodes 1, 2 and 3 used for left shoulder, arm and forearm, respectively
b. Upper–body Subnetwork 2 – Right Side: Nodes 4, 5 and 6 used for right shoulder, arm and forearm, respectively
c. Lower–body Subnetwork 3 – Left Side: Nodes 7, 8 and 9 used for left lower back, thigh and shank, respectively
d. Lower–body Subnetwork 4 – Right Side: Nodes 10, 11 and 12 used for right lower back, thigh and shank, respectively
e. Lower–back Subnetwork 5: Node 13 used for the slave located on the back of the exoskeletal device (that node is used for connecting the IMUs and accelerometers)

Based on the above description, it can be observed from the prototype that the first subnetworks for the upper–body are connected on the same junction module and the

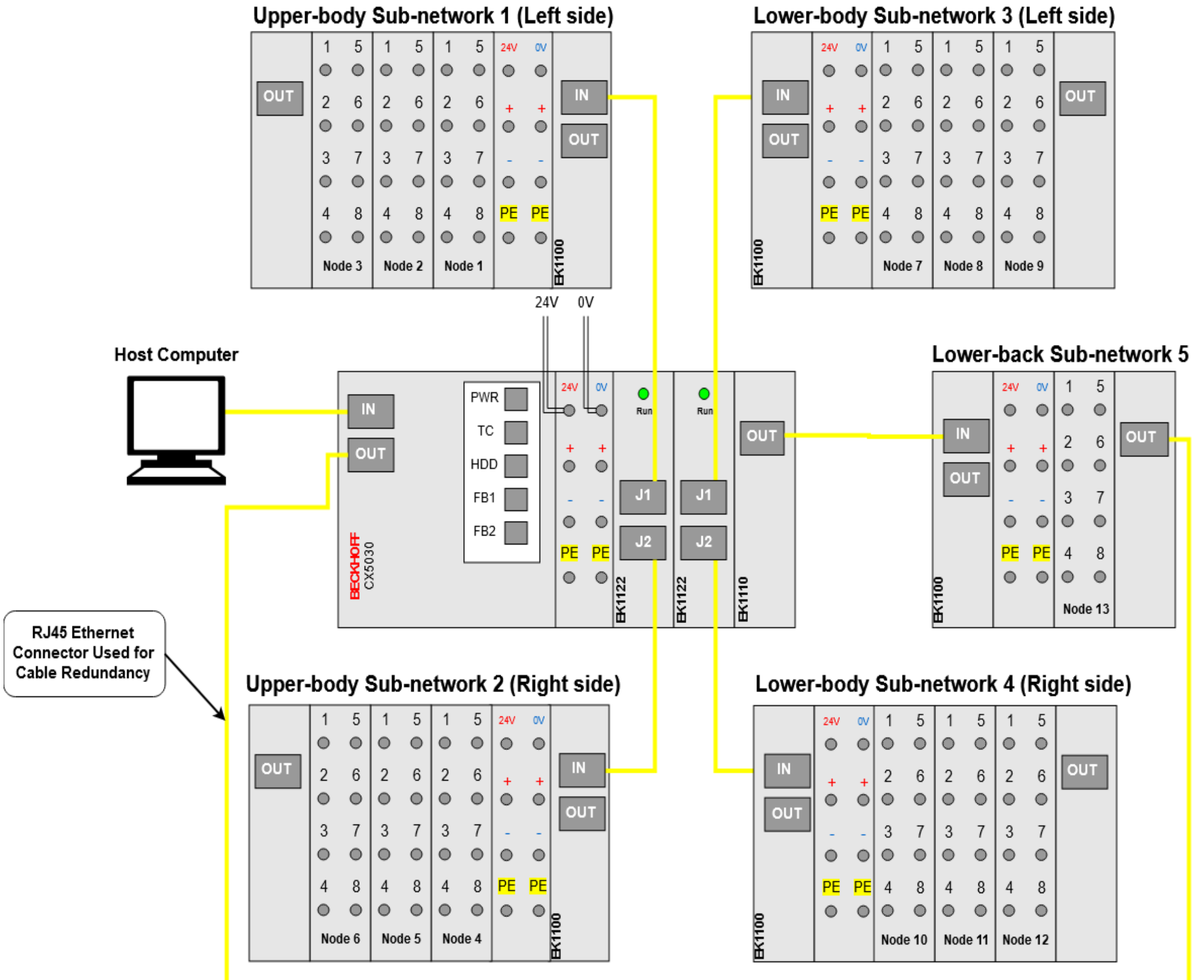

Figure 4.9: Prototype design of the communication system

same concept applies for the lower–body sub–networks, which are connected on their own junction module. Two junction modules (2–ports each) have been selected instead of one (4–ports) in order to increase the efficiency on the communication, wiring and have a fault tolerant network. According to the technical specifications of the EK1122 junction module from Beckhoff [121], it is able to decrease the propagation delay on the hardware by 50% by using a 2–port junction module. The last subnetwork (for the back node) is simply attached on a coupler device which is connected on the master device. Moreover, it should be mentioned that in each subnetwork there are input and output slaves which are processing the telegram sent from the master device. In order to apply the frame size optimisation algorithm, is is needed to place the nodes in such a way that the outputs will be processed first and the inputs last. Even if more nodes connected on the network, the nature of the application allows to physically change the position of each node, due to the relatively small network.

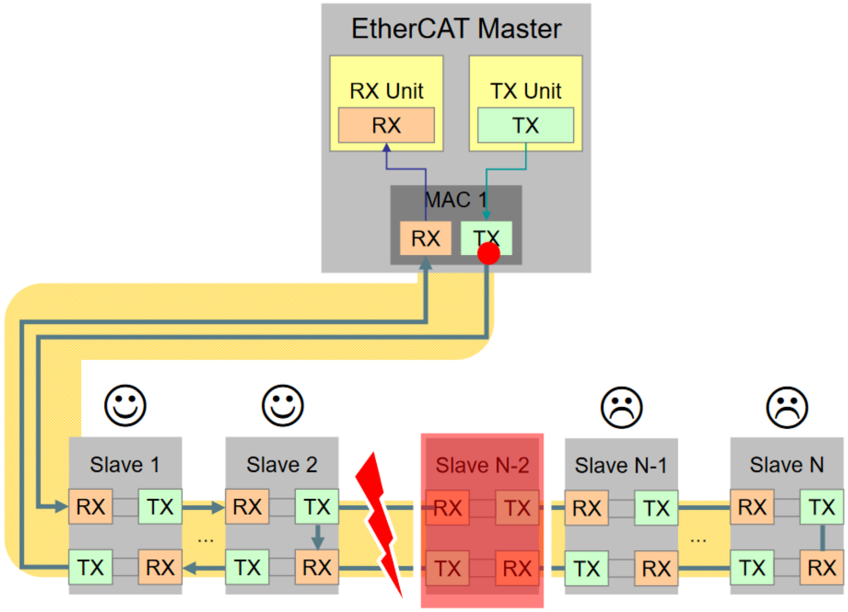

Figure 4.10: Case of node failure without using cable redundancy feature [122]

Another remarkable feature that is introduced in prototype design is the cable redundancy. In order to use this feature, a second ethernet port is required on the master side as well as on the last node on the network. The failures that can occur in the network are cable and node failures. For example, in case that in a network of 10 nodes the failure occurs in node 5, then the rest of the slaves will not be processed from the protocol if cable redundancy feature is not used. Representation of such example is shown in Figure 4.10.

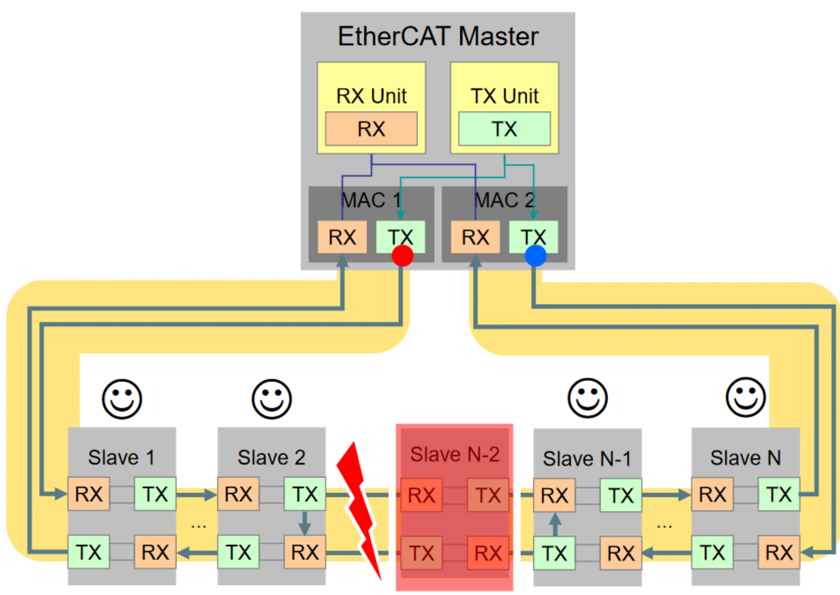

Figure 4.11: Case of node failure when using cable redundancy feature [122]

On the other hand, in case that cable redundancy feature is used then it is possible to have undisrupted communication in the network with a recovery time of less than 15 μs. This means that even motion applications with very short cycle times can continue working smoothly when a cable breaks. There is no need to physically modify the nodes or replace any broken cables. Representation of such example is shown in Figure 4.11 and the RJ45 Ethernet connector used for cable redundancy concept is also presented in Figure 4.9.

4.6 Summary

In this chapter a simulation model of the selected communication architecture was presented. The simulations performed with the aid of OPNET software. The simulations focused, mainly, on the calculation of the communication cycle time and the length of the transmitted data. As mentioned in the previous sections, the bandwidth of motion was assessed to be 10 Hz for walking and 40 Hz for running. Based on that, the sample rate of the control loop was chosen to be 2 kHz, resulting a network period of 500 μs. Three different models have been simulated in order to obtain the results for the throughput and the network delays. Two different network topologies have been simulated to evaluate the performance of the protocol. Each model consisted of different number of slaves and special attention paid on the tree topology since it has been selected to be used for the actual system setup. The simulation results were compared with the theoretical approach discussed in this chapter. These results from the simulations have shown that they match the theoretical approach presented in this chapter. Moreover, it has been found that the proposed topologies are capable of transferring the required amount of data (as introduced in table 3.3, page 57) by achieving the maximum bit–rate provided by the protocol. It is worth noting that from both theoretical and simulation approaches has been found that the size of the frame that can be transferred on the network is significantly smaller than the available frame provided by EtherCAT protocol (max. of 1500 bytes). Thus, more sensors/nodes could be added on the network in the future.

In addition, an optimisation algorithm for reducing the size of the frame by 50% and the communication cycle time examined in this chapter. The final design of the network architecture proposed based on the requirements for real–time and fault tolerant communications. Finally, cable redundancy concept has been discussed in details. Due to the fact that exoskeletons have moving parts, there is a high chance that one or more nodes will fail to provide the needed information due to broken cables/wires. Thus, cable redundancy can be used to provide undisrupted communication without loosing valuable measurements.

Chapter 5

Sensors, Software and Prototype Setup

5.1 Introduction

This chapter introduces a novel design of the single–joint prototype constructed at University of Leeds. This single–joint will be a part of the whole exoskeletal device that will be manufactured for the final stage of the project. The design of the prototype is an effort of the exoskeleton engineers of mechanical designers worked for this project and mentioned in the acknowledgement section of this report.

In section 5.3, the sampling rate that is used for the development of electronics is discussed, based on a motion capture study that has been conducted. The results from this study have been evaluated for the purpose of selecting the sensors that will be used for the prototype and will meet the required specifications of the sampling rate. The sensors that have been chosen for this project are described in section 5.4. Section 5.5 concludes by introducing the architecture used for the control electronics and software, based on the proposed mechanical designed of the single–joint.

5.2 Mechanical Design of the Prototype

An exoskeleton single–joint was built from the mechanical designers of this project in order to be used for the validation of experimental work that will be conducted at a later stage. The design must fulfil the requirements that has been set for this project and discussed in Appendix A. A simple representation of the single joint mimicking the movement of a human leg is depicted in Figure 5.2. The actual joint prototype shown in Figure 5.1 should follow the wearer during normal walking, minimise the force applied to the human and maintain the balance when external forces occur. The total mass of the prototype is 32.86 kg and the links are made of aluminium, the kneecap and brackets holding hydraulic pistons are made of stainless steel and the rest of the parts of the joint are made of aluminium alloy 6061. This design is novel, since no such configuration has been found in the literature of exoskeletons.

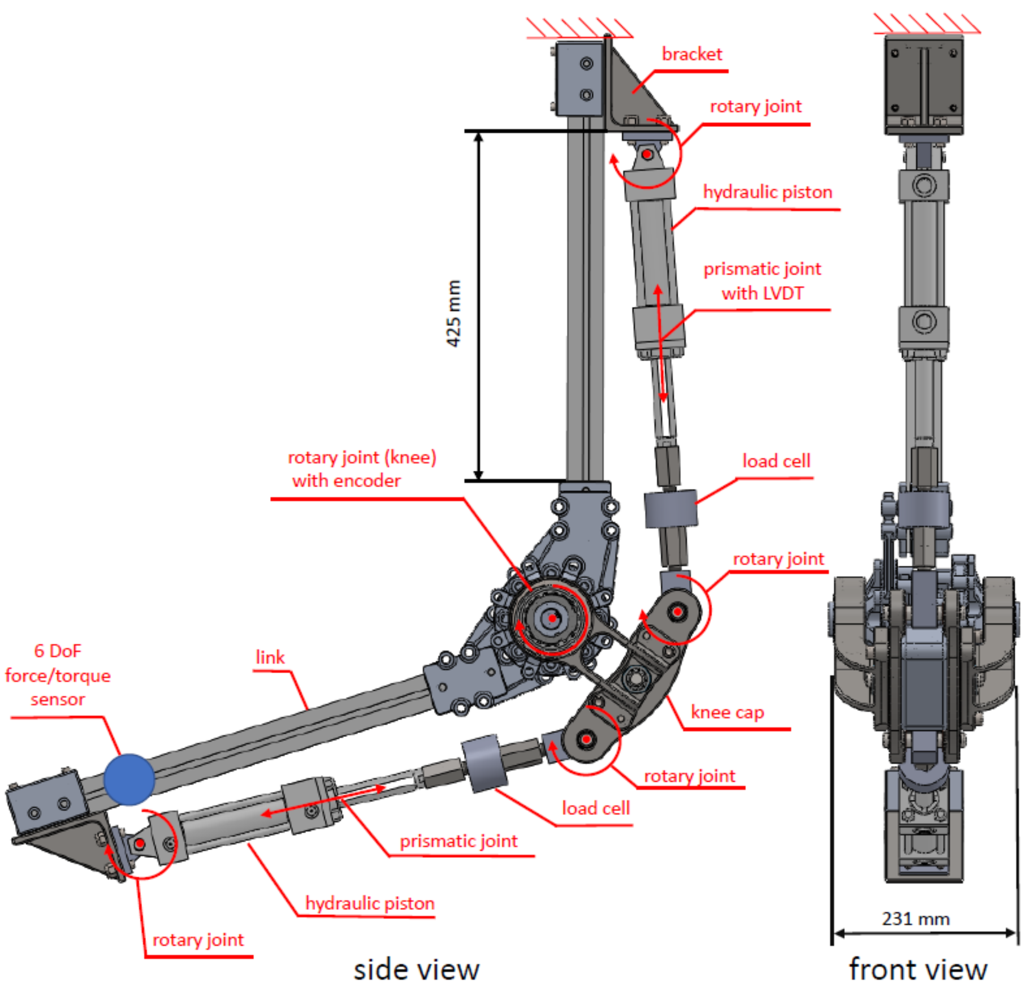

Figure 5.1: Prototype design of the single–joint

According to Figure 5.1, the sensors used are placed on different locations on the single–joint. The flexion and extension of the actuators are measured by the Linear Variable Differential Transformer (LVDT) placed in parallel with the upper and lower actuators. Moreover, there are two load cells placed at the end of actuator rods and are measuring the forces applied by the actuators and at a later stage they will be capable of measuring the load carried from the whole exoskeleton. An absolute encoder that is placed at the centre of the joint is measuring the angular displacement of the prototype. Finally, a 6 degree of freedom Force/Torque sensor measuring the force that was applied on the whole joint is attached on the lower link. The Force/Torque sensor is not used for the experimental work that will be analysed in the next section. It has been used by the control systems' engineer of this project for the validation of the controlling algorithms that are discussed extensively in [123].

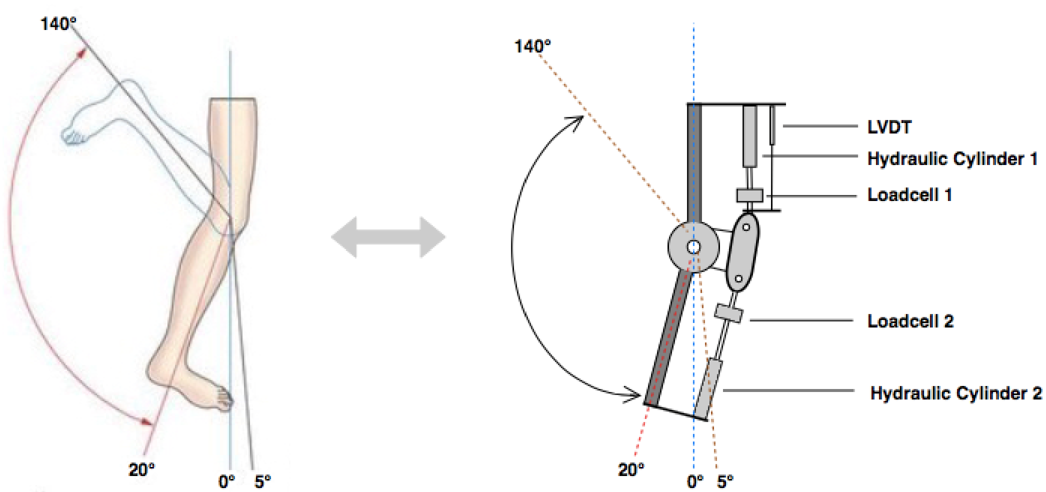

Figure 5.2: Motion of exoskeleton's lower extremity

5.3 Sampling Rate and Bandwidth of Motion

The nature of operation of an exoskeleton requires high bandwidth and fast sampling rate in order to process all the data in a small amount of time for the considered tasks. The sensors that are connected on the device must sample the signals as fast as possible and the sampling rate should either be equal to the minimum sampling rate considered or faster than that. In addition, the real–time communication system should be able to process the data as fast as the sampling rate. Therefore, in order to determine the minimum value of the sampling rate for the control system, the bandwidth of motion of exoskeleton segments has to be examined.

The sampling rate that has been selected to be used for the exoskeleton built for this project, is derived from the motion capture study conducted in the School of Biomedical Sciences at University of Leeds. The subject was a 29–year–old male, weighing 92.3 kg and is 182 cm tall. The subject performed several activities during this study, in order to record the motion of the human body and determine the bandwidth that should be used for the control system that will be designed for exoskeleton. The motion capture study examined extensively by the control systems' engineer of this project and is presented in [123]. From this study, it has been derived that if running is also considered as a task for the exoskeleton, then the minimum sampling rate that should be used is approximately 1.6 kHz. Thus, EtherCAT seems to be the most appropriate communication protocol to deploy the control algorithm due to the high performance of the protocol, since it can process the data at a minimum of 2.8 kHz. The highest sampling rate that can be used with this protocol is up to, approximately, 83 kHz, depending on the number and the type of the slaves/nodes that are attached to the protocol.

5.4 Sensors Attached on the Prototype

According to Figure 5.1, there are several sensors attached on the prototype which are used to obtain different measurements from the single–joint. The sensors used to conduct the experiments for this research are: a LVDT (Linear Variable Differential Transformer), two load cells and an SSI absolute encoder. The sensors have been selected in accordance with the requirements for the communication protocol and the control system which have been derived from the motion capture study.

5.4.1 Linear Variable Differential Transformer Sensor

According to the prototype in Figure 5.1, a LVDT (Linear Variable Differential Transducer) is used to measure the flexion and extension of the hydraulic pistons. The sensor that used is manufactured from Solartron and it is the S-Series AS10 (shown in Figure 5.3 [124]).

The sensor operates on the principle of movement of a core with respect to secondary coils, while the primary coil is excited by alternating current. A typical structure of a LVDT is depicted in Figure 5.4. According to the technical specifications [125] of the AS10 LVDT that is used for this project, the sensor produces an analogue output voltage of ± 10 V, proportional to the displacement. The displacement that can be measured

Figure 5.3: Linear Variable Differential Transducer (LVDT) – S–Series AS10 [124]

from the sensor is ± 50 mm with a maximum range of 100 mm. The bandwidth of the sensor is 460 Hz, which is sufficient for tasks considered in Appendix A.

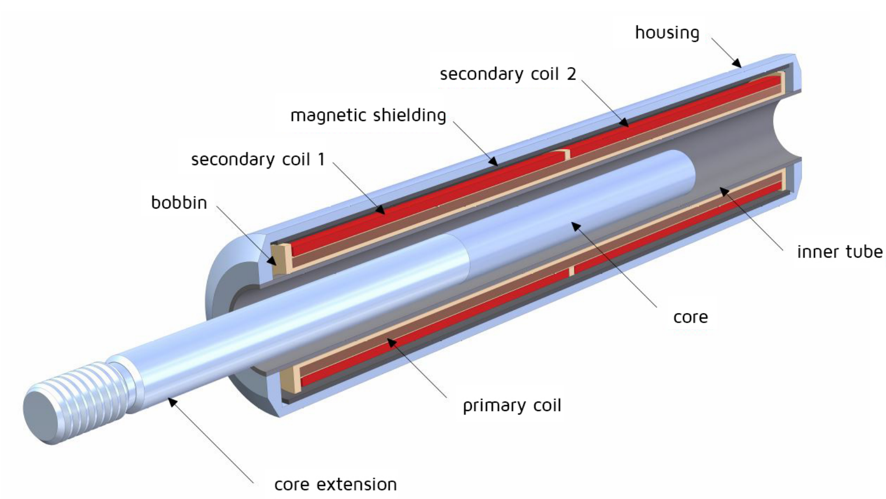

Figure 5.4: Typical structure of LVDT [126]

5.4.2 Load Cell Sensor

As shown in the prototype in Figure 5.1, there are two load cells placed at the ends of the rods of the hydraulic pistons. The load cells are manufactured by Novatech and the model is the F256–Z4616. The load cell is depicted in Figure 5.5.

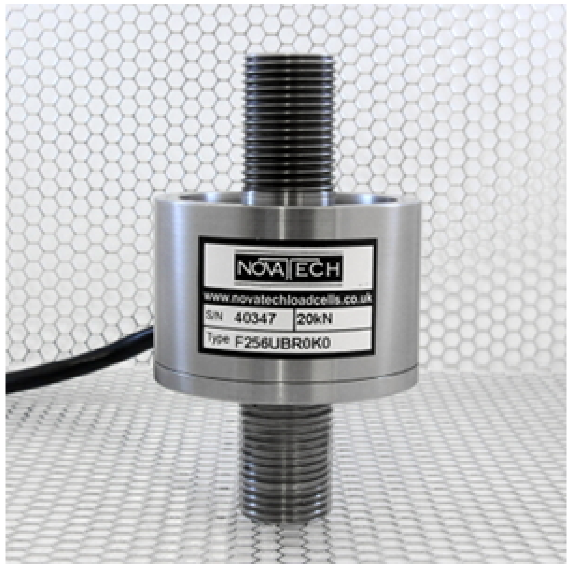

Figure 5.5: Load cell sensor – Novatech F256–Z4616 [127]

According to the technical specifications of the device [128], the load cells have a measurement range of ±20 kN. However, the development of the load cells requires the connection with an additional external amplifier device in order to amplify the output signal. An SGA Analogue Strain Gauge Load Cell Amplifier has been used for that purpose, where the output of the amplifier has been configured to ±10 V for the range of the ±20 kN. Based on the technical specifications of the Strain Gauge Amplifier in [129] and [130], there is a built–in second order low pass filter with a cutoff frequency range between 1 Hz up to 5 kHz. Based on the measured minimum bandwidth frequency (derived from the motion capture to be 10 Hz), the cutoff frequency has been configured to 50 Hz. In addition, the sensitivity of the sensor has a value of 2 mV/V.

The most common type of strain gauge loadcells consists of an insulating flexible backing which supports metallic foil pattern. The formula for calculating the strain gauge resistance is the following:

$$R = \rho \times \frac{l}{A} \tag{5.1}$$

where R – is the resistance of the strain gauge, ρ – is the resistivity, l – length of the strain gauge and A – is its cross-sectional area. Based on the same equation, it can be seen that the resistance increases when the strain gauge is under tension and decreases when the strain gauge is under compression.

The linear relationship between the strain of the strain gauge and the change in its resistance can be derived from the following formula:

$$\frac{dR}{R} = K \times (\frac{dl}{l}) = K \times \varepsilon \tag{5.2}$$

where K – is the 'gauge factor' and ε – is the ratio of strain. The resistance of a strain gauge loadcell is usually measured using a Wheatstone Bridge. The Wheatstone Bridge is an electrical circuit that used to measure the overall change in the resistance, increase the sensitivity of the measured signal and reduce the effects of temperature.

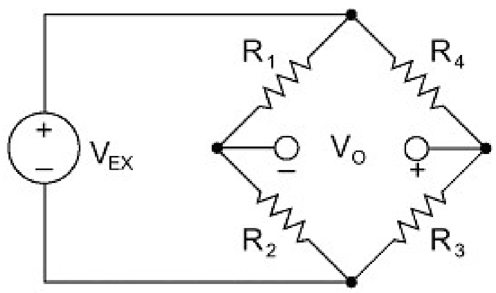

Figure 5.6: Wheatstone bridge circuit use in strain gauge load cells for calculating the resistance change

According to Figure 5.6, the Wheatstone Bridge circuit includes two parallel voltage divider circuits. The voltage divider rule is:

$$V_{out} = V_{in} \times \frac{R_b}{R_a + R_b} \tag{5.3}$$

Therefore, based on voltage divider rule, the output voltage of the Wheatstone Bridge of the strain gauge loadcell can be derived as:

$$V_{out} = V_{EX} \times (\frac{R_3}{R_4 + R_3} - \frac{R_2}{R_1 + R_2}) \tag{5.4}$$

From this equation, it can be seen that when $\frac{R_2}{R_1+R_2} = \frac{R_3}{R_4+R_3}$, then the output voltage of the Wheatstone Bridge, V_{out}, will be equal to zero. In such case, then the Bridge is balanced. Any changes introduced to any of the resistances in the Bridge, will result in a non–zero output voltage. Thus, by replacing any of the resistances with an active strain gauge, any change that will happen in the strain gauge will result in an unbalanced bridge and produce a non–zero value for the output voltage.

5.4.3 Encoder Sensor

Safety is the most significant factor for an exoskeleton that a human is wearing to perform different activities during the day. An exoskeleton has the upper and lower joints which need to be monitored and controlled according to the results that were received from the monitoring process. Thus, it is essential to understand the range of motion for each joint in order to avoid serious injuries that can be caused on the human body of the user of the exoskeleton. Therefore, an encoder can, for example, be placed at the knee joint of the exoskeleton in order to monitor the range of motion of the knee and provide the appropriate feedback to the controller.

As shown in Figure 5.1, an encoder is used to measure the angular displacement (flexion/extension) of the joint. The device is an absolute encoder manufactured from Hengstler, with the model AC36. The exact model number, according to the specification from Hengstler in [131], p. 5, is AC36 0014 A R.41 SD B. Based on the same datasheet, the encoder has an overall length of 36 mm and a diameter of 38.1 cm. The device is depicted in Figure 5.7.

Figure 5.7: AC36 optical absolute encoder [131]

The device has a resolution of 14–bits for the measurement of angular displacement with 10,000 rpm of continuous operation. The interface that is used is the Synchronous Serial Interface (SSI) using binary coding. It is also equipped with SinCos interface with 1 V peak–to–peak. The bandwidth of the sensor is 500 kHz, allowing a maximum baud–

rate of 1 MHz. According to the control system specifications discussed previously, the allowable bandwidth of the sensor is able to fulfil the minimum requirements of bandwidth of 400 Hz (or 1.6 kHz if running is considered) of the exoskeleton segments.

In order to understand the way an encoder is operating; the principle of operation should be examined. As previously mentioned, the encoder that was employed for this project is using the absolute measurement system. The main difference between the absolute and incremental measuring systems, is depicted in Figure 5.8.

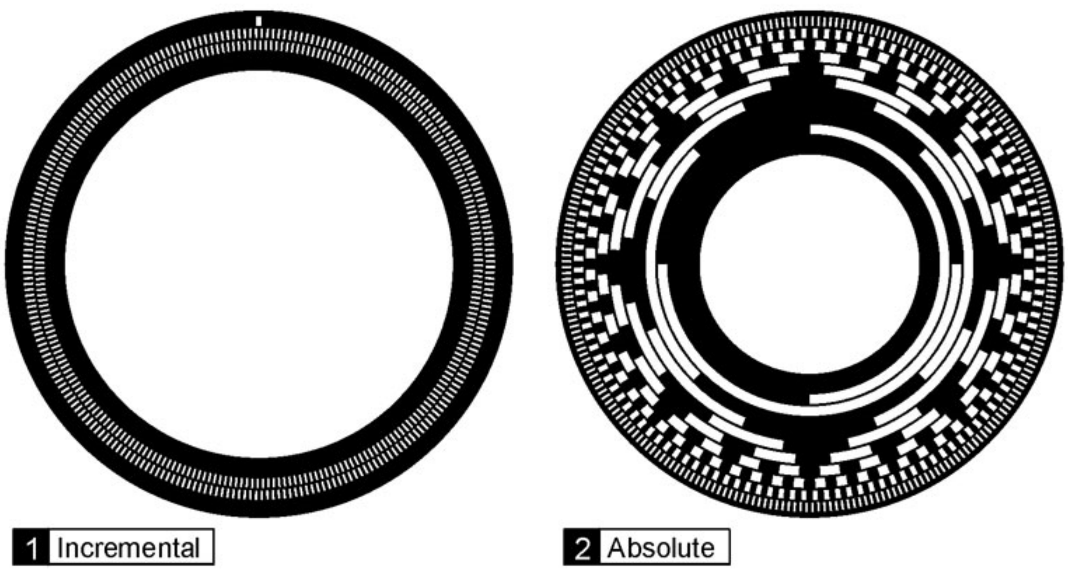

Figure 5.8: Incremental and absolute measuring systems [132]

One of the advantages of an absolute encoder is that it is capable of providing unique position values once power supply unit is turned on. The encoder disc that is placed on the internal of the device has unique marks or slot and the disc is able to record each of these unique values when the shaft of the encoder is moving. Moreover, the absolute encoders are divided into two main categories, the single–turn and multi–turn. The single turn is used to record the angular displacement in one turn (across 360^o from the starting position). Once the shaft reaches the starting position, the encoder's disk starts measuring again from the beginning. At the other end, in multi–turn encoders the same principle of operation with the single–turn is applied, but the encoder's disc is also counting the total number of revolutions of the shaft.

Regarding the coding of an absolute encoder, there are main categories that can be used, the 'Binary' and 'Gray' coding. When binary coding is used, the device is able to provide a binary output number that reflects to the position of the shaft. However, every time the position of the disc is altered, there might be several binary bits that have to be shifted, which can lead to the recording of invalid position. The error introduced by this coding method is negligible and can be ignored. On the other end, the gray coding method is a one–step code, where only one bit needs to be moved from its initial position to the next one when the shaft is moving. Finally, the interfaces that can be used for an absolute encoder are the SSI, which stands for Synchronous Serial Communication, and BiSS, which stands for Bidirectional Serial Synchronous. Based on the technical specifications of each interface, BiSS seems to be a more advanced interface, by providing a transmission rate up to 10 MHz without compensating the cable length, compared to the SSI interface which has a transmission rate of up to 1.5 MHz and the cables should have a fairly small length.

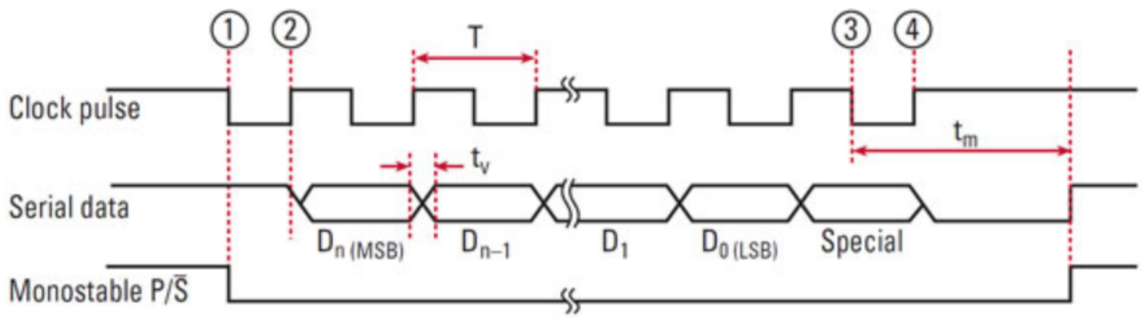

Figure 5.9: Serial Synchronous Interface (SSI) communication

Nevertheless, due to the nature of application, the SSI seems to be the most reliable, efficient and cost–effective solution. By using SSI interface, only two twisted pair of lines are needed, one for the clock and the other for the transmission of the data. In addition, when the transmission of data takes place in SSI, the data are transmitted synchronously with the clock by starting with the Most Significant Bit (MSB). The nature of operation of SSI transmission can be described as follows and also depicted in Fig. 5.9:

1. When there is no data transmission, both the clock and the data line signals remain high (H or binary 1);

2. When a clock sequence changes for the first time from Low (L or binary 0) to High (H or binary 1) to then the bit–parallel data will be stored in the input latch of the shift register in order to ensure that during the data transmission the bits cannot be changed;

3. When the clock is at the High (H or binary 1) position, the data transmission starts with the MSB;

4. For every rising edge of the clock signal, the next significant bits are placed on the output data line;

5. Once the Least Significant Bit (LSB) placed on the data line, the clock signal is changing from High to Low which indicates the end of data transmission.

5.5 EtherCAT Electronics and Software

EtherCAT electronics and real–time software have been deployed to develop the aforementioned sensors for the single–joint prototype examined in section 5.2. The sampling rate of the control loop has been configured at 2 kHz, which meets the minimum requirement of 1.6 kHz when running which is considered as a task.

5.5.1 EtherCAT Electronics

The 'brain' of all the electronics attached on the single–joint is the CX2030 embedded PC from Beckhoff [133]. The device is built around an Intel Core processor. The chip features dual–core Intel i7 2610UE, with a clock of 1.5 GHz and a 128 KB integrated NOVRAM operating as persistent memory. The processor is programmed using TwinCAT 3, a software tool integrated on Microsoft Visual Studio [134].

A block diagram of the hardware of EtherCAT electronics is depicted in Figure 5.10. According to the technical specification of the CX2030, in order to take measurements from different sensors and devices, dedicated EtherCAT terminals are required. These terminals are modular I/O systems consisting of electronic terminal blocks. For the sensors used for this research, the master device (CX2030) communicates with the peripherals via the following terminals:

- **EL3102 [135]:** a 2–channel analog input terminal that handles differential input signals in the range of ± 10 V with a resolution of 16–bits. It features an input filter with 5 kHz limit frequency, which is well above the minimum sampling rate of 1.6 kHz. The measuring error of the terminal found to be $< \pm 0.3\%$. This terminal is used to connect the LVDT sensor with the master device (CX2030) and acquire the measurements.

- **EL3162 [135]:** a 2–channel analog input terminal that handles single–ended input signals in the range between 0 and 10 V with a resolution of 16–bits. It features an input filter with 5 kHz limit frequency, which is well above the minimum sampling rate of 1.6 kHz. The measuring error of the terminal found to be

$< \pm 0.3\%$. This terminal is used to connect the loadcell sensors with the master device (CX2030) and acquire the measurements.

- **EL5002 [136]:** a 2–channel SSI interface terminal which allows the direct connection with two SSI encoders. The terminals have an internal clock that generates a pulse for reading the encoder and makes the incoming data stream available to the controller as a data word in the process image. It features a serial input of 24–bit width. It has a maximum data rate of 1 MHz, which is more than the minimum sampling rate of 1.6 kHz. Other essential features of the terminal are the: adjustable baud–rate, coding method (Binary or Gray) and data length.

Finally, an external SGA Analogue Strain Gauge Load Cell Amplifier is used to amplify the output signal from the loadcells. The gain of the amplifier has been configured to 1.99 mV/V (which is close to the 2 mV/V of the sensitivity of the loadcells, mentioned in 5.4.2). The non–linearity error of the amplifier has been found to be 0.03% of the full–range. Also, the SGA features an offset cancelling circuit and a selectable filter, which has been configured between 10 Hz and 50 Hz to cover the bandwidth required for the control system.

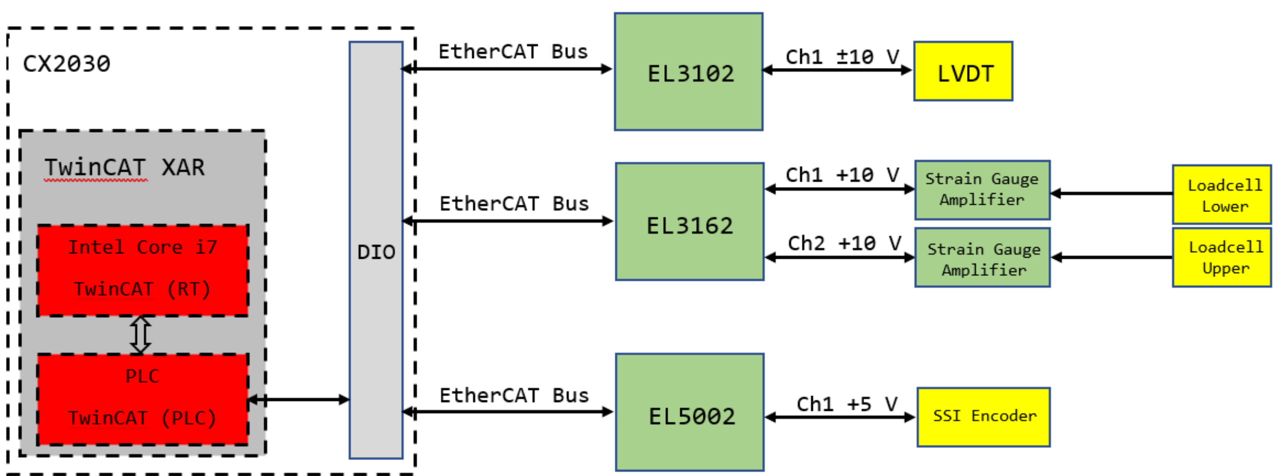

Figure 5.10: Hardware block diagram of EtherCAT electronics

5.5.2 Software Implementation Methodology

In order to conduct the experiments that will be discussed in section 6, software is required to meet the specifications which have been examined in this section (for example, the minimum sampling rate of 1.6 kHz). Thus, in order to meet these requirements, a hard real–time system is required, otherwise the operation of the whole system will fail. A working counter is initiated from TwinCAT software to detect the devices and terminals that are connected on the network. Then, TwinCAT is initialised in the CX2030 embedded pc in order to establish the communication with the peripherals, such as the LVDT, the loadcells and the encoder that are attached on the network via the dedicated terminals mentioned before. Once the communication cycle time configured from the user, then the system is following a state–machine developed in the software. The states are the following:

a. *TwinCAT Initialisation on the CX2030* — once the power supply switched on, CX2030 is initialising TwinCAT that is installed on its embedded hard drive disc;

b. *Network Initialisation* — master device sends initialisation commands on the network to detect the terminals attached and the topology that is used;

c. *Idle* — waiting for the user to send any commands from TwinCAT software on the host computer;

d. *Run* — master transmits the telegram to the slaves on the network, reads from the input nodes, writes on the output nodes and then telegrams are returned back to the master following the same path. The whole process is triggered by a timer/clock that has been configured by the user;

e. *Data Processing* — master is performing data processing of the tasks included in the telegram

The timer used for the real–time application has been configured to provide a communication cycle time of 500 μs. According to the formula $T = \frac{1}{f}$, the sampling rate will be 2 kHz, which is capable to process the tasks that will be performed by the exoskeleton. Finally, the real–time system is able to convert the measured raw values of the sensors into human readable forms and display these values in TwinCAT software in order to validate the measurements.

5.6 Summary

In this chapter the technical specifications of the sensors that were selected to meet the requirements for range and bandwidth were discussed. The prototype design of the single joint presented along with the location of each sensor on the exoskeleton frame. The sampling rate and bandwidth of motion derived from the motion capture study were analysed and it has been found that the minimum sampling rate of the control loop that will be used for the experiments is 2 kHz. Sensors were selected to meet requirements for the range and bandwidth. An electronics architecture was proposed by presenting the hardware block diagram of EtherCAT electronics. Moreover, a software architecture was proposed allowing for implementation of EtherCAT communication protocol presented in Chapter 6.

Chapter 6

Experimental Work and Results

6.1 Introduction

In this chapter the experimental work conducted for EtherCAT is presented along with the development of the sensors that were used for the single joint and presented in section 5.2 (Figure (5.1)). The purpose of the experiments is to aid in the testing and validation of the communication strategy used for this project. The experiments that are presented in this section do not include any experiments for the actuators attached on the exoskeleton single–joint. The actuators have been tested by the controls' engineer of the this project. The control algorithm that has been developed for this project will be deployed in a future implementation, in order to assess the overall performance of the system. Nevertheless, the experiments have been conducted in collaboration with Mr. Napora to validate the results obtained from the sensors. Mr. Napora is responsible for developing and implementing the control algorithm. An initial set of experiments has been conducted using NI cRIO–9024 as the master device in order to evaluate EtherCAT protocol with LabVIEW and assess the performance of this specific experimental setup using a different master device. The implementation with NI's device is discussed thoroughly in Appendix B.

6.2 Implementation Priorities

Before conducting any experimental work, priorities have been set in order to assure the normal operation of network, based on the specifications of the exoskeleton project and the nature of application. Each of these priorities are discussed below:

a. Configuration of the timer/clock of the communication system in order to achieve the minimum value of sampling rate, which is 1.6 kHz (as examined in detail in section 5.3, page 92). The timer for this experiment has been configured at 500 μs, which is a frequency of 2 kHz. That configuration could be changed by increasing the value of the timer if higher sampling rate is needed, although, higher delays might be introduced due to the fact that some of the hardware devices that will be used in the network, will not be able to support sampling rates of more than 5 kHz (such as the EL3102 terminal as presented in 5.5.1, page 100). Thus, the sensors have been tested using a sampling rate of 2 kHz, which is sufficient for the experiments of this research. Nevertheless, it should be noted that particular attention should be paid when configuring the sampling rate, since any changes might affect the overall performance of the network.

b. Optimisation of the topology in order to introduce the feature of distributed clocks in a future implementation of the network, when the whole exoskeleton device will be manufactured. According to [137], EtherCAT distributed clocks is a feature that can be deployed on the network. That technology enables the synchronisation of all the slave clocks with a reference clocks that has been selected by the user. The slave device serving as a reference clock is, usually, the very first slave attached to the network. Nevertheless, it should be mentioned that in order to use the distributed clocks feature, part or all of the network slaves must support that feature. Therefore, according to the potential topology presented in section 3.4.3.1, the nodes should be configured in such way where the first slave will be capable to serve as a reference clock for the whole network. That feature could increase the overall performance of the communication between the nodes and reduce the total amount of the cycle time needed to process all the data.

c. Deploy of frame size optimisation algorithm described in section 4.5. This task can be implemented once it is guaranteed that the two aforementioned tasks are applied successfully. Failure of the algorithm is an extremely undesirable condition that could affect the topology of the network, the communication cycle time and, in the worst case scenario, lead to the failure of the normal operation [1].

6.3 Equipment Setup and Software Development of the Sensors

In this section the hardware setup and the software development are described. This includes the hardware connections of the sensors to the master device via the dedicated EtherCAT terminals and the software implementation of each sensor using TwinCAT software.

6.3.1 LVDT Development

6.3.1.1 Hardware Setup

Based on the analysis in section 5.4.1, the S–Series AS10 LVDT sensor produces analog output measurements in the range of ± 10 V with a 16–bit resolution. Thus, the EtherCAT terminal should be able to read the whole range of measurements. For this purpose, the EL3102 EtherCAT terminal has been used. The hardware connection of the LVDT sensor with the master device CX2030 is depicted in Figure 6.1.

According the figure below, the sensor is connected at the same external power unit where the CX2030 is connected in order to use the same ground in order to avoid the noise in the communications between the master device and the sensor. The external power unit provides a 24 V DC supply on both devices. In addition, from the same figure, it can be seen that a 10 kΩ is connected between the green and yellow wires of the transducer in order to reduce the calibration error and increase the accuracy of the measurements. On the other end of the CX2030, an ethernet cable is connected to the host computer in order to send the commands for the data acquisition system through TwinCAT software.

[1]Note to reader: the frame size optimisation algorithm has not been used on the experiments discussed in the following sections, nevertheless, it is a priority that should be taken into account when designing the network for the exoskeleton project of this research.

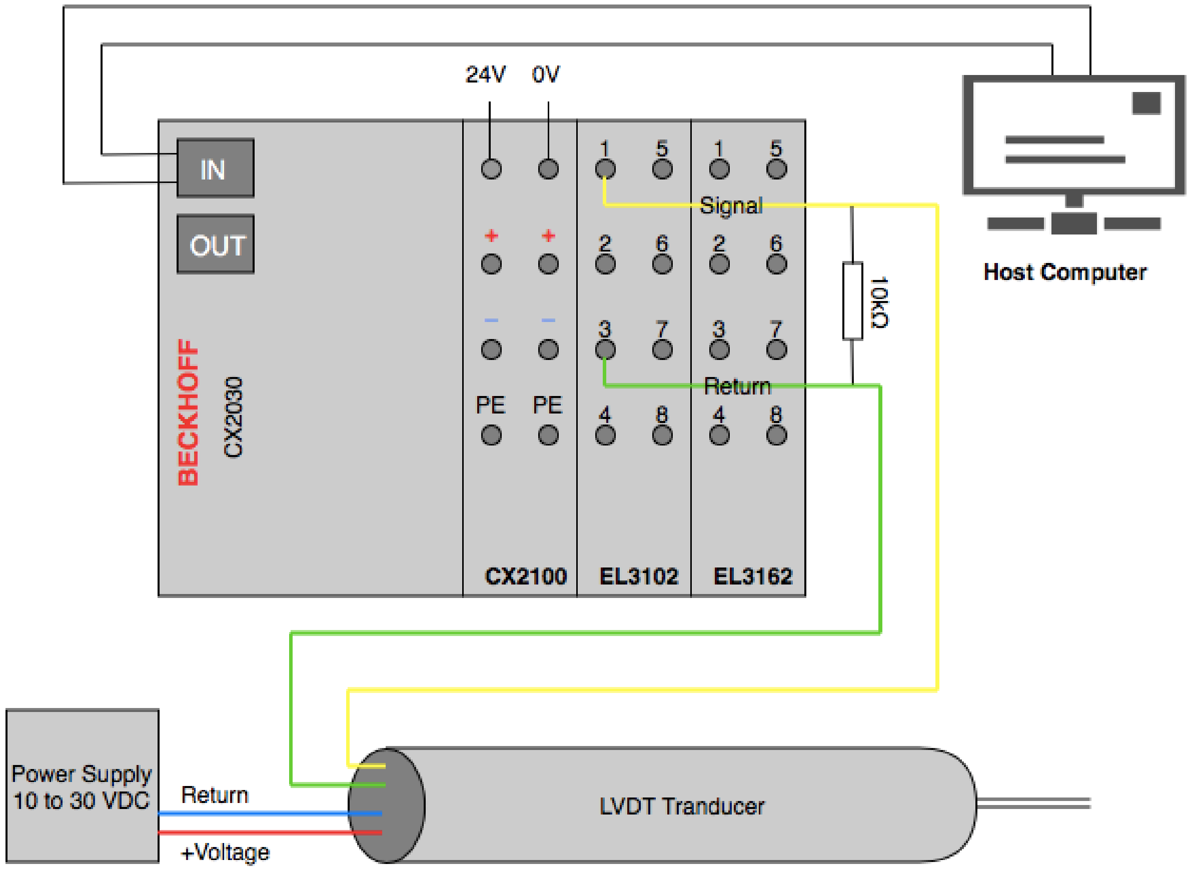

Figure 6.1: LVDT hardware connection with CX2030

6.3.1.2 Software Development of the LVDT

The software that will be used to acquire the measurements from the LVDT sensors will be developed using TwinCAT. As mentioned before, the LVDT is an analog sensor and provides analog readings in the range of ±10 V. Before moving on the part of reading the values from the sensor, a list of variable should be declared in TwinCAT, using a Global Variable list. Since the master device is reading raw values from the sensor, an analogue input variable will be declared with the name `iiAnalogueIn_1`. On the other hand, in order to provide the raw measurement values within the software, an analogue output variable will be declared with the name `iqAnalogueOut_1`. Both input and output variables will be of type `int`, which stands for ‘integer’. The declaration of the variables in TwinCAT are shown in Appendix C, section C.1, Figure C.1 (other variables included in the global variables list presented in Appendix D are used for different purposes in the project). Table 6.1 is summarising the input and output variables that used for the implementation of the LVDT sensor.

Table 6.1: Analogue inputs and outputs of the LVDT sensor

Variable	**Name**	**Type**
Analogue Input 1	iiAnalogueIn_1	INT
Analogue Output 1	iqAnalogueOut_1	INT

Due to the flexibility of the communication protocol, there is no need to define the register address of the terminal where the LVDT will be attached. EtherCAT allows to manually link the variables used to the dedicated terminals. According to [138], variable linking is the process used in TwinCAT to connect PLC variables to hardware I/O. This creates an abstract layer between PLC addressed variables and hardware/fieldbuses. This allows the PLC to connect to multiple fieldbusses at the same time. Once the variable linking process completed, then a function has been developed in order to acquire the measurements from the sensor. Since analogue terminals produce -32767 to 32767 for -10 to 10 V, there is a needs for a universal function to convert these bit numbers into real numbers. The form of the function block is depicted in Figure 6.2.

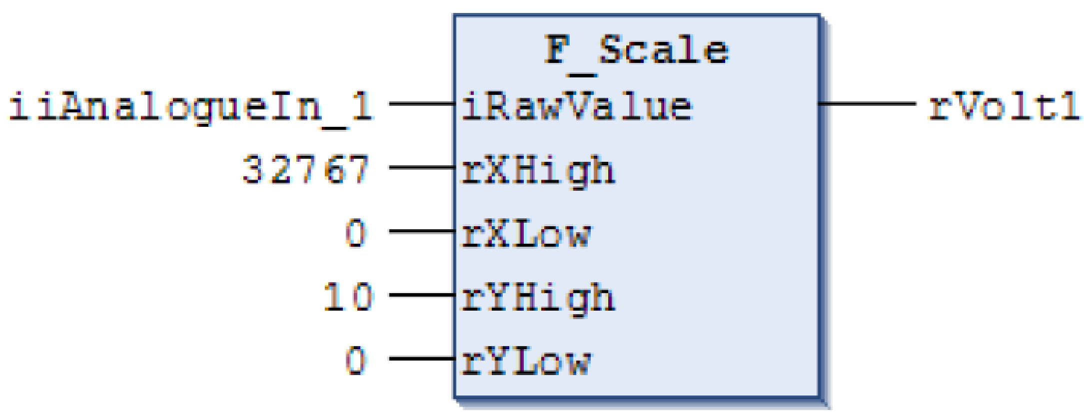

Figure 6.2: Universal function block for conversion of raw values into real numbers for LVDT experiment

Table 6.2: Variables used in TwinCAT to read the raw values from LVDT sensor

Variable	**Name**	**Type**
Raw Value Reading	iRawValue	INT
Highest Raw Value	rXHigh	REAL
Lowest Raw Value	rXLow	REAL
Highest Scale Value	rYHigh	REAL
Lowest Scale Value	rYLow	REAL

According to figure 6.2 on page 109, the algorithm of the function developed for reading the values from the sensor, shown in Appendix C, section C.1, Figure C.2 (description of each variable used included in the comments of the source code). Table 6.2 summarises the variables and their type that used to read the raw values from the LVDT sensor.

Finally, to convert the raw values of the LVDT into human readable form, a conditional statement should be used to check the real–time value of the voltage, compare it with the position of the shaft of the sensor and display the actual measurement within the software. The conditional statement used for this purpose depicted in Appendix C, section C.1, Figure C.3. The pseudocode presented below, describes briefly the conditional statement that has been used to acquire the actual distance in centimetres.

Algorithm 2 Conversion of measured voltage into position of the shaft in centimetres

Read the raw values from the EL3102 analogue EtherCAT terminal
Convert the raw analogue values into readable form (voltage)
if measuredVoltage > 0 **then**
    PositionOfTheShaft [in cm] = (10 - measuredVoltage) * 0.5
else if measuredVoltage = 0 **then**
    PositionOfTheShaft [in cm] = 5
else if measuredVoltage < 0 **then**
    PositionOfTheShaft [in cm] = (10 - measuredVoltage) * 0.5
else
    Print error message
end if

6.3.1.3 Experimental Results

Once all the above functions and algorithms are established, the implementation can be downloaded on the target/master device in order to examine the output results from the measurements. The real–time values of the variables used, can be observed in the Main Program window of the software as shown in Figure C.4.
The output results include the following measurements:

- `rVolt1` is measuring the output voltage of the sensor (can take values in the range of ±10 V);
- `Global_IO.iiAnalogueIn_1` is measuring the real–time raw values of the sensor with 16–bit resolution (can take values in the range of ±32767);

- `rLength1` is displaying the position of the shaft of the LVDT sensor in real time, based on the measured voltage (rVolt1).

Table 6.3 on page 112 presents the output results from eleven different measurements obtained by the LVDT sensor. A figure showing the output result in TwinCAT software is depicted in Appendix C, section C.1, Figure C.4

In the results depicted in Figure C.4, it can be seen that when the iron core of the LVDT (as can be seen in Figure 6.3) is placed in–between the secondary coil 1 and secondary coil 2, then the output voltage is approximately zero. Output voltage of zero indicates that the shaft of the sensor has travelled a distance of 5 cm, as can be seen from the `rLength` output value. The following diagram of Figure 6.3 is a representation of the linear relationship between the measurement range and the output voltage. It can be seen that the output voltage is inversely proportional to the measurement range. Thus, when the iron core of the sensor moves to the left, the output voltage increases while the measurement range decreases (and vice versa when the iron core moves to the right).

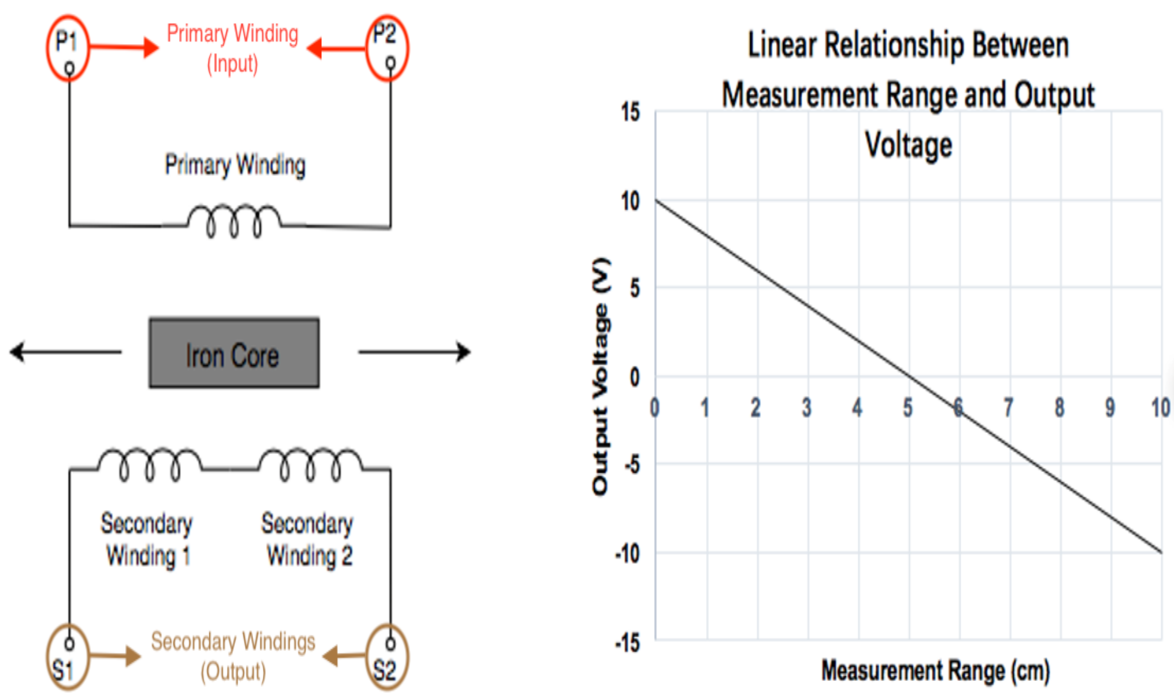

Figure 6.3: Output results of the LVDT sensor showing the output voltage of the sensor and the position of shaft in cm

The above experiments were designed based on the ideal working conditions of the LVDT, but in fact, the LVDT does not perfectly represent accurate readings. For example, as mentioned earlier, there is residual voltage at zero instead of 0 V when the core is in the middle position, the residual voltage at zero has a significant negative impact on the accuracy, causing the displacement transducer to be insensitive near the middle position.

The main cause is that there is a small residual voltage left due to factors like winding capacitance and variances in the magnetic materials. Internal or external signal conditioning electronics compensate for this residual voltage, producing a true electrical zero output.

The measurements of the distances travelled by the shaft and the output voltages recorded, are summarised in table 6.3:

Table 6.3: Expected against measured values of the voltages [V] and distances [cm] recorded in this experiment – [M] letter stands for 'Measurement'.

	Voltage (V)		**Distance (cm)**	
	Expected	*Measured*	*Expected*	*Measured*
M1	10	9.93	0	0.001
M2	8	8.07	1	0.99
M3	6	5.96	2	1.98
M4	4	4.05	3	2.98
M5	2	1.97	4	3.97
M6	0	0.00061	5	5
M7	-2	-1.93	6	5.98
M8	-4	-4.06	7	7.02
M9	-6	-6.05	8	8.03
M10	-8	-7.93	9	9.01
M11	-10	-9.96	10	10

6.3.2 Loadcell Development

6.3.2.1 Hardware Setup

Based on the analysis in section 5.4.2, the F256-Z4616 loadcell sensor produces analog output measurements in the range of 0–10 V with a resolution of 16–bits. In fact, the loadcell could produce negative voltage up to -10 V. Negative voltage can be used to measure the tension. However, the nature of this application requires only to measure the compression force. Thus, no negative voltages will be measured in the experiments that will follow. Therefore, to measure the analog signal of the loadcell, the EL3162 EtherCAT terminal will be attached on the network. In addition, since the output signal of the sensor is relatively small, an SGA (Strain Gauge Amplifier) has been used to amplify the signals received from the loadcell. The hardware connection of the loadcell and the SGA is depicted in Figure 6.4.

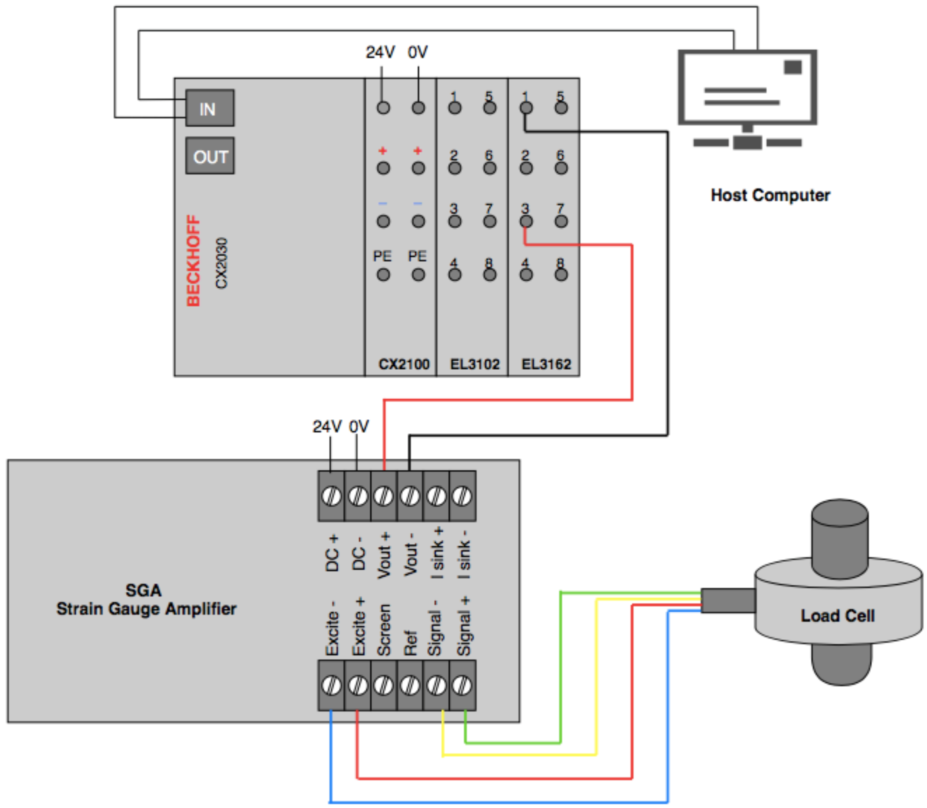

Figure 6.4: Loadcell hardware connection with CX2030 and SGA

According to figure 6.4, the SGA and the CX2030 master device, are connected to the same power source, where the grounds of the external power unit have been connected together in order to eliminate any potential noise that might be introduced to the communications. The SGA provides a ± 10 V excitation voltage for the built-in bridge circuit of the load cell. As described in section 5.4.2, the gain of the SGA has been configured at 1.99 mV/V and the cut–off frequency at 50 Hz.

6.3.2.2 Software Development of the Loadcell

The software that will be used to acquire the measurements from the LVDT sensors will be developed using TwinCAT. Before moving on to the development of the algorithm that will be used for the measurements from the loadcell, the sensitivity concept of the loadcell needs to be further examined. The results of this analysis will be deployed in the algorithm in order to provide the output results in human readable form.

In general, the sensitivity (S) of a loadcell can be described as the ratio between the output voltage and the excitation voltage when the loadcell reaches its nominal force of 1 kN under the excitation voltage of 10 V. A sensitivity of 2 mV/V means that a force transducer produces an output signal of 2 mV at nominal force, when supplied with one volt. Thus

$$S = \frac{V_{out}}{V_{ex}} = 2\ mV/V \tag{6.1}$$

According to the specifications, the excitation voltage will be

$$V_{in} = V_{ex} = 10\ V \tag{6.2}$$

and the output voltage will be

$$V_{out} = S \times V_{in} = 2(mV/V) \times 10(V) = 20\ mV \tag{6.3}$$

Therefore, by having a gain of 2 mV/V, the amplified output voltage will be

$$V_{amplified} = \frac{V_{out}}{Gain} = \frac{20(mV)}{2(mV/V)} = 10\ V \tag{6.4}$$

which is the maximum voltage that can be measured from the EL3162 EtherCAT terminal. Thus, the resolution of the force that can be measured from the loadcell, has been found to be the ratio between the maximum rated force of the loadcell and the amplified output voltage, thus

$$Resolution = \frac{1000(N)}{10(V)} = 100\ N/V \tag{6.5}$$

Finally, by taking into account the above analysis, the algorithm that will measure the force from the loadcell sensor can be developed in TwinCAT software. An approach similar to the development of the LVDT will be followed, since the loadcell is providing analog results. The developed software, will be used to translate the raw values of the measurements into human readable values. According to Figure C.1 (Appendix C, section C.1), for this experiment, the `iiAnalogueOut_2` from the Global Variable Lis is selected to represent the input data acquired from the loadcell sensor. In addition, as mentioned in the previous sections, this variable should manually be linked to the related terminal, that is to say to the EL3162 terminal where the sensor is connected. Table 6.4 is summarising the input and output variables that were used for the implementation of the LVDT sensor.

Table 6.4: Analogue inputs and outputs of the LVDT sensor

Variable	**Name**	**Type**
Analogue Input 2	iiAnalogueIn_2	INT
Analogue Output 2	iqAnalogueOut_2	INT

A function block similar to the one used for the LVDT (Figure 6.2), will also be used for this experiment. The new function block is depicted in Figure 6.5.

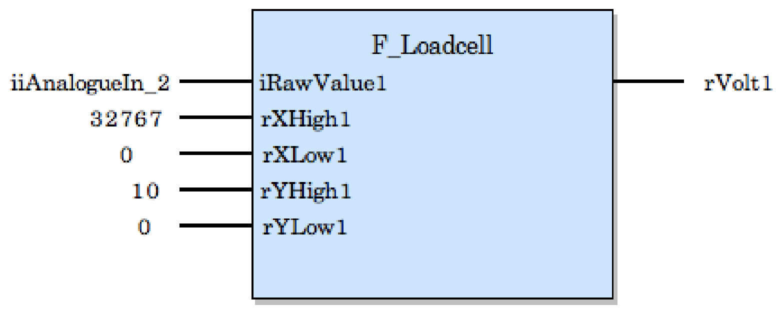

Figure 6.5: Universal function block for conversion of raw values into real numbers for loadcell experiment

Table 6.5: Variables used in TwinCAT to read the raw values from LVDT sensor

Variable	**Name**	**Type**
Raw Value Reading	iRawValue1	INT
Highest Raw Value	rXHigh1	REAL
Lowest Raw Value	rXLow1	REAL
Highest Scale Value	rYHigh1	REAL
Lowest Scale Value	rYLow1	REAL

Based on figure 6.5, since the loadcell is not providing any negative output voltages, it has been configured to measure raw values in the range of 0 and 32767 and the voltages in the range of 0 to 10 V. The real–time output voltage can be obtained by using the variable `rVolt1` of the function block. The algorithm that has been developed to read the measurements from the loadcell sensor is depicted in Appendix C, section C.2, Figure C.5.

Based on equation 6.5 in the previous page, the resolution of force measured by the loadcell has been calculated and can be used in the algorithm in order to provide the output result in terms of Newtons (N). The expression that was used to convert the real–time raw values into Newtons is the following

$$F\_force = 100 \times F\_Loadcell \tag{6.6}$$

6.3.2.3 Experimental Results

Once all the above functions and algorithms established, the implementation can be downloaded on the target/master device in order to examine the output results from the measurements. The real–time values of the variables used, can be observed in the Main Program window of the software as shown in Figure 6.6.

```
// Scale of the loadcell
rVolt1[0.0125] := F_Loadcell(
iRawValue1 := Global_IO.iiAnalogueIn_2[41],
rXHigh1 := 32767,
rXLow1 := -32767,
rYHigh1 := 10,
rYLow1 := -10);
// loadcell force
rForce[1.25] := F_force(
iRawValue1 := Global_IO.iiAnalogueIn_2[41],
rXHigh1 := 32767,
rXLow1 := -32767,
rYHigh1 := 10,
rYLow1 := -10);
```

Figure 6.6: Output results of the loadcell sensor showing the output voltage of the sensor and the measured load/force in kN

The output results include the following measurements:

- `rVolt1` is measuring the output voltage of the sensor (can take values in the range of ±10 V);
- `Global_IO.iiAnalogueIn_2` is measuring the real–time raw values of the sensor with 16–bit resolution (can take values in the range of ±32767);
- `rForce1` is displaying the force measured by the loadcell sensor in real–time, based on the measured voltage (rVolt1) and the equation used to calculate the actual measured force in terms of Newtons.

It should be mentioned that during the development, the algorithm has been developed in order to also measure the tension force; hence, measuring negative voltage. That might be used in a future implementation since there might be the need to measure the tension force of the loadcell. This configuration does not affect the performance of the communications. In order to obtain the measurements from the loadcell, an external device has been used to apply axial compression force to the loadcell. The maximum force that was applied from that device was 1.25 kN, which matches the output results shown in figure 6.6. The same value has been obtained from the force meter that is attached on the external device that applies the compression of the loadcell. Additional measurements have been obtained and it has been found that all the readings are matching the output values that have been displayed in the algorithm.

6.3.3 Absolute SSI Encoder Development

6.3.3.1 Hardware Setup

The connection of the encoder on the CX2030 is different compared to the connections of the load cell and the LVDT. The encoder is not an analogue device; thus, it should be connected to a dedicated terminal that provides the SSI interface. Therefore, the EL5002 terminal will be used for that purpose. This terminal allows the direct connection of two SSI encoders. The internal interface circuit generates a pulse for reading the encoder and makes the incoming data stream available to the controller as a data word in the process image. Various operating modes, transmission frequencies and bit widths can be permanently stored in a control register. The hardware connection of the encoder with the CX2030 master device is depicted in Figure 6.7.

According to figure 6.7 on page 118, the encoder is connected on a 5 V power supply. Any voltage above 5.5 V can damage the encoder. Apart from the power supply, the rest of the cables are connected to the dedicated terminal (EL5002), such as Clock, /Clock, Data and /Data. The clock pins are generating a pulse to read back the data from the encoder. It should be mentioned here that the (+) and (-) pins of the PSU Terminal should also be connected on the 24 V power supply. These pins will provide the power for the internal circuit of the EL5002 terminal which includes the clock for the encoder.

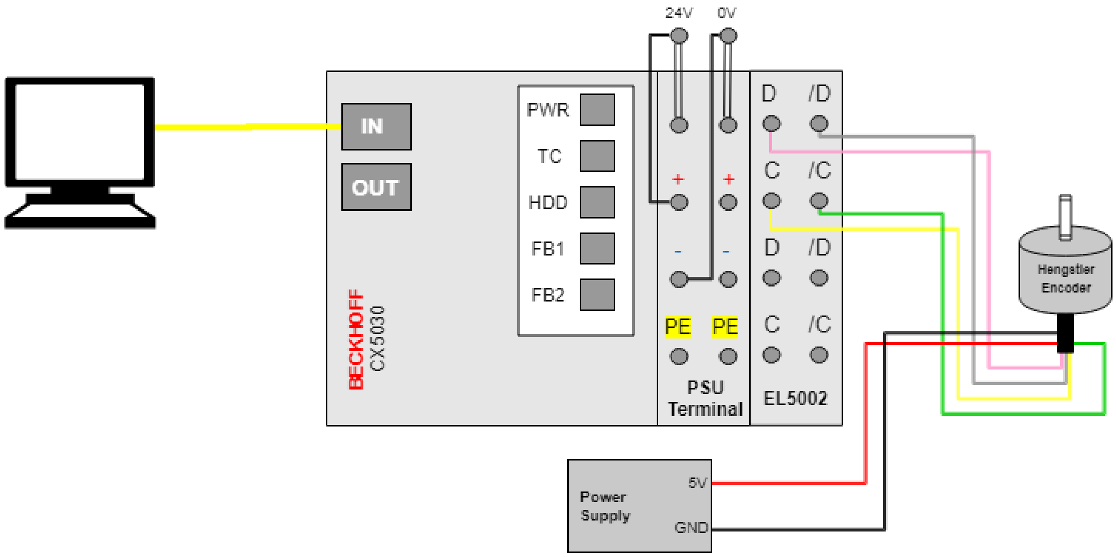

Figure 6.7: Encoder hardware connection with CX2030

6.3.3.2 Software Development of the SSI Encoder

Once all the connections established on the hardware side, the encoder should be configured using the TwinCAT software. These configurations should be done at the very beginning to ensure that the output data from the encoder will be in human readable form. First of all, a new NC task should be created within the software, in order to allow TwinCAT to recognise the encoder device. This step will allow the configuration of the SSI settings, the scaling factor of the encoder and the encoder's mask and submask. These configurations are described thoroughly below.

a. **Configuration of encoder's mask**: The parameter 'Encoder Mask' (maximum encoder value) can be used to set the maximum number of available bits. By default, this is set to 0xFFFFFFFF, which corresponds to 32 bits (20 single–turn bits and 12 multi–turn bits). The calculation is based on the following equation:

$$GM_{max} = 2^{SingleturnBits+MultiturnBits} - 1 = 2^{20+12} - 1 = (4,294,967,295)_{10} = (0xFFFFFFFF)_{16} \tag{6.7}$$

For this application, an encoder which only supports single–turn operation of size 14–bits is used. Thus, the calculation for the encoder that is used will be the following:

$$GM_{max} = 2^{SingleturnBits+MultiturnBits} - 1 = 2^{14+0} - 1 = (16,383)_{10} = (0x00003FFF)_{16} \tag{6.8}$$

b. **Configuration of encoder's submask**: The parameter 'Encoder Sub Mask' (absolute range maximum value) indicates how many bits of the maximum encoder value is single–turn bits. The default setting is 20 (and therefore 12 multi–turn bits). The calculation is based on the following equation:

$$GM_{ST} = 2^{SingleturnBits} - 1 = 2^{20} - 1 = (1,048,575)_{10} = (0x000FFFFF)_{16} \quad (6.9)$$

For this application, an encoder which only supports single–turn operation of size 14–bits is used. Thus, the calculation for the encoder that is used will be the following:

$$GM_{ST} = 2^{SingleturnBits} - 1 = 2^{20} - 1 = (16,383)_{10} = (0x00003FFF)_{16} \quad (6.10)$$

c. **Configuration of encoder's scaling factor**: The value can be calculated with the formulas specified below. The calculation is based on the assumption that one revolution corresponds to 360deg. The number of single–turn bits is taken into account in the calculation of the scaling factor. Therefore, for the calculations of the scaling factor of the attached encoder, the following formula will be used:

$$SF = \frac{distanceperround}{2^{SingleturnBits}} = \frac{360\,\deg}{2^{14}} = 0.02197265625 \quad (6.11)$$

d. **Configuration of SSI Settings of the EL5002 terminal**: The next step is to configure the SSI settings of the EL5002 terminal which will be used from the internal circuit of that specific terminal. These configurations are depicted on the Figure 6.8. The most important settings are the SSI–coding, SSI–baudrate, SSI–frame type, SSI–frame size and SSI–data length. For this part, the SSI–coding has been configured for '*Dual Code*'. Regarding the baudrate, according to manufacturer's specification, the encoder can support up to 500 kBaud; thus, it is configured to operate at its maximum frequency. For the SSI–frame size, due to the fact that the encoder is single–turn 14–bits, that setting configured accordingly at '*Singleturn 13bit*'. Finally, the '*SSI–frame size*' and '*SSI–data length*' represent the size of the data that will be transmitted on the bus. It is only 13–bits out of the total 14–bits, since the last bit is used as power failure bit.

8000:0	SSI Settings	RW	> 19 <
8000:01	Disable frame error	RW	FALSE
8000:02	Enable power failure bit	RW	FALSE
8000:03	Enable inhibit time	RW	FALSE
8000:04	Enable test mode	RW	FALSE
8000:06	SSI-coding	RW	Dual code (0)
8000:09	SSI-baudrate	RW	500 kBaud (3)
8000:0F	SSI-frame type	RW	Singleturn 13 bit (1)
8000:11	SSI-frame size	RW	0x000D (13)
8000:12	SSI-data length	RW	0x000D (13)
8000:13	Min. inhibit time[µs]	RW	0x0000 (0)

Figure 6.8: SSI settings of EL5002 EtherCAT terminal

6.3.3.3 Experimental Results

Once all the above configurations established, the implementation can be downloaded on the target/master device in order to examine the output results from the measurements. The real–time values of the encoder, can be observed in the Main Program window of the software as shown in Figure 6.9.

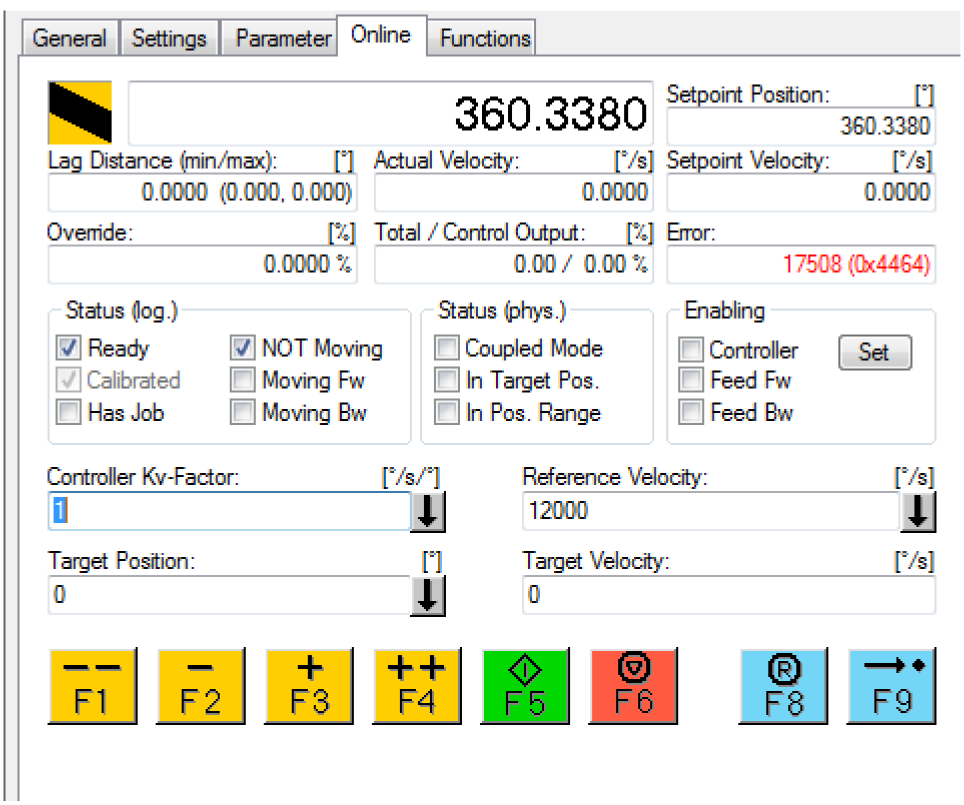

Figure 6.9: Real–time encoder measurements

According to figure 6.9 on page 120, it can be observed that there is a small error in the measurements from the encoder. That error is possibly noise that is introduced in the transmission of the data from the encoder to the CX2030 master. In a future implementation, a filter to reduce or even eliminate the noise in the transmissions, can be used and deployed in the control algorithm that will be used for the whole system.

Moreover, further measurements have been acquired in order to validate the experimental results and examine the output values from the encoder. In these measurements, different angular positions have been used in order to be compared with the measured values displayed in the software window. These measurements and their results are presented in table 6.6.

Table 6.6: Expected against measured values of the angular displacement – [M] letter stands for 'Measurement'

	Angular Displacement (degrees)	
	Expected	*Measured*
M1	45	45.03
M2	90	89.92
M3	135	135.37
M4	180	180.26
M5	225	225.45
M6	270	270.27
M7	315	315.44
M8	360	360.34

6.4 Discussion

The sensors that have been tested above, are able to meet the specifications for this project and achieve the needed performance for real–time communications. Nevertheless, since the controls algorithm has not been deployed on the communication system, it is not possible to assess the performance of the whole system. Moreover, the exoskeletal device has not been manufactured yet. Therefore, the results have been validated based on the theoretical and simulation approaches.

The first section discusses the issues occurred when experimenting with the LVDT sensor. As mentioned before, the sensor might become insensitive during some measurements, which could affect the overall performance of the communication system.

Accuracy is one of the most critical factors for sophisticated systems such as exoskeletons.

The second section presents a brief evaluation of the control algorithm when using myRIO from NI. This algorithm has been tested extensively by Napora in [123]. The discussion will critically assess the results of these experiments and the drawbacks of using low–level communication strategies.

6.4.1 LVDT Measurement Issues

The above experiments were designed based on the ideal working conditions of the LVDT, but the LVDT does not perfectly represent accurate readings. For example, as mentioned earlier, there is residual voltage at zero instead of 0V when the core is in the middle position. The residual voltage at zero has a significant negative impact on the accuracy, causing the displacement transducer to be insensitive near the middle position.

The main cause is that there is a small residual voltage left due to factors like winding capacitance and variances in the magnetic materials. Internal or external signal conditioning electronics compensate for this residual voltage, producing a true electrical zero output. It has been found that such issues could occur due to the following:

- **Fundamental Component**: Since the two secondary windings parameters of the LVDT are not completely identical, when the core is in the middle position, its equivalent circuit parameters such as mutual inductance, self–inductance and resistance cannot be exactly the same, thereby causing the magnitudes of the induced electromotive forces of the two secondary windings to be unequal. In addition, due to the resistance of the primary windings, the iron loss of the magnetic conductive material, the unevenness of the material, the existence of the winding turn–to–turn capacitance, etc., the excitation current of the primary winding is different from the phase of the magnetic flux generated.

- **High Order Harmonic**: The higher harmonic components are mainly caused by the nonlinearity of the magnetisation curve of the magnetically permeable material. Due to the effects of hysteresis loss and ferromagnetic saturation, the excitation current and the flux waveform are inconsistent in the production of a non-sinusoidal (mainly third harmonic) flux. Hence, a non–sinusoidal potential is induced in the secondary windings. In addition, distortion of the excitation current waveform will also result in higher order harmonic components in the residual voltage at zero. The zero residual voltage affects the normal operation of the circuit and even affects the measurement results of the LVDT. For an exoskeleton, a sophisticated system that requires high coupling with the human, some errors are not allowed. Therefore, it is necessary to take measures to reduce residual voltage at zero of LVDT to reduce the adverse effects caused by it. Although the zero residual voltage cannot be completely eliminated.

6.4.2 Control Strategy

The middle level algorithm described in [123] with low level coupled controller was implemented using LabView on MyRIO. The novel design of prototype with two opposing actuators connected with a knee cap was used. The joint has only one degree of freedom. Its upper link is vertically attached to the test frame. Consequently, only the lower link will be able to perform certain tasks during the tests. A static test was performed on the controller in the setup with a robotic knee attached in parallel. Next, a dynamic test, where a user displaces the joint with 60 kg load attached to it, was conducted. The results that will be evaluated are the angular displacement measure by the encoder, the bandwidth of motion and the forces measured by the loadcells attached on the hydraulic actuators.

6.4.2.1 Static Evaluation of the Controller

For the first test, there is no load attached on the prototype. The prototype is moved with the used of the hydraulic actuators which are controlled from myRIO device. For this first test it has been found that the joint has an angular displacement in the range [-14, -87.275] degrees, with an absolute value of 73.275 degrees [123]. This range of movements satisfies the requirements presented in 5.2. Further range of movements might be considered for additional tasks performed by the exoskeleton (running, squating etc.)

In addition, as mentioned before, it has been found from the motion capture study, that the bandwidth of motion should be 10 Hz for gait and at least 1.6 kHz if running is also considered as a task. From the test performed with myRIO, it can be seen that the bandwidth of motion is less than 0.01 Hz [123], which is below the required bandwidth of 10 Hz. This bandwidth also satisfies the minimum requirements for the nature of this application.

Finally, it can be seen from the experiments that during static intervals, the absolute force felt by the wearer of the exoskeleton is less than 5 N. However, when the joint is moving, it has been found that higher forces introduced, but the absolute values do not exceed 20 N. These measurements are vital in order to optimise further the controller to reduce the human–machine interaction force in the future.

6.4.2.2 Dynamic Evaluation of the Controller

To test the controller for a case where displacement is closer to normal operation (operated by a human), the test rig was adapted so that the joint was able to be moved by hand with load attached to it. Additional 60 kg of load have been used for the purpose of this test. Based on the experimental results, the angular displacement seems to be close to the range for the previous, where no load has been on the prototype joint. Accordingly, it is in the range of [-18, -82.275]. Moreover, the bandwidth of motion has been increased to 0.5 Hz, but still satisfies the required bandwidth of 10 Hz for gait.

Finally, the human–machine interaction force has been measured at 20 N when the load is attached to the prototype. However, if heavier loads are carried from the exoskeleton, the human–machine interaction force will be increased and will affect the control of the whole system. Therefore, particular attention should be paid when developing and optimising the control algorithm.

6.4.2.3 Critical Evaluation of the Controller

It was demonstrated that the prototype under governance of middle level controller with low level coupled control of hydraulic actuator enables the joint to be used in an enhancive exoskeleton governed by force control laws. It was shown that if the joint is held at constant angle, the human–machine interaction force is minimised. It was shown as well that the controller successfully governs the joint when it is displaced by a human operator and the bandwidth of motion is within the required limit of 10 Hz for gait.

Nevertheless, the controller was not able to achieve a control loop rate of 2 kHz, which is needed when considering running as a task to be performed by the exoskeleton. The results obtained from the experimental setup show that when the bandwidth is set at 1 kHz, the presence of jitter is higher when the control loop is set to a faster period. The jitter is lower when the control loop period is set to 5 ms and 10 ms. This suggests that this setup would be suitable for applications that do not require high frequency control loops. When the bandwidth was set to run at 2 kHz, the software showed a warning stating that stability is not guaranteed for frequencies above 1 kHz. Time of execution of loop iteration between 3 and 6 ms allows for successful governance, and will allow the movement with bandwidth up to 10 Hz but the application might fail if higher bandwidths need to be used.

Taking everything into consideration, it has been found myRIO device cannot provide an adequate solution for this application. The setup fails to update input values at a frequency above 1 kHz, and the presence of such jitter would cause the exoskeleton to fail. Therefore, real–time communications and fast sampling rates cannot be achieved. According to NI, for applications with higher–performance requirements such as control loops at more than 1 kHz, LabVIEW FPGA Module should be used with Scan Mode. In this case, it is necessary to assemble the network with NI EtherCAT slaves (NI-9144), because these devices have on–board FPGA, which allows the use of 40 MHz clock, enabling the accomplishment of faster sampling rates. Although, such devices might add extra weight on the exoskeleton and limit the space for other electronics and components that need to be used for the on–board communications.

6.5 Summary

This chapter has presented the results obtained from the experiments when using EtherCAT protocol and CX2030 embedded PC to interface the sensors that are used by the exoskeleton. The implementation priorities that have been set are discussed prior to the experiment. The hardware setup of the sensors along with the software implementation in TwinCAT covered. To ensure the accuracy of the measurements, configurations should be done on each EtherCAT terminal. Although the experimental results from the LVDT and encoder sensors were of high accuracy, it was shown that for the loadcell an SGA amplifier should be used to amplify the output signal received from the sensor.

Moreover, it was demonstrated that the controller allows for operation with bandwidth of joint angular displacement up to 0.6 Hz. Further test are required to determine if the joint is able to follow gait, that is input signal with bandwidth up to 10 Hz. The required sampling rate of 2 kHz was achieved by configuring the communication cycle time at 500 μs. A critical evaluation of the control strategy developed for this project is presented at the end of this chapter. The results of this analysis were used to estimate the communication cycle time of the system that will be used for the final design of the exoskeleton. Based on this approach, it has been deemed that the communication cycle between all slaves and the master can occur in 33.68 μs, which in theory means that 93% of the control loop time can be available for the master to compute the algorithms deployed.

Section II - Power Systems

Chapter 7

Potential Power Sources Suitable for the Exoskeleton

7.1 Introduction

An increasing demand for energy has been reported over the past years for power–hungry applications such as exoskeletons. Conventional power sources such as fossil–fuel and environmental concerns are driving forces toward renewable and wireless power transmission energy sources. Moreover, gas, oil and coal energy sources are being depleted quickly and their reserves are becoming insufficient and intended for future use. In addition, due to greenhouse gas emissions these energy sources are environmental unfriendly. Thus, renewable energy sources are becoming more essential over the years.

Full–body exoskeletons usually have high hydraulic and electrical power requirements to perform certain tasks and ensure the energetic autonomy of the robot. Hydraulic power is used for locomotion of the joints and, in general, of the whole exoskeleton by moving the actuators and electric power is essential to deliver adequate amount of power for the on–board electronics, such as sensors, microprocessors and other peripheral devices. At the same time, the power source that will be used by exoskeletons should be lightweight. In addition, safety of the user is another important factor that should be considered. Exposure in various safety hazards, such as electrocution or electric shock, potential explosion of fuel, emitting radiation and CO2 emissions could pose a risk to user. Therefore, there is a great need for developing a compact power system that will meet the power requirements of the robot. Furthermore, a standalone and self sufficient power system for exoskeletons is an essential factor that should be considered in order to achieve longer times of operation and especially when exoskeletons are utilised in remote environments. Thus, a portable power source can be used to provide a feasible and reliable solution.

This chapter outlines the widely adopted power sources that can be used by exoskeleton. In section 7.3 conventional power sources, such as non–rechargeable primary cells, internal combustion engines and solar panels, are analysed and performance metrics are presented. Section 7.4 is reviewing the potential energy harvesting technologies that could be used for the exoskeleton examined in this project and previous related work is also presented to evaluate their suitability. Section 7.5.1 examines the wireless power transmission technology along with the methods and implementation techniques that can be used to develop a WPT system. The near–field technology is evaluated in terms of transfer efficiency, distance and frequency of operation. The chapter concludes by reviewing the limitation, challenges and safety concerns when using wireless power transmission systems in line with humans.

7.2 Widely Adopted Power Sources for Exoskeletons

Among the developments described in the previous chapters, the most critical are power supply systems to allow the new electronic–based equipment to function effectively for activities up to 72 hours (or more) in length. This challenge requires several different approaches. Power and energy systems should be considered as a solution. Power systems include the energy sources and sinks as well as energy management and control. Therefore, adequate power is needed for the electronics and the on–board communications of the exoskeleton, in order for the systems to be able to operate smoothly.

Apart from the communications and electronics, several other applications for the exoskeletal device require portable energy. Such applications include sensors, motors, encoders, embedded computers and hydraulics. In addition, in order for an exoskeleton to be effective, the electronics are critical. Nowadays, batteries are able to provide the adequate energy and become the main power supply for the exoskeleton. However, there are many different types of power sources that should be considered in order to effectively power up an exoskeletal device. The power sources and solutions that will be discussed in the following sections are summarised in the following:

a. Traditional power sources

- Non–rechargeable primary cells
- Internal combustion engines
- Electrochemical fuel cells
- Tethered solutions

b. Energy harvesting technologies

- Thermoelectric devices
- Regenerative breaking
- Piezoelectric devices
- Solar panels (PV–cells)

c. Wireless Power Transmission (WPT) technologies

- Near–field
- Far–field

7.3 State of the art and Current Challenges

One of the main challenges when designing an exoskeletal device is the successful delivery of power to all devices that need electrical charge to operate smoothly. Even though there are many power sources nowadays of sufficient energy density to sustain a full–body exoskeleton, the amount of operation time for portable solutions is limited. This is due to the high energy needs that an exoskeleton requires for the actuators and the on–board electronics.

Currently, there are few power sources that are capable of delivering sufficient amount of energy to operate an exoskeleton for up to few hours. These power sources are, basically, portable and can be carried by the wearer of the device. Some of the most advanced solutions that can be used delivering power to the exoskeleton are outlined below along with the disadvantages of using each solution.

7.3.1 Non-Rechargeable Primary Cells

As stated in [139] "*Non–rechargeable primary cells tend to have more energy density and store it longer than rechargeable secondary cells, but then replacement cells must be transported into the field for use when the primary cells are depleted, of which may be a special and uncommon type*". In addition, rechargeable batteries could be used as an alternative technology. However, this solution may be insufficient due to the fact that a rechargeable station should be carried from the wearer that must rapidly recharge the batteries. On the other end of the spectrum, in case that a rechargeable station is not available, then depleted cells should be able to replace the existing batteries that have been slowly charged [139].

Primary cells could be important when charging of the battery is impractical or impossible due to environmental constraints, such as for exoskeletons deployed in the military field. In addition, devices such as pacemakers are using primary cells in order to provide sufficient energy in the long term. High specific energy, long storage times and instant readiness are the key factors that make the primary cells a potential solution for several different applications. Figure 7.1 represents the comparison between primary and secondary batteries in terms of the energy that can be stored and delivered.

The performance of the batteries depends on the chemistry that is used to manufacture them. There are many different chemistries that can be used when designing batteries. The chemistries that have been used to manufacture batteries, are capable to differentiate the energy characteristics of the cell and provide a sufficient solution for several applications. For non–rechargeable cells, alkaline and lithium primary can be used. On the other hand, for rechargeable cells, lead acid, NiMH and Li-ion chemistries can be used. Figure 7.2 illustrates the performance of batteries with different chemistry.

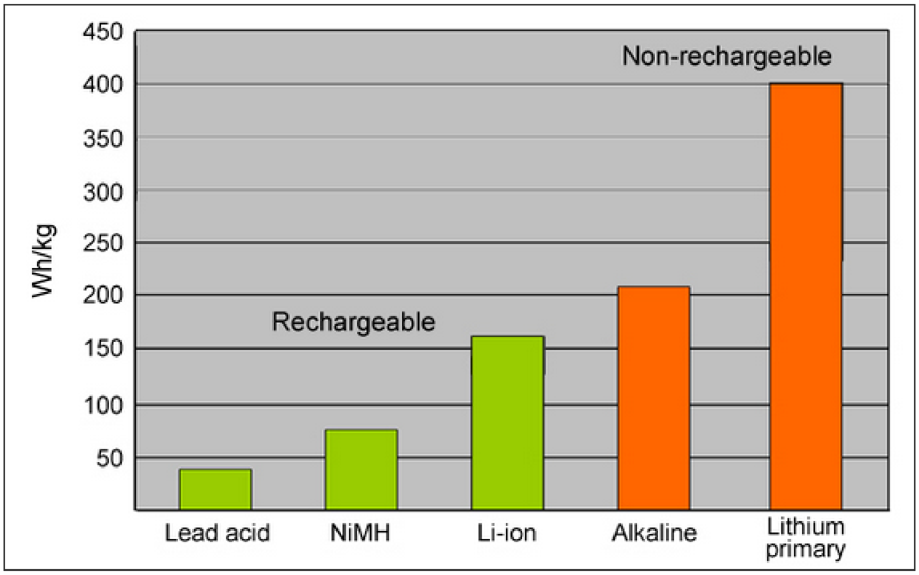

Figure 7.1: Primary and secondary cells comparison [140]

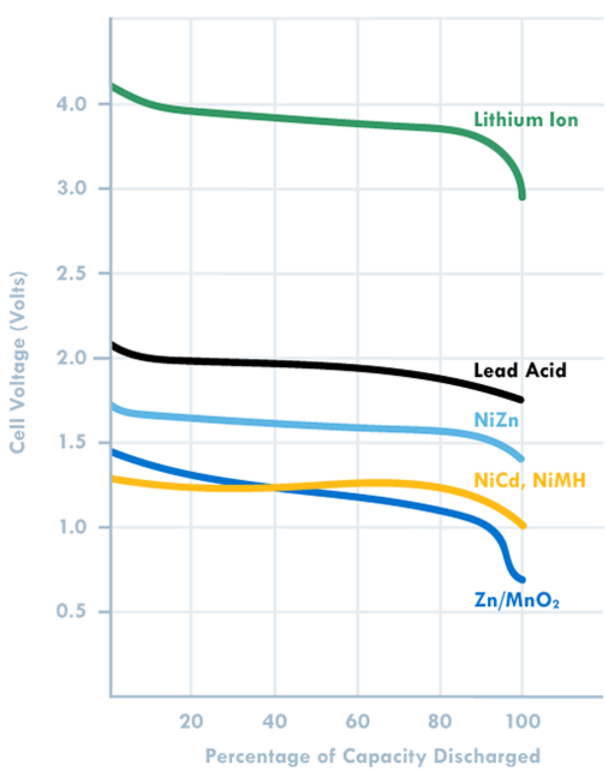

Figure 7.2: Voltage plot based on battery chemistry [140]

Another factor that should be considered is the energy that can be stored in the battery and the power that can be delivered when the battery operates under normal conditions. Both aspects are dependent on the chemistry that is used by the cell. In addition, temperature of the battery should also be monitored in order to ensure the stability of the whole power system.

7.3.1.1 Advantages

Using primary cells can have many advantages depending on the application. Firstly, the energy density of a primary cell is high and there is no need to compromise the design of the power system to accommodate recharging. Moreover, it is found to be the most promising technology for low cost and low drain applications since they can be replaced easily or removed from the power system to be charged on a charging station. For applications that require a single use of the battery, such as military missiles, primary cells are the most suitable solution. Low cost, convenience and wide availability are making primary batteries a suitable alternative for basic applications.

7.3.1.2 Disadvantages

On the other hand, primary cells are not suitable for power–hungry applications, such as exoskeletons. The short life time and the cost of continuous replacement are making them unsuitable for high drain devices. In addition, the overall efficiency is a factor that should be considered when using non–rechargeable batteries since they can only produce 2% of the power that is used during the manufacturing process. Finally, more waste is produced when disposing non–rechargeable batteries which could pose an environmental risk.

Taking everything into account, non–rechargeable primary cells can only be used when the power requirements are not that high. Based on the power requirements of this project, exoskeleton is a device that drains a lot of power to perform certain tasks. Thus, primary cells could be highly efficient when using them only for the on–board electronics of the exoskeletal device, since the energy load has been found to be between 20 and 150 watts.

7.3.2 Internal Combustion Engines

Internal combustion (IC) engine power supplies offer high energy output. However, the fuel consumption continues even when they are idle or operating at low power levels.

On the other hand, the solution of engines that do not idle is possible, although there is a great need for energy storage for a starting system that will be able to rapidly accelerate the engine to full operating speed. Apart from that, such solution should be extremely reliable so that the engine will not fail to start up immediately [139].

Utilisation of standalone and highly efficient power systems in hydraulic–based robots is essential nowadays to maintain a sustainable operation. Power sources that are capable of generating both hydraulic and electrical power could be capable of fulfilling the energy requirements of a device such as exoskeleton. The hydraulic power will be used from the actuators and the electrical power can be used for the on–board communications and, in general, for the electronics that are attached to the exoskeletal device. In the past, it has been seen that Kazerooni et al. [1] have developed a hydraulic–electric power unit (HEPU) that was able to deliver 2.3 kW of hydraulic power and 220 W of electric power at 15 VDC. Their design of the HEPU was capable to deliver a sufficient amount of power that was needed from BLEEX to operate smoothly. The IC had a weight of 27 kg (without fuel on its tank). There are no reported attempts to measure the overall weight of the IC when the tank is full, which could affect the performance of BLEEX since more weight needs to be carried by the device.

Specifications of ICs vary depending on the application. This research focuses on robotics applications and more specifically on human wearable robotics such as exoskeletons. Kazerooni et al. in [1] have presented four different versions of internal combustion engines that can be used for exoskeletons to provide hydraulic and electric power. The main specifications of these ICs are summarised on table 7.1.

Table 7.1: Performance Metrics of Four Different Versions of Internal Combustion Engines Presented in [1]

Specifications/Generation	**1st Generation**	**2nd Generation**	**3rd Generation**	**4th Generation**
Engine	Honda GX31	Honda GXH50	Fuji BT50SA	ZDZ-80
Hydraulic Power	750	1 kW	1.1 kW	2.3 kW
Electrical Power	120	100 W	120 W	220 W
Efficiency (%)	16	13	6	8.1

7.3.2.1 Advantages

Using ICs for robotic applications can have many advantages. First of all, the ICs have a really small size when comparing them with the external combustion engines. In addition, they are safer to operate and they can be used for applications that do not have high power requirements. Their portability is also making them a suitable alternative solution to deliver the required amount of power. Finally, the efficiency can be higher than their counterparts and they do not need frequent maintenance, which explains why the overall cost could be decreased.

7.3.2.2 Disadvantages

Although the internal combustion engines are a highly efficient solution for autonomous robotics, there are many factors that should be considered when designing or using an IC. For example, in order for an engine to provide sufficient power to the exoskeleton, it should, typically, operate at high speed which will introduce higher vibration and sound levels. Such effects could be undesirable when operating the exoskeleton. In addition, depending on the weight of the IC, the fuel consumption could be increased which will increase the overall cost of the system when operating under normal conditions. Furthermore, when the engine is working in high revolutions it will become extremely hot. Therefore, a cooling system should also be attached to the exoskeleton, which, on the other hand, will increase the overall weight. Finally, particular attention should be paid to the safety regulations of operating a fuel engine either indoors or outdoors. For indoor applications, the safety regulations are very strict due to the aforementioned factors, such as noise, fuel consumption, gas emissions, high temperatures and many more. Thus, these factors make it virtually impossible to use an IC for robots that will be used mainly indoors. On the other hand, devices that will be used outdoors could deploy ICs since the safety regulations are not that strict. Most of the exoskeletons that are deployed for military purposes, are using fuel engines to extend the time of operation and provide a more efficient system when using the device under several different environmental conditions. Nevertheless, use of ICs on the battlefield could, also, pose a safety risk since fuel is a highly flammable substance that can cause explosion during combat.

7.3.3 Electrochemical Fuel Cells

Another solution that should be considered as a potential source of power is the electrochemical fuel cells such as Solid Oxide Fuel Cells (SOFCs), Alkaline Fuel Cells (AFCs), Molten Carbonate Fuel Cells (MCFCs) and many more. It could be considered as one of the most efficient solutions since it could provide instantaneous energy like batteries and conserve the fuel source when not needed. The refuelling process is easy to be performed with liquid such as methanol. Although, the normal operating temperature of a SOFC is around 600 °C which makes compulsory the use of a cooling system [139, 141]. Table 7.2 summarises the most known electrochemical fuel cells along with the performance metrics.

Table 7.2: Performance Metrics of Well Known Electrochemical Fuel Cells

Type of Fuel Cell	Output Power (W)	Temperature of Operation (°C)	Efficiency	Application
Alkaline Fuel Cells (AFCs)	10 - 200 kW	∼80	∼65%	Commercial & Research
Solid Acid Fuel Cells (SAFCs)	10 W - 1 kW	200 - 300	∼50%	Commercial & Research
Molten Carbonate Fuel Cells (MCFCs)	100 MW	∼650	∼60%	Commercial & Research
Tabular Solid Oxide Fuel Cells (TSOFCs)	∼100 MW	∼1000	∼65%	Commercial & Research

7.3.3.1 Advantages

Fuel cells are sharing some common characteristics with the combustion engines due to the fact that they rely on electrochemistry to operate. The fuel cells could be used from devices that convert electrochemical energy into other forms of energies that needed to be used by the robotic devices. Therefore, fuel cells can combine the advantages of both engines and batteries [142]. First of all, the fuel cells has been found to be more efficient than combustion engines since they are able to produce electric power directly from chemical energy. Another factor that should be considered when examining the advantages of the fuel cells is their solid form, which means that there are no parts that are moving under normal operation of a robot. With solid fuel cells, vibrations that are produced from combustion engines could be eliminated and the noise could be reduced when operating under normal conditions [142, 143].

Further to the advantages of the electromechanical fuel cells is the independent scaling between power and capacity. On the other hand, batteries, usually, provide limited capacity and power which are configured during the manufacturing process. When the energy requirements are high, performance of the batteries is poor. Instead, fuel cells can perform better even in the megawatt range (power plant). In addition, fuel cells provide higher energy densities and can be used continuously by refuelling. On the other side, batteries need to be replaced or recharged, a process that could be time consuming and costly [142, 144].

7.3.3.2 Disadvantages

On the contrary, apart from the aforementioned advantages of using fuel cells, there are some serious disadvantages that should be considered when using them in robotics applications. The first and the most important disadvantage is the cost that was introduced when implementing fuel cells. This is a major barrier for fuel cells and it has been seen that it could mostly be used for highly specialised applications (such as spaceships). Another factor that should be considered is the power density of the fuel cell. Even though the power density of fuel cells has been increased over the years, it has been found that it is highly inefficient to use them for portable or automotive applications [141].

Moreover, another limitation introduced from using fuel cells is the fuel availability and the storage process. Hydrogen gas appeared to be the most efficient solution when using fuel cells, although it is a fuel that has high cost, is not widely available and it is difficult to store [145]. Other alternatives that can be used are gasoline, methanol and formic acid, though they cannot be used on their initial form and they require chemical processing before using them for the fuel cells. Thus, such issues with the previously mentioned fuel alternatives could affect the overall performance of the fuel cell.

Lastly, when working with fuel cells, high temperatures will be introduced to the system. In order to operate a fuel cell smoothly, the cooling system is an essential requirement to avoid the potential risk of explosion and meet the safety regulations. In addition, gas emissions should be taken into consideration when consuming fuel, since the emissions could be poisonous and put the operator's health at risk.

Taking everything into account, it can be noticed that electromechanical fuel cells are one of the most efficient solutions. There are many advantages of using them for robotic applications and they are able to provide sufficient amount of energy for an exoskeleton. Nevertheless, there are potential risks and limitations that should be considered and, according to the literature, it will not be easy to overcome the challenges of using fuel cells.

7.3.4 Tethered Solutions

According to the previous chapters, the energy requirements of the exoskeleton examined in this research, are high and could reach the range of a few kilowatts. Hence, stable and continuous delivery of power is essential. A tethered solution would be an efficient and reliable solution for robotics applications. For a long time, tethers have been extensively used in various areas including under–water, ground and aero–space environments.

There are many advantages of using tethered solutions. First of all, there is the continuous power supply through the tether. For robotics deployed in the field, this could be essential for providing sufficient amount of power. Robots can have further endurance and last longer than systems using batteries as power source. In addition, the size of the robot can also be reduced since there is no need to develop an on–board power supply, thus it will be more lightweight and could move more efficiently in narrow spaces [146].

Since tether can be a sophisticated physical link in form of cable, it can also be used in the means of communication between the exoskeletal device and the base station. Moreover, tether can also be utilised to as a medium to supply the hydraulic fluids that are needed by the actuators. Accordingly, communications, power and hydraulic fluids can all be included in a single cable that will be attached to the robot. In addition, wired communication link will provide a more reliable solution by reducing the risk of missing data during the transmission process [147].

On the other hand, when using a tethered solution, there are a few drawbacks that need to be considered. Distance of travel could be one of these, since the tether might have limited length, thus the robot will not be able to operate for longer distances. Also, in the case that one of the links (communication, power or hydraulics) fail, it will be difficult to detect the malfunctioning part since all of the above links are wrapped in a single cable that is attached to the robot. In such case, the whole cable should be disassembled or replaced by a new one, a process that could be time consuming and increase the cost of the project. Another disadvantage is the wiring complexity of the physical link, which is, usually, undesirable for robots such as exoskeletons.

Taking all the above into consideration, tethered solution has been seen to perform well for exoskeleton projects, such as Raytheon XOS–2 [19], and is able to provide the required amount of power that is needed by the device. For the individual research, tethered option has been considered as a back–up solution in case that the wireless power transmission (WPT) fails to meet the energy needs of the exoskeleton. The table on the following page summarises the pros and cons of the power sources examined above.

Table 7.3: Summary table of Pros and Cons for Non-Rechargeable Primary Cells, Internal Combustion Engines, Electrochemical Fuel Cells and Tethered Solutions

Pros and Cons/ Power Sources	**Non-Rechargeable Primary Cells**	**Internal Combustion Engines**	**Electrochemical Fuel Cells**	**Tethered Solutions**
Pros	-High energy density -Can be replaced easily -Can be removed easily for recharging -Suitable for standalone applications -Fairly low cost	-Small size compared to external combustion engines -Safer operation under normal environmental conditions -Portability -High efficiency -Do not require frequent maintenance	-High efficiency -Low vibration and noise levels -High performance compared to primary cells -High energy density -Solid form	-Continuous supply of power -Low cost -Lightweight -High efficiency
Cons	-Not suitable for power hungry applications -Short life span -Low efficiency (approx. 2%) -Environmental risk when disposed	-High noise and vibration levels when operate at high speeds -High operation temperatures -Increased cost of fuel -Virtually impossible to use for indoor applications -Fuel is highly flammable and can cause explosion -CO2 emissions	-High manufacturing costs -Low efficiency for automotive and portable applications -Low fuel availability -Limited storage/stock -High operation temperatures -CO2 emissions	-Reduced distance of travel due to limited length of the tether -Wiring complexity of the physical link -Difficult to detect malfunctioning parts

7.4 Energy Harvesting Technologies

An alternative solution to overcome the challenges of using the aforementioned power sources, such as internal combustion engines, electromechanical fuel cells and batteries, is the energy harvesting. The approach of scavenging energy from human motion, temperature change and sunlight, can provide a more efficient solution to deliver power to the instruments, components and electronic devices used by the exoskeleton. In the past, energy harvesting solutions have been used effectively for several applications, such as solar–powered calculators and electronic self–winding wristwatches. Thus, it has been found that scavenging energy from different sources can provide an alternative solution for delivering power to electronic devices and replace batteries or any other source of energy, depending on the application requirements.

Energy harvesting technology has been deployed successfully for several years to extract energy from different sources, such as wind and water. Wind turbine farms and hydroelectric plants have been used extensively to provide a reliable solution to the increasing energy needs both for robotics and commercial applications. Another example of the extensive use of energy harvesting solutions nowadays is the generative braking that is used is hybrid and electric cars to generate power and charge the on–board batteries when the car is braking.

Another remarkable solution of extracting energy are the solar panels which can help to collect the sunlight and convert it into electrical power. Solar power scavenging has been found to be one of the most reliable and efficient solutions, depending on the application and the weather conditions. Solar panels that have been used to supply power for industrial applications, are capable of delivering power in the range between watts and up to a few megawatts.

Thermoelectric devices and piezoelectric sensors can also be used to harvest energy from human motion and vibrations. However, when using thermoelectric devices to extract energy, the high amount of energy that is released to the environment needs to be considered. Therefore, there is an increasing need to develop and manufacture new devices that will harvest energy more efficiently and reliably. On the other hand, piezoelectric sensors are capable of providing a small amount of energy that would be sufficient for the on–board electronics of an exoskeleton.

Considering all the previous solutions for scavenging energy, there are also limitations and challenges that need to be taken into account when using each technology or a combination of them on a hybrid system. Each solution is discussed in the following sections along with previous related work and experiments conducted from other researchers. In addition, the challenges of using the aforesaid technologies are outlined and discussed briefly at the end of this chapter.

7.4.1 Thermoelectric Devices

For the past decade, technology has been linked closely to the human body and to the methods of how to extract several different readings that could be processed from small wearable devices and provide a report for specific measurements from the human body. In addition, small wearable device do not need high amount of energy to operate or charge their internal batteries. Consequently, technology has started focusing on the methods on how to extract energy from the human body and use it for the wearable devices.

Based on the literature, an average person needs between 2000 and 2500 calories per day under normal conditions. The amount of energy that is used by the human body is approximately $1.07*10^7$ joules per day [148]. This amount of energy can be produced from body fat which, in turn, is coming from the food consumed during the day. The food contains several different nutrition sources from which the human body is capable of extracting sufficient amount of energy to 'operate' during the day. In addition, under certain weather conditions or when someone is working out (e.g. jogging, lifting weights, walking etc.) the body is releasing the energy to environment in the form of heat. Thus, there is a considerable amount of energy that can be harvested from the human body by using thermoelectric devices to capture the heat dissipated. There are many challenges that need to be considered when developing such devices, which will have a minimal interference with the natural functions and will not limit the motions of the human body.

Based on Winter at [149], the amount of mechanical energy that the human body is producing is between and 15% and 30%; thus, the rest of the energy produced from the food consumption is dissipated into the atmosphere in the form of heat. Therefore, a device that will be able to harvest/capture this energy and convert it into electrical energy, would help to power up small electronic devices, such as smartphones, smartwatches etc. When developing such device, the maximum efficiency that the device is able to provide needs to be considered, in order to estimate the total amount of power that can be harvested. By using Carnot's equation the efficiency of a device that converts heat into mechanical energy can be calculated. The optimal efficiency can be achieved at the environmental temperature of 0^oC.

$$efficiency = \frac{T_{body} - T_{ambient}}{T_{body}} \tag{7.1}$$

In equation 7.1, T_{body} is the normal temperature of the human body (37^oC = 310 Kelvin) and $T_{ambient}$ is the environmental temperature (0^oC = 273 Kelvin). In addition, the conversion of heat into electricity is dependent on the efficiency of the thermoelectric materials that will be used. That efficiency can be calculated by using the following equation [150].

$$\mu = \frac{\Delta T}{T_h} * \frac{\sqrt{1+ZT} - 1}{\sqrt{1+ZT} + \frac{T_c}{T_h}} \tag{7.2}$$

In equation 7.2, μ is the efficiency of the device, T_h is the hot temperature, T_c is the cold temperature, ΔT is the difference between hot and cold temperatures ($\Delta T = T_h - T_c$) and ZT is the figure of merit for the device [150]. In addition, the figure of merit varies when using different thermoelectric materials. A typical value of the figure of merit for thermoelectric generators is approximately ZT $\approx$ 1. During the past years, only small improvements have been applied to thermoelectric generators in order to increase the figure of merit [151]. Therefore, it is obvious that by developing new materials with higher figure of merit, the overall performance of the thermoelectric generators can be increased.

Moreover, the efficiency of the thermoelectric device can also be affected by the environmental and body temperatures. Therefore, the efficiency will be higher when the difference between the two temperatures is greater and vice versa. Based on the Figure 7.3, page 143 and equation 7.2, the efficiency of a device with a ZT=1 and at an environmental temperature of 0^oC is 2.2%. It can, also, be observed that when the temperature decreases and/or the figure of merit (ZT) increases, then the efficiency is higher.

Another factor that should be taken into account when implementing a thermoelectric device to capture energy from human body is the mechanisms through which heat is lost when dissipated to the environment. These two mechanisms are known as heat transfer and heat loss (sensible heat and latent heat, respectively). It should, also, be mentioned that the thermoelectric devices are able to capture only the sensible heat and convert it into electricity.

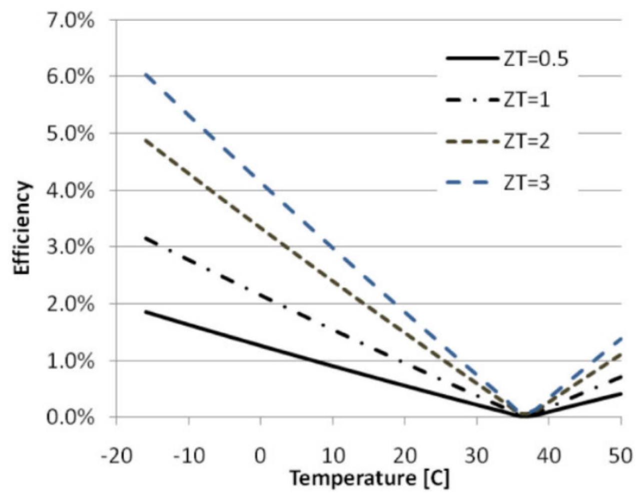

Figure 7.3: Efficiency of thermoelectric generator under different environmental temperatures [152]

According to [148], the heat that is released into the atmosphere in the form of heat during normal walking is around 100W. Therefore, based on Figure 7.3 and equation 7.2, a thermoelectric device with an efficiency of 2.2% can provide approximately 2 W of electric power that can be stored or used for other electronic devices. Although, in order to capture this small amount of energy, there are many parts of the human body that need to be covered using specific thermoelectric materials. Covering the whole body with a thermoelectric suite will, also, be a challenge that needs to be addressed. Therefore, considering all the above results and the challenges that are introduced when developing thermoelectric devices, it can be concluded that such methods and technologies would be more efficient for low power applications where the energy requirements are not that high.

7.4.2 Regenerative Braking

In the recent years, regenerative braking has been used extensively in automotive industry and, more specifically, in hybrid and electric vehicles. It is a technique that is used to capture energy from the vehicles kinetic energy, convert it back to electrical energy or store it in storage devices, such as batteries, ultracapacitors and ultrahigh–speed flywheels [153–155]. The energy in the storage devices can be used again in order to move the vehicle and it is called "regenerative" due to the fact that the energy can be captured and used again. On its early stage, regenerative braking technology had an efficiency ratio between 45% and 55%. For the energy needs of the first electric cars that have been deployed, that seemed to be a sufficient amount of energy to be generated and stored at the on–board batteries. However, since then, the technology has been advanced and today the EVs that are deploying this system have an efficiency of at least 66% by optimum use of the available technology [155]. Back in 2007, Tesla has been shown that one of its first EV models, the Tesla Roadster, was able to use the regenerative braking system with a net efficiency of at most 64% [156]. Van Sterkenburg et al. [157] through their simulations on a simple regenerative braking system have shown that the system is able to provide a maximum efficiency of up to 85%. The efficiency they achieved is dependent on the operating conditions and depicted in Figure 7.4. Another interesting study has been presented by Serkan et al. in [158], where the efficiency of their system was able to achieve a surprising ratio of 94.1%. Although the simulations are very promising for achieving high efficiencies, under real world conditions, the efficiency of regenerative braking system can reach an average level between 80% to 85% [159].

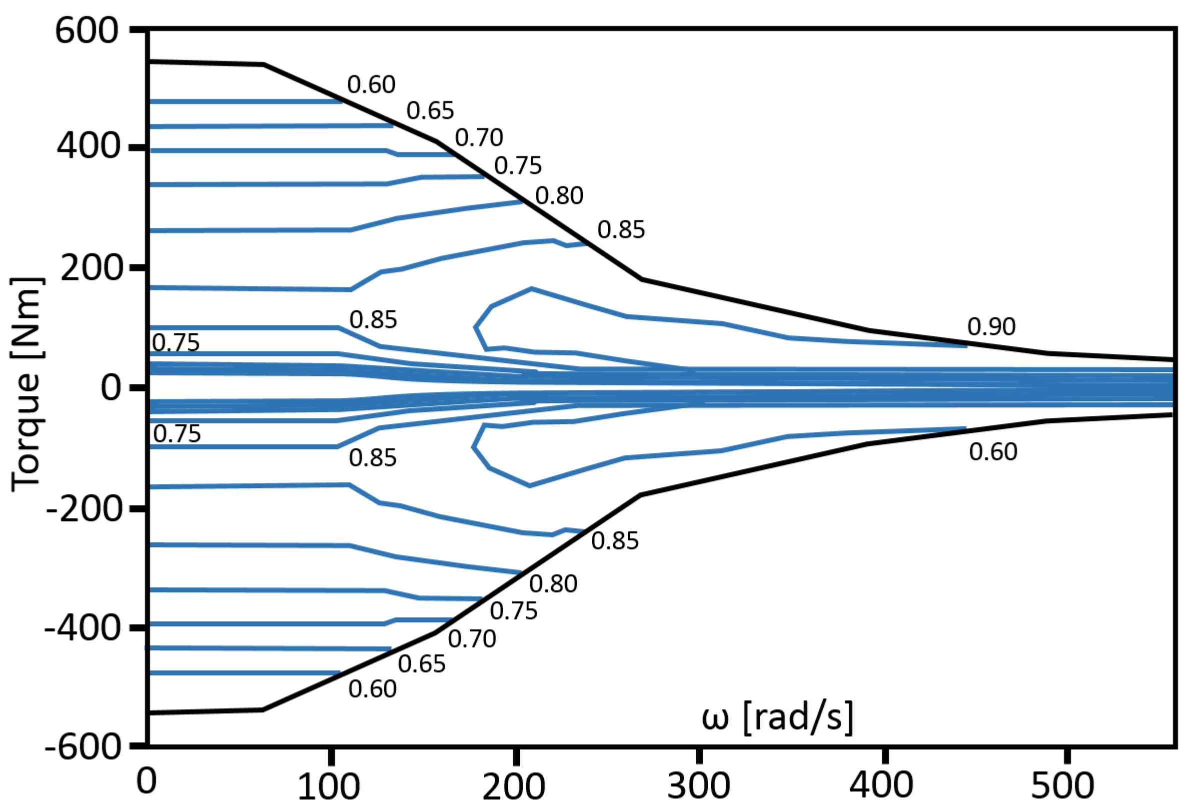

Figure 7.4: Efficiency of the combination of given electric motor and inverter [157]

Therefore, regenerative braking technology can also be used in this project to harvest energy from human motion. Mechanical energy that is produced from human motion can be converted into electrical energy and used by the on–board electronics. In order to use the generative braking to extract energy from human motion, the following main factors must be considered:

- Positive Work Phase where the muscles of the human body generate the motion when performing positive mechanical work

- Negative Work Phase where the previously produced energy is absorbed and act as brakes to stop the motion when performing negative mechanical work

In [149], Winter has described the two aforementioned phases as follows:

- Positive Work is the work performed when the muscle is shortened (known as concentric contraction) and the use of positive energy will increase the metabolic cost

- Negative Work is the work done when the muscle is lengthened (known as eccentric contraction) and the muscle torque acts in the direction opposite to the angular velocity of the joint

In this manner, during the negative work of the muscle, a device that will create resistance and produce energy, could be placed. Such device will use the generative breaking technology and, theoretically, will not limit the natural motions of the joints. The idea for deploying such device is that during the negative work of the muscle, an electric generator can be used in order to reduce the load on the muscle and, at the same time, generate electrical power. In addition, in order to use a device that will generate power from human motion, the way in which the motion is utilised needs to be considered. According to the human body anatomy, knee and elbow joint motions are, basically, single DOF movements, while other joints, such as shoulders, can perform more complex movements. Thus, it is needed to focus more on the joints with single DOF in order to minimise the complexity of the device that will be used and decrease the metabolic cost. Moreover, according to Riemer et al. in [152], in order to design the device the maximum torque of the joint during each motion should be a known variable due to the fact that a device that will convert mechanical into electrical power needs to withstand torques of similar magnitude to maximum joint torque. Failure to identify the torque of each joint will increase the overall metabolic cost since the device will be heavier. Therefore, based on the same research, heel strike, ankle and knee motions are the potential candidates that will contribute to the energy harvesting process. As mentioned above, the regenerative breaking device will be used during the negative phase and heel strike, ankle and knee joints seem to provide the highest amount of negative work during normal walking [152].

One of the main factors that should be taken into account when designing a device that will use the regenerative braking is the efficiency of the device in terms of the energy that it can harvest from specific motions. The efficiency of regenerative breaking device attached on the knee is expressed as the ratio between the difference of electrical power output and the difference in metabolic cost of a particular activity with and without a device [152]. Thus, to derive the efficiency, the following equation is used

$$efficiency = \frac{\Delta electrical\_power}{\Delta metabolic\_power} \tag{7.3}$$

The difference in metabolic cost is expressed by the energy spent to generate electrical power and the energy spent by the wearer to carry the device. Therefore, the weight of the device will also affect the efficiency of the whole system. Taking everything into account, a knee joint device that is deployed to generate power during the negative phase of the knee motion has been proposed by Niu et al. in [160] and has been developed by Donelan et al. in [161] and [162]. The design of the knee joint device is depicted in Figure 7.5.

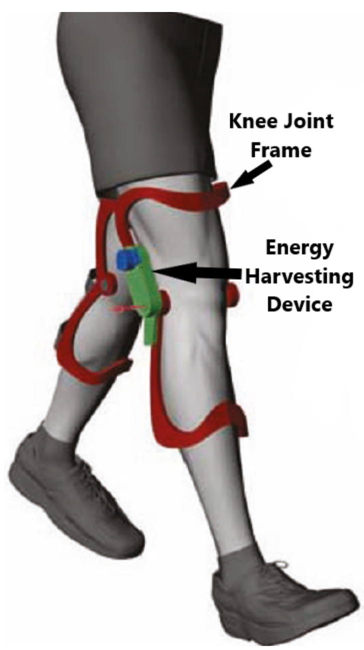

Figure 7.5: Knee joint device deploying regenerative breaking technology to harvest energy from the knee motion [161]

The joint device of the figure 7.5 has a weight of 1.6 kg, has an efficiency of approximately 70% and is capable of harvesting electrical power in the range between 17 W and 25 W. The amount of the harvested power is dependent on the walking pace of the operator. The device is configured in such way to work during the negative phase of the knee motion.

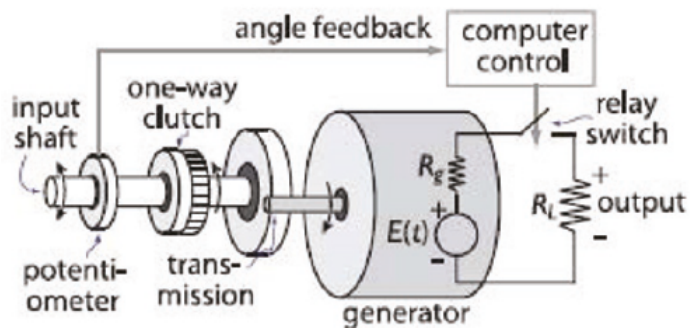

Figure 7.6: Schematic diagram of the knee joint device used for harvesting energy from the knee motion [161]

This has been implemented by driving a gear train through a unidirectional clutch that is only transmitting to a DC brushless motor when the knee extends. The device is not engaged at all during the knee flexion, due to the one–way clutch that is used. The DC motor is used in the device to serve as the generator of the electrical power. Then, the generated electrical power is dissipated by a load resistor. The schematic and chassis of the device implemented by Donelan et al. in [161] are depicted in Figures 7.6 and 7.7, respectively.

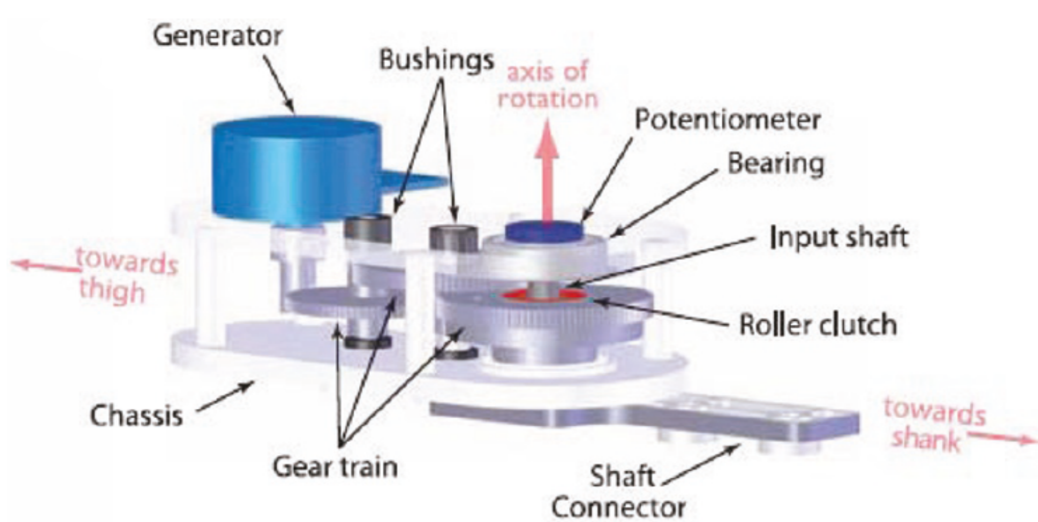

Figure 7.7: Chassis design of the knee joint device used for harvesting energy from the knee motion [161]

Taking all the above into account, a device similar to that developed by Donelan et al. in [161], can be used for this project. Based on the prototype design presented in 5.1, there is no need for addition knee brace that will hold the regenerative braking system. The device can be attached to the exoskeleton frame either on the knee joint or to the kneecap. Both places are performing specific motions and have 1 DOF. It should also be mentioned that since the regenerative braking device is not directly attached to the human knee joint but to the exoskeleton frame, the resistance applied to the motion can be increased in order to harvest more energy from the device. However, it should be considered that the resistance to the motion must not be higher than the torque of the exoskeleton joint. A torque of higher magnitude on the device will require stronger transmission and will, eventually, increase the weight of the device and the metabolic cost.

Finally, based on the aforementioned, by attaching regenerative braking systems on both exoskeleton knee joints and caps, the amount of energy that can be harvested could, theoretically, be up to 100 W. However, typical conversion losses up to 50% should, also, be considered. Consequently, it will be reasonable to believe that the amount of energy that can be generated could be up to 50 W [152]. Although regenerative braking is one of the most efficient technologies to harvest energy from human motion without significantly increasing the metabolic cost, there are still limitations and challenges that need to be taken into consideration when implementing this technology. The challenges that need to be overcome to reach an optimum target when harvesting energy with this technology, are discussed on the final section of this chapter.

7.4.3 Piezoelectric Devices

Another method for harvesting energy from human motion is the used of the piezoelectric devices. The piezoelectric effect converts kinetic energy in the form of vibrations or shocks into electrical energy. Piezoelectric generators (energy harvesters) offer a robust and reliable solution by converting normally wasted vibration energy in the environment to usable electrical energy. They are ideal in applications that need to charge a battery, super capacitor, or directly power remote sensor systems. In the past, many researchers have developed piezoelectric devices to generate energy from heel–strike motion. Some of the devices built in the past are using methods to capture the energy during the stance phase (the phase in which the foot is on the ground) and some other devices are using methods to capture the energy during walking when the sole of the shoe is bending. In both cases, the devices are targeting the energy that would have been lost to the environment if piezoelectric sensors were not used. The following paragraphs are presenting some of the devices and experimental results that have been obtained from previous related work.

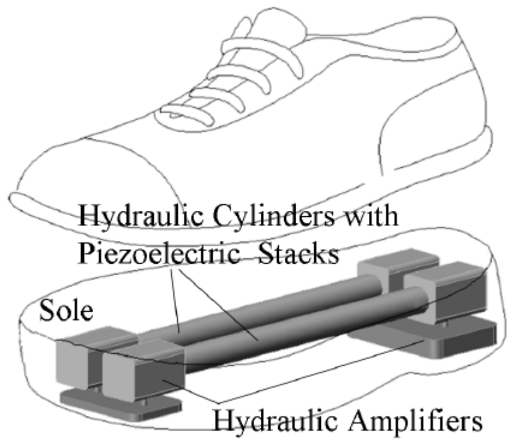

Figure 7.8: Piezoelectric device of two hydraulic cylinders with piezoelectric stacks [163]

A remarkable attempt to harvest energy during the heel–strike, has been presented by Antaki et al. in [163]. The generator used in this device consisted of two hydraulic cylinders that was placed within the shoe sole and contained lead zirconate titanate piezoelectric stacks (PZT). The main idea for developing this device was to harvest energy during the gait cycle, which will be used to power up artificial organs. From the experiments conducted by Antaki et al., it has been found that the prototype was able to generate power up to 675 mW when the subjects was walking and up to 2.1 W when the subject was running. An overall average power of 6.2 W could be generated from a 75 kg individual. The design of this piezoelectric device is depicted in Figure 7.8. The main drawback of this device is that it is bulky and heavy.

Another attempt to use piezoelectric sensors in a shoe sole has been presented by Kendall et al. in [164]. In their research, Kendall et al. have presented two different designs of the piezoelectric device. The first design was containing sheets made of Polyvinylidinefluoride (PVDF). These sheets had the same shape with the shoe sole and they were able to accept any form of stress under bending. This design was able to generate an average power of 1.1 mW with a peak voltage of ±60 V. The second design was made from piezoelectric composite material using a uniform strip. This design was able to generate an average power of 1.8 mW with a peak voltage of 150 V. Later improvements of the aforementioned design were found to provide a power output of 1.3 mW for the PVDF stack and 8.3 mW for the uniform strips [165]. The same group has, also, developed another piezoelectric device, which was a shoe with a magnetic rotary device. The magnetic rotary module was able to produce a maximum power of 1.61 W during the heel strike and an average of 58.1 mW during the entire gait [166]. The design of the shoe is depicted in Figure 7.9.

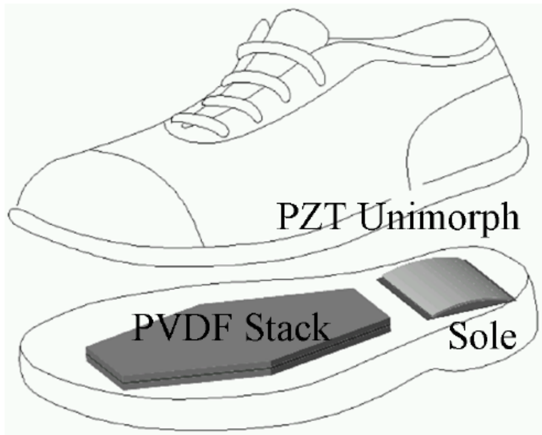

Figure 7.9: PVDF stack and PZT uniform strip of the piezoelectric device [164]

An area where the piezoelectric generators have, also, been used successfully, is the prosthetic knee implant. Prat et al. in [167, 168] have presented a piezoelectric devices attached to a knee implant and was able to produce 850 μW of continuously regulated power with 19% of electrical efficiency and 20% of electromechanical efficiency. According to their research, piezoelectric transduction has many advantages when using a device that is attached to the knee, due to the fact that the forces applied to the knee can be three times higher than the body weight. The design of the piezoelectric device is depicted in Figure 7.10.

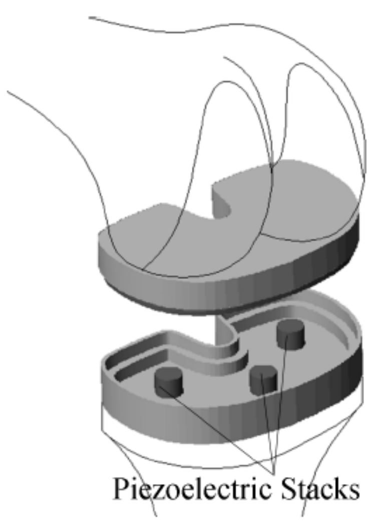

Figure 7.10: Piezoelectric device attached to knee implant [167]

Taking everything into account, a key advantage of developing any of the above–mentioned piezoelectric devices is the fact that they can be mounted on an existing shoe or surgically placed into the human body. In this way, there is no need to develop another external device that could be bulky or increase the overall weight. However, the main drawback in using piezoelectric devices is the relatively small amount of power that can be generated. From previous related work presented above, it has been found that the output power can have a maximum value of 2 W. Therefore, such device cannot be used for this project, since the exoskeleton has high energy requirements. Nevertheless, there might be some on–board electronics that could take advantage of the small amount of power that can be produced by the piezoelectric devices.

7.4.4 Solar Panels (Photovoltaic-Cells)

For many years, solar energy has been one of the most efficient and reliable sources of renewable energy and it has been gaining more and more attention due to the continuous climate change. This form of energy can be found without any extra cost and it is widely available compared to other sources of energy that might have high costs or are difficult to be captured or extracted. It has been found from the scientists that the total amount of solar energy supplied to the earth in one day is capable to provide power for the whole world for one year [169]. In addition, solar energy is considered as a 'clean' source of energy due to the fact that there are no gas emissions or any other harmful substances that are released in the atmosphere when using this form of energy. In the last decades, solar energy has been converted into electricity and used in many different applications, such as vehicular, industrial, residential and many more.

Since the ancient years, sunlight has been used mainly for heating and lighting purposes. In the 18th century, French scientists use solar power for first time to deliver power to a steam engine that was used to print newspapers [170]. Later in this century, Fritts has built the first solar panel made of selenium and with an efficiency of 1% [171]. During the years, the efficiency of solar panels has been increased gradually. However, due to the high costs of the solar cells, all commercial applications were limited to novelty solutions in 1950s [172]. Nevertheless, over the last two decades, the technology has been advanced, costs have been decreased and solar panels have been used widely to supply sufficient amount of power for several different applications.

Solar panels contain photovoltaic (PV) cells that are able to convert the sunlight into electrical power and store it or provide it directly to the electronic devices that need it to operate. Although, the light can be reflected, absorbed or passed through the PV cell only the absorption process is needed to produce electricity. The PV cell is made of two layers of different semiconductors. The first layer is an ‘n–type’ semiconductor with electrons that have negative charge and the second layer is a ‘p–type’ semiconductor that has a positive charge. The combination of these two layers will provide a p–n junction that will create an electric field. Additional components might also be connected with the PV cells in order to form a complete system that will provide the energy to operate a water pump, to switch on the lights and many more. In general, a PV cell is relatively small and can produce about 2 W of power [173]. Hence, in order to increase the output power of a PV cell, many PV cells need to be combined together that will form a module. In addition, modules can also be combined to form an array which, in turn, will provide even higher output power. Figure 7.11 is showing the form of a single PV cell, the module that is made from a combination of PV cells and the array that is made from a combination of modules [174].

The semiconductors that are included in the PV cells can be made of several different types of materials or even a combination of them. Each type has different characteristics and different performance. The three main types of materials that are used to manufacture PV cells are silicon, polycrystalline thin film and single–crystalline thin film. Khaligh et al. in [174] have described thoroughly the benefits and drawbacks of using different types of materials for the PV cells. A solar energy system is, also, classified into two systems. The first one is the passive system that is used to control the amount of power that is captured from the PV cells and takes part in the distribution of the energy to the devices, components or appliances that are connected to the grid. The second system is known as active since it involves electrical and mechanical components and mechanisms, that are taking part on the capturing of the solar energy [174].

A fully functional solar energy system consists of many different components and devices that are taking part in different processes, from capturing to inverting the DC to AC load. Such system is depicted in Figure 7.12. Based on the same figure, batteries are optional but usually all solar energy systems have batteries to store any excessive amount of energy or provide the sufficient energy to the grid during off–peak periods. In addition, a DC/DC converter is essential to operate at the desired current or voltage to match the maximum available power from the PV module.

Finally, based on the nature of this project, solar panels might not be able to be used from the exoskeleton since it will operate, mainly, indoors. For indoor places, the light density is significantly low and the amount of energy that could be capture is up

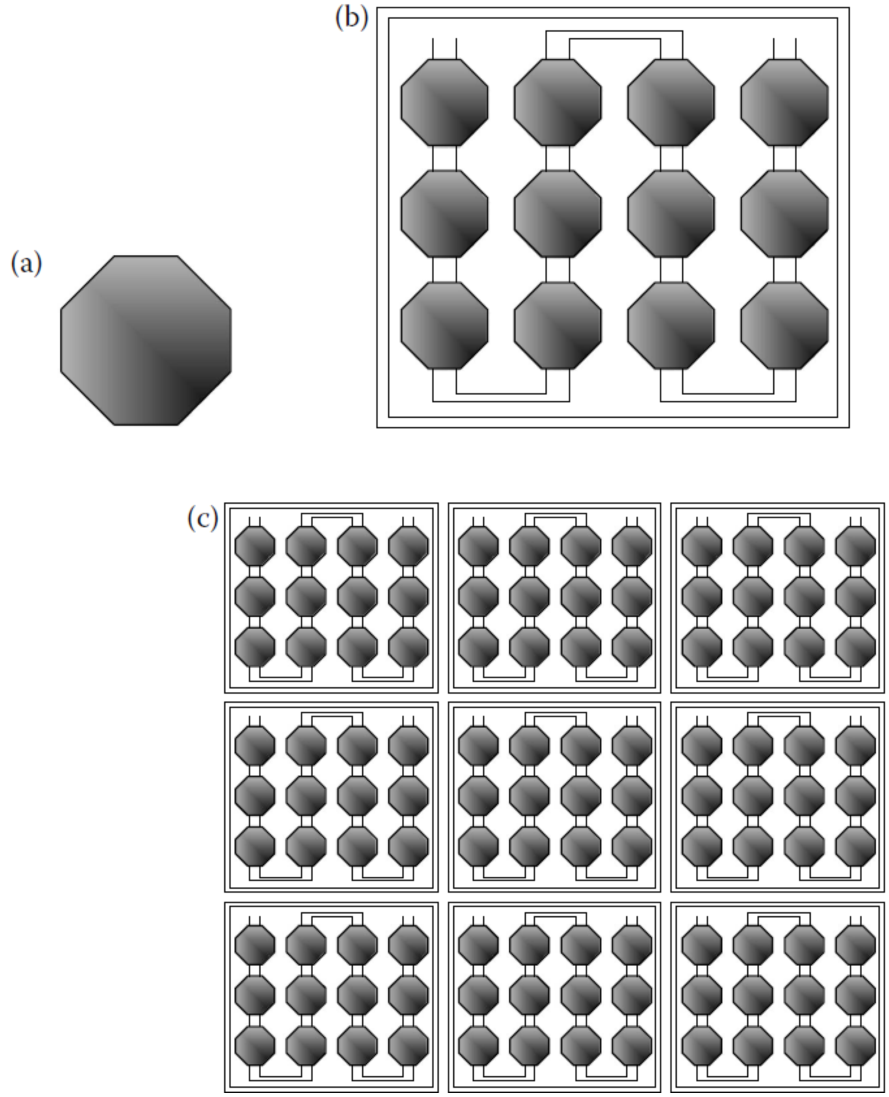

Figure 7.11: (a) PV Cell, (b) Combination of PV Cells forming a module and (c) Combination of modules forming an array [174]

to a few watts. In addition, due to the solid design of the exoskeletal device, the solar panels must be in the form of ultra–thin and flexible films that can be attached on the device, without interfering with the user's motions. Therefore, solar panels will be considered as a back–up solution when the exoskeleton is operating outdoors, where the density of the light that is coming from the sun is higher.

7.4.5 Limitations and Challenges

The use of energy harvesting technologies seems to be very promising to capture energy that otherwise would be wasted. Although, there are many challenges and limitations that need to be overcome in order to design an energy harvesting system

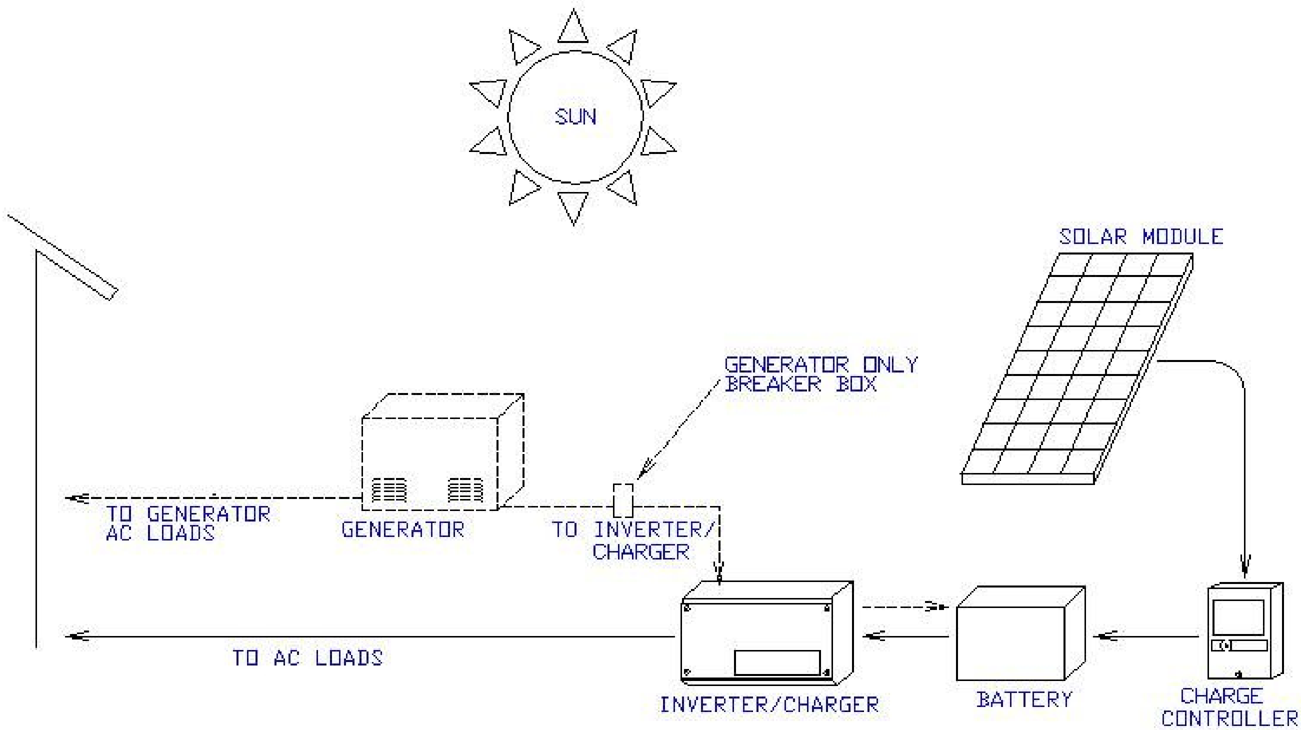

Figure 7.12: Example of a simple solar power system [174]

that would be of high efficiency and reliability. The following list is describing briefly the main challenges and limitations that can occur when implementing each of the aforementioned harvesting technologies.

- **Thermoelectric Devices:** There are many challenges that need to be addressed in designing a reliable system that will be able to harvest energy from human body motions and operate in high temperatures. In order to achieve high efficiency for the system, extensive engineering design needs to be performed in order to balance the flow of the heat between the modules and maximise the temperature gradient across them. In addition, the efficiency of the system is also decreased since the heat that is dissipated from the human body to the environment is relatively high and only a small amount of this heat can be captured and be converted into electricity. For this reason, there is a need to research in the development of new materials that will be able to increase the efficiency of thermoelectric devices by capturing higher amounts of heat [175]. Furthermore, thermoelectric device can face a relatively high electrical output resistance which is an undesirable condition since the output power delivered to the load will be decreased, which in turn, will decrease the efficiency of the system. Another practical limitation is the low thermal conductivity. In cases where thermal conductivity should be high in order to drive excessive heat away from other electronic devices, the thermoelectric generators will fail to capture all the heat, which is unfavourable since it will make the device virtually useless [176].

- **Regenerative Braking:** Apart from the high efficiency that can be achieved when using regenerative braking technology, there are some limitations to overcome when implementing the system proposed in 7.4.2 and presented in Figure 7.5. The first challenge is the limit to the power absorption. The generator is not capable of capturing all the energy produced during the gait cycle. Such limitation is coming from the change in direction and speed of the knee. On the other hand, when using a gear with a changing transmission ratio to keep the generator rotation speed constant, the losses will become higher due to friction. In addition, a high gear ration will increase the weight of the device, which in turn will increase the metabolic cost. Equally important is the control approach that need to be improved when using such device. A control algorithm need to be developed in order to operate the device in a more reliable way. Finally, there are physical limitations that need be addressed when designing a device with regenerative braking technology.

- **Piezoelectric Devices:** The main challenge that is introduced when using piezoelectric devices, is the relatively small amount of output energy they can provide. Due to the nature of operation of such devices and the nature of the application examined in this project, it will be possible to generate more than a few watts that can be used for the on–board electronics of the exoskeleton. In addition, the efficiency of the piezoelectric devices is not at a desirable level and there are considerable losses during normal operation. In addition, the materials from which the sensors are made are of high cost and will increase the complexity of the system during the design process. Furthermore, while working with vibrations, these devices are prone to pick up unwanted vibrations introduced in the system by several external or internal factors. Finally, to the best of author's knowledge, the literature is very limited and there are no remarkable attempts to exploit the full functionality and characteristics of such devices.

- **Solar Panels (PV–Cells:)** As already mentioned in 7.4.4, the solution of a solar energy harvesting system is on its own is a challenge due to the fact that the exoskeleton will mainly operate indoors and such system will only be used as a back–up when the device is operating in the open field. Apart from this challenge, there are other challenges that need to be addressed when using system to harvest energy from the sunlight. First of all, there is the high cost of such system. The initial cost of purchasing or manufacturing a solar energy system can be dramatically increased if all the components that will be needed to have a fully functional system considered. Nevertheless, solar technologies are developing, it can be assumed that the cost will be decreased in the near future. On the other hand, solar energy systems are weather dependent. Considering a system that is constantly operating under rough weather conditions (rain, snow etc.), then the efficiency could go down to 10%. In addition, if the energy captured from the sunlight is not used directly, then it needs to be stored in large batteries, which, in turn, will lead to a higher cost. Finally, if the energy storage is considered as an option for the exoskeleton, then batteries need to be used to store the energy. Accordingly, the batteries need to be carried from the exoskeleton and the overall weight of the device will, in fact, be increased along with the metabolic cost of the wearer. Hence, all the above limitations and challenges need to be considered when using a solar energy harvesting system.

7.5 Wireless Power Transmission

7.5.1 Introduction

Traditional power supplies with cords have become less popular during the past years due to the limitations they introduce in mobility and the high cost in large–scale projects. In addition, the durability of traditional cords are dependent on the environmental conditions and the reliability can be affected in cases where one or more cords will fail to supply the needed power. On the other hand, batteries can be an alternative solution for the traditional power supplies. Although, technology behind batteries has not been advanced enough for robotics applications. For this reason, this alternative may be unreliable in certain conditions. Moreover, the batteries tend to have a short lifespan which, in turn, can increase the cost when it comes to the replacement with another unit and increase the overall weight when more batteries need to be used to deliver sufficient amount of power.

To overcome the challenges and limitation of using traditional power supplies and batteries, technology has advanced and allowed the wireless transfer of electromagnetic waves. This technology is known as Wireless Power Transmission (WPT) technique and, nowadays, is widely used for many applications, such as mobile wireless charging, wireless sensor networks, medical implants and drones or for large–scale applications such as electric vehicles or spaceships. The WPT term is used to describe the wireless power transmission of electromagnetic energy through an electromagnetic field, using different technologies and techniques. The first reported attempt to use wireless power transmission has been seen Maxwell back in 1868, where he derived a mathematical model to express the electromagnetic currents. After a few years, Hertz has discovered the radio waves and he conducted experiments to prove that the electromagnetic waves produced by the transmitter can be wirelessly transferred to the receiver [177].

Later, the next reported attempt to use WPT has been presented by Nikola Tesla in 1897 [178]. Tesla has used the inductive coupling technique to implement WPT and he showed that the Tesla coils used were able to produce high AC currents. That experiment seemed to be the basis for implementing long–distance power transmission using radio communications. Later, based on Tesla's experiments, Brown [179] was able to implement a system capable of transferring wirelessly 475 W of power using microwaves and with an efficiency of 54%. Recently, MIT has implemented a WPT system that was able to lit up a 60 W light bulb that was placed 2 meters away from the transmitter coil [180]. Since then, technology and research have been advanced on the WPT techniques and methods and significant improvements have already been deployed in many different fields.

Nowadays, WPT is used widely by many industries, such as automotive and space. Engineers have started implementing charging stations for charging wirelessly the on–board batteries of electric vehicles. On the other end, laser beams are used to transmit power and data on the space stations and satellites. Moreover, for the past few years, wireless charging of mobiles phones is used extensively in order to avoid the wiring complexity and the increased cost of replacing any broken wires. In addition, WPT has also been used for inspection robots that are deployed either on the military field or in industry (such as pipeline inspection robots, UAVs etc.).

In the following sections, the basic concepts of implementing WPT are discussed along with the applications that extensively use WPT to charge or supply continuous power. At the end of the chapter, methods of implementation of WPT are, also, presented briefly and the performance comparison in presented by reviewing previous related work. Finally, limitations, challenges and safety concerns of the WPT are outlined in order to identify any potential risks of using this technology.

7.5.2 Applications of Wireless Transfer of Power

During the past decades many technologies have been introduced to the market in order to assist people with their everyday life and make it more reliable and efficient. The main target for introducing a new technology is its user and environmental friendliness. In addition, portable and wearable devices have become more and more popular, a result that led to the increasing need for longer battery life of these devices in order to be able to operate for at least a one day. Conventionally, charging these devices require a wall charger with a wire that will be attached on the device's side. This could introduce potential issues both for the safety of the user and the device itself. On the other hand, the user needs always to carry specific chargers and wires for several different electronic devices. Consequently, wireless power transmission (WPT) is an environmental and user–friendly technology that can be used as an alternative to the conventional chargers and wires. In addition, WPT has attracted more and more interest in the consumers market as well as in the scientific community. WPT has been found to be one of the most advanced and essential technologies that is featured in new robotic applications and consumer electronics. The following subsections are presenting briefly some of the applications where WPT is used.

7.5.2.1 Wireless Charging

Wireless power transmission has been first used in the recent years to transfer power in short ranges in order to charge small electronic devices such as smartphones, smartwatches, tablets, PCs and PDAs. As the term of wireless power transmission suggests, the transfer of electric current to a specific device has been achieved without the need for the device to be in physical contact with the wireless charger. Some of the first attempts to charge a mobile phone wirelessly has been presented by Hui et al. in [181], where they designed, manufactured and tested a wireless charger for mobile phones, MP3 and CD players using multilayer PCB spiral winding matrices to generate uniform magnetomotive force over a planar surface.

A few years later, based on Hui's research and experiments, Taylor et el. [183] have implemented a system to wirelessly transfer power to a laptop computer using magnetic induction to eliminate the need for charging the laptop by plugging in the power cable. For their experiments, authors state that they have completely removed the battery from the laptop in order to make sure they can power it up using only the wireless charger. According to their experimental results, they were able to transfer

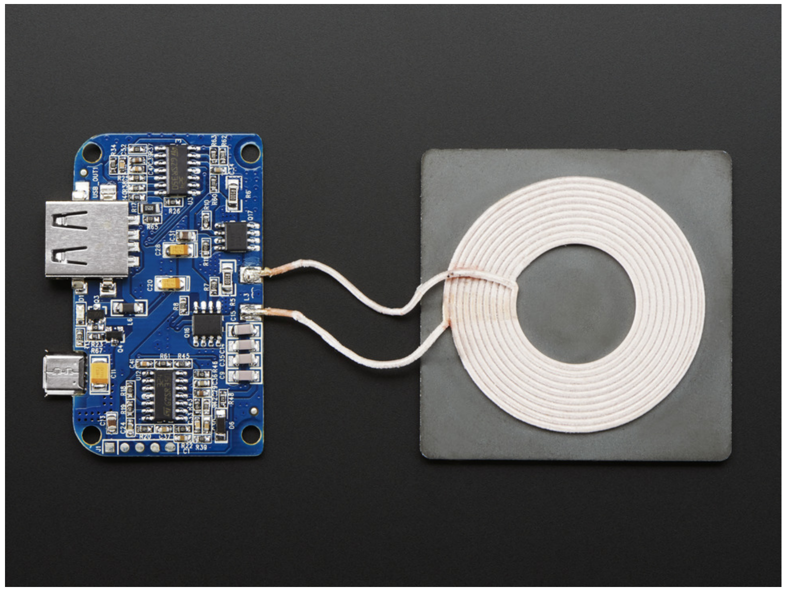

Figure 7.13: Universal Qi wireless charging transmitter [182]

power of more than 20 W with an efficiency of nearly 60%. Since 2010, Qi technology is widely used as a wireless charging standard for providing 5-15 watts of power for small electronic devices. Qi standard was developed by Wireless Power Consortium and since then more than 650 companies have adapted this standard [184]. Qi technology is using an electromagnetic field and inductive coupling to send energy from the transmitter to the receiver. On the transmitter side, there is an induction coil that is creating an alternating electromagnetic field. This electromagnetic field is picked up by the receiver and is converted back to electrical current to charge the battery of an electronic device. A universal Qi wireless charging transmitter is depicted in Figure 7.13.

On the other hand, wireless charging has been used lastly by many researchers to charge the batteries of electric vehicles. An interesting research has been presented by McDonough in [185] where he manufactured a system capable of transmitting wirelessly power between 700 W and 1.5 kW with efficiencies of 64% and 90%, respectively (a prototype of McDonough's system setup is depicted in Figure 7.14). The resonant frequency he achieved was at 160 kHz with a coupling factor of approximately 20%. He concluded that a better efficiency could be achieved in a future implementation of the same system.

Another remarkable research has been presented by Zheng et al. in [186], where they have designed and implemented a wireless charger capable of transferring up to 4 kW with an efficiency of 98%. The distance, between the receiver in their experiments, was variable between 4 and 8 cm. In addition, the operating frequencies that have been

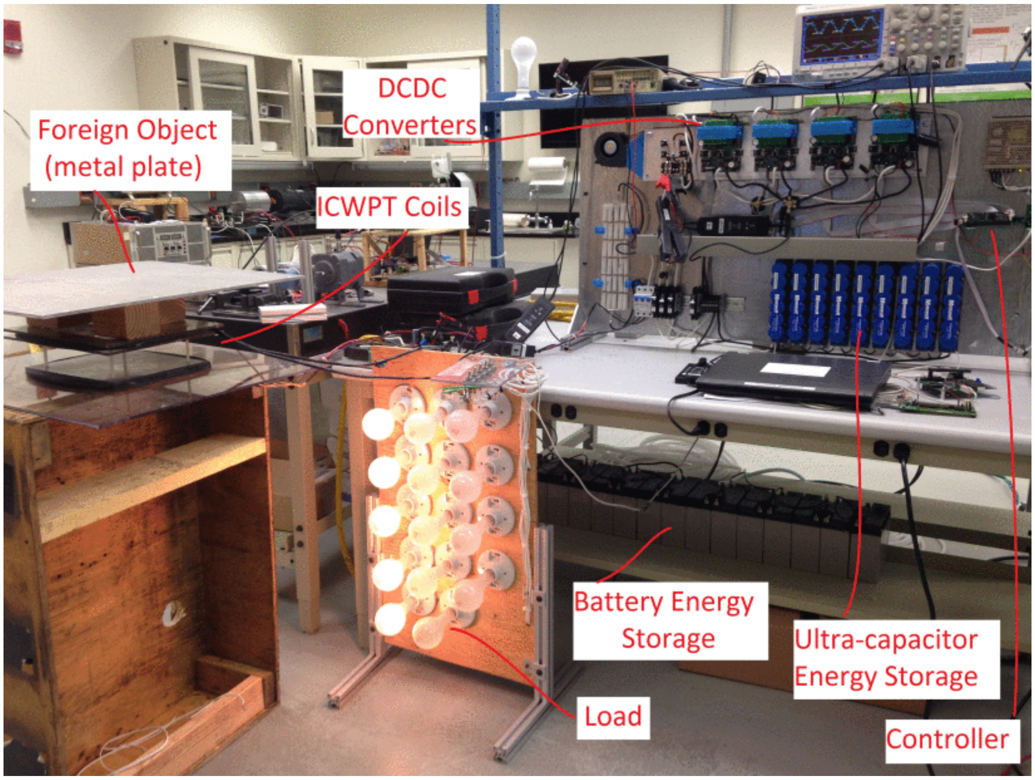

Figure 7.14: Prototype setup of McDonough's charger [185]

tested were between 10 and 300 kHz. The optimal frequency to achieve the maximum efficiency at 4cm of distance between the coils, were 191.5 kHz. The charging process in their experiments lasted approximately 5 hours to perform a full charge (a prototype of Zheng's system setup is depicted in Figure 7.15).

7.5.2.2 Medical Implantations

Among the aforementioned WPT applications, medical implantable microsystems have attracted strong attention due to their ability to replace or assist the functionality of organs in the human body. Microsystems such as endoscopic capsules, nerve stimulators and implantable monitors have been introduced in [187–192]. The medical devices that have been used can either be implanted in the human body or attached on the skin. In both cases, they need power to operate smoothly, transmit data and charge the on–board batteries that they might have. Thus, WPT is coming to solve the problem of using wires to charge any implantable devices. The widely adopted technique used for implementing WPT in medical devices is the inductive coupling (will be discussed in details later in this chapter). There are other methods that also studied, such as magnetic resonance and microwave transmissions due to their advantages (directivity,

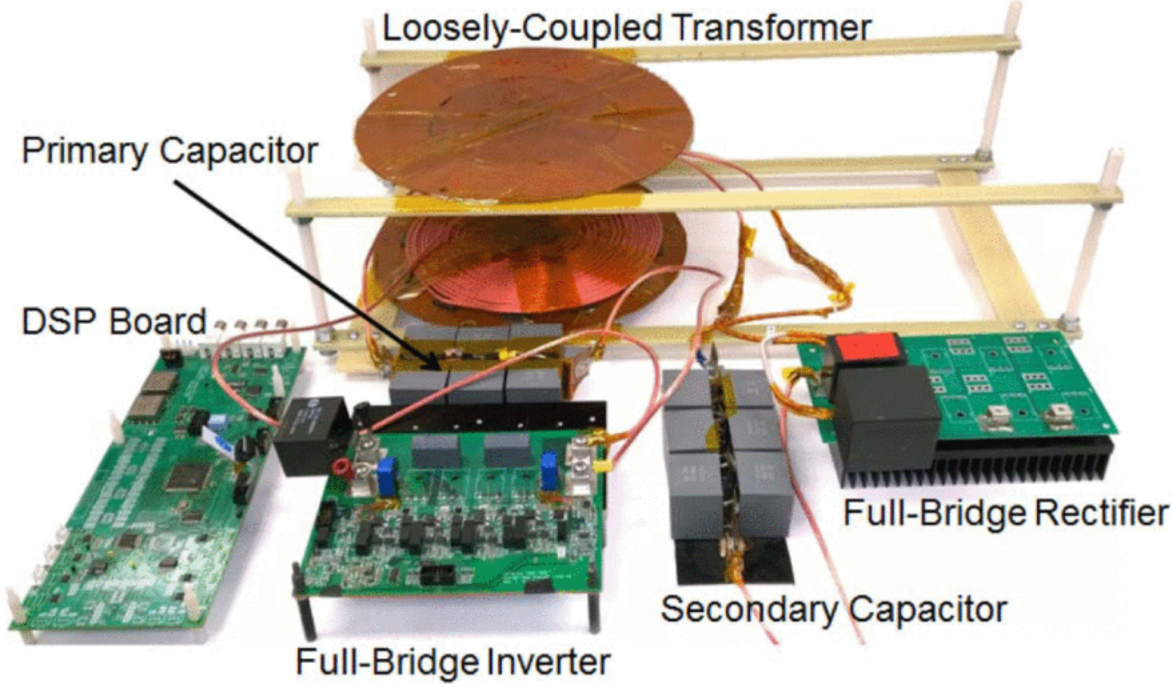

Figure 7.15: Prototype setup of Zheng's charger [186]

range etc.). Although, operating in high frequencies could introduce a potential risk to human health.

Lin et al. in [193] they have implemented a batteryless implantable CMOS SoC to effectively reduce the pain by using low stimulation voltage of the dorsal root ganglion. Their method to implement the pain control device is based on pulsed radio–frequency (PRF) stimulation. The implantable device is using an RF frequency of 402 MHz for the stimulation process and the external charger (tuned at the frequency of 1 MHz) is using the inductive coupling method to charge the implantable device. The authors mentioned that depending on the WPT method that has been used for the charging process, the implantable device can operate for up to six months without recharging. The power that can be transferred to the implantable device is relatively low (up to 9.5 mW), though, it is sufficient to operate smoothly for long periods. Finally, the efficiency of the transmission has been found to be approximately 80%. A prototype of the stimulator module along with the measured thermography is depicted in Figure 7.16.

Another remarkable attempt to transfer power wirelessly to implantable devices has been implemented by Park et al. in [194]. The authors have suggested a helical coil that can be implemented on the sleeve of the clothes and can transfer energy to a device implanted in the human body. The helical coil induces magnetic field to the inside of

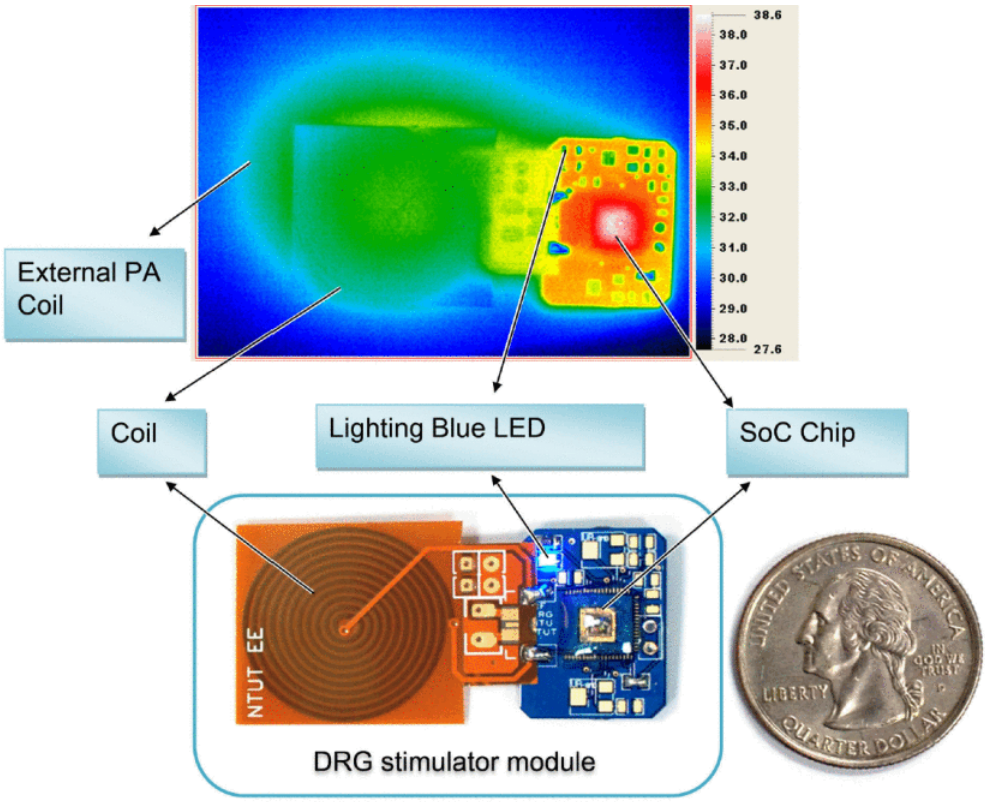

Figure 7.16: Prototype of the stimulator and measured thermography [193]

the arm when the induced current flows in the coil inside the body. Therefore, all the devices that are located around the inner coil can pick up the power transferred from the outer coil. According to the same research, the magnetic field lies on the ISM band (13.56 MHz). There are no reported experimental results of this device, but only a proposed design which can be found in [194].

An interesting implementation of a motion–free endoscopic capsule used for inspection, has been presented by Wang et al. in [195]. The system they have developed has a two–hop transfer mechanism and is capable of transferring a maximum 90 mW of power (and an average of 24 mW) with an efficiency of 3.04% over a distance of 1 m. The power that is available for the device is relatively low, although, it is more than enough to charge and operate the endoscopic capsule. The experiments they have conducted confirmed that the frequency of 13.56 MHz is the optimum choice to have an efficient and reliable submission. In addition, an estimation of the electromagnetic radiation safety for their system has been estimated to be approximately 0.1 W/kg for a person with weight of 80 kg and their estimation complies with the International Council on Non–ionising Radiation Protection guidelines.

Finally, Liu et al. [196], have implemented a WPT system for charging an implantable pacemaker. Their proposed system was capable of transferring up to 6.3 W of power to the pacemaker at an operating frequency of 160 kHz and with a maximum efficiency of 90%. The power could successfully be transmitted over a distance of 12 cm and used to charge the batteries of the pacemaker. Their system is using a novel approach for the implementation of WPT from implantable medical devices, since they achieved the maximum performance at a relatively low transmission frequency. In the past, researchers were using frequencies of up to few hundred MHz which could introduce potential risk on the human health. Thus, under this low frequency, the radiation effects on the human body could be decreased dramatically.

7.5.2.3 Military Applications

In the recent years, WPT has also been introduced in the military field and promises to change the way a soldier, a vehicle or a UAV is operating on the battlefield. For many years, soldiers were carrying large batteries on their backpacks in order to supply power to vital instruments needed on the battlefield. However, batteries could weigh over 20 kg and could introduce potential risks of being carried them under extreme weather conditions (extremely hot/cold environment, contact with rain/snow etc.). Thus, there is a great need to implement new methods and technologies for the power distribution on the military applications.

The first reported attempt to use WPT in the military field is coming from the US military where they deployed an initial prototype on the QinetiQ Talon robots to Afghanistan. These prototypes are used to recharge the batteries of the robot. On their initial implementation, robots needed to be docked to an armoured vehicle to charge its batteries. Lastly, there are attempts to extend this task by using transmitters that will charge the batteries wirelessly, without the need for the robot to return to the charging station [197].

Over the past few years, there is a large number of potential applications where WPT has been deployed. Some of the most known applications are the following [197]:

- Wireless transmission of power from the soldier's vest to the helmet, in order to supply power to helmet–mounted devices (such as night vision device etc.)
- Wireless transmission of power from the armoured vehicle's seat to the soldier's vest in order to recharge the batteries carried in the backpack
- Wireless power transmission from armoured vehicle to UAVs/UGVs/UUVs to recharge the batteries and extend their time of operation

- Wireless power transmission from the soldier's vest to any handheld devices to recharge batteries (such as battery recharging for handheld radio communication device)

On the other end of the spectrum, acoustic/ultrasonic communications have been used widely to communicate with submarines and, in general, for underwater communications. According to Lazarus et al. [198], acoustic wireless power transmission using airborne acoustic/ultrasonic waves can provide a feasible and efficient solution for long–range applications. Another remarkable attempt to use wireless power transmission using lasers has been reported in 1980s during the US Strategic Defence Initiative [199]. In 2004, JAXA and the Osaka Institute for Laser Technology have reported an attempt to implement direct solar pumped laser with an efficiency of 37% and capable on delivering on its full configuration up to 1 GW of power [200, 201]. Finally, the European Space Agency (ESA) [202] has designed a four parallel laser system connected to 1.5 m diameter telescope capable of transmitting 6 kW of power and receive, on the other side, 650 W of power. Since then, there are very few reported attempts to use any other method or technique to achieve an efficient and reliable transmission of power over greater distances on the military field. Most of the projects have become confidential and without publishing any experimental results.

7.5.3 Methods and Implementation techniques of Wireless Power Transmission

The methods that are used to transfer power wirelessly are divided into two categories, the near–field WPT and the far–field WPT. Classification of each category is based on the transfer distance, the principal mechanism used and the amount of power that can be transferred. The following sections describe briefly the two main categories of WPT methods, the implementation techniques that can be deployed to transmit power wirelessly, performance comparison of the two WPT methods along with previous related work. Finally, limitations, challenges and safety concerns are also discussed in the final section of this chapter.

7.5.3.1 Classification of Wireless Power Transmission Methods

Based on the air gap between the transmitter and receiver coils, the WPT transmission methods are divided into the following two categories:

- **Near–field WPT (Non–radiative)** is used to transmit power over a few centimetres or up to a few meters (e.g. distance between the transmitter and receiver coils can vary between 0.1 cm and 5 meters). In near–field WPT, distances greater than 5 meters can decrease the efficiency of the transmission exponentially and introduce high latency and losses. In addition, the transmission frequencies vary between a few Hz and up to several kHz. The main techniques used to establish near–filed WPT are the inductive coupling, magnetic resonance coupling and capacitive coupling. All three implementation techniques will be discussed further below.

- **Far–field WPT (Radiative)** is used to transmit power over several meters or up to a few hundred kilometres. When implementing far–field power transmission, particular attention should be paid to the manner of establishing stable communication between the transmitter and receiver coils, since the efficiency for this method is relatively low compared to the near–field method. The frequency band that is used is extremely high (up to several GHz). Moreover, there are several implementation techniques for far–field WPT, such as lasers, microwaves, ultrasound and many more. A couple of these techniques will be discussed further in a later section below.

7.5.3.2 Implementation Techniques of Wireless Power Transmission

Each method of the WPT technology has one or more implementation techniques. Selection of each technique is based on the nature of the application, the transfer distance and the amount of power that need to be transmitted.

Near–filed WPT is a promising solution for that can provide sufficient power to wireless sensor networks, smartphones, laptops, wearable devices, medical implants, electric vehicle and many more. The techniques used to transfer power in near–field applications are the following:

- **Capacitive Coupling** is using capacitors for the transfer of power in a circuit or a wireless power system by producing alternating electric signals for the transmission of power between the anode and cathode. The transmitter is generating an AC voltage that is applied on the transmitter plate. On the other end, the receiver plate by using electrostatic induction, is receiving the oscillating electric field that will supply the receiver's circuit with AC current. By increasing the frequency, the amount of transmitted power can also be increased exponentially.

Along with frequency, if the capacitance between the transmitter and receiver plates increased, then greater amount of power can be transmitted between the two circuits. The coupling provides a medium for the AC signals while blocking the DC energy. This technique is also widely known as electrostatic or AC coupling [203–208].

- **Inductive Coupling** is the technique where power is transferred between two coils. The transmitter's coil is producing a magnetic field that is picked up by the receiver's coil. Both coils are forming a transformer. The transmitter coil is creating an oscillating magnetic field by the AC current that is flowing through it. On the other side, the receiver's coil is receiving the magnetic field and creating and alternating EMF which, in turn, creates an AC current flows through the receiver's circuit. That current can be fed directly to the devices that need it to operate or it can be converted to DC (by using AC/DC converter) to be used for other purposes [203, 206, 207].

- **Magnetic Resonance Coupling** is another form of inductive coupling where two resonant circuits that are tuned under the same frequency are capable of exchanging energy by using magnetic fields. Both circuits are connected to a resonator with specific value of capacitance. Resonance is used to increase the range of the power transfer and the coupling efficiency. The basic concept of magnetic resonance coupling is that the coil ring operating as the transmitter is using the current flowing through the coil to generate a magnetic field with high resonance. If the transmitter is tuned at the same resonant frequency and is near the transmitter, it can pick up the magnetic field and generate AC current that will flow through the load circuit of the transmitter. Maximum transfer efficiency can be achieved by using magnetic resonance coupling due to the fact that this technique features a tunnelling effect on the magnetic field preventing the EM waves from propagating through air [206, 207, 209, 210].

Far–field WPT could also be an alternative choice for transferring sufficient amount of energy over large distances. Nowadays, far–field WPT is used to transfer power to satellites, to robots deployed on the battlefield and many more applications. Some of the widely used techniques for far–field WPT are the following:

- **Microwave Transmission** has been used to establish WPT over a large distance by using more directional radio waves by making use of shorter wavelength of the microwave range electromagnetic radiation. The operating frequency of microwaves for WPT systems is usually in the range 1 GHz to 1000 GHz [211]. Depending on the nature of application and the environmental conditions, microwave transmissions can achieve high transfer efficiency. Microwave WPT has been developed and tested for several space applications [209].

- **Laser Transmission** has been found to be a remarkable solution to transfer power wirelessly over long range. The main mechanism for the laser transmission can be defined as the conversion of electricity into laser beam which is pointing at a PV cell that is capable of converting the laser beam back to electrical energy [202]. Laser beam has been used in several different fields, such as military to power various kinds of sensors [212], consumer applications to deliver power stationary and moving devices [213].

7.5.4 Performance Metrics of Wireless Power Transmission

When implementing wireless power transfer systems, there are specific performance metrics that should be taken into account in order to develop a highly efficient and reliable system capable of transferring the required amount of energy over different ranges. Hence, the key factors that need to be considered are the frequency of operation, efficiency of power transfer and the transfer distance. The following sections are discussing briefly these key factors. Previous related work will be summarised in a later section of this chapter. Therefore, the following subsections intend to outline the basic performance metrics without referring to any work or experiments conducted from other researchers.

7.5.4.1 Transfer Distance

One of the most critical factors that should be considered when designing and implementing a WPT system is the transfer distance or the air gap between the transmitter and the receiver. The transfer distance varies when using different implementation techniques or methods.

Firstly, inductive coupling is considered as the technique for short–range applications. Even though the efficiency is relatively high when transferring over short distances, however when the distance increases the system can become unstable. It is worthy of note that the amount of power that can be transferred by using this technique increases exponentially when efficiency increased. On the other hand, when magnetic resonant coupling is used, the transfer distance can be significantly increased, but at the same time the transfer efficiency will be decreased. Magnetic resonance coupling can be considered as a type of implementation technique for mid–range applications. In addition, capacitive coupling could also be used to implement near–field WPT. Capacitive coupling can be used for short–range applications. Although, once more, when the distance increases, then the transfer efficiency can be significantly decreased. The overall transfer efficiency of the capacitive coupling technique is less than that of magnetic resonant and inductive couplings.

In general, there are certain limits when implementing each technique. Roughly, capacitive coupling can be used for distances up to several millimetres, inductive coupling for distanced between 0.5cm to 40cm and magnetic resonant coupling for distances between 0.5m to 5m. As mentioned, even when using a specific technique for a WPT system, the distance between the transmitter and receiver coils can be increased, although with the cost of lower efficiency. Thus, there is a great need to define the energy requirements of the application from its initial stage in order to select the most efficient and reliable technique for the WPT. Finally, improvements can be applied to the current techniques or a hybrid system integrating all the techniques can be implemented to achieve the best transfer efficiency with the maximum output power.

On the contrary, transfer distance for far–field WPT applications varies from several meters to several hundred kilometres. The different techniques that can be used to implement such systems provide different rates for the transfer distance, with laser beams being one of the most advanced, reliable and efficient systems at the same time. The efficiency in far–field applications is a drawback, though there are many reported attempts from the scientific community to improve the efficiency using different methods, mechanisms and approaches. Some of these researches will be presented later in this chapter.

7.5.4.2 Efficiency of Power Transfer

The next critical factor that needs to be considered when implementing a WPT system, is the efficiency of power transfer. The efficiency of a WPT system can be defined as the power received from the receiver coil divided by the overall input power supplied on the transmitter coil. As mentioned above, efficiency of power also depends on the techniques that are used to establish wireless transmission of power.

Regarding the near–field techniques, it has been seen that the efficiency can be relatively high. Inductive coupling can provide efficiencies of up to 98%, although to achieve such efficiency there is a need to find the optimum distance between transmitter and receiver coils and perfectly align both sides. The distance between the coils can be increased slightly, yet that will decrease the transfer efficiency. On the other hand, capacitive coupling can deliver power wirelessly with efficiencies up to 85%. Although, it needs to be considered that this method can be used for short–range applications which means that even a slight increase in the distance between the transmitter and receiver coils will dramatically affect the power transfer efficiency. Finally, magnetic resonant coupling can be used –as aforesaid– for mid–range applications (up to a few meters). By using this technique, efficiencies of up to 70% can be achieved and transfer great amount of power. It has to be mentioned, that the overall efficiency of the magnetic resonant and inductive couplings can be increased by achieving a high rate for the coupling coefficient between the resonators and by increasing the operating frequency. In contrary, such approach might increase the complexity of the circuits used on the system.

On the other hand, for far–field applications, the efficiency has been found to be up to 50%, depending on the technique used, the environmental conditions and the frequencies used. An average efficiency that can be achieved for laser and microwave techniques is approximately 30%. Several methods have been deployed to increase the efficiency for far–field applications and establish reliable and stable communications. It has to be mentioned that due to the nature of these techniques, the WPT system that need to be implemented can be huge and occupy a lot of space in a lab on in a whole plant. NASA and other space organisations have built such WPT plants to transmit and receive power from satellites that are travelling around earth. The following figure 7.17 is showing a comparison in performance between the near and far field techniques.

7.5.4.3 Frequency

The operating frequency that can be used for a WPT system varies from a few hertz up to several GHz, depending on the application, the WPT methods and techniques that used to implement such system. For inductive coupling, it has been seen from the literature that the frequency range of 20–40 kHz has been used as a base frequency, when the distance between the transmitter and the receiver is up to 10 cm. Magnetic resonant coupling has been using frequencies between 1–12.5 MHz when the coils of the system have a distance of up to 5 m. In the capacitive coupling technique, frequencies of up to 1 MHz have been used for distances of up to a few mm. All of the above frequencies for the near–field WPT has been used as base frequencies for several systems. Furthermore,

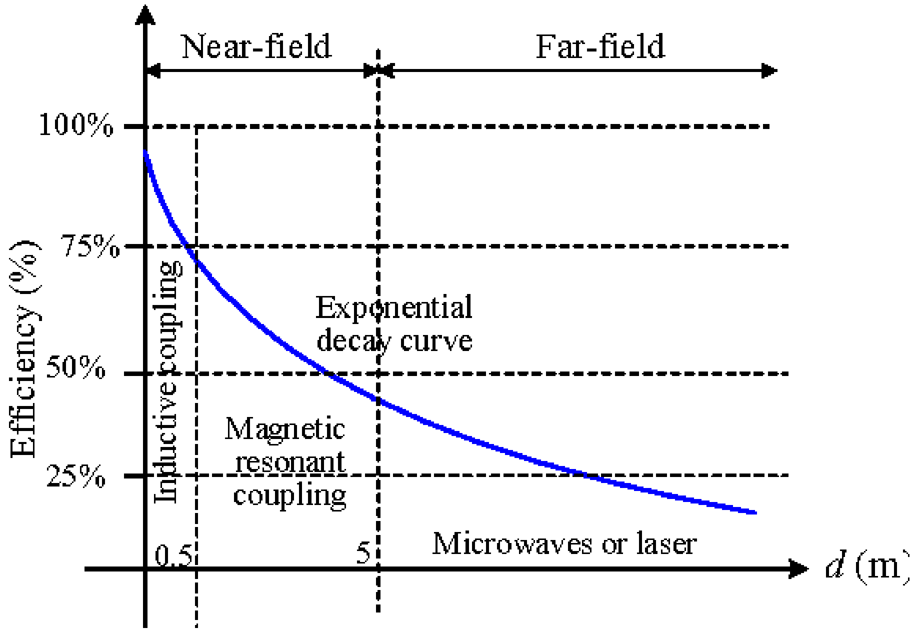

Figure 7.17: Efficiency of different WPT techniques [214]

it has been found that when the frequency increased, then the distance between the coils can be increased as well. For example, with a frequency of 2 MHz the transfer distance can be up to 50 cm, but with a frequency of 30 MHz the distance can be increased up to 100 cm. Nowadays, the far–field techniques are based on electromagnetic radiation and they usually operate in the frequency band of 2.4-5.8 GHz. There are also attempts to even use up to few THz to establish communication between the receiver and transmitter. Table 7.4 outlines the performance metrics for near–field WPT techniques and Table 7.5 the performance metrics for far–field WPT techniques.

Table 7.4: Performance Metrics for Near–Field WPT Techniques

WPT Metrics	**Near–Field**		
	Inductive Coupling	**Magnetic Resonant Coupling**	**Capacitive Coupling**
Frequency	125-150 kHz	5.92-12.5 MHz	Up to MHz
Output Power (W)	Up to 5	4.2	Up to 1
Distance	0.5-40 cm	0.5-5 m	Up to several mm
Efficiency (%)	70-90	40-60	85
Application/example	Wireless Charging	WSN/UAV	Smart card or small robots

7.5.5 Previous Related Work

This section is presenting a summary of previous reported attempts to implement wireless power transmission systems for near–field applications. The table that follows

Table 7.5: Performance Metrics for Far–Field WPT Techniques

WPT Metrics	**Far–Field**		
	Laser	**Microwave**	**Acoustic**
Frequency	Up to GHz (or even THz)		
Output Power (W)	Up to several hundred		
Distance	Up to several kilometres		
Efficiency (%)	10-40		
Application/example	Satellites, Space Stations and UAVs	WSN/UAV	Undersea Applications

outlines the work from other scientists, organisations and researchers, along with the technique of WPT used in their project, the frequency of operation, distance between the receiver and transmitter coils, the maximum output power, the power efficiency and, finally, the application for which the WPT system has been developed. Related work for far–field WPT is not presented in the following table, due to the nature of the application of this project. The exoskeleton needs a great amount of power to operate smoothly and without any risk for the operator's health. For this reason, far–field applications are not suitable for this project since the amount of power they can provide for an indoor application is relatively low and the human might be exposed to high levels of radiation when radiative techniques are used for indoor applications.

As mentioned in the previous sections, the near–field WPT techniques can be classified into the following three categories: inductive coupling, magnetic resonant coupling and capacitive coupling. There are several different methods and approaches to implement these techniques and transfer power wirelessly. Figure 7.18 shows some of these methods for implementing WPT systems. Finally, table 7.6 outlines briefly the most remarkable works and experiments conducted by other researchers. The review of their research has been analysed thoroughly, although the most significant factors related to WPT (frequency, distance, output power etc.) are presented in the table below. Some of these experiments have been mentioned in the previous sections and the following table summarises all the previous related work.

7.5.6 Limitations, Challenges and Safety Concerns

Although there are many advantages of using wireless power transmission systems in robotics or any other application, the limitations that have been introduced to the design or implementation process, the challenges of using WPT systems in line with

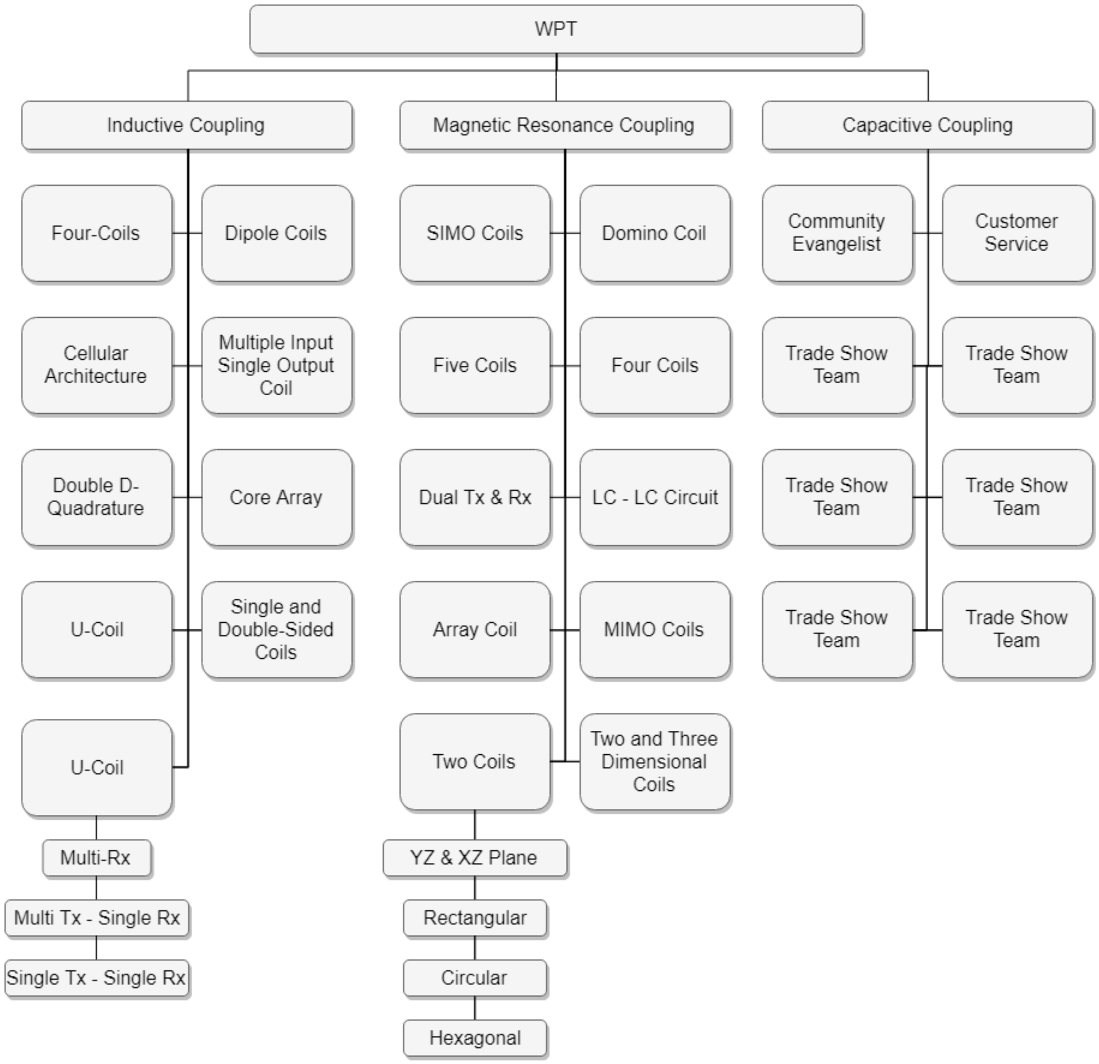

Figure 7.18: Near–field WPT techniques classification

humans and the potential safety risks need to be considered.

First of all, since wireless technology is used to transfer power, there are many security risks that need to be considered. In many applications that use wireless technology especially for data communication purposes, many attacks from external sources have been recorded, trying to harm the infrastructure of a communication system. Thus, there is a great need to design and implement advanced security measures due to the fact that wireless technology is weak to external attacks and breaches. Regarding the wireless power transmission, RF–based systems seem to be the most vulnerable to attacks. At the same time, safety of using WPT systems is another challenge that need to be considered. When WPT systems are used along with human presence, then there are many safety risks for human's health due to the exposure to radiation. Humans are exposed to electromagnetic fields which may introduce a safety risk. In addition,

Table 7.6: Summary of previous related work for near–field wireless power transmission

WPT Technique	Method of Implementation	Power (W)	Frequency	Distance (m)	Efficiency (%)	Application	Source
Capacitive Coupling	Parallel Plates	100	848 kHz	0.0125	94	Slip Ring Replacement	[215]
	Double–Sided LCLC	2400	1 MHz	15	90.8	Electric Vehicle	[216]
	Single Active Switch	1034	200 kHz	Unknown	90.1	Consumer Electronics	[217]
	Conformal Bumper	1068	540 kHz	60	92	Electric Vehicle	[218]
	Single Plate	7.6	840 kHz	0.05	41	General Purpose	[219]
	Matrix Charging Pad	1.6	449 kHz	0.05	54	Consumer Electronics	[220]
Magnetic Resonant Coupling	DD Topology Pad	3300	85 kHz	20	Unknown	Electric Vehicle	[221]
	Conventional Tx–Rx Coils	100000	10-100 kHz	26	80	Electric Vehicle	[222]
	Conventional Tx–Rx Coils	1000	20.15 kHz	15.6	96	Electric Vehicle	[223]
	Two Tx Coils – Two Rx Coils	70	3 MHz	24	90	Car Interior Components	[224]
	Dual Tx – Dual Rx	2100	40 kHz	7	94	Electric Vehicle	[225]
	LC-LC Series Topology	3000	80 kHz	20	95	Electric Vehicle	[226]
Inductive Coupling	Single/Double Sided Coils	1500	20 kHz	7	95	Electric Vehicle	[227]
	Single Tx – Multi Rx	27000	20 kHz	24	74	Electric Vehicle	[228]
	Single Tx – Multi Rx	315	20 kHz	17.5	91	Electric Vehicle	[229]
	Single Tx – Single Rx	180000	60 kHz	7	95	Electric Train	[230]
	Single Tx – Single Rx	2000	33 kHz	10	∼90	Electric Vehicle	[231]
	Single Tx – Single Rx	4000	300 kHz	8	98	Electric Vehicle	[186]

implementation of WPT may be a challenge in clinical experiments due to the high frequencies that can be used. According to IEEE Standards [232], the exposure of humans to radiation in the range of 3 kHz to 100 GHz in public surroundings can be 10 W/m^2. Therefore, when working with RF–based systems, the frequencies can go up to a few GHz for the transceivers in order to transmit the required amount of power. Moreover, in medical applications, WPT can also be challenging since there are tissues on the human body that can absorb the transmitted energy. Finally, for biomedical applications, the alignment of the transmitter and receiver coils is a critical factor. Implementation of WPT in the medical field seems to be the most challenging ones, since configuration of the transceivers and electrical properties of the propagation channel could affect the overall performance of the system.

Conversely, more challenges have been encountered in the implementation of the WPT due to the growing need to transfer greater amounts of power. Practical implementation of such systems can be another challenge in terms of the electromagnetic field, electromagnetic compatibility and other thermal aspects. An example is the charging pads that are used to charge wirelessly the mobile phones nowadays. As it is widely known, smartphone batteries are attached to the rear of the device with no or limited air circulation. In this manner, the power loss or power consumption from other components that are connected to the logic board of the device can be high. Moreover, the AC charging flux needs special considerations since the AC flux can induce high eddy currents on the electronic circuit and the metallic components of the device, which will result in damaging the circuit by increasing the internal temperature. Therefore, a mechanism that will extremely reduce these losses and the internal temperature, is necessary. In addition, special attention needs to be paid on other metallic components, devices and materials that are attached on the device, since high interferences could be introduced with the cost of low efficiency on the WPT system.

Furthermore, the transfer distance and the power efficiency of a WPT system was the first challenge that scientists needed to face since the very first time that wireless power transmission was used in the 19th century. During the years, many methods, mechanisms and techniques have been developed to overcome such challenges, but, there are still drawbacks that need to be considered. One of the most important challenge is the orientation between the transmitters and receivers of the WPT system. In order to achieve greater distance and high efficiency for the transmission, there should be perfect alignment between the coils. Slight deficiencies of the transmitter or receiver coils are considerable, but at the same time the efficiency will be lower. Also, when the transmitter needs to communicate with several receivers in order to achieve wireless power transmission with multiple devices, it needs to be taken into account that the mutual coupling between the receivers will introduce undesired effects such as interference. For this reason, tuning is required in order to tune each receiver at an optimal frequency.

Similarly, transceivers size and weight continue to pose a challenge to the implementation of a WPT system. Usually, there are no issues on the design of the receiver coil but, mostly, there are many impracticalities when it comes to the design and implementation of the transmitter's coil. A remarkable example is the endoscopic capsules where the transmitter needs to be connected on a wall outlet to transmit the power to the device. Thus, there is a need to use small batteries of high capacity which, at the same time, they need to be as lightweight as possible. Finally, the main/ mechanism to transmit power wirelessly is the presence of an electronic circuit with transmitter coil(s) and, on the other side, an electronic circuit with receiver coil(s) that will pick up the power that is transmitted. It should be mentioned that, usually, the transmitter's side is connected to high voltage sources, depending on the application. Therefore, particular attention should be paid to the supply voltage and the components that will be used to convert AC to DC (if needed), otherwise, exposure to high voltages and currents could introduce new challenges and safety risks for the implementation of the WPT system.

7.6 Summary

The first section of this chapter investigated the widely adopted power sources that can be used to deliver sufficient amount of power to an exoskeletal devices. Some of the power sources that have been examined are non–rechargeable primary cells, internal combustion engines, electromechanical fuel cells and tethered solutions. The advantages have been discussed as well as the drawbacks that can be noticed from using each one of them. It has been noted that due to the nature of the application of this project, tethered solutions are the most efficient and reliable for providing the power the exoskeleton requires for performing certain tasks.

The second section of the chapter includes a thorough analysis and discussion for the energy harvesting technologies that can be used in this project. The analysis included technologies such thermoelectric devices, regenerative breaking, piezoelectric devices and sensors and solar panels. It has been understood that two of the most advanced technologies that can be used for the project are the regenerative breaking and the solar panels. On the other hand, based on performance metrics on the thermoelectric and piezoelectric devices, it has been found that these solutions are not capable of delivering high amounts of power. Low efficiency of piezoelectric and thermoelectric is also a factor that has been examined in this section. Moreover, the use of solar panels for the exoskeleton poses a major challenge since the device has been designed to operate mainly indoors, which explains why the amount and density of light is relatively low. Conversely, regenerative breaking technology has seen tremendous progress in the automotive industry and has been used extensively on the EVs, although the components that need to be used to implement this technology can increase the overall cost. The section concludes with the limitations and challenges of the aforementioned technologies. Brief discussion about energy harvesting and conventional power sources is taking place at the end of this section.

The final section of the chapter is presenting thoroughly the wireless power transmission (WPT) technologies, along with the methods and techniques of implementation and everyday applications where WPT is used extensively. In addition, performance metrics such as the transfer efficiency, distance frequency have been examined in order to identify the most suitable candidate that can be used in this project. Previous studies from other researchers and scientists are presented in this section. Their work is summarised in a table that outlines the implementation technique, frequency of operation, efficiency of power transfer, distance between the transmitters and receivers and, lastly, the nature of application. Lastly, limitations and challenges for designing, implementing and using WPT systems are examined. Even though there are many approaches to overcome most of the challenges that can arise, there are also safety and security concerns when these systems are used with humans. A study on the IEEE standards is presented at the end of the section in order to identify the maximum allowable limits for using wireless systems either in public or private applications.

Finally, table 7.7 summarises all the technologies and potential power sources analysed in this chapter. The table provides an overview of each power source technology and includes basic performance specifications.

Table 7.7: Summary and Performance Metrics of Power Sources Reviewed in this Chapter

Power Source Technology	**Method of Implementation**	**Power**	**Efficiency (%)**	**Application**
Traditional Power Sources	Non-Rechargeable Primary Cells	Varies	Up to 99	Commercial & Research
	Internal Combustion Engines	Up to few kW	25 - 30	Automotive & Research
	Electrochemical Fuel Cells	$\sim$100 MW	20 - 60	Commercial & Research
	Tethers	Varies	Up to 90	Commercial & Research
Energy Harvesting	Thermoelectric Devices	Up to few mW	Up to 10	Commercial & Research
	Regenerative Braking	Few hundred W	Up to 90	Automotive & Research
	Piezoelectric Devices	Up to few W	Up to 30	Commercial & Research
	Solar Panels (PV-Cells)	Few W up to several MW	Up to 25	Commercial & Research
Wireless Power Transmission	Near-Field	Few hundred kW	Up to 90	Commercial & Research
	Far-Field	Few hundred W	Up to 60	Commercial & Research

Chapter 8

Simulations of Wireless Power Transfer System

8.1 Introduction

In this chapter, a simulation study of a wireless power transfer system is presented along with the results obtained from the simulations. These results include the efficiency of the WPT system, the frequency of operation and the maximum amount of power that can be transmitted. The purpose of these is to aid in the analysis and testing of the potential strategy for the WPT system to be developed.

The second section of the chapter outlines the simulation objectives that have been set for the simulation approach in order to identify the most essential factors that need to be taken into consideration. In addition, due to the nature of the application for this project, the human gait needs to be analysed in order to identify which WPT technology can fulfil the requirements of the exoskeleton and how the WPT system can be integrated in the human body or the exoskeleton frame. The analysis of the human gait will discuss briefly the posture of the human body and contact of the lower extremities with the ground during normal walking.

In the third section of the chapter, the design and simulation approach of the potential WPT system is presented. The implementation techniques and methods are discussed along with the design of the transmitter and receiver coils. For the initial stage of the simulations, the proposed design of the coils has been simulated with the aid of COMSOL software in order to examine the electromagnetic field distribution between the coils during the wireless transmission of power. In these simulations, different angles of rotation for the receiving antenna are tested. These angles have been derived from the analysis of the human gait and, especially, from the different angles of the human foot when performing certain activities.

The next section of the chapter is presenting and reviewing the experimental results of the WPT system, such us the frequency of operation, the efficiency of the system and the coupling coefficient of the coils for vertical and horizontal alignments. In addition, the design of the coils has been completed with a finite element analysis (FEA) software to avoid the disadvantages of the traditional method. The FEA analysis will help to calculate the mutual inductance for the WPT system that will be simulated. The chapter concludes with a proposed design for a WPT system that will be capable of transferring sufficient amount of power to operate a heavy duty device such as the exoskeleton. The implementation method and technique of this proposed system are discussed.

8.2 Simulation Objectives

Prior to any simulations, the objectives for the work to be done to obtain the expected results with regard to the theoretical approach of a WPT system presented in the previous chapter need to be set. The following list outlines the objectives that have been set for the simulations:

- Acquire basic understanding of the main aspects of WPT systems, with focus on the implementation techniques and methods of this technology.
- Survey potential WPT strategies for transferring high amounts of power and determine which technology is suitable for the exoskeleton.
- Understand and assess the main technical aspects of the suitable WPT system.
- Design and simulate the proposed WPT system to evaluate the performance, efficiency and reliability.
- Propose a novel solution of using the simulated WPT system to transmit continuous power to the exoskeletal device, based on the power requirements specified for the exoskeleton of this project.

8.3 Human Gait Analysis

Human body is capable of numerous manoeuvres in the environment using both lower and the upper extremities as well as the core. Among all of those, the task of walking is the most basic [58], [56]. To realise this aspect of human locomotion the lower–body part of the exoskeleton couples with the user for the purpose of gait augmentation or restoration. Consequently, understanding of the gait process is of paramount importance for designing an exoskeleton. During walking, the majority of human segments displacement occurs in the sagittal plane. The main joints involved in walking are the hip, knee and the ankle, which is built of the talocrural (flexion–extension) and the subtalar joint (inversion–eversion). Most generally operation of a leg in normal gait in healthy person can be divided into two phases with different functions: stance phase (approx. 62% of the gait cycle duration) and swing phase (approx. 38%).

In order to use a WPT system of high efficiency and reliability, it is required to use the most suitable implementation technique to establish the wireless transmission between the transmitter and receiver coils. In Magil's research for this project [233], it has been found (by means of simulation) that the least amount of power that will be needed for the exoskeleton is approximately 1.3 kW. Therefore, based on this requirement, a near–field method seems to be the most suitable solution in order to reduce the exposure to high radiation and transfer high amount of power. According to the initial design of the exoskeleton device presented in Figure 3.12 58, a WPT system can be implemented where the receiver coils will be attached at the soles of the frame and the transmitter coils can be placed on the floor that will be modified for this purpose. [Note to reader: the proposed design of this WPT system will be discussed at the end of this chapter in section 8.6.]

As mentioned in the literature above, the exoskeleton is a device that will be worn by a human and it will use his/her motions as information to operate accordingly. Thus, there is a great need to examine the human gait cycle with focus on the angular displacement of the foot during normal walking, where the proposed WPT system will be placed. In Figure 8.1 cycle of normal gait is depicted.

From the figure 8.1, it can be noticed that the angular displacement of the foot varies depending on the walking phase. The angular displacement of the foot is in the range of approximately 0 and 67.5 degrees. The analysis should be performed in order to identify the movement of the human leg and, especially, the sole of the foot where the coils will be attached. The results of the human gait analysis will be used to simulate the WPT system and thereby the coupling effect between the transmitter and receiver coils. The coupling coefficient is one of the most essential factors of the WPT systems since they provide information about the alignment of the coils and the efficiency of the transmission under different angles of rotation. The design of the

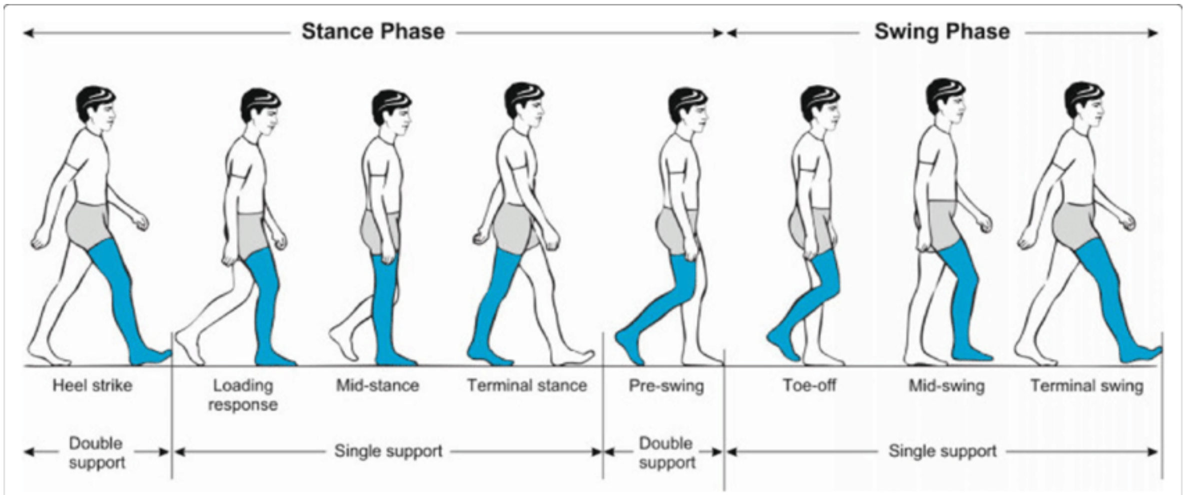

Figure 8.1: Human gait cycle [234]

proposed coils is discussed in the next section along with the simulations performed to obtain the coupling coefficient for specific angles of rotation and the distribution of the electromagnetic field between the coils.

8.4 Design and Simulation of the WPT System

8.4.1 WPT Implementation Method and Technique

As mentioned in chapter 7 of this report, in order to design and implement a WPT of high efficiency and reliability, the energy requirements of the relevant application need to be specified first. Based on the simulations performed, the exoskeleton will need at least 1.3 kW of electric power to operate. Therefore, there is a need to identify which method and technique is the most suitable for transferring that amount of power.

From the human gait analysis, it has been observed that the maximum distance between the foot and the ground is usually 5 cm. Hence, the corresponding between the transmitter and the receiver coils will be in the range of 0 (full contact with the ground) and 5 cm. Having said that, a near–field (non–radiative) will be used to implement the WPT system. Based on the analysis in section 7.5.3.1 of the previous chapter, near–field methods are used to transfer power over a few centimetres (or up to a few metres if needed). Any greater distance between the coils can reduce the overall efficiency. In addition, the transmission frequencies of the near–field varies between a few Hz and up to several kHz.

On the other hand, there are different implementation techniques for the near–field method. Such techniques are the inductive coupling, magnetic resonance coupling and capacitive coupling. Based on the nature of the application studied in this project, magnetic resonance coupling seems to be the most efficient and reliable technique for the implementation of the wireless power transmission. According to the literature, magnetic resonance coupling can provide high efficiencies and a wide range of operation frequencies for the potential WPT system to be developed. Previous related work based on this technique has shown that it is the most suitable for advanced and power–hungry applications. Most of nowadays applications using WPT systems, are deploying the magnetic resonance coupling technique to achieve the best possible efficiencies and high amounts of transferable power. The proposed design of the transmitting and receiving coils/antennas is depicted in the next section, with the aid of COMSOL software. Magnetic resonance coupling is assessed also by presenting performance metrics of the WPT system to be used in this project.

8.4.2 Initial Design of Antennas Based on Selected WPT Technique

Prior to the simulations of the complete WPT to be used in this project, the antennas that will be used for the power transmission need to be designed. For the initial stage of the simulations, COMSOL software has been selected in order to address the concept of WPT by studying the electric–field and energy coupling effects between two circular loop antennas. The basic plan for the simulations in COMSOL is to use a transmitting antenna of fixed orientation, while the receiving antenna is rotating. The coupling effect between the antennas is investigated in terms of S–parameters. The design of the antennas is depicted in Figure 8.2.

The design consists of two circular loop antennas enclosed by an air domain (the air domain is not included in figure 8.2). Furthermore, a thin copper layer has been used as material for the design of the antennas. At the lumped ports of each antenna, a 50 Ω of reference impedance has been used to excite the antennas. The electric field distribution and power flow are shown in the section below, where results of the simulations are presented.

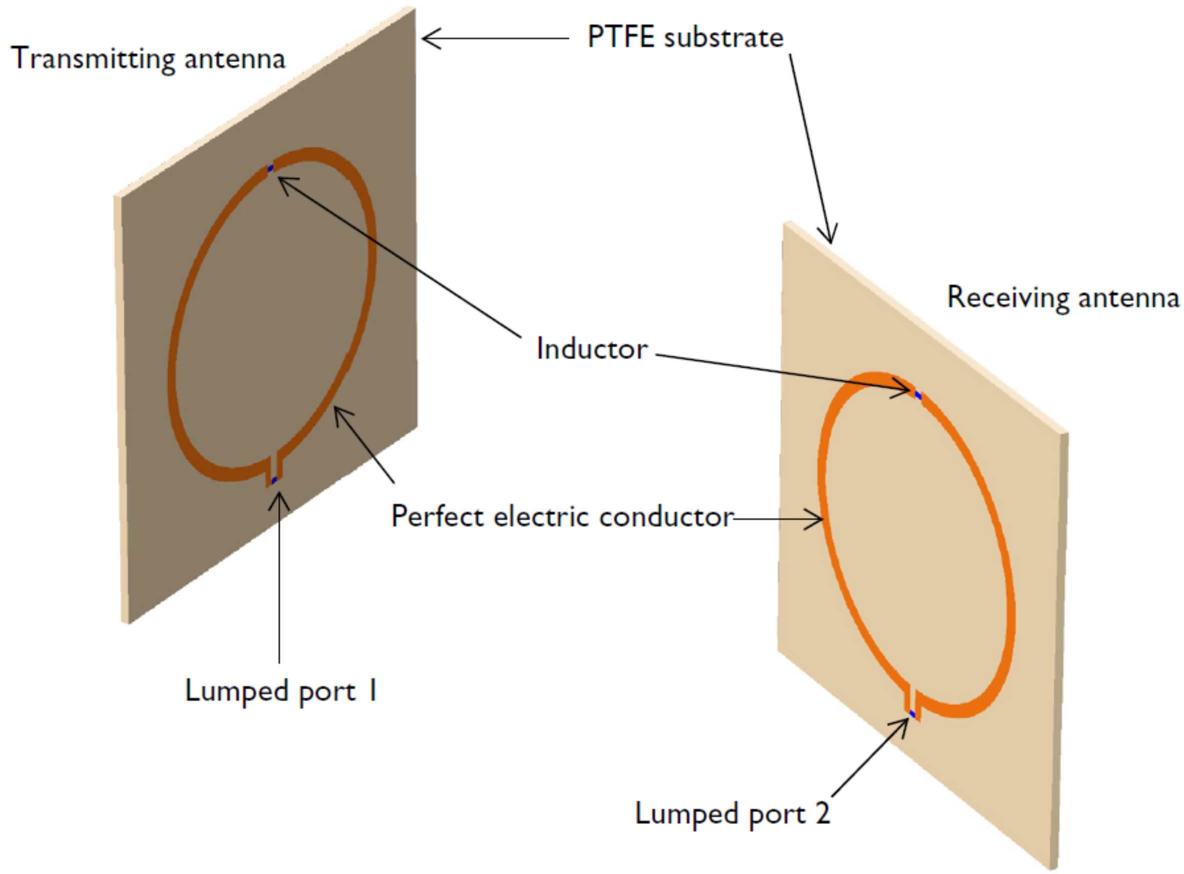

Figure 8.2: Initial design of antennas for the investigation of the coupling effect

8.4.2.1 Electric Field Distribution and Power Flow of the Proposed Design

The simulations have been performed by using frequencies in the range of 0 to 60 kHz. From these simulations, it has been observed that the best coupling coefficient between the receiver and transmitter coils has been achieved at 25 kHz. Thus, COMSOL has been configured at the frequency of 25 kHz. The following figures are presenting the distribution of the electric field and the power flow between the transmitter and the receiver.

The figures 8.3 to 8.7 are showing the electric field distribution and the power flow when the receiving antenna is rotating. This simulation has been performed with respect to the human gait analysis, where it has been seen that the angular displacement of the sole of the human foot varies between 0 and 67.5 degrees. In addition, considering that the receiving antenna will be attached to the sole, the coupling effect between the antennas needs to be investigated. The rotation angles that simulated are from 0 to 90 degrees with a step of 22.5 degrees per simulation. The arrows shown in the figures are indicating the flow of the power.

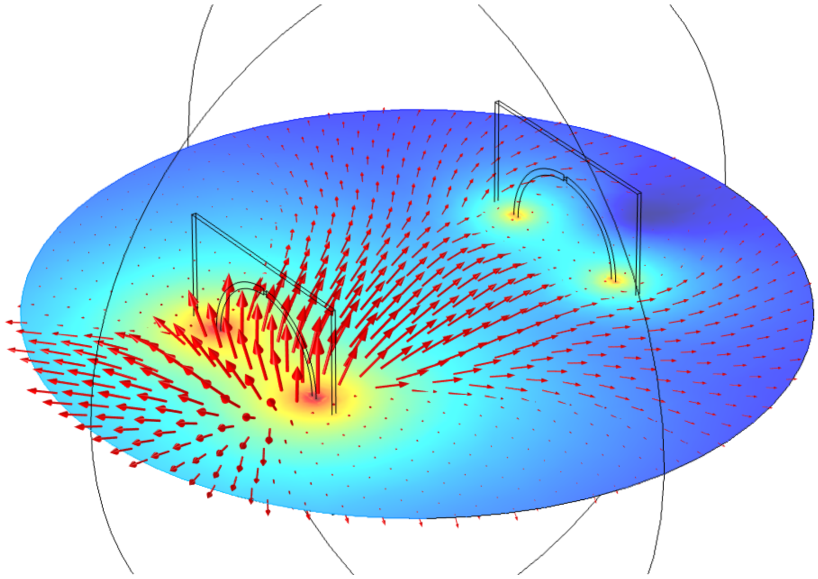

Figure 8.3: Representation of electric field distribution and power flow while receiving antenna is at 0 degrees

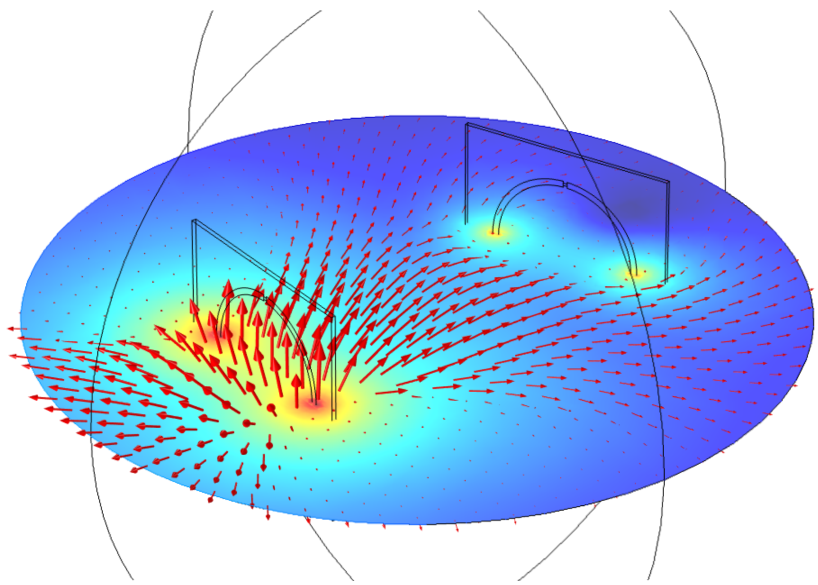

Figure 8.4: Representation of electric field distribution and power flow while receiving antenna is at 22.5 degrees

It can be seen that when the antennas are facing each other (receiving antenna at 0 degrees) there is a strong coupling between the transmitter and the receiver. By increasing the angle of rotation for the receiving antenna at 22.5 degrees, it can be observed that the coupling between the antennas is not as strong as in 0 degrees. When the receiving antenna is at 90 degrees as shown in Figure 8.7, there is no coupling area around the antenna and the power transmitted from the transmitting antenna is released to the environment.

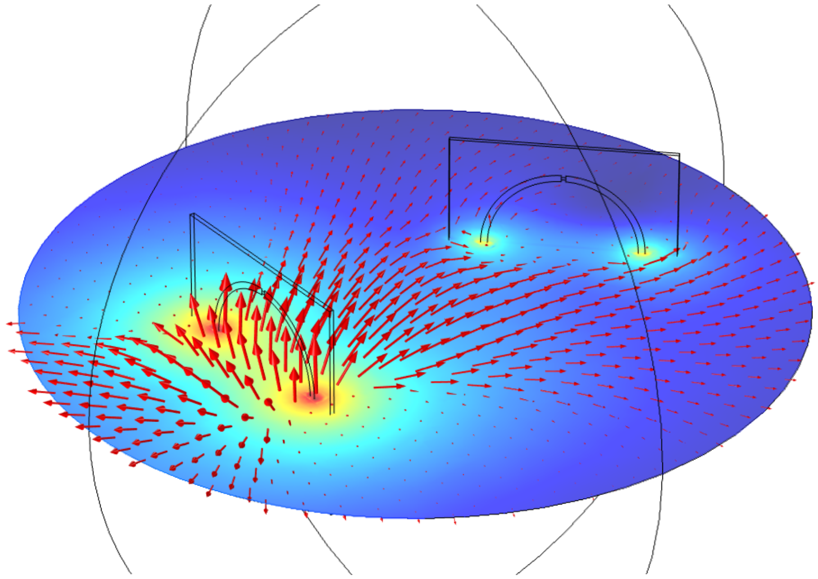

Figure 8.5: Representation of electric field distribution and power flow while receiving antenna is at 45 degrees

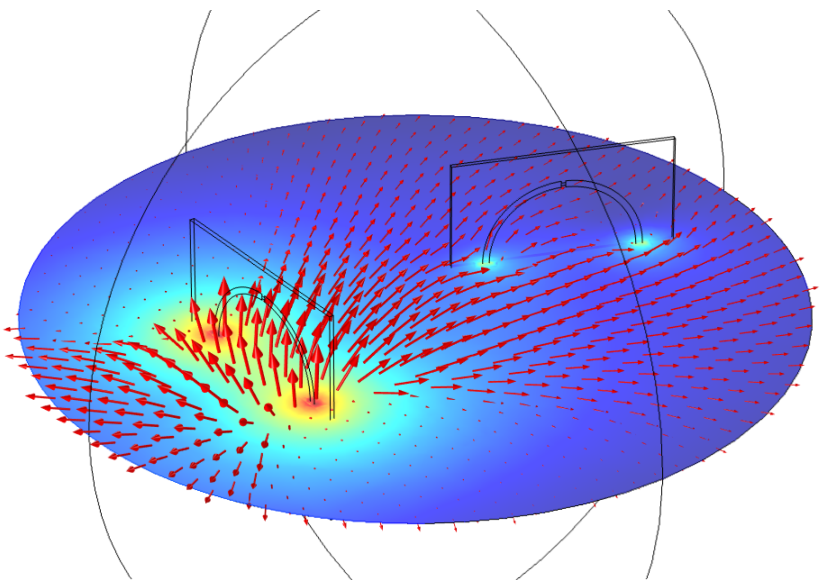

Figure 8.6: Representation of electric field distribution and power flow while receiving antenna is at 67.5 degrees

The above simulations have been performed to gain a better understanding of the coupling effect between the transmitting and receiving antennas for the WPT to be used for this project and observe potential losses during the transmission or when the antennas are not aligned perfectly. The results of these simulations will assist on the final design of the WPT system and will help to estimate the overall efficiency for the transmission that is discussed in the following sections.

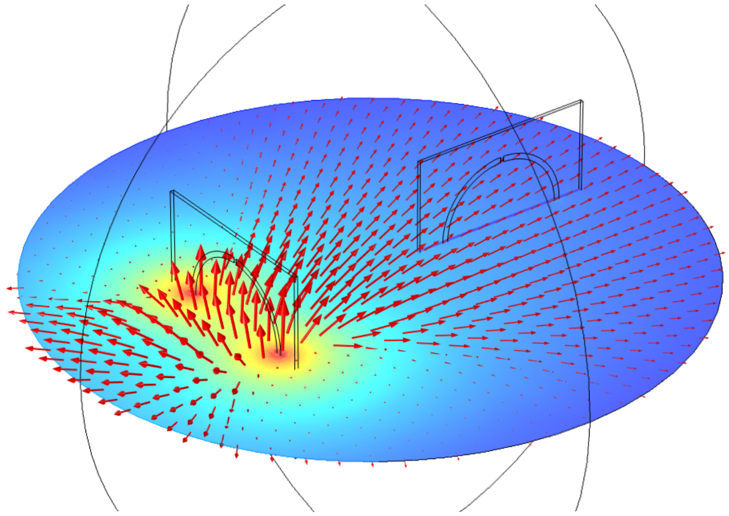

Figure 8.7: Representation of electric field distribution and power flow while receiving antenna is at 90 degrees

8.5 Simulation Results and Discussion

Once the two identical antennas/coils examined in COMSOL for their coupling effect and the distribution of the electric field during the transmission, the simulation model will be tested using Maxwell and Simplorer in order to obtain the results regarding the performance of the system, the reliability in terms of the amount of transmitted power with respect to the application of this project and the efficiency of the power transfer. The following sections are presenting the coils that have been designed using finite element analysis software (FEA) and the results obtained from the simulations of proposed WPT system.

8.5.1 Finite Element Analysis of the Simulation Model

As mentioned previously, based on the literature and the nature of this application, the technique that will be used to implement the wireless power transmission system is the magnetic resonance coupling. This technique has been selected due to the high performance that it can provide in terms of frequency of operation, transmission efficiency and amount of transmitted power.

In general, when the circuit is tuned under the same resonant frequency, the coils of the WPT system are capable of transmitting power with high efficiency. The exchange of power may become weaker at other frequencies [235]. For this reason, the frequency where the system provides the highest amount of power with the best possible efficiency needs to be found. In order to have a transmission of high efficiency, the system should work at the resonant frequency. Thus, to implement such system, the mutual and self–inductances of the coils that will be used for the wireless power transmission should be calculated.

Usually, these parameters can be calculated using formulas or by direct measurements of the physical system [235–237]. Nevertheless, depending on the design parameters of the coils (shape, size, number of turns etc.), these calculations can become more complex. Thus, the FEA software can be used to avoid these calculations and obtain the needed parameters that will be used for the WPT system. In addition, FEA software such as Maxwell is capable of visualising the magnetic field distribution between the coils that will help in the electromagnetic shielding design of the system.

The Tx and Rx coils with the aid of ANSYS Maxwell software. Two identical helix coils have been designed with 8 turns for each coils. The proposed design of the coils perform well when having only few turns. It has been found that while increasing the number of turns, the system is becoming more complex and it needs more computing power to perform the analysis. Thus, the design has been simplified to reduce the complexity of simulations. In order to perform the simulations, excitation current has been applied at the faces of the terminals of each coil. This configuration will help to visualise the distribution of the magnetic field when the current is flowing through the coils and obtain the values for the mutual inductance and, hence, the coupling coefficient. The coupling coefficient is a key factor in WPT systems, since it can provide an estimate of the transfer efficiency. The mutual inductance can be calculated using the following formula.

$$M = k\sqrt{L_1 L_2} \tag{8.1}$$

where M is the mutual inductance in Henrys, K is the coupling coefficient and $L_{1,2}$ is the inductance of the coils in Henrys. The materials that used for the design of the coils is copper. The initial design of the Tx and Rx coils is depicted in Figure 8.8.

The initial design has been simplified in order to simulate the model and obtain the values for the coupling coefficient between the coils. A sweep parameter analysis has been performed in Maxwell to obtain these values. In this analysis, the software is testing the coupling coefficient of the coils under two different conditions. The first simulation is testing the coupling coefficient in the vertical axis in the range of 5 and 200 cm. The second simulation is testing the coupling coefficient in the horizontal axis (distance between the centres of the coils) in the range of 0 and 120 cm. Coupling

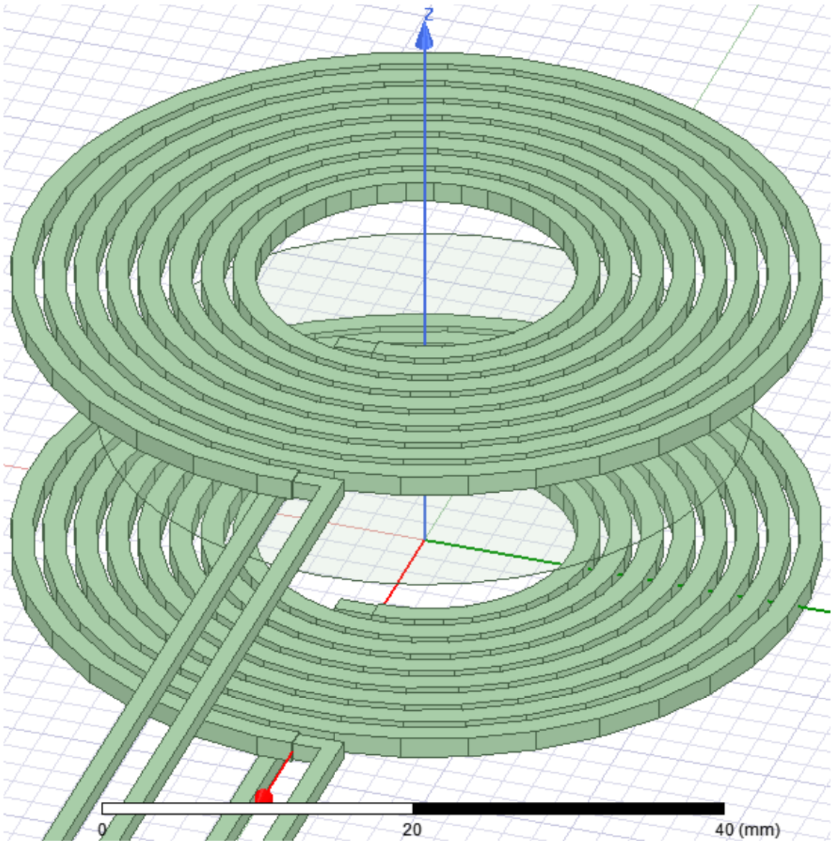

Figure 8.8: Tx and Rx coils design in Maxwell

coefficient vs vertical distance and coupling coefficient vs horizontal distance graphs are depicted in Figures 8.9 and 8.10, respectively.

For the second simulation, the vertical distance between the coils has been set at the fixed value of 50 mm and only the horizontal distance is variable. It can be observed that when the Rx is moving on the horizontal axis, the coupling between the coils is becoming weaker. Finally, the designed model has been tested for the distribution of the magnetic field at a fixed vertical distance of 50 mm. The first test has be performed without the shield between the coils. The results of this test depicted in Figure 8.11.

For the second test, an aluminum shield has been placed between the coils. The shielding has been done in order to reduce the distribution of the electromagnetic field and make the system safer when it is used in line with humans. Radiation can pose a high risk for human health. Therefore, there is a need to design the system in such way where the radiative effects will not introduce undesirable conditions. The shield has been designed with the aid of Maxwell software. A second simulation has been performed and the results of the distribution of the electromagnetic field are depicted in Figure 8.12.

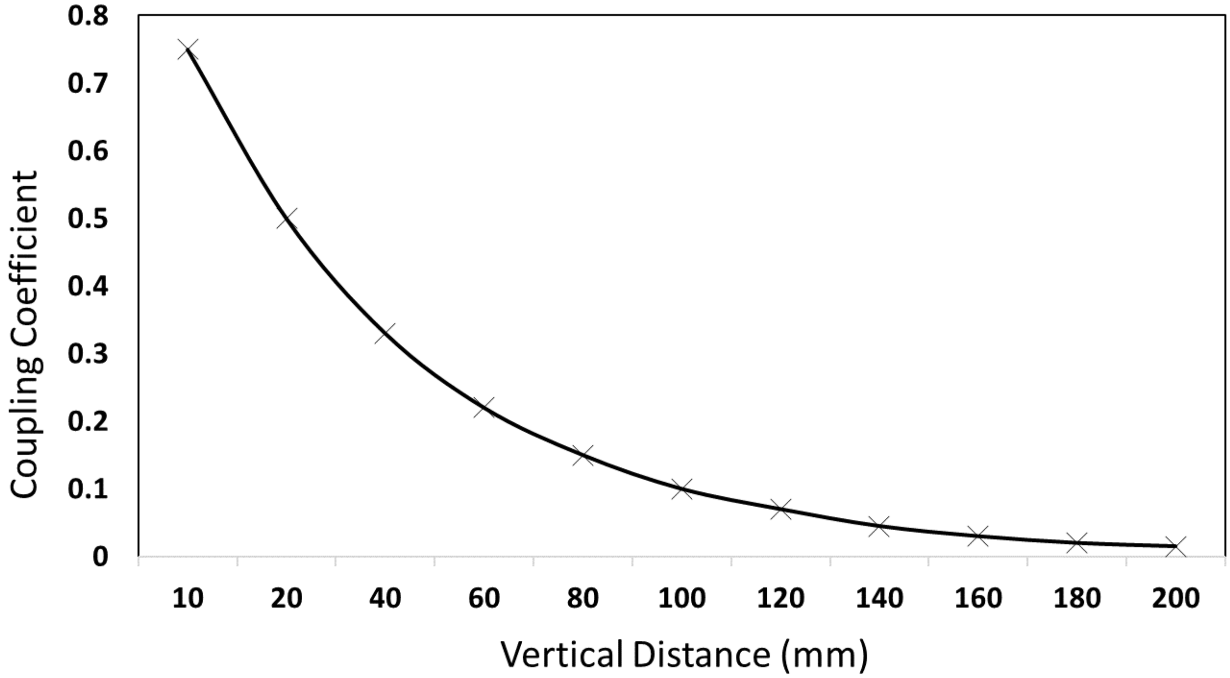

Figure 8.9: Coupling coefficient vs vertical distance

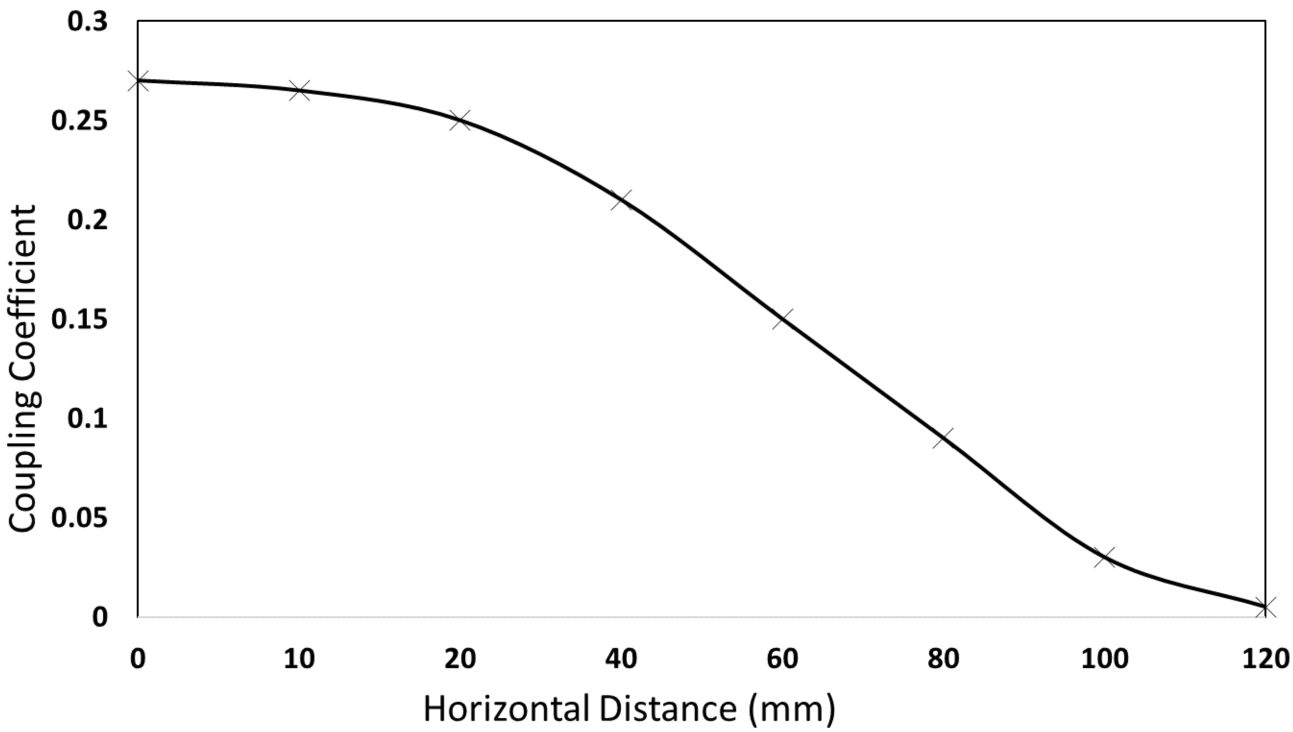

Figure 8.10: Coupling coefficient vs horizontal distance

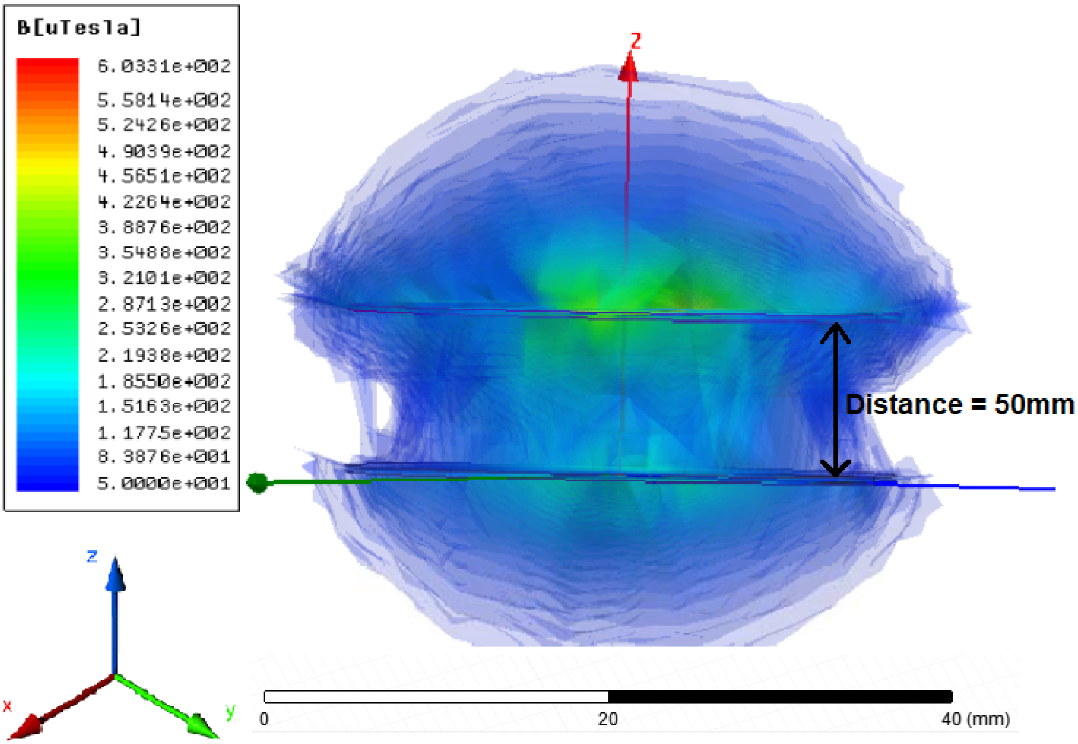

Figure 8.11: Distribution of magnetic field without shielding

In order to reduce further the strong electromagnetic fields, more shields could be placed on the top of the Rx coil (along the Z axis). The radiation will be limited to a specific region without compromising the efficiency of the WPT system. For the simulations performed in this project, only one shield has been used in order to represent the reduction of the electromagnetic field distribution. Future implementation will include more shields on the design that will help to identify the maximum level at which the magnetic field distribution can be reduced.

8.5.2 Efficiency of Power Transfer and Frequency of Operation

Once the design of the Tx and Rx coils of the WPT system has been finalised, the coils can be imported into ANSYS Simplorer software for further analysis, in terms of the operation frequency, maximum achievable power and primary/secondary voltages and currents. The initial circuit design in Simplorer is depicted in Figure 8.13. The circuit parameters have been configured based on the finite element analysis (FEA) performed previously. It can be seen from the circuit schematic that two inductors of values 44.308 uH and 44.32 uH, respectively, are used to represent the coils designed in Maxwell. The values for the inductance of each coil obtained from the parametric sweep

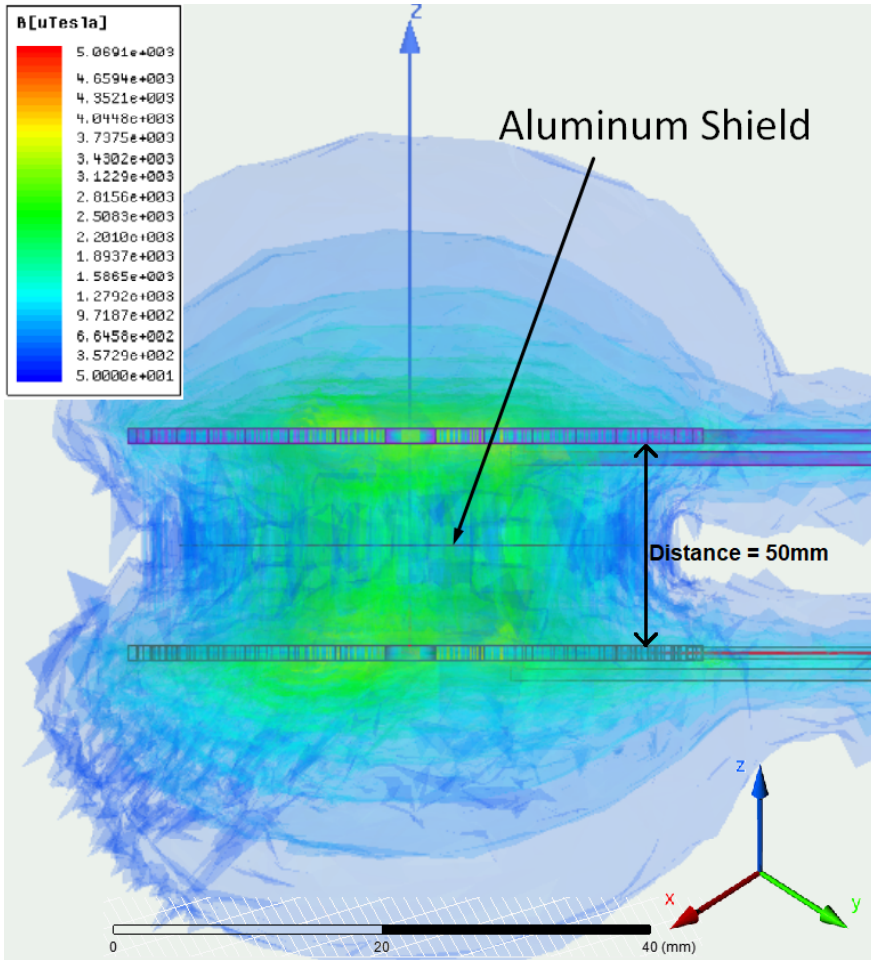

Figure 8.12: Distribution of magnetic field with shielding

analysis discussed previously. Finally, the coupling coefficient has been calculated before with the aid of Maxwell software and presented in Figure 8.9. Thus, by substituting all the known values in formula 8.1, the value for the coupling coefficient obtained by the finite element analysis can be verified. The circuit presented in 8.13 can be used as a tool to perform the simulations and obtain the results that will be needed for the evaluation of the performance of the system.

The circuit of this figure has been designed in such way to provide the best possible coupling factor K. The circuit presented in figure 8.13 forms a resonator on both sides (receiver and transmitter). It should be mentioned that the circuit examined is using a parallel–parallel (P–P) contactless power transfer system. While the system is in resonance, a huge amount of energy can be stored with lower excitation. If the energy intake speed ratio of the system is larger than the energy loss ratio of the system, energy accumulation occurs. In this circuit, the energy oscillates between the coils (which stores energy in the magnetic field) and capacitors (which store energy in an electric field) at a certain resonance frequency. The two resonators of the figure have been placed close to one another in order to form a link and be able to exchange energy. The efficiency of the energy exchange varies depending on each resonator and the coupling ratio K. The dynamics of a system with two resonators can be identified from the coupling mode theory or from equivalent circuit analysis of the connection system for the resonator. Moreover, the components $L1$ and $L2$ are the transmitter and receiver resonator coils, respectively. Each coil has a capacitor in parallel so that a resonator can be formed. R_{ac1} and R_{ac2} resistors denote unwanted resistance (including ohmic and radiation losses) in the coil and the resonance capacitor for each resonator. AC load resistance is shown as *Rload*.

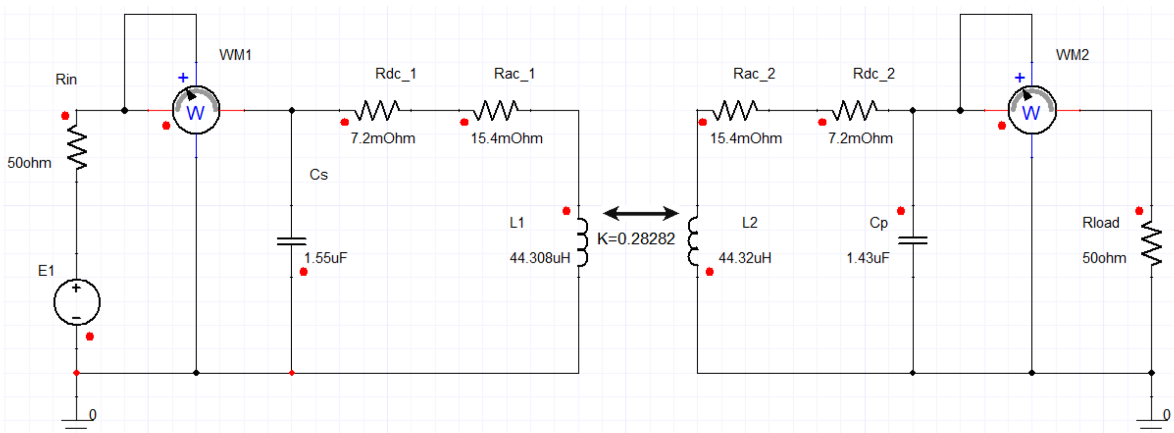

Figure 8.13: Initial circuit design based on the parameters obtained by the finite element analysis

Nevertheless, in order to achieve more accurate results for the WPT system described in this section, the coils designed with the aid of Maxwell software need to be imported into Simplorer. It should be mentioned that some of the components introduced in the initial circuit, need to be changed to run the simulations of the new circuit. The final circuit design of the WPT system is depicted in Figure 8.14. The configuration of the circuit has been changed from P–P to S–P (series–parallel). Furthermore, in order to achieve maximum power delivery on the transmitter's side, for the resonant circuit RLC all the components should be in series to achieve the maximum current that will flow through the transmitter's coil. On the receiver's side, the capacitor *Cp* is placed in parallel with the receiver's coil in order to achieve the maximum voltage that will flow across the load resistor *Rload*.

Firstly, a transient analysis has been performed on the final circuit using Simplorer software. This analysis will provide the voltages and currents in the primary and

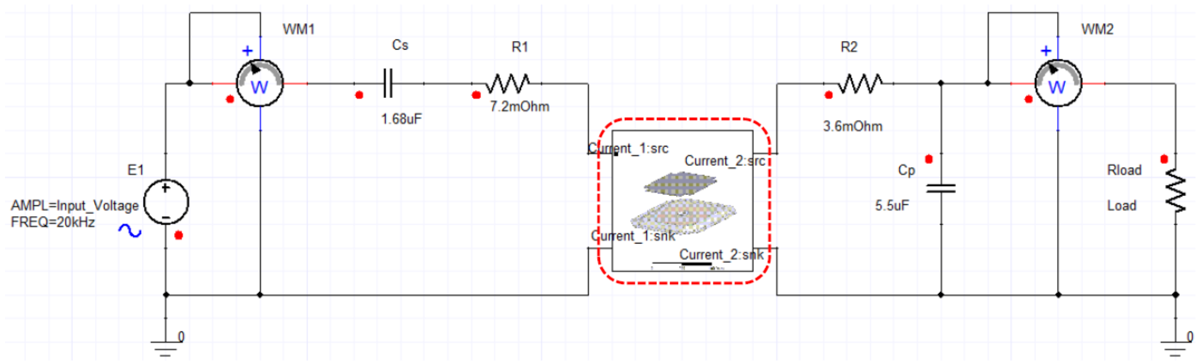

Figure 8.14: Final circuit design with the coils designed in Maxwell

secondary circuits that are used in the WPT system. The results of the transient analysis are depicted in Figure 8.15.

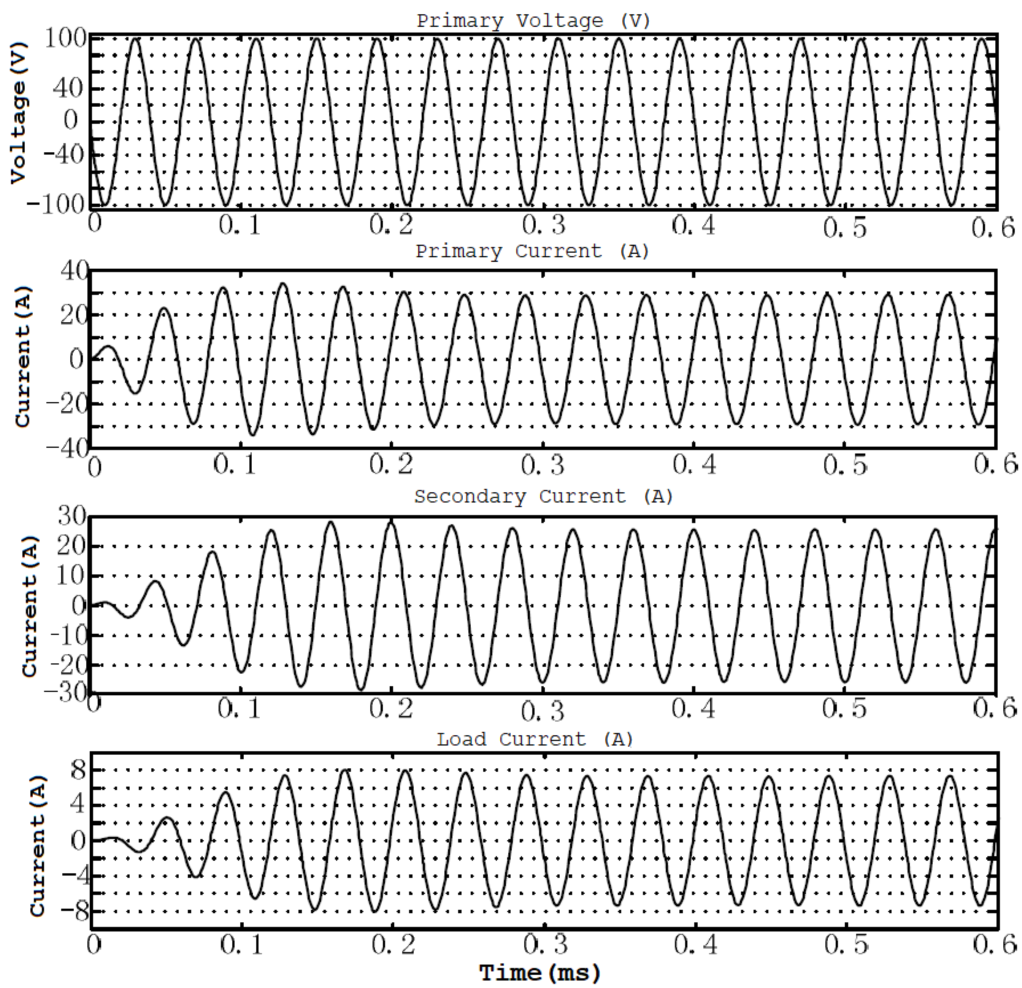

Figure 8.15: Transient analysis results of the final design of the WPT system

From the results, it can be seen that when AC voltage is applied on the transmitter's circuit, there is a current that is flowing through the load. In addition, the transmitter circuit is capable of transferring power wirelessly to the receiver's circuit due to the resonance between them. From the results it can also be observed that there are few losses, but they are negligible and do not affect the overall performance of the system. Such losses are acceptable as far as they are not reducing the transfer efficiency and the amount of power transmitted to the load.

The next simulation performed with the circuit presented in Figure 8.14 is testing the efficiency of the WPT system and the total amount of power that can be transferred from the source to the load under different frequencies. In this way, by using Simplorer an AC analysis in the range of 0 Hz and 60 kHz has been set up. From these simulations, it has been found that the system performs well in the range of kHz where it is capable of transferring the sufficient amount of power that the exoskeleton will need to operate. Finally, from the simulations the results for the input and output power of the circuit as well as the efficiency of the WPT system were obtained. The results from these simulations are depicted in Figures 8.16 and 8.17.

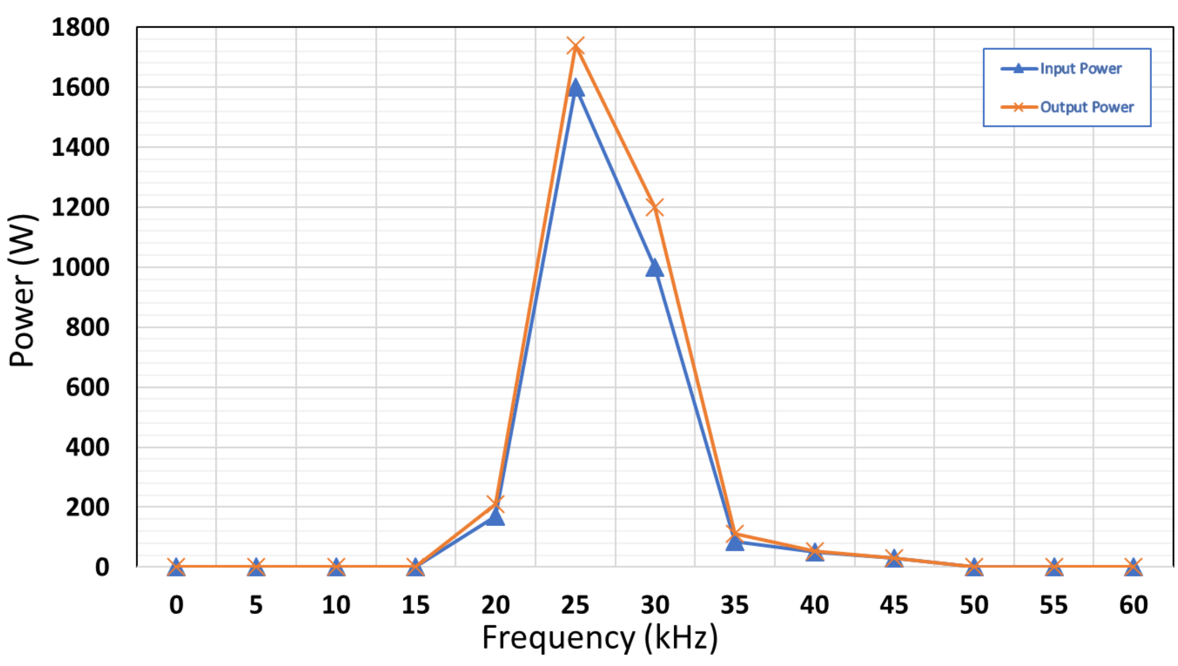

Figure 8.16: Input and output power vs frequency of the simulation model

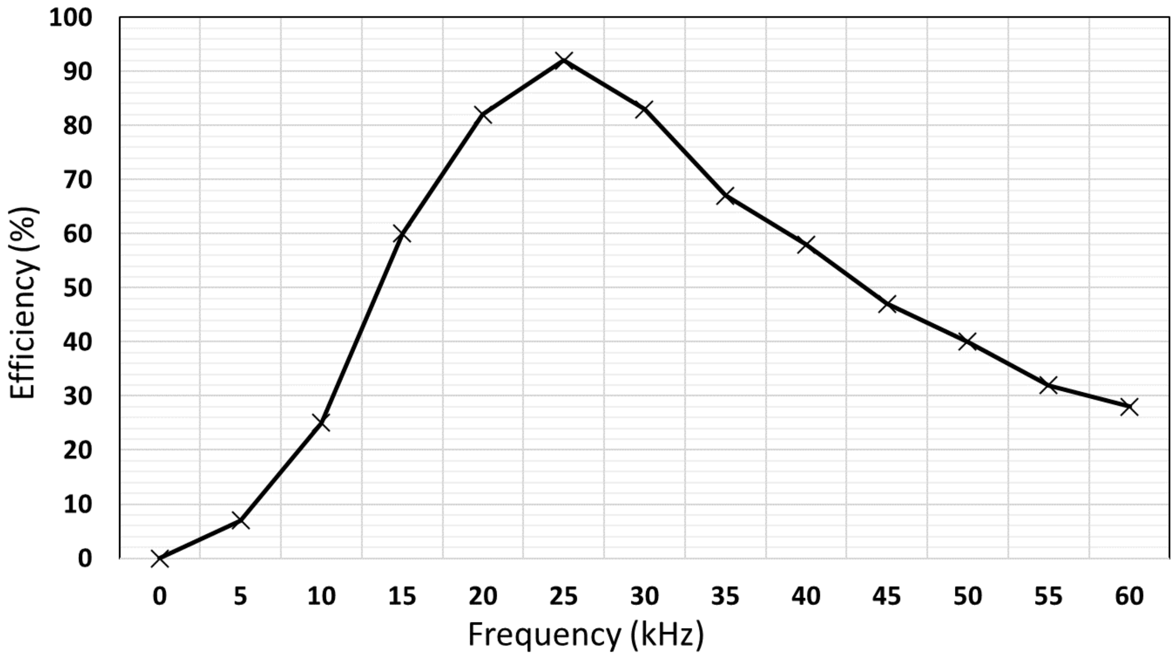

Figure 8.17: Efficiency vs frequency of the simulation model

From the figures 8.16 and 8.17 it can be seen that the simulated model can achieve a peak output power of 1600 W with an input power of 1739 W. Based on these results, the efficiency can be calculated by using the following formula.

$$\eta = \frac{P_{out}}{P_{in}} = \frac{1600}{1739} = 0.92 = 92\% \tag{8.2}$$

Taking everything into account, it seems that the model designed for this simulation approach with the aid of Maxwell and Simplorer performs well under certain conditions. The implementation technique that is tested in the simulations is the magnetic resonant coupling and the configuration of the simulation model has been done in accordance with the specifications and requirements of this specific technique.

8.6 Proposed Design of a WPT System for Continuous Power Delivery to the Exoskeletal Device

As mentioned in the background research for WPT systems, near–field (non–radiative) method seems to be the most suitable for short–range power transfer due to its high efficiency, different implementation techniques and lower exposure to electromagnetic fields which, in turn, can provide a system that will comply with the health and safety regulations as well as with the IEEE Standards. Near–field WPT techniques can be used to address the energy consumption problem in exoskeletons with a strong potential for both indoor assistive and enhancive solutions. The operational time of an exoskeleton is normally limited by the battery capacity and it can only work for a limited amount of time. Several studies have emphasised different methods to prolong the operational time of batteries. Although these efforts have shown an improvement in power consumption, their power consumption/operational time remains a performance bottleneck and its feasibility is the key factor that impedes deployment in vast areas.

Taking the above factors into account and with respect to the nature and power requirements of the application examined in this project, there is a great need for a wireless power transmission system that will be safe for the human health and capable of delivering high amount of power with the best possible transmission efficiency. The implementation method that has been simulated in the above sections is the magnetic resonant coupling and it has been seen that it performs well under certain conditions. Thus, based on the simulation approach, this WPT system can be integrated on the exoskeleton and meet the power needs specified in the above sections.

Nevertheless, in order to achieve the best possible efficiency for the proposed WPT system, the receiver coils that will be attached to the exoskeleton should be near the transmitter coils (preferably within 10 cm). Therefore, based on the prototype design presented in Figure 3.12 (chapter 3, section 3.4.2), it can be seen that a potential place for the coils is at the soles of the exoskeletal device. As mentioned previously, the exoskeleton will be worn by a user and it will mimic his/her motions. Accordingly, the soles of the device will be in continuous contact with the ground/earth (either both soles or one at a time). Based on this approach, the transmitter coils can be placed on or under the floor that will be modified for this purpose.

When it comes to the implementation of the transmitter coils, the factor that one coil is not sufficient to provide uninterrupted power to the exoskeleton needs to be considered. The user that will wear the device will, usually, move/walk constantly and perform certain activities. For this reason, there is a need for continuous power without any failures in the transmission. That factor can be addressed by using an array of coils that will be placed on the modified floor and will cover the whole area at which the exoskeleton will move. Representation of a WPT system with array coils is depicted in Figure 8.18.

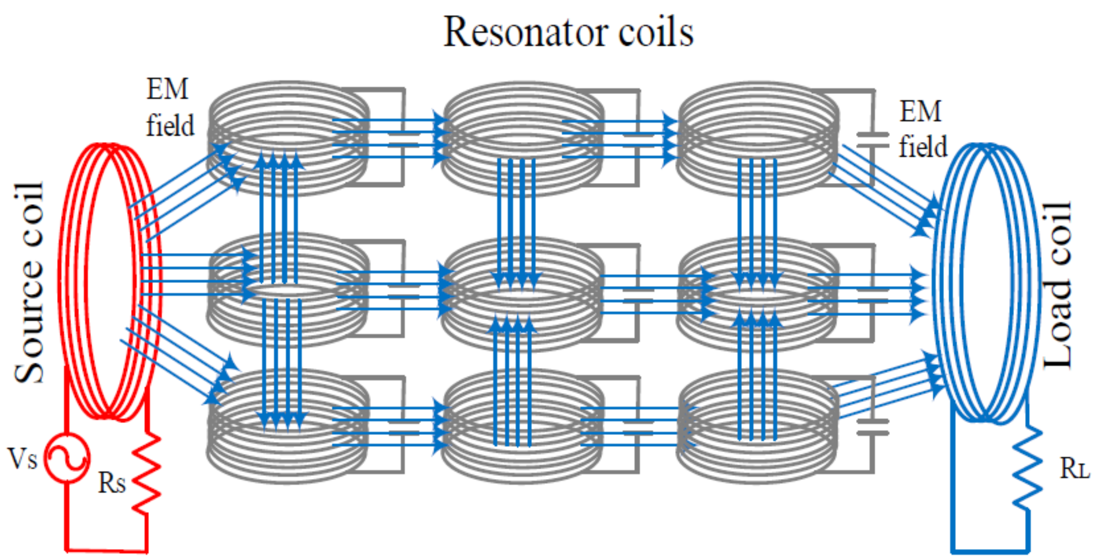

Figure 8.18: WPT system with array coils

By implementing this approach, the receiver coils will be in continuous coupling with one or more transmitter coils at the same time and be able to receive the power needed for the on–board electronics and actuators of the exoskeleton. There are cases where the receiver coils will not be in perfect alignment (either horizontally or vertically) with the transmitter coils, although the system will still be able to pick up the transmission signal an exchange energy. That effect has been tested in this project with the aim of COMSOL and Maxwell in the previous sections, where the vertical and horizontal positions were changed dynamically to evaluate the performance. Even under greater than 10 cm distances, it has been proved that the WPT system is capable of transferring electric power but with the cost of lower efficiency. It should also be mentioned that another simulation has been performed where the angular displacement of the receiving coil was changing dynamically to evaluate the coupling coefficient of the WPT system. Both simulations are discussed in the previous sections extensively.

Therefore, by taking the aforementioned into account, a WPT system can be implemented to serve as the power supply for the exoskeleton. The proposed system can be represented by the block diagram depicted in Figure 8.19. Such system has been evaluated by Nutwong et al. in [238], where they have tested the performance of a simple

WPT system with one receiver and several transmitters. In their research they have also evaluated the coupling coefficient of their system when the receiver is under two different conditions: (a) when the receiver is close to the centre of one of the transmitter coils and (b) when the receiver is between two transmitters. Multiple transmitter coils are excited by the inverter circuit. Detection switches are placed between the receiver coil and the rectifier circuit. The DC output voltage (V_{out}) is sensed and transmitted to the primary circuit via wireless communication devices. The primary-side controller is used to select the transmitter coil pattern and regulate the output voltage. The secondary-side controller is used to control the detection switches and send feedback data wirelessly.

The inverter circuit consists of (n+2) MOSFET switches with antiparallel diodes, where "n" is the number of transmitter coils. The excitation of each transmitter coil is controlled by excitation switches. Compensation capacitors are connected in series with each transmitter coil. A rectifier circuit with four diodes and a filter capacitor are included on the output. The detection switches are located in front of the rectifier circuit. When these diodes are on, then the receivers resonant circuit form a resonant configuration. With proper switching frequency on the primary side, the secondary circuit experiences a line communication. The detection switches are designed to exhibit the bidirectional–carrying and bidirectional–blocking characteristics, which make them similar to an ideal switch. The operation of the system depicted in figure 8.19 is divided into the two following main categories:

- **Normal Mode:** In normal mode, the transmitter and receiver coils are perfectly or partially aligned and the charging process of the load is initiated. Thus, when the system is operating in this mode, the transmitter is able to transfer power wirelessly. On the other side, the receiver will pick up this power and transfer it to the load to either charge any potential batteries that will be connected to the system or directly power up the on–board electronics attached on the exoskeleton;

- **Detection Mode:** The detection mode serves as an approach in determining a proper transmitter coil pattern before the charging process. In more details, every time that this mode is active, the system is loading a predefined coil pattern in order to provide the most efficient charging process. The detection mode is activated prior to normal mode.

Finally, the basic operating principal of the proposed WPT system is depicted in Figure 8.20.

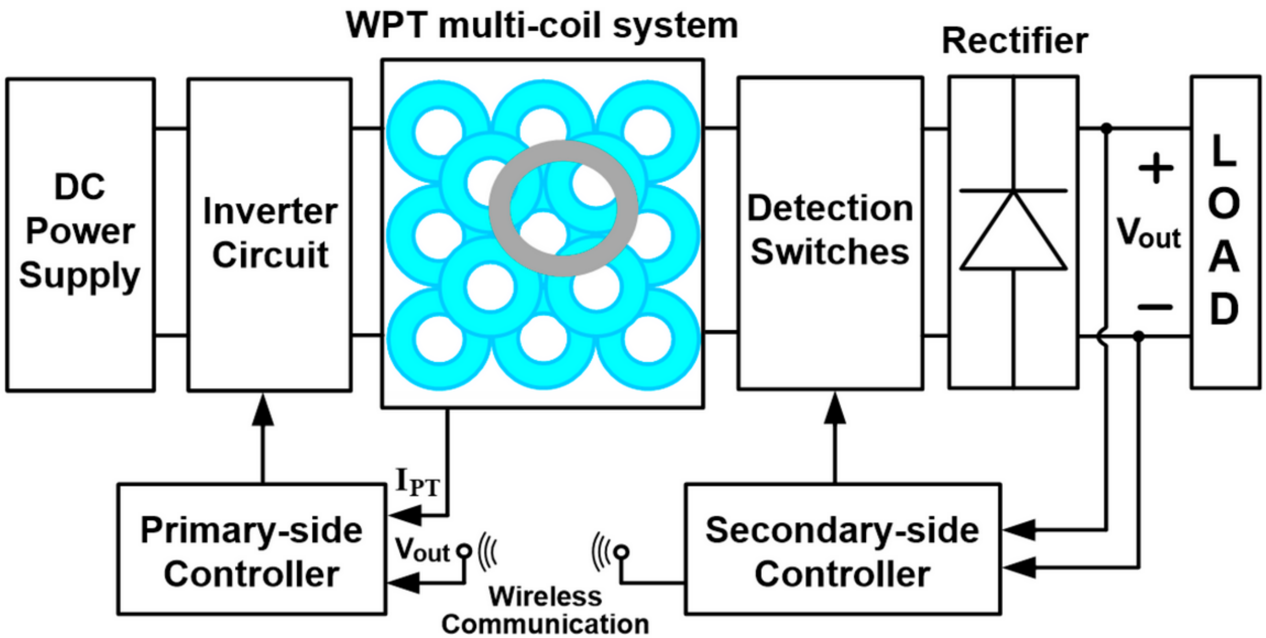

Figure 8.19: Block diagram of the proposed wireless power transmission system

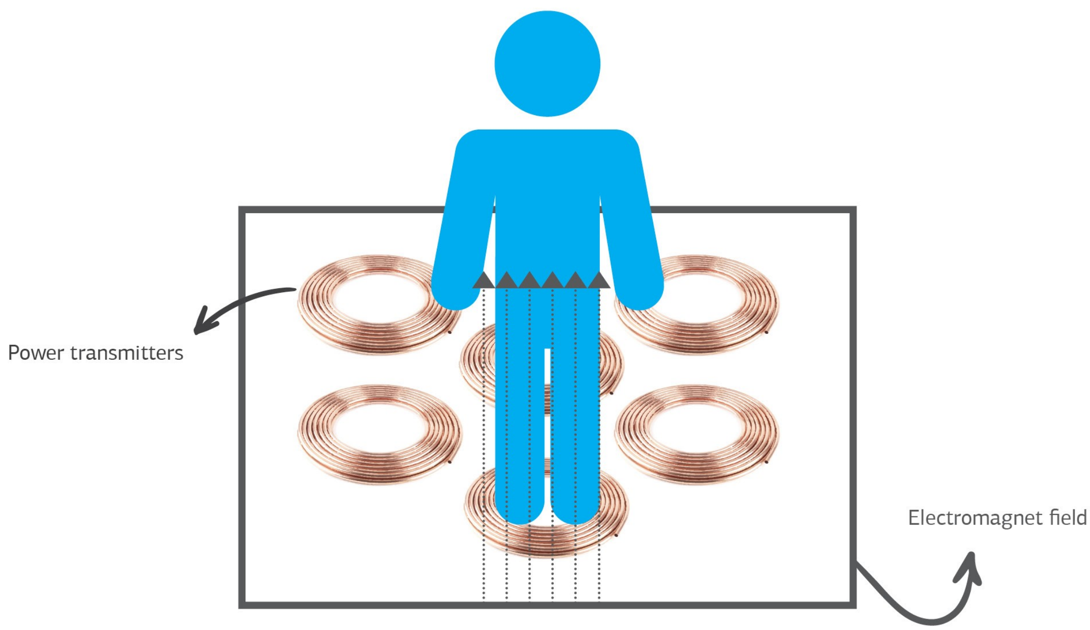

Figure 8.20: Basic operational principal of the proposed WPT system

8.7 Summary

The first section of this chapter presented the simulation objectives that has been set based on the literature review in WPT systems and the requirements for this project. These objectives have been followed step by step in order to obtain the expected results with regard to the theoretical approach presented in the previous chapter of this report.

The second section is presenting the analysis of the human gait. This analysis has been conducted in order to gain a better understanding of the human gait and its phases, with focus on the motions of the foot, its contact with the ground and the angular displacement when human performs certain activities. The results proved to be essential for designing the antennas that have been used in the simulations. In addition, the angular displacement of the foot has been studied since it is a parameter that need to be tested in the simulations to evaluate the coupling coefficient of the WPT system. The final part of this section is investigating the potential places and areas on the exoskeleton frame that can be used to attach the transmitting and receiving coils. The prototype design of the exoskeleton has been studied thoroughly and it has been found that the sole of the exoskeleton can be a possible area where the receiving antenna can be integrated and exchange power with a transmitting circuit that can be placed on the floor.

Third section of the chapters presents the implementation method and technique that will be followed to design and simulate the WPT system. Defining these is essential at a first stage in order to estimate the performance of the system that will be simulated. Since the exoskeleton is a device that needs a human to operate, a near–filed method is discussed with focus on the magnetic resonant coupling due its technical specifications and the high efficiency that it can provide. Next, an initial design of the antennas is presented along with the parameters that have been configured in COMSOL software during the design process. These antennas have been simulated to investigate the distribution of the electric field and the power flow when the transmitting antenna has a fixed position and the receiving antenna is rotating with different angles on every simulation. The results of the simulations have been discussed briefly and it has been seen that the antennas have strong coupling for the different angles used, except the case where the receiving antenna rotated by 90 degrees. This simulation has been performed with respect to the human gait study in order to visualise the coupling of the antennas when the angular displacement is changing dynamically.

The results from COMSOL have been analysed thoroughly in order to design the final system that will be simulated in the next section with the aid of ANSYS Maxwell and Simplorer. Firstly, the design of the coils has been done in Maxwell and their parameters such as self–inductance, coupling coefficient and mutual inductance have been obtained from the simulations by using finite element analysis software. The final design of the coils is presented in this section along with the coupling coefficient between them when the distance is changing vertically and horizontally. It has been found that a relatively good coupling coefficient for the model that used in the simulations can be achieved. Next, the electromagnetic field distribution of the coils is presented as well as the methods on how to reduce the exposure to radiation and provide a safer system by using aluminum shielding. The efficiency and the maximum output power are also presented in this section, which have been obtained from the AC and Transient analysis performed in Simplorer. From these simulations it can be seen that the system is able to transmit at least 1600 W of power with an efficiency of 92% and an operating frequency of 25 kHz.

The final section of the chapter is proposing the development of a sophisticated physical layer approach for self–aware rechargeable floor and energy efficient WPT for exoskeletons. The design of the proposed system is based on the implementation of an array of coils that can be integrated to the floor that will be modified for this purpose and will be able to continuously deliver power to the exoskeleton device. A potential solution for the proposed system is discussed and the block diagram included in the analysis to provide a visual representation of the WPT system. This approach seems to be a promising solution for an efficient WPT system that will deliver uninterrupted power to the exoskeleton.

Finally, the approach that adopted in the system that proposed to provide continuous and uninterrupted power wirelessly, can be challenging due health hazard concerns. The user of the exoskeleton could be exposed to electromagnetic radiation which can introduce a safety risk. Thus, particular attention should be paid when manufacturing and testing the proposed design in order to overcome or limit the challenges and safety concerns that examined thoroughly in 7.5.6.

Chapter 9

Summary, Conclusions and Future Work

9.1 Summary

In Chapter 1 the aims and objectives of the research are outlined. The aims of the individual research were to determine the most suitable communication strategy for an enhancive full–body exoskeleton coupling with the operator's segments and develop a basic prototype of the selected communication system to successfully transfer data between modules and other on–board electronic devices. In addition, this study seeks to review the potential power sources that can be used to deliver sufficient amount of energy to operate the exoskeleton, such as energy harvesting and wireless power transmission technologies and identify the challenges of using these technologies for power–hungry applications. This information is to be used to design and simulate a dynamic model that will address these challenges and provide a novel solution of the optimum design methodology for enhancive exoskeletons. This section summarises the research objectives and results found.

Acquire basic understanding for an enhancive full–body exoskeleton, with focus on the communication and power system aspects.

The requirements of designing and manufacturing exoskeletons were gathered from the literature review and presented in Chapter 2. From these, requirements for communication and power systems are derived. Classification of exoskeletons and control strategies are also reviewed to obtain a better understanding of the main factors that should be considered during the design process. Special emphasis is placed on the communication approach and architecture used in BLEEX. This is a first step on identifying the main aspects of using a real–time communication systems in exoskeletons. Current state and challenges are also presented.

Survey potential communication/network strategies for the entire robot and determine which communication systems are suitable for the exoskeleton.

In Chapter 3 potential communication strategies suitable for an exoskeleton device were described. Advanced communication protocols that are used extensively in industry were discussed, along with any previous related work. The main specifications of each protocol were reviewed and compared to select the most suitable candidate to be used for this project. Evaluation of the technical specifications of each protocol in terms of available hardware, bit rate, topologies, message size and maximum number of connected nodes/slaves were presented. A scoring scheme has been adopted to quantify the features of each protocol. In order to derive the score of the different aspects, the potential nodes locations on the exoskeleton prototype presented. Lastly, it has been shown that EtherCAT is the most suitable candidate due to the greatest range of available hardware, the bigger frame size, the support of several different topologies or even a combination of them and, lastly, the highest bit rate compared to other communication protocols. Finally, the real–time characteristics as well as the low complexity and high reliability were the main aspects for choosing EtherCAT.

Choose sensors and electronics for a novel single joint prototype, which is intended to be a base for further development and serve as a platform for proving the successful operation of the communication network. Develop electronics and software for the platform.

The sensors and electronics that will be used to develop a novel joint prototype are described in Chapter 5. Linear Variable Differential Transformer (LVDT), load cells with SGA amplifiers and absolute encoders were interfaced to CX2030 embedded PC, on which the control algorithms and other functions will be executed. The software that is controlling these devices and sensors was written in TwinCAT. The technical specifications of each device were discussed to assess the performance and limitations they will introduce. Lastly, the software implementation methodology is discussed thoroughly along with the communication characteristics that should be configured on the master device (CX2030) during the experimental process.

Construct communication–oriented model of the device and simulate the proposed communication strategy for the exoskeleton, on the level of the entire device, to gain insight into communication related issues. Evaluate the performance and assess its stability, efficiency, reliability and robustness.

This was done in Chapter 4. Firstly, the simulation approach and objectives are discussed. This approach is based on the performance and the protocols that are used to operate Ethernet protocol. It has been seen that EtherCAT is based on the characteristics of conventional Ethernet that is used widely in industry. The simulations have been performed with the aid of Riverbed Modeler (previously known as OPNET). The data exchange interval is the factor that is examined thoroughly in order to calculate the execution time of each separate task and the overall communication cycle time of the simulation model. Equations were derived for the calculation of these elements. In the next step three different simulation models have been designed to assess the performance of the network. Each model consisted of different number of the slaves and different topologies. Moreover, throughput of each model has been obtained from the simulations. It was shown that the results from the simulations were matching those obtained by the theoretical approach. Also, an approach to increase the overall performance of the network is discussed and an algorithm for the frame size optimisation is presented. It has been seen that by using this algorithm, the size of the frame can be reduced by 50% when the output nodes are physically placed before the input nodes. Lastly, a design methodology of the whole communication system is discussed and a prototype of this design is presented. The cable redundancy feature is also introduced in that prototype and is used to avoid potential network failures during normal operation.

Implement an experimental setup to assess the feasibility of the proposed communication protocol. Validate the theoretical and simulation approaches.

This was done in Chapter 6. An experimental setup developed to test the sensors and electronic devices that will be connected on EtherCAT network. Firstly, the implementation priorities were discussed to identify the objectives that should be met from the experiments, based on the simulation results and the literature review. The hardware setup of LVDT, load cell and encoder were presented. The software configurations that were made for each device in TwinCAT are also discussed. It was shown that the LVDT was capable of measuring the distance of travel with a small error due to residual voltage left. However, that error did not affect the performance of the communications and the output results. On the other hand, it has been remarked that when experimenting with the load cell, the output voltage was extremely low and the measurement were became inaccurate when applying higher loads on the sensor. To avoid that, a strain gauge amplifier has been used to obtain accurate measurements and filter the output results. Filtering is also needed for the encoder device to obtain results of high accuracy. Although the experiments for each device and sensor conducted successfully, the results cannot be fully evaluated since the control algorithm has not been deployed on EtherCAT network. However, the control strategy developed by the controls' engineer of this project were discussed and critically evaluated. From this evaluation it has been found that the control algorithm can be deployed on EtherCAT protocol in the future. Lastly, an estimation of the communication cycle time based on the proposed network topology is presented. It has been found from calculations that the overall communication cycle time is 33.68 μs which means that when the control loop configured at 2 kHz, then the master will still have 466.32 μs for the computation of other algorithms.

Assess the main technical specifications of potential power sources and technologies that can be used for exoskeletons and determine which technology is the most suitable candidate.

The potential power sources that are suitable for exoskeletons are presented in Chapter 7. Firstly, the widely adopted power sources, such as non–rechargeable primary cells, internal combustion engines, electromechanical fuel cells and tethered solutions are discussed. Their technical specifications are outlined along with related work and experiments performed by other scientists. Moreover, energy harvesting technologies, such as regenerative breaking, thermoelectric devices, piezoelectric devices and solar panels were reviewed, in terms of their technical specifications. Based on the overall performance and efficiency, it has been found that regenerative breaking is the most promising solution for providing adequate amount of electric energy for the on–board electronics of the exoskeleton. Lastly, wireless power transmission methods and implementation techniques have been discussed. Previous related work has been presented in addition to the performance metrics for each WPT technology. Furthermore, it has been concluded that due to the nature of the application examined in this project, magnetic resonant coupling is the most suitable candidate for the implementation of the WPT system to be used. High efficiencies, frequencies of operation and transfer distances were the main factors for selecting this implementation technique.

Simulate and propose a novel solution of using wireless power transmission technologies for the final structure of the exoskeleton, based on the power requirements that have been specified for this application.

This was done in Chapter 8. The simulation model of a WPT system has been designed with the aid of COMSOL and ANSYS Maxwell. From the simulation results it has been seen that the WPT system is capable of transferring up to 1.8 kW of electric power with an efficiency of more than 90%. In addition, the electromagnetic field distribution of the coils has been examined in order to identify if the WPT system poses a risk of exposure to radiation when the system is used in line with humans. It has been seen that shielding of the coils can reduce the distribution of the electromagnetic field and, in turn, the exposure to radiation. Finally, a WPT system for continuous power delivery to the exoskeleton is presented. This system is capable of transferring up to a few kilowatts of electric power and can be used as a standalone solution for the exoskeleton. The implementation technique is based on an array of transmitting coils that can be mounted on the floor and transfer energy when the receiving coils of the exoskeleton entering the area of coverage.

9.2 Conclusions

Looking at the summary it can be concluded that the individual research has successfully presented an approach for using a real–time protocol, such as EtherCAT, to establish the on–board communications. The results of the analysis shown that EtherCAT is the most suitable candidate for the exoskeleton project. The superiority of EtherCAT in terms of bit–rate and availability of hardware were deterministic factors that positioned the protocol above the rest. As it was demonstrated, the real–time communication system was successfully used as part of a full–body enhancive exoskeleton. The work has clearly shown that the sensors and devices attached to the protocol were capable of transmitting the data packets using a control loop execution frequency of 2 kHz which was derived from the motion capture study.

An investigation into simulation of a real–time communication system for a full–body enhancive exoskeleton gave guidelines for the final design of the protocol. Throughput, network delays and communication cycle time were obtained from the simulations used to provide an estimation on the performance of the protocol when several nodes/slaves are attached on the network. Furthermore, by comparing the simulation results with the theoretical approach, it has been found that the length of the data that are travelling around the network can be larger, which means that more data packets can fit in the protocol frame when the network is operating under the same period/frequency. Moreover, the analysis of the frame size optimisation algorithm has shown that the frame transmission time can be reduced by 50% when the output terminals are physically placed before the input terminals. A design methodology for inclusion of the frame size optimisation algorithm presented with respect to the proposed network topology discussed in Chapter 3.

Moreover, a research on the power sources suitable for the exoskeleton has been presented in this report. Conventional power sources (e.g. rechargeable primary cells and internal combustion engines), energy harvesting solutions (e.g. regenerative breaking and solar panels) and wireless power transmission technologies (e.g. near and far–field solutions) have been reviewed. The analysis has clearly shown that wireless power transmission is the most suitable method to deliver sufficient amount of power that will be used both by the on–board electronics and the hydraulic valves. The near–field solution of magnetic resonant coupling has been found to be the most promising candidate for the WPT system to be used by the exoskeleton. The potential WPT system has been tested by means of simulations and from the results obtained it can be deduced that wireless power transmission technology can be used as a standalone solution to meet the energy requirements of the exoskeleton. Transfer efficiency and amount of transmitted power of the simulation model have been evaluated in order to estimate the performance of the system. Finally, the research concludes by proposing a novel design methodology for implementing a WPT system that can be deployed to deliver undisrupted power to the exoskeleton. That system is based on the magnetic resonant coupling technique by using an array of transmitting coils mounted on the floor. These coils will be capable of transferring energy to the receivers when they enter the area of coverage. Further improvements and considerations for the simulation model will be discussed in future work sections.

9.3 Future Work

Following the research presented in this report, there are further issues and expansions to be explored in the future:

a. Further research could be conducted on the control strategies of the exoskeleton and which approach should be followed in order to develop a robust control and communication system. The integration of control and communication in networked control systems has made the design and analysis of such systems a great theoretical challenge for conventional control theory. Such an integration also makes the implementation of networked control systems a necessary intermediate step towards the final convergence of control, communication, and computation. The role of integrated communication and control systems is to coordinate and perform interrelated functions, ranging from real–time multi–loop control to information display and routine maintenance support. Thus, it is essential to understand the main characteristics of a control system and how a control algorithm can be integrated into the communication system to provide a robust solution;

b. A successful approach for simulating the selected communication protocol was proposed. Nevertheless, there might be room for improvements by optimising the network topology to further improve the performance of the communication system. Topology optimisation aims at achieving the stability of the network architecture, and then further enhances network performance. Most of them are based on improving the physical architecture parameters of the network, such as the number of nodes, the distance between nodes, and the link relationship between nodes and so on;

c. The simulation model designed to assess the performance of EtherCAT protocol is not making use of the frame size optimisation algorithm. Since this algorithm can be deployed to reduce the overall communication cycle time, it is interesting to investigate the behaviour of the simulation model in a future implementation;

d. Although the sensors attached to the prototype tested successfully using EtherCAT protocol, the overall performance of the communication system cannot be fully evaluated since the control algorithm has not been deployed. Further experiments must be carried out in the future by integrating the algorithm into EtherCAT system;

e. Communication system was shown to perform well when the sampling frequency was configured at 2 kHz (period of 500 μs). This frequency has been derived from the motion capture study. In the future it is advisable to assess the performance of the system setup using sampling rates of up to 20 kHz;

f. The configuration of the communication system at the current stage did not take into account the optimisation of the distributed clocks. This is a feature that can be used in EtherCAT protocol to increase the stability of the network and achieve higher performance. It remains a research question where and how to best incorporate this in the implementation process of the network in order to avoid undesirable effects, such as high jitter;

g. As seen in the simulation process of the WPT system, the power that can be transmitted is sufficient to meet the energy requirements of the exoskeleton. It remains as future work to investigate the behaviour and performance of the proposed design by means of experiments under real–world conditions;

h. The simulation results of the WPT system has shown that the electric power that can be transmitted to the exoskeleton, could reach the scale of a few kilowatts. A future implementation will integrate a monitoring and controlling system, which will help to avoid undesirable effects during the power transmission;

i. Further investigation should be done on the selection of the sensors that will be attached to the exoskeleton, since they would have to be robust, while providing sufficient measurement quality. For sensors and actuators, industrial Ethernet (such as EtherCAT) is often excessively robust and powerful. These systems usually require point–to–point communications rather than a fieldbus, and their bandwidth requirements are normally low. Thus, each sensor should be selected in such way to meet the real–time characteristics of the communication protocol examined in this work.;

j. Moreover, research into the environment that the exoskeleton will be used in might give rise to an indication of the time needed to perform certain amount of operations. This information can be used to further optimise both the communication and WPT systems.

k. Although limitations, challenges and safety concerns, when using WPT systems, have been discussed thoroughly in this report (Section 7.5.6, page 171), further research should be performed on the techniques and methods of reducing electromagnetic radiation and other potential safety hazards, especially when humans involved in the experimental process and, either indirectly or directly, interact with the WPT system.

Bibliography

[1] J. Raade, K. Amundson, and H. Kazerooni. Development of hydraulic–electric power unit for mobile robots. In *Fluid Power Systems and Technology, ASME 2005 International Mechanical Engineering Congress and Exposition on*, pages 27–34, November 2005.

[2] N. Mizen. *Design and Test of a Full-Scale, Wearable, Exoskeletal Structure*. Technical report, Cornell Aeronautical Laboratory, Inc., March 1964.

[3] N. Mizen. *Preliminary Design of a Full–Scale, Wearable, Exoskeletal Structure*. Technical report, Cornell Aeronautical Laboratory, Inc., 1963.

[4] R. S. Mosher. Handyman to hardiman. In *SAE Technical Paper*. SAE International, 02 1967. Accessed: 2019-07-08.

[5] B Makinson J. *Research and Development Prototype for Machine Augmentation of Human Strength and Endurance – Hardiman I Project*. Technical report, General Electric Company, May 1971.

[6] B Fick R. and B Makinson J. *Final Report on Hardiman I Prototype for Machine Augmentation of Human Strength and Endurance*. Technical report, General Electric Company, August 1971.

[7] A. Chu, H. Kazerooni, and A. Zoss. On the biomimetic design of the Berkeley Lower Extremity Exoskeleton (BLEEX). In *Robotics and Automation, 2005. ICRA 2005. Proceedings of the 2005 IEEE International Conference on*, pages 4345–4352, April 2005.

[8] H. Kazerooni. Exoskeletons for human power augmentation. In *Intelligent Robots and Systems, 2005. (IROS 2005). 2005 IEEE/RSJ International Conference on*, pages 3459–3464, August 2005.

[9] A. Zoss, H. Kazerooni, and A. Chu. On the mechanical design of the Berkeley Lower Extremity Exoskeleton (BLEEX). In *Intelligent Robots and Systems, 2005. (IROS 2005). 2005 IEEE/RSJ International Conference on*, pages 3465–3472, August 2005.

[10] A. B. Zoss, H. Kazerooni, and A. Chu. Biomechanical design of the Berkeley Lower Extremity Exoskeleton (BLEEX). *IEEE/ASME Transactions on Mechatronics*, 11(2), April 2006.

[11] H. Kazerooni and R. Steger. The Berkeley Lower Extremity Exoskeleton. In *Journal of Dynamic Systems, Measurement, and Control, Transactions of the ASME*, volume 128, pages 14–25 vol.1, March 2006.

[12] H. Kazerooni, J-L. Racine, A. Chu, and Zoss A. Lower extremity enhancer, December 2011. US Patent 8,070,700 B2.

[13] Exobionics webpage. `http://www.eksobionics.com/`. Accessed: 2014-07-31.

[14] Berkeley Robotics & Human Engineering Laboratory webpage. `http://bleex.me.berkeley.edu/`. Accessed: 2014-07-30.

[15] H. Kazerooni. Exoskeletons for human performance augmentation. In *Springer Handbook of Robotics*, pages 773–793. Springer Berlin Heidelberg, 2008.

[16] G. Mone. Popular Science: Building the Real Iron Man. `http://www.popsci.com/scitech/article/2008-04/building-real-iron-man`, Accessed: 2014–05–23.

[17] S.C. Jacobsen, M.X. Olivier, and B.J. Maclean. Biomimetic mechanical joint, August 27 2013. US Patent 8,516,918.

[18] C. Kovalsky and G. Shields. Raytheon: Raytheon Unveils Lighter, Faster, Stronger Second Generation Exoskeleton Robotic Suit. `http://raytheon.mediaroom.com/index.php?s=43&item=1652`, Accessed: 2014–05–23.

[19] Army Technology. Raytheon XOS 2 Exoskeleton, Second–Generation Robotics Suit, United States of America. `http://www.army-technology.com/projects/raytheon-xos-2-exoskeleton-us/`, Accessed: 2014–05–23.

[20] M. Bergamasco, F. Salsedo, S. Marcheschi, N. Lucchesi, and M. Fontana. A novel compact and lightweight actuator for wearable robots. In *Robotics and*

Automation (ICRA), 2010 IEEE International Conference on, pages 4197–4203, May 2010.

[21] N. Lucchesi, S. Marcheschi, L. Borelli, F. Salsedo, M. Fontana, and M. Bergamasco. An approach to the design of fully actuated body extenders for material handling. In *RO–MAN, 2010 IEEE*, pages 482–487, September 2010.

[22] S. Marcheschi, F. Salsedo, M. Fontana, and M. Bergamasco. Body extender: Whole body exoskeleton for human power augmentation. In *Robotics and Automation (ICRA), 2011 IEEE International Conference on*, pages 611–616, May 2011.

[23] K. Yamamoto, K. Hyodo, M. Ishii, and T. Matsuo. Development of power assisting suit for assisting nurse labor. *JSME International Journal Series C Mechanical Systems, Machine Elements and Manufacturing*, 45(3):703–711, 2002.

[24] K. Yamamoto, M. Ishii, H. Noborisaka, and K. Hyodo. Stand alone wearable power assisting suit – sensing and control systems. In *Robot and Human Interactive Communication, 2004. ROMAN 2004. 13th IEEE International Workshop on*, pages 661–666, September 2004.

[25] T. Yoshimitsu and K. Yamamoto. Development of a power assist suit for nursing work. In *SICE 2004 Annual Conference*, volume 1, pages 577–580, August 2004.

[26] M. Ishii, K. Yamamoto, and K. Hyodo. Stand–alone wearable power assist suit – development and availability. In *Journal of Robotics and Mechatronics*, volume 17, pages 575–583, 2005.

[27] J.E. Pratt, B.T. Krupp, C.J. Morse, and S.H. Collins. The RoboKnee: an exoskeleton for enhancing strength and endurance during walking. In *Robotics and Automation, 2004. Proceedings. ICRA '04. 2004 IEEE International Conference on*, volume 3, pages 2430–2435 Vol.3, April 2004.

[28] K. Kong and D. Jeon. Fuzzy control of a new tendon–driven exoskeletal power assistive device. In *Advanced Intelligent Mechatronics. Proceedings, 2005 IEEE/ASME International Conference on*, pages 146–151, 2005.

[29] K. Kong and D. Jeon. Design and control of an exoskeleton for the elderly and patients. *Mechatronics, IEEE/ASME Transactions on*, 11(4):428–432, August 2006.

[30] K. Kong, M. Tomizuka, H. Moon, B. Hwang, and D. Jeon. Mechanical design and impedance compensation of SUBAR (Sogang University's Biomedical Assist Robot). In *Advanced Intelligent Mechatronics, 2008. AIM 2008. IEEE/ASME International Conference on*, pages 377–382, July 2008.

[31] K. Kong, J. Bae, and M. Tomizuka. Control of rotary series elastic actuator for ideal force–mode actuation in human – robot interaction applications. *Mechatronics, IEEE/ASME Transactions on*, 14(1):105–118, February 2009.

[32] K. Kong, H. Moon, B. Hwang, D. Doyoung Jeon, and M. Tomizuka. Impedance compensation of SUBAR for back–drivable force–mode actuation. *Robotics, IEEE Transactions on*, 25(3):512–521, June 2009.

[33] K. Kasaoka and Y. Sankai. Predictive control estimating operator's intention for stepping–up motion by exoskeleton type power assist system HAL. In *Intelligent Robots and Systems, 2001. Proceedings. 2001 IEEE/RSJ International Conference on*, volume 3, pages 1578–1583 vol.3, 2001.

[34] H. Kawamoto and Y. Sankai. Comfortable power assist control method for walking aid by HAL–3. In *IEEE International Conference on Systems, Man and Cybernetics, 2002.*, volume 4, page 6, October 2002.

[35] H. Kawamoto and Y. Sankai. Power assist system HAL–3 for gait disorder person. In K. Miesenberger, J. Klaus, and W. Zagler, editors, *Computers Helping People with Special Needs*, volume 2398 of *Lecture Notes in Computer Science*, pages 196–203. Springer Berlin Heidelberg, 2002.

[36] S. Lee and Y. Sankai. Power assist control for walking aid with HAL–3 based on EMG and impedance adjustment around knee joint. In *Intelligent Robots and Systems, 2002. IEEE/RSJ International Conference on*, volume 2, pages 1499–1504 vol.2, 2002.

[37] S. Lee and Y. Sankai. Power assist control for leg with HAL–3 based on virtual torque and impedance adjustment. In *Systems, Man and Cybernetics, 2002 IEEE International Conference on*, volume 4, pages 6 pp. vol.4–, October 2002.

[38] H. Kawamoto, S. Lee, S. Kanbe, and Y. Sankai. Power assist method for HAL–3 using EMG–based feedback controller. In *IEEE International Conference on Systems, Man and Cybernetics, 2003.*, volume 2, pages 1648–1653 vol.2, October 2003.

[39] H. Kawamoto, S. Kanbe, and Y. Sankai. Power assist method for HAL–3 estimating operator's intention based on motion information. In *Robot and Human Interactive Communication, 2003. Proceedings. ROMAN 2003. The 12th IEEE International Workshop on*, pages 67–72, October 2003.

[40] S. Lee and Y. Sankai. The natural frequency–based power assist control for lower body with hal–3. In *Systems, Man and Cybernetics, 2003. IEEE International Conference on*, volume 2, pages 1642–1647 vol.2, October 2003.

[41] H. Kawamoto and Y. Sankai. Power assist method based on phase sequence driven by interaction between human and robot suit. In *Robot and Human Interactive Communication, 2004. ROMAN 2004. 13th IEEE International Workshop on*, pages 491–496, September 2004.

[42] T. Hayashi, H. Kawamoto, and Y. Sankai. Control method of robot suit HAL working as operator's muscle using biological and dynamical information. In *Intelligent Robots and Systems, 2005. (IROS 2005). 2005 IEEE/RSJ International Conference on*, pages 3063–3068, August 2005.

[43] K. Suzuki, Y. Kawamura, T. Hayashi, T. Sakurai, Y. Hasegawa, and Y. Sankai. Intention–based walking support for paraplegia patient. In *Systems, Man and Cybernetics, 2005 IEEE International Conference on*, volume 3, pages 2707–2713 Vol. 3, October 2005.

[44] H. Kawamoto, T. Hayashi, T. Sakurai, K. Eguchi, and Y. Sankai. Development of single leg version of HAL for hemiplegia. In *Engineering in Medicine and Biology Society, 2009. EMBC 2009. Annual International Conference of the IEEE*, pages 5038–5043, September 2009.

[45] H. Kawamoto, S. Taal, H. Niniss, T. Hayashi, K. Kamibayashi, K. Eguchi, and Y. Sankai. Voluntary motion support control of Robot Suit HAL triggered by bioelectrical signal for hemiplegia. In *Engineering in Medicine and Biology Society (EMBC), 2010 Annual International Conference of the IEEE*, pages 462–466, August 2010.

[46] M. Shingu, K. Eguchi, and Y. Sankai. Substitution of motor function of polio survivors who have permanent paralysis of limbs by using Cybernic Voluntary Control. In *IEEE International Conference on Robotics and Biomimetics (ROBIO), 2009*, pages 504–509, December 2009.

[47] H. Kawamoto, T. Shiraki, T. Otsuka, and Y. Sankai. Meal–assistance by Robot Suit HAL using detection of food position with camera. In *Robotics and Biomimetics (ROBIO), 2011 IEEE International Conference on*, pages 889–894, December 2011.

[48] T. Otsuka, K. Kawaguchi, H. Kawamoto, and Y. Sankai. Development of upper–limb type HAL and reaching movement for meal–assistance. In *Robotics and Biomimetics (ROBIO), 2011 IEEE International Conference on*, pages 883–888, December 2011.

[49] H. Satoh, T. Kawabata, and Y. Sankai. Bathing care assistance with Robot Suit HAL. In *Robotics and Biomimetics (ROBIO), 2009 IEEE International Conference on*, pages 498–503, December 2009.

[50] T. Kawabata, H. Satoh, and Y. Sankai. Working posture control of Robot Suit HAL for reducing structural stress. In *Robotics and Biomimetics (ROBIO), 2009 IEEE International Conference on*, pages 2013–2018, December 2009.

[51] Cyberdyne webpage. `http://www.cyberdyne.jp/`. Accessed: 2014-08-19.

[52] K. Amundson, J. Raade, N. Harding, and H. Kazerooni. Hybrid hydraulic–electric power unit for field and service robots. In *Intelligent Robots and Systems, 2005. (IROS 2005). 2005 IEEE/RSJ International Conference on*, pages 3453–3458, August 2005.

[53] W. Huo, S. Mohammed, J. C. Moreno, and Y. Amirat. Lower limb wearable robots for assistance and rehabilitation: A state of the art. *IEEE Systems Journal*, PP(99):1–14, 2014.

[54] L. Mertz. The next generation of exoskeletons: Lighter, cheaper devices are in the works. *IEEE Pulse*, 3(4):56–61, July 2012.

[55] S. Jacobsen and M. Olivier. Contact displacement actuator system, August 2008. WO Patent App. PCT/US2007/016336.

[56] M. Nordin and V. H. Frankel. *Basic Biomechanics of the Musculoskeletal System*. Lippincott Williams & Wilkins, 3rd edition, 2001.

[57] BS EN ISO 13482:2014. Robots and robotic devices – safety requirements for personal care robots. The British Standards Institution.

[58] J. Rose and J. G. Gamble. *Human Walking*. Lippincott Williams & Wilkins, 3rd edition, 2006.

[59] V. Medved. *Measurement of Human Locomotion*. CRC Press, 2001.

[60] J. Wheeler, B. Rohrer, D. Kholwadwala, S. Buerger, R. Givler, J. Neely, C. Hobart, and P. Galambos. In–sole MEMS pressure sensing for a lower extremity exoskeleton. In *Biomedical Robotics and Biomechatronics, 2006. BioRob 2006. The First IEEE/RAS-EMBS International Conference on*, pages 31–34, February 2006.

[61] R. A. R. C. Gopura, K. Kiguchi, and D. S. V. Bandara. A brief review on upper extremity robotic exoskeleton systems. In *2011 6th International Conference on Industrial and Information Systems*, pages 346–351, August 2011.

[62] C. J. et al. Yang. A Review of exoskeleton-type systems and their key technologies. In *Journal of Mechanical Engineering Science 2008 222: 1599*, volume 22, pages 1599–1612, March 2008.

[63] M Vukobratovic, D Hristic, and Z Stojiljkovic. Development of active anthropomorphic exoskeletons. *Medical and Biological Engineering*, 12:66–80, 02 1974.

[64] C-J Yang, Jiafan Zhang, Y-M Dong, and Yexin Zhang. A review of exoskeleton–type systems and their key technologies. *Proceedings of The Institution of Mechanical Engineers Part C-journal of Mechanical Engineering Science - PROC INST MECH ENG C-J MECH E*, 222:1599–1612, 08 2008.

[65] OECD. Population projections. `https://www.oecd-ilibrary.org/content/data/data-00538-en`, 2014. Accessed: 2019–07–22.

[66] K. Kiguchi, K. Iwami, M. Yasuda, K. Watanabe, and T. Fukuda. An exoskeletal robot for human shoulder joint motion assist. *IEEE/ASME Transactions on Mechatronics*, 8(1):125–135, March 2003.

[67] Yang Shen, Peter Ferguson, Ji Ma, and Jacob Rosen. *Upper Limb Wearable Exoskeleton Systems for Rehabilitation: State of the Art Review and a Case Study of the EXO-UL8 – Dual-Arm Exoskeleton System*, pages 71–90. January 2018.

[68] Y. Sankai. HAL: Hybrid Assistive Limb based on Cybernics. In M. Kaneko and Y. Nakamura, editors, *Robotics Research*, volume 66 of *Springer Tracts in Advanced Robotics*, pages 25–34. Springer Berlin Heidelberg, 2011.

[69] S. Karlin. Raiding iron man's closet [geek life]. *IEEE Spectrum*, 48(8):25–25, August 2011.

[70] Army technology (2014). Raytheon XOS 2 Exoskeleton, Second-Generation Robotics Suit. `https://www.army-technology.com/projects/raytheon-xos-2-exoskeleton-us/`. Accessed: 2018-08-03.

[71] Y. Sankai. Leading edge of cybernics: Robot suit HAL. In *SICE–ICASE, 2006. International Joint Conference*, October 2006.

[72] A. Tsukahara, Y. Hasegawa, and Y. Sankai. Standing–up motion support for paraplegic patient with robot suit HAL. In *Rehabilitation Robotics, 2009. ICORR 2009. IEEE International Conference on*, pages 211–217, June 2009.

[73] R. Lai and A. Jirachiefpattana. *Communication Protocol Specification and Verification*. Springer US, Boston, Kluwer Academic, 1 edition, 1998.

[74] S. Kim, G. Anwar, and H. Kazerooni. High–speed communication network for controls with the application on the exoskeleton. In *American Control Conference, 2004. Proceedings of the 2004*, volume 1, pages 355–360 vol.1, June 2004.

[75] G. Buttazzo. *Hard Real–Time Computing Systems*. Springer US, Boston, Springer Science+Business Media, LLC, 3rd edition, 2011.

[76] R. Froschauer and F. Auinger. A survey on the integration of the FlexRay bus in distributed automation and control systems. In *2009 2nd International Symposium on Logistics and Industrial Informatics*, pages 1–6, September 2009.

[77] N. Navet, Y. Song, F. Simonot-Lion, and C. Wilwert. Trends in automotive communication systems. *Proceedings of the IEEE*, 93(6):1204–1223, June 2005.

[78] C. Gang, Y. Dong, and C. Rensheng. Developing trend of industrial fieldbus control system. In *Electronic Measurement and Instruments, 2007. ICEMI '07. 8th International Conference on*, pages 1–765–1–768, August 2007.

[79] B. Galloway and G. P. Hancke. Introduction to industrial control networks. *IEEE Communications Surveys Tutorials*, 15(2):860–880, February 2013.

[80] National Instruments webpage. `http://www.ni.com/white-paper/9731/en/`. Accessed: 2016–06–06.

[81] Microchip webpage. http://ww1.microchip.com/downloads/en/AppNotes/00713a.pdf. Accessed: 2016–06–06.

[82] Texas Instruments. 3.3-V CAN TRANSCEIVER - SN65HVD233-EP. http://www.ti.com/lit/ds/symlink/sn65hvd233-ep.pdf. Accessed: 2016–06–06.

[83] Y. S. Cha and B. J. You. Design and implementation of mobile humanoid robot control system based on dual network. In *Robotics and Biomimetics (ROBIO), 2009 IEEE International Conference on*, pages 251–256, December 2009.

[84] H. Kimm. Distributed event-triggered robot control system over Controller Area Network. In *Industrial Technology (ICIT), 2012 IEEE International Conference on*, pages 522–526, March 2012.

[85] Yu-Kyoung Sung, Byung-Hun Hwang, Jung-Shik Kong, Bo-Hee Lee, and Jin-Geol Kim. Messages scheduling for a humanoid robot in the CAN. In *Industrial Electronics Society, 2004. IECON 2004. 30th Annual Conference of IEEE*, volume 3, pages 2470–2474 Vol. 3, November 2004.

[86] M. Ruff. Evolution of local interconnect network (LIN) solutions. In *Vehicular Technology Conference, 2003. VTC 2003-Fall. 2003 IEEE 58th*, volume 5, pages 3382–3389 Vol.5, October 2003.

[87] ST Microelectronics. LIN Application Note. http://www.st.com/web/en/resource/technical/document/application_note/CD00004273.pdf. Accessed: 2016–06–06.

[88] LIN Consortium. LIN Specification PackageRevision 2.2A. http://www.lin-subbus.org. Accessed: 2016–06–06.

[89] Yi-Nan Xu, Y. E. Kim, K. J. Cho, J. G. Chung, and M. S. Lim. Implementation of FlexRay communication controller protocol with application to a robot system. In *Electronics, Circuits and Systems, 2008. ICECS 2008. 15th IEEE International Conference on*, pages 994–997, August 2008.

[90] National Instruments webpage. http://www.ni.com/white-paper/3352/en/. Accessed: 2016–06–06.

[91] S. Mackay, E. Wright, D. Reynders, and J. Parl. Practical industrial data networks: Design, installation and troubleshooting. In *Electronics, Circuits and*

Systems, 2004. ICECS 2004. 11th IEEE International Conference on, pages 181–197, August 2004.

[92] PROFIBUS Nutzerorganisation. PROFIBUS System Description, Technology and Application. http://www.profibus.com/nc/download/technical-descriptions-books/downloads/profibus-technology-and-application-system-description/download/14844/, Accessed: 2016–06–06.

[93] F. He, W. Tong, and Q. Wang. Synchronization control strategy of multi-motor system based on profibus network. In *2007 IEEE International Conference on Automation and Logistics*, pages 3029–3034, August 2007.

[94] Yi Chen and Xiaokun Shi. A real-time communication solution based on profibus. In *Advanced Intelligence and Awareness Internet (AIAI 2011), 2011 International Conference on*, pages 288–292, October 2011.

[95] EtherCAT Technology Group. EtherCAT - The Ethernet Fieldbus. http://www.ethercat.org/download/documents/ETG_Brochure_EN.pdf. Accessed: 2016–06–06.

[96] EtherCAT Technology Group. Technical Introduction and Overview. http://www.ethercat.org/en/technology.html. Accessed: 2016–06–06.

[97] S. Marcheschi, F. Salsedo, M. Fontana, and M. Bergamasco. Body extender: Whole body exoskeleton for human power augmentation. In *Robotics and Automation (ICRA), 2011 IEEE International Conference on*, pages 611–616, May 2011.

[98] C. Meijneke, W. van Dijk, and H. van der Kooij. Achilles: An autonomous lightweight ankle exoskeleton to provide push-off power. In *5th IEEE RAS/EMBS International Conference on Biomedical Robotics and Biomechatronics*, pages 918–923, August 2014.

[99] National Instruments. PROFIBUS Interfaces for NI LabVIEW, LabVIEW Real-Time. http://www.ni.com/pdf/products/us/cat_profibus_interfaces.pdf. Accessed: 2016–06–06.

[100] A. Techmer and P. Leteinturier. Implementing flexray on silicon. In *International Conference on Networking, International Conference on Systems and Interna-*

tional Conference on Mobile Communications and Learning Technologies (ICNI-CONSMCL'06), pages 34–34, April 2006.

[101] Infineon. FlexRay Communication Controller SAK-CIC310-OSMX2HT Data Sheet. `http://www.infineon.com/dgdl/Infineon-CIC310-DS-v02_02-en.pdf?folderId=db3a304317a748360117f45a9c863e84&fileId=db3a3043183a955501189de9f8b8404c`. Accessed: 2016–06–06.

[102] National Instruments. OPERATING INSTRUCTIONS AND SPECIFICATIONS - CompactRIO NI cRIO-9081/9082. `http://www.ni.com/pdf/manuals/375714a.pdf`. Accessed: 2016–06–06.

[103] Microchip. High-Speed CAN Transceiver - MCP2551. `http://ww1.microchip.com/downloads/en/DeviceDoc/21667f.pdf`. Accessed: 2016–06–06.

[104] Microchip. LIN Transceiver with Voltage Regulator - MCP2021A/2A. `http://ww1.microchip.com/downloads/en/DeviceDoc/20002298C.pdf`. Accessed: 2016–06–06.

[105] Beckhoff Automation. Beckhoff - New Automation Technology - Main Catalog 2015. `https://www.beckhoff.com/english.asp?download/catalog.htm`. Accessed: 2016–06–06.

[106] Siemens. SIMATIC NET - PROFIBUS Networks - Manual. `https://w3.siemens.com/mcms/industrial-communication/en/support/ik-info/Documents/profn2_e.pdf`. Accessed: 2016–06–06.

[107] Helmholz. Brief Instruction FLEXtra multiRepeater. `https://www.helmholz.de/dnl/FLEXtra_multiRepeater_Brief_instruction_en_3.pdf`. Accessed: 2016–06–06.

[108] D. Natale, M. *Network Topology and Bus Length. In: Understanding and using the Controller Area Network*. Springer US, 2008.

[109] Texas Instruments. Controller Area Network Physical Layer Requirements.

[110] C. C. Wang, C. L. Chen, J. J. Li, and C. Y. Juan. Configurable active star design for automobile FlexRay systems. In *2012 IEEE International Conference on Consumer Electronics (ICCE)*, pages 301–302, January 2012.

[111] ELMOS Semiconductor. Flexray active star device–e981.56. http://www.elmos.com/fileadmin/2013/02_products/01_interface/06_flexray/e981-56_elmos_is.pdf, Accessed: 2018–11–28.

[112] J.-L. Ch. Racine. PhD Disseration: Control of a Lower Extremity Exoskeleton for Human Performance Amplification. University of California, Berkeley, 2003.

[113] The technical response to the question: 'Why EtherCAT?'. EtherCAT – the Ethernet fieldbus. http://www.ethercat.org/pdf/ethercat_e.pdf. Accessed: 2018–04–21.

[114] J. Jasperneite, M. Schumacher, and K. Weber. Limits of increasing the performance of industrial ethernet protocols. In *2007 IEEE Conference on Emerging Technologies and Factory Automation (EFTA 2007)*, pages 17–24, September 2007.

[115] G. Cena, S. Scanzio, A. Valenzano, and C. Zunino. A distribute-merge switch for EtherCAT networks. In *2010 IEEE International Workshop on Factory Communication Systems Proceedings*, pages 121–130, May 2010.

[116] Mladen Knezic, Branko Dokic, and Zeljko Ivanovic. Performance evaluation of the switched EtherCAT networks with VLAN tagging. *Serbian Journal of Electrical Engineering*, 9:33–42, January 2012.

[117] M. Knezic, B. Dokic, and Z. Ivanovic. Increasing EtherCAT performance using frame size optimization algorithm. In *ETFA2011*, pages 1–4, September 2011.

[118] G. Prytz. A performance analysis of EtherCAT and PROFINET IRT. In *2008 IEEE International Conference on Emerging Technologies and Factory Automation*, pages 408–415, September 2008.

[119] G. Cena, S. Scanzio, A. Valenzano, and C. Zunino. A distribute-merge switch for ethercat networks. In *2010 IEEE International Workshop on Factory Communication Systems Proceedings*, pages 121–130, May 2010.

[120] G. Cena, S. Scanzio, A. Valenzano, and C. Zunino. Performance analysis of switched ethercat networks. In *2010 IEEE 15th Conference on Emerging Technologies Factory Automation (ETFA 2010)*, pages 1–4, Sep. 2010.

[121] Documentation EK1122, EK15xx EtherCAT Junctions. https://download.beckhoff.com/download/document/io/ethercat-terminals/ek1122_ek15xxen.pdf. Accessed: 2018–04–23.

[122] EtherCAT – The Ethernet Fieldbus. https://www.ethercat.org/download/documents/EtherCAT_Introduction_EN.pdf. Accessed: 2018–04–23.

[123] G. M. Napora. *Control Aspects of a Full–body Enhancive Robotic Exoskeleton*. PhD thesis, University of Leeds, UK, 2018.

[124] Solartron Metrology LVDT Displacement Transducers, S Series. https://solartron.cdistore.com/manufacturer/solartron/lvdt-linear-variable-displacement-transformer/s-series. Accessed: 2018–04–27.

[125] S-Series Displacement Transducers. https://www.klinger.fi/wp-content/uploads/migrated/attachment/Solartron_S_Series_LVDT_Anturit_Esite.pdf. Accessed: 2018–04–27.

[126] Inductive Sensors (LVDT). https://www.lvdt.eu/. Accessed: 2018–04–27.

[127] F256 Axial Compensated Loadcell. https://www.novatechloadcells.co.uk/ds/f256.htm. Accessed: 2018–04–27.

[128] F256 Axial Compensated Loadcell. https://www.novatechloadcells.co.uk/pdf/F256.pdf. Accessed: 2018–04–27.

[129] LCM Systems. SGA Analogue Strain Gauge Load Cell Amplifier. http://www.lcmsystems.com/res/SGACasedAnalogueLoadCellStrainGaugeAmplifier.pdf. Accessed: 2018–04–27.

[130] Mantracourt. SGA A SGA D Strain Gauge Load Cell Amplifier Signal Conditioner. https://www.mantracourt.com/userfiles/documents/sga_manual.pdf. Accessed: 2018–04–27.

[131] Hengstler – Technical Datasheet Absolute Encoder AC 36 – BiSS / SSI. https://www.hengstler.de/gfx/file/shop/encoder/AC36/Datasheet_AC36-BiSS_SSI_en.pdf. Accessed: 2018–04–27.

[132] C. Gonzalez. What's the Difference Between Absolute and Incremental Encoders?. https://www.machinedesign.com/motion-control/what-s-

difference-between-absolute-and-incremental-encoders. Accessed: 2018–04–27.

[133] Manual – CX2020, CX2030, CX2040 Embedded PCs. https://download.beckhoff.com/download/document/ipc/embedded-pc/embedded-pc-cx/cx2000_hwen.pdf. Accessed: 2018–04–28.

[134] TwinCAT 3 Engineering. https://www.beckhoff.com/twincat3/. Accessed: 2018–04–28.

[135] Documentation, EL31xx–00xx Analog Input Terminals (16 Bit). https://download.beckhoff.com/download/document/io/ethercat-terminals/el31xxen.pdf. Accessed: 2018–04–28.

[136] Documentation, EL500x SSI Sensor Interface Terminals. https://download.beckhoff.com/download/document/io/ethercat-terminals/el500xen.pdf. Accessed: 2018–04–28.

[137] EtherCAT Distributed Clocks – default settings. https://infosys.beckhoff.com/english.php?content=../content/1033/ethercatsystem/2469102219.html&id=. Accessed: 2018–04–28.

[138] TwinCAT 3 – eXtended Automation (XA). https://download.beckhoff.com/download/document/catalog/Beckhoff_TwinCAT3_042012_e.pdf. Accessed: 2018–04–28.

[139] National Research Council Committee on Soldier Power/Energy Systems. *Meeting the Energy Needs of Future Warriors*. The National Academies Press, Washington D.C., 1st edition, 2004.

[140] D. Durbin and Q. Horn. *BU-106: Advantages of Primary Batteries*. https://batteryuniversity.com/learn/article/primary_batteries. Accessed: 2019–07–08.

[141] B. Sorensen and G. Spazzafumo. 4 – fuel cell systems. In *Hydrogen and Fuel Cells (Third Edition)*, pages 221 – 272. Academic Press, third edition, 2018.

[142] P. R. O'Hayre. Fuel cells for electrochemical energy conversion. *EPJ Web of Conferences*, 189:00011, 01 2018.

[143] X. Li. Chapter One - Thermodynamic Performance of Fuel Cells and Comparison with Heat Engines. In *Advances in Fuel Cell*, volume 1, pages 1 – 46. Elsevier Science, 2007.

[144] F. Barbir. Chapter Ten - fuel cell applications. In *PEM Fuel Cells (Second Edition)*, pages 373 – 434. Academic Press, Boston, second edition, 2013.

[145] K. Burke. 4.02 - Current perspective on hydrogen and fuel cells. In *Comprehensive Renewable Energy*, pages 29 – 63. Elsevier, Oxford, 2012.

[146] X. Xiao, Y. Fan, J. Dufek, and R. Murphy. Indoor UAV localization using a tether. pages 1–6, August 2018.

[147] S. Ajwad and J. Iqbal. Recent advances and applications of tethered robotic systems. *Science International*, 26:2045–2051, January 2014.

[148] McArdle W. D., Katch F. I., and Katch V. L. *Exercise physiology : nutrition, energy and human performance*. Wolters Kluwer–Lippincott Williams and Wilkins, 7th edition, 2010.

[149] A. D. Winter. Biomechanics and motor control of human movement, fourth edition. *Power Electronics, IEEE Transactions on*, September 2009.

[150] G. J. Snyder. Small thermoelectric generators. *Electrochemical Society Interface*, 17(3):54–56, September 2008.

[151] M. S. Dresselhaus, G. Chen, M. Y. Tang, R. G. Yang, H. Lee, D. Z. Wang, Z. F. Ren, J. P. Fleurial, and P. Gogna. New directions for low–dimensional thermoelectric materials. *Advanced Materials*, 19(8):1043–1053, 2007.

[152] R. Riemer and A. Shapiro. Biomechanical energy harvesting from human motion: Theory, state of the art, design guidelines, and future directions. *Journal of neuroengineering and rehabilitation*, 8:22, April 2011.

[153] K.T. Chau. 21 - Pure electric vehicles. In *Alternative Fuels and Advanced Vehicle Technologies for Improved Environmental Performance*, pages 655 – 684. Woodhead Publishing, 2014.

[154] J.A.A. Hartley, R.G. McLellan, J. Richmond, A.J. Day, and I.F. Campean. Regenerative braking system evaluation on a full electric vehicle. In *Innovations in*

Fuel Economy and Sustainable Road Transport, pages 73 – 86. Woodhead Publishing, 2011.

[155] P. Tawadros, N. Zhang, and A. Boretti. 17 - Integration and performance of regenerative braking and energy recovery technologies in vehicles. In *Alternative Fuels and Advanced Vehicle Technologies for Improved Environmental Performance*, pages 541 – 563. Woodhead Publishing, 2014.

[156] G. Soldberg. The Magic of Tesla Roadster Regenerative Braking. `https://www.tesla.com/en_GB/blog/magic-tesla-roadster-regenerative-braking`. Accessed: 2019–07–15.

[157] S. Van Sterkenburg, E. Rietveld, F. Rieck, B. Veenhuizen, and H. Bosma. Analysis of regenerative braking efficiency – a case study of two electric vehicles operating in the rotterdam area. In *2011 IEEE Vehicle Power and Propulsion Conference*, pages 1–6, September 2011.

[158] S. Dusmez and A. Khaligh. A compact and integrated multifunctional power electronic interface for plug-in electric vehicles. *Power Electronics, IEEE Transactions on*, 28:5690–5701, December 2013.

[159] M. Brown. Regenerative Braking Efficiency. `http://large.stanford.edu/courses/2016/ph240/brown1/`. Accessed: 2019–07–15.

[160] P. Niu, P. Chapman, R. Riemer, and X. Zhang. Evaluation of motions and actuation methods for biomechanical energy harvesting. In *2004 IEEE 35th Annual Power Electronics Specialists Conference (IEEE Cat. No.04CH37551)*, volume 3, pages 2100–2106 Vol.3, June 2004.

[161] J. M. Donelan, Q. Li, V. Naing, J. A. Hoffer, D. J. Weber, and A. D. Kuo. Biomechanical energy harvesting: Generating electricity during walking with minimal user effort. *Science*, 319(5864):807–810, 2008.

[162] Q. Li, V. Naing, and J. M. Donelan. Development of a biomechanical energy harvester. *Journal of NeuroEngineering and Rehabilitation*, 6(1):22, June 2009.

[163] J. F. Antaki, G. E. Bertocci, E. C. Green, T. Rintoul A. Nadeem, R. L. Kormos, and B. P. Griffith. A gait–powered autologous battery charging system for artificial organs. *Asaio Journal (American Society for Artificial Internal Organs : 1992)*, 41(3):M588–M595, 1995.

[164] J. Kymissis, C. Kendall, J. Paradiso, and N. Gershenfeld. Parasitic power harvesting in shoes. In *Digest of Papers. Second International Symposium on Wearable Computers (Cat. No.98EX215)*, pages 132–139, October 1998.

[165] N. S. Shenck and J. A. Paradiso. Energy scavenging with shoe–mounted piezoelectrics. *IEEE Micro*, 21(3):30–42, May 2001.

[166] J. Y. Hayashida. *Unobtrusive Integration of Magnetic Generator Systems into Common Footwear*. PhD thesis, Massachusetts Institute of Technology, MIT, 2000.

[167] S. R. Platt, S. Farritor, K. Garvin, and H. Haider. The use of piezoelectric ceramics for electric power generation within orthopedic implants. *IEEE/ASME Transactions on Mechatronics*, 10(4):455–461, August 2005.

[168] S. R. Platt, S. Farritor, and H. Haider. On low-frequency electric power generation with pzt ceramics. *IEEE/ASME Transactions on Mechatronics*, 10(2):240–252, April 2005.

[169] R. Pelc and R. M. Fujita. Renewable energy from the ocean. *Marine Policy*, 26(6):471 – 479, 2002.

[170] S. Rahman. Alternate sources of electric energy. *IEEE Potentials*, 7(2):22–25, May 1988.

[171] C.B. Panchal, J Larsen-Basse, L.R. Berger, J.A. Berger, B.J. Little, H.C. Stevens, J.B. Darby, L.E. Genens, and D.L. Hillis. Otec biofouling-control and corrosion-protection study at the seacoast test facility: 1981-1983. *Argonne National Laboratory Report ANLIOTEC-TM-5*, July 1985.

[172] T. Fournier. Open cycle-ocean thermal energy conversion: Experimental study of flash evaporation. In *OCEANS '85 - Ocean Engineering and the Environment*, pages 1222–1229, November 1985.

[173] V.L. Bruch. An assessment of research and development leadership in ocean energy technologies. *Sandia National Laboratories: Energy Policy and Planning Department, USA, Techical Report SAND93-3946*, April 1994.

[174] A. Khaligh and O.C. Onar. *Energy harvesting: Solar, wind, and ocean energy conversion systems*. January 2017.

[175] I. Petsagkourakis, K. Tybrandt, X. Crispin, I. Ohkubo, N. Satoh, and T. Mori. Thermoelectric materials and applications for energy harvesting power generation. *Science and Technology of Advanced Materials*, 19(1):836–862, 2018.

[176] A. Kandemir, A. Ozden, T. Cagin, and C. Sevik. Thermal conductivity engineering of bulk and one-dimensional si-ge nanoarchitectures. *Science and Technology of Advanced Materials*, 18:187, March 2017.

[177] D. J. Cichon and W. Wiesbeck. The heinrich hertz wireless experiments at karlsruhe in the view of modern communication. In *Proceedings of the 1995 International Conference on 100 Years of Radio*, pages 1–6, September 1995.

[178] N. Tesla. The transmission of electrical energy without wires. `http://www.tfcbooks.com/tesla/1904-03-05.htm`, March 1905. Accessed: 2019–07–15.

[179] W. C. Brown. The history of power transmission by radio waves. *IEEE Transactions on Microwave Theory and Techniques*, 32(9):1230–1242, September 1984.

[180] M. Kesler. Highly Resonant Wireless Power Transfer: Safe, Efficient, and over Distance. `https://witricity.com/wp-content/uploads/2016/12/White_Paper_20161218.pdf`, 2013. Accessed: 2019–07–15.

[181] S. Y. R. Hui and W. W. C. Ho. A new generation of universal contactless battery charging platform for portable consumer electronic equipment. *IEEE Transactions on Power Electronics*, 20(3):620–627, May 2005.

[182] Adafruit. Universal Qi Wireless Charging Transmitter. `https://www.adafruit.com/product/2162?gclid=CjwKCAjwkrrbBRB9EiwAhlN8_D7PeDAiQ_cTufMLqxpqmaxgPDElKbrGoJou0XoDXwnyhu_2D2BEXBoC_NsQAvD_BwE`, 2019. Accessed: 2019–07–18.

[183] J. A. Taylor, Z. N. Low, J. Casanova, and J. Lin. A wireless power station for laptop computers. In *2010 IEEE Radio and Wireless Symposium (RWS)*, pages 625–628, January 2010.

[184] Wireless Power Consortium. Qi - mobile computing. `https://www.wirelesspowerconsortium.com/qi/`, 2019. Accessed: 2019–07–18.

[185] M. McDonough. Integration of inductively coupled power transfer and hybrid energy storage system: A multiport power electronics interface for battery-powered

electric vehicles. *IEEE Transactions on Power Electronics*, 30(11):6423–6433, November 2015.

[186] C. Zheng, J. Lai, R. Chen, W. E. Faraci, Z. Ullah Zahid, B. Gu, L. Zhang, G. Lisi, and D. Anderson. High-efficiency contactless power transfer system for electric vehicle battery charging application. *IEEE Journal of Emerging and Selected Topics in Power Electronics*, 3(1):65–74, March 2015.

[187] M. W. Baker and R. Sarpeshkar. Feedback analysis and design of rf power links for low-power bionic systems. *IEEE Transactions on Biomedical Circuits and Systems*, 1(1):28–38, March 2007.

[188] G. Wang, W. Liu, M. Sivaprakasam, M. Zhou, J. D. Weiland, and M. S. Humayun. A dual band wireless power and data telemetry for retinal prosthesis. In *2006 International Conference of the IEEE Engineering in Medicine and Biology Society*, pages 4392–4395, August 2006.

[189] M. Catrysse, B. Hermans, and R. Puers. An inductive power system with integrated bi-directional data-transmission. *Sensors and Actuators A: Physical*, 115(2):221 – 229, 2004. The 17th European Conference on Solid-State Transducers.

[190] C. M. Zierhofer and E. S. Hochmair. Geometric approach for coupling enhancement of magnetically coupled coils. *IEEE Transactions on Biomedical Engineering*, 43(7):708–714, July 1996.

[191] R. R. Harrison. Designing efficient inductive power links for implantable devices. In *2007 IEEE International Symposium on Circuits and Systems*, pages 2080–2083, May 2007.

[192] U. Jow and M. Ghovanloo. Design and optimization of printed spiral coils for efficient transcutaneous inductive power transmission. *IEEE Transactions on Biomedical Circuits and Systems*, 1(3):193–202, September 2007.

[193] C. Lin, H. Chiu, M. Lin, C. Chang, I. Ho, P. H. Fang, Y. C. Li, C. L. Wang, Y. Tsai, Y. Wen, W. Shih, Y. Yang, and S. Lu. Pain control on demand based on pulsed radio-frequency stimulation of the dorsal root ganglion using a batteryless implantable cmos soc. In *2010 IEEE International Solid-State Circuits Conference - (ISSCC)*, pages 234–235, February 2010.

[194] B. W. Ha, J. A. Park, H. J. Jin, and C. S. Cho. Energy transfer and harvesting for rf-bio applications - invited. In *2015 IEEE MTT-S 2015 International Microwave Workshop Series on RF and Wireless Technologies for Biomedical and Healthcare Applications (IMWS-BIO)*, pages 54–55, September 2015.

[195] T. Sun, X. Xie, G. Li, Y. Gu, Y. Deng, and Z. Wang. A two-hop wireless power transfer system with an efficiency-enhanced power receiver for motion-free capsule endoscopy inspection. *IEEE Transactions on Biomedical Engineering*, 59(11):3247–3254, November 2012.

[196] C. Liu, C. Jiang, J. Song, and K. T. Chau. An effective sandwiched wireless power transfer system for charging implantable cardiac pacemaker. *IEEE Transactions on Industrial Electronics*, 66(5):4108–4117, May 2019.

[197] J. Muhs. Alleviating the battlefield battery burden with wireless power. `http://mil-embedded.com/articles/alleviating-battlefield-battery-burden-wireless-power/`, 2011. Accessed: 2019–07–18.

[198] V. F. Tseng, S. S. Bedair, and N. Lazarus. Acoustic wireless power transfer with receiver array for enhanced performance. In *2017 IEEE Wireless Power Transfer Conference (WPTC)*, pages 1–4, May 2017.

[199] J. O. Dickey, P. L. Bender, J. E. Faller, X X Newhall, R. L. Ricklefs, J. G. Ries, P. J. Shelus, C. Veillet, A. L. Whipple, J. R. Wiant, J. G. Williams, and C. F. Yoder. Lunar laser ranging: A continuing legacy of the apollo program. *Science*, 265(5171):482–490, 1994.

[200] M. Mori, H. Kagawa, H. Nagayama, and Y. Saito. Current Status of Study on Hydrogen Production with Space Solar Power Systems (SSPS). In H. Lacoste and L. Ouwehand, editors, *Solar Power from Space - SPS '04*, volume 567 of *ESA Special Publication*, page 3, December 2004.

[201] H. Suzuki, K. Kisara, M. Niino, and M. Mori. Overview of studies on space solar power systems and elemental technology development. *Materials Science Forum - MATER SCI FORUM*, 631-632:3–8, October 2009.

[202] C. Cougnet, E. Sein, A. Celeste, and L. Summerer. Solar power satellites for space exploration and applications. *Journal of the British Interplanetary Society*, 59(8):290–296, November 2006.

[203] R. Erfani, F. Marefat, A. M. Sodagar, and P. Mohseni. Transcutaneous capacitive wireless power transfer (c-wpt) for biomedical implants. In *2017 IEEE International Symposium on Circuits and Systems (ISCAS)*, pages 1–4, May 2017.

[204] R. Erfani, F. Marefat, A. M. Sodagar, and P. Mohseni. Modeling and characterization of capacitive elements with tissue as dielectric material for wireless powering of neural implants. *IEEE Transactions on Neural Systems and Rehabilitation Engineering*, 26(5):1093–1099, May 2018.

[205] R. Erfani, F. Marefat, A. M. Sodagar, and P. Mohseni. Modeling and experimental validation of a capacitive link for wireless power transfer to biomedical implants. *IEEE Transactions on Circuits and Systems II: Express Briefs*, 65(7):923–927, July 2018.

[206] L. Mateu, T. Drager, I. Mayordomo, and M. Pollak. Chapter 4.1 - Energy harvesting at the human body. In *Wearable Sensors*, pages 235 – 298. Academic Press, Oxford, 2014.

[207] S. Valtchev, E. Baikova, and L. Romba. Electromagnetic field as the wireless transporter of energy. *Facta universitatis - series: Electronics and Energetics*, 25:171–181, January 2012.

[208] H. S. Gougheri and M. Kiani. Optimal wireless receiver structure for omnidirectional inductive power transmission to biomedical implants. In *2016 38th Annual International Conference of the IEEE Engineering in Medicine and Biology Society (EMBC)*, pages 1975–1978, August 2016.

[209] A. Banerji, T. Datta, G. Bandyopadhyay, S. K. Biswas, A. Banerji, and A. Banerji. Wireless transfer of power: Status and challenges. In *2016 International Conference on Intelligent Control Power and Instrumentation (ICICPI)*, pages 251–257, October 2016.

[210] A. Karalis, J.D. Joannopoulos, and M. Soljacic. Efficient wireless non-radiative mid-range energy transfer. *Annals of Physics*, 323(1):34 – 48, 2008. January Special Issue.

[211] Q. Chen, K. Ozawa, Q. Yuan, and K. Sawaya. Antenna characterization for wireless power-transmission system using near-field coupling. *IEEE Antennas and Propagation Magazine*, 54(4):108–116, August 2012.

[212] S. Ul Haq. Wireless power transmission “a potential idea for future”. *International Journal of Scientific and Engineering Research*, Volume 6:Page 933, March 2015.

[213] A. Stein. Wi–Charge Wins CES 2018 Best of Innovation Award. `https://www.businesswire.com/news/home/20180110006324/en/Wi-Charge-Wins-CES-2018-Innovation-Award#new_tab`, 2018. Accessed: 2019–07–18.

[214] A. M. Jawad, R. Nordin, S. K. Gharghan, H. M. Jawad, and M. Ismail. Opportunities and challenges for near-field wireless power transfer: A review. *Energies*, 10(7), 2017.

[215] D. C. Ludois, M. J. Erickson, and J. K. Reed. Aerodynamic fluid bearings for translational and rotating capacitors in noncontact capacitive power transfer systems. *IEEE Transactions on Industry Applications*, 50(2):1025–1033, March 2014.

[216] F. Lu, H. Zhang, H. Hofmann, and C. Mi. A double-sided LCLC-compensated capacitive power transfer system for electric vehicle charging. *IEEE Transactions on Power Electronics*, 30(11):6011–6014, November 2015.

[217] J. Dai and D. C. Ludois. Single active switch power electronics for kilowatt scale capacitive power transfer. *IEEE Journal of Emerging and Selected Topics in Power Electronics*, 3(1):315–323, March 2015.

[218] J. Dai and D. C. Ludois. Capacitive power transfer through a conformal bumper for electric vehicle charging. *IEEE Journal of Emerging and Selected Topics in Power Electronics*, 4(3):1015–1025, September 2016.

[219] C. Liu, A. P. Hu, and N. . C. Nair. Modelling and analysis of a capacitively coupled contactless power transfer system. *IET Power Electronics*, 4(7):808–815, August 2011.

[220] C. Liu, A. P. Hu, B. Wang, and N. C. Nair. A capacitively coupled contactless matrix charging platform with soft switched transformer control. *IEEE Transactions on Industrial Electronics*, 60(1):249–260, January 2013.

[221] H. Jiang, W. Li, M. Tabaddor, and C. Mi. Optimization and safety evaluation of a 3.3 kw wireless ev charger. In *2015 IEEE Transportation Electrification Conference and Expo (ITEC)*, pages 1–5, June 2015.

[222] J. Shin, S. Shin, Y. Kim, S. Ahn, S. Lee, G. Jung, S. Jeon, and D. Cho. Design and implementation of shaped magnetic-resonance-based wireless power transfer system for roadway-powered moving electric vehicles. *IEEE Transactions on Industrial Electronics*, 61(3):1179–1192, March 2014.

[223] H. Kim, C. Song, D. Kim, D. H. Jung, I. Kim, Y. Kim, J. Kim, S. Ahn, and J. Kim. Coil design and measurements of automotive magnetic resonant wireless charging system for high-efficiency and low magnetic field leakage. *IEEE Transactions on Microwave Theory and Techniques*, 64(2):383–400, February 2016.

[224] M. Chabalko, J. Besnoff, M. Laifenfeld, and D. S. Ricketts. Resonantly coupled wireless power transfer for non-stationary loads with application in automotive environments. *IEEE Transactions on Industrial Electronics*, 64(1):91–103, January 2017.

[225] Y. Li, R. Mai, T. Lin, H. Sun, and Z. He. A novel WPT system based on dual transmitters and dual receivers for high power applications: Analysis, design and implementation. 10(2), 2017.

[226] Z. Wang, X. Wei, and H. Dai. Design and control of a 3 kW wireless power transfer system for electric vehicles. *Energies*, 9(1), 2016.

[227] M. Chigira, Y. Nagatsuka, Y. Kaneko, S. Abe, T. Yasuda, and A. Suzuki. Small-size light-weight transformer with new core structure for contactless electric vehicle power transfer system. In *2011 IEEE Energy Conversion Congress and Exposition*, pages 260–266, September 2011.

[228] J. Huh, S. W. Lee, W. Y. Lee, G. H. Cho, and C. T. Rim. Narrow-width inductive power transfer system for online electrical vehicles. *IEEE Transactions on Power Electronics*, 26(12):3666–3679, December 2011.

[229] R. Mai, L. Ma, Y. Liu, P. Yue, G. Cao, and Z. He. A maximum efficiency point tracking control scheme based on different cross coupling of dual-receiver inductive power transfer system. *Energies*, 10(2), 2017.

[230] S. Lee, J. Kim, and J. Lee. Development of a 60 khz, 180 kW, over 85power transfer system for a tram. *Energies*, 9(12), 2016.

[231] M. Ibrahim, L. Pichon, L. Bernard, A. Razek, J. Houivet, and O. Cayol. Advanced modeling of a 2–kW series–series resonating inductive charger for real electric

vehicle. *IEEE Transactions on Vehicular Technology*, 64(2):421–430, February 2015.

[232] IEEE Standards Association. IEEE C95.1–2019 – IEEE Approved Draft Standard for Safety Levels with Respect to Human Exposure to Electric, Magnetic and Electromagnetic Fields, 0 Hz to 300 GHz. `https://standards.ieee.org/standard/C95_1-2019.html`, 2019. Accessed: 2019–07–22.

[233] T. Magil. *LEADUE – Leeds Enhancive Action at a Distance Upper–Body Exoskeleton*. PhD thesis, University of Leeds, UK, 2019.

[234] M. Moltedo, T. Bacek, T. Verstraten, C. Rodriguez-Guerrero, B. Vanderborght, and D. Lefeber. Powered ankle–foot orthoses: The effects of the assistance on healthy and impaired users while walking. *Journal of NeuroEngineering and Rehabilitation*, 15, December 2018.

[235] C. Zhu, K. Liu, C. Yu, R. Ma, and H. Cheng. Simulation and experimental analysis on wireless energy transfer based on magnetic resonances. In *2008 IEEE Vehicle Power and Propulsion Conference*, pages 1–4, September 2008.

[236] A. P. Sample, D. T. Meyer, and J. R. Smith. Analysis, experimental results, and range adaptation of magnetically coupled resonators for wireless power transfer. *IEEE Transactions on Industrial Electronics*, 58(2):544–554, February 2011.

[237] T. Linlin, H. Xueliang, L. Hui, and H. Hui. Study of wireless power transfer system through strongly coupled resonances. In *2010 International Conference on Electrical and Control Engineering*, pages 4275–4278, June 2010.

[238] S. Nutwong, A. Sangswang, and S. Naetiladdanon. An inverter topology for wireless power transfer system with multiple transmitter coils. *Applied Sciences*, 9(8), 2019.

[239] *Customer Needs in the Exoskeleton Project – draft 4*. Technical report, University of Leeds, April 2014.

Appendix A

Customer Needs:
Activities to be performable by the device

Appendix A in the Customer Needs [239] lists following tasks:

Table A.1: Activities to be performable by the device [239]

Unique Identifier	**Activity**
NA-1	Walk on level ground
NA-2	Walk on rough terrain
NA-3	Run
NA-4	Squat
NA-5	Get up from a fallen position
NA-6	Walk up the stairs
NA-7	Walk up the slopes
NA-8	Walk down the stairs
NA-9	Walk down the slopes
NA-10	Go through doorways
NA-11	Walk on level ground with load
NA-12	Walk on rough terrain with load
NA-13	Run with load
NA-14	Squat with load
NA-15	Get up from a fallen position with load
NA-16	Walk up the stairs with load

NA-17	Walk up the slopes with load
NA-18	Walk down the stairs with load
NA-19	Walk down the slopes with load
NA-20	Go through doorways with load
NA-21	Deadlift
NA-22	Overhead shoulder press (with bar)
NA-23	Vertical jump
NA-24	Bench press (with bar)
NA-25	Horizontal push (full body)
NA-26	Horizontal pull (full body)
NA-27	Biceps curl (with bar)
NA-28	Bent over row (with bar)
NA-29	Pull down

Appendix B

Initial Experimental Setup with NI cRIO–9024

In the following sections an EtherCAT communication system implemented with NI and Beckhoff Automation hardware is described. The feasibility of this setup is evaluated for the exoskeleton.

B.1 Experimental Setup

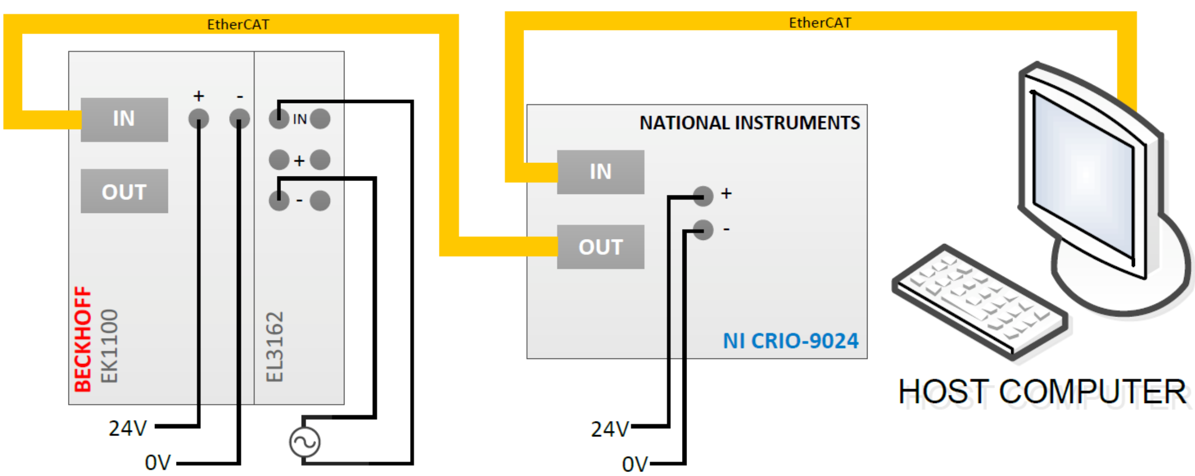

Figure B.1: Connection diagram of the EtherCAT experimental setup

The experimental setup uses an NI cRIO–9024 as a master. For the slave module, an EtherCAT coupler EK1100, coupled with an EtherCAT terminal EL3162 from Beckhoff Automation were used. The terminal has two analogue inputs with a resolution of 16–bits each with a sampling frequency of 20 kHz. The host computer running LabVIEW was connected to the master through a standard Ethernet cable, which itself was connected to the slave also with a standard Ethernet cable. Both the master and slave devices were powered with DC voltage. Analogue input 1 from the EL3162 was connected to an analogue signal generator. A diagram of the connection is shown in Figure B.1.

The setup was configured in LabVIEW from the host computer following the guidelines from NI. In this setup, the slave device is a third–party product, therefore, for this device to be recognised by LabVIEW, specific files (xml files) provided by Beckhoff Automation were imported. The configuration of the LabVIEW project is depicted in Figure B.2.

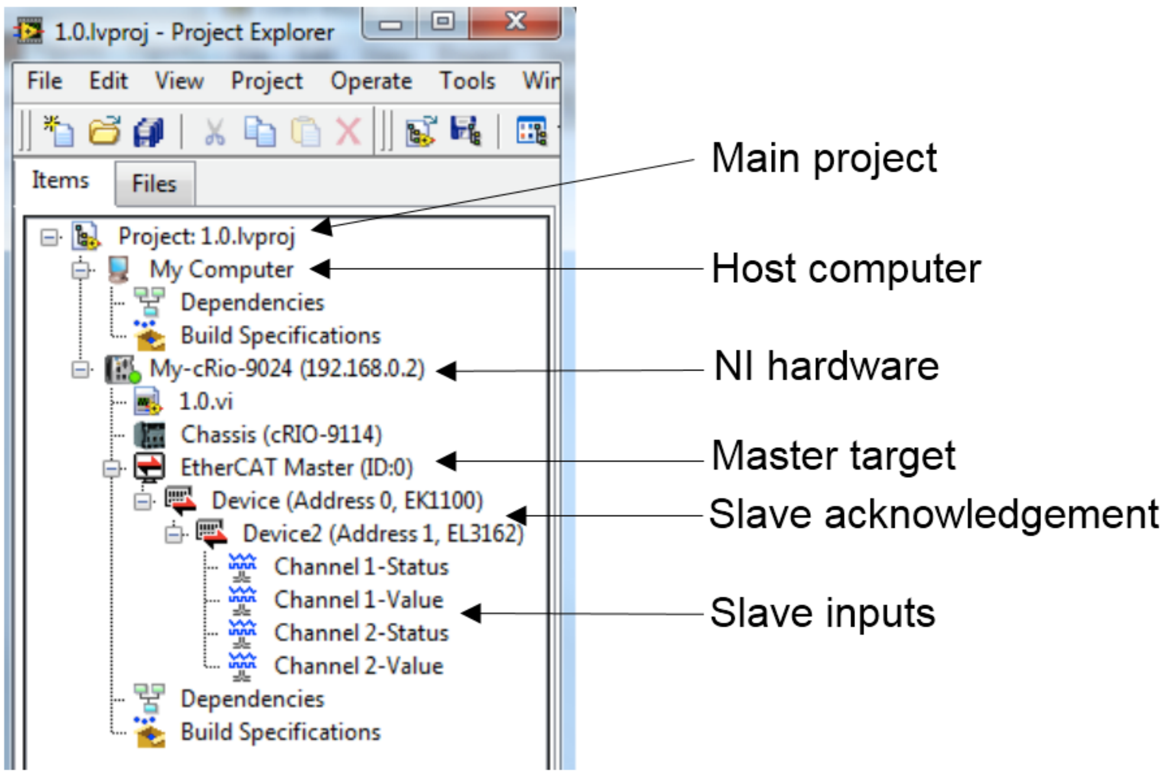

Figure B.2: Configuration of the LabVIEW project

The setup uses LabVIEW Real–Time, which employs "Compact RIO Scan Mode". The Compact RIO Scan Mode allows to reduce development time and programme complexity because it automatically detects the I/O modules, which become available to be dragged directly into the user's program. Using this mode the I/O variables can be updated at a rate up to 1 kHz.

A program was created in LabVIEW to read voltage from channel 1 of the EtherCAT terminal, which was connected to a 70 Hz sine wave from the signal generator. The program runs inside a timed–loop structure, which forces its body to execute at specified rates. The program is depicted in Figure B.3. Sections of the program are numbered:

a. initialises the array before program execution to save computing time;

b. is the difference of time in μs, between the present time and previous time;

c. saves values into the arrays

d. saves difference of time vs number of iterations

e. saves voltage vs elapsed time

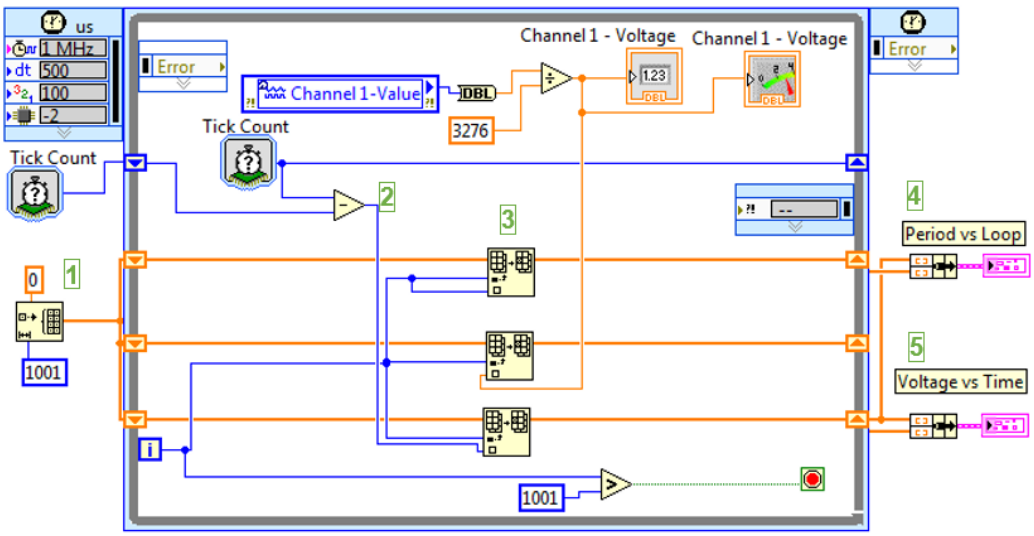

Figure B.3: LabVIEW program

The control loop was run with periods of 10 ms, 5 ms, 1 ms, 500 μs, 200 μs, and 50 μs. Six sets of data were collected, each one for 1,000 iterations with the Scan Mode configured at default 1 kHz (1ms period). Another set of data was collected for 1,000 iterations with the Scan Mode configured at 2 kHz (500 μs period) and control loop period of 500 μs. As depicted in Figure B.4, LabVIEW does not guarantee stability with the Scan Mode at frequencies above 1 kHz.

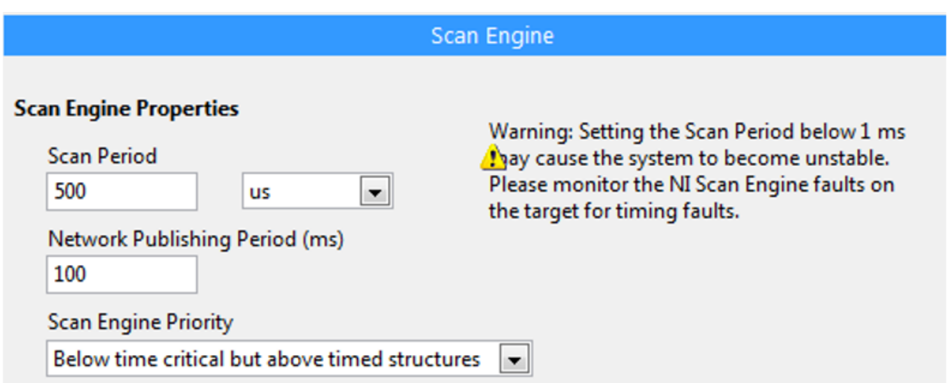

Figure B.4: Scan Mode configuration warning

B.2 Experimental Results

The data was imported to Matlab for statistical analysis. The Matlab code found at the end of this Appendix was used to process the data. A summary of the statistical analysis for the data collected with the Scan Mode set at 1 kHz is shown in Table B.1. In the table, "Loop Execution Time" refers to the time between starting points of two immediate iterations, and "Measurement Update Time" refers to the time between points when the input value changes.

Table B.1: Summary of collected data with Scan Mode set as 1 kHz

Set Control Loop Period	**Mean [μs]**		**Standard Deviation from Measure Mean Value**		**Min [μs]**		**Max [μs]**	
	Loop Execution Time	Measurement Update Time	Loop Execution Time	Measurement Update Time	Loop Execution Time	Measurement Update Time	Loop Execution Time	Measurement Update Time
10 ms	10000	10000	0.4%	0.4%	9927	9950	10053	10053
5 ms	5000	5000	0.7%	0.7%	4921	4939	5057	5057
1 ms	1000	1010	2.4%	10%	923	946	1063	2008
500 μs	500	1014	18.95%	11.6%	347	963	651	2006
200 μs	250	1008	27.4%	8.8%	161	974	480	2000
50 μs	136	1009	55%	12.9%	92	746	355	1992

It can be seen in the table that when the control loop is set to run at higher speeds the standard deviation is higher than when run at lower speeds. This indicates the presence of jitter, which means that the control loop sometimes executes at a longer or shorter times. Measurement Update Time (input value update period) also suffers from jitter. The jitter is higher when the control loop time is set at higher speeds. The jitter of the control loop set at a period of 1 ms is shown in Figure B.5. The jitter of the time between samples of the input value is shown in Figure B.6. The data obtained with the Scan Mode set at 2 kHz (500 μs period) with the control loop period set at 500 μs are shown in Table B.2.

Table B.2: Comparison between Scan Modes at 1 and 2 kHz for T=500μs

Scan Mode	**Mean [μs]**		**Standard Deviation from Measure Mean Value**		**Min [μs]**		**Max [μs]**	
	Loop Execution Time	Measurement Update Time	Loop Execution Time	Measurement Update Time	Loop Execution Time	Measurement Update Time	Loop Execution Time	Measurement Update Time
1 kHz	500	1014	18.95%	11.6%	347	963	651	2006
2 kHz	500	1009	3.76%	6.62%	448	978	561	1517

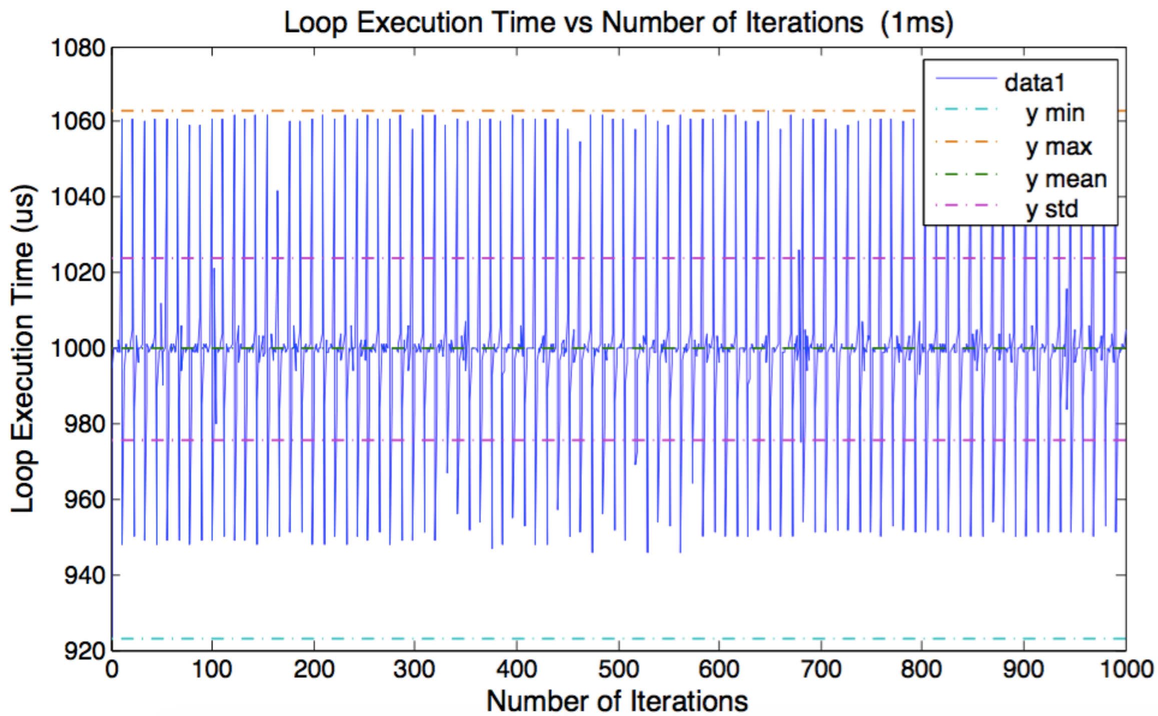

Figure B.5: Loop execution time vs number of iterations (1ms)

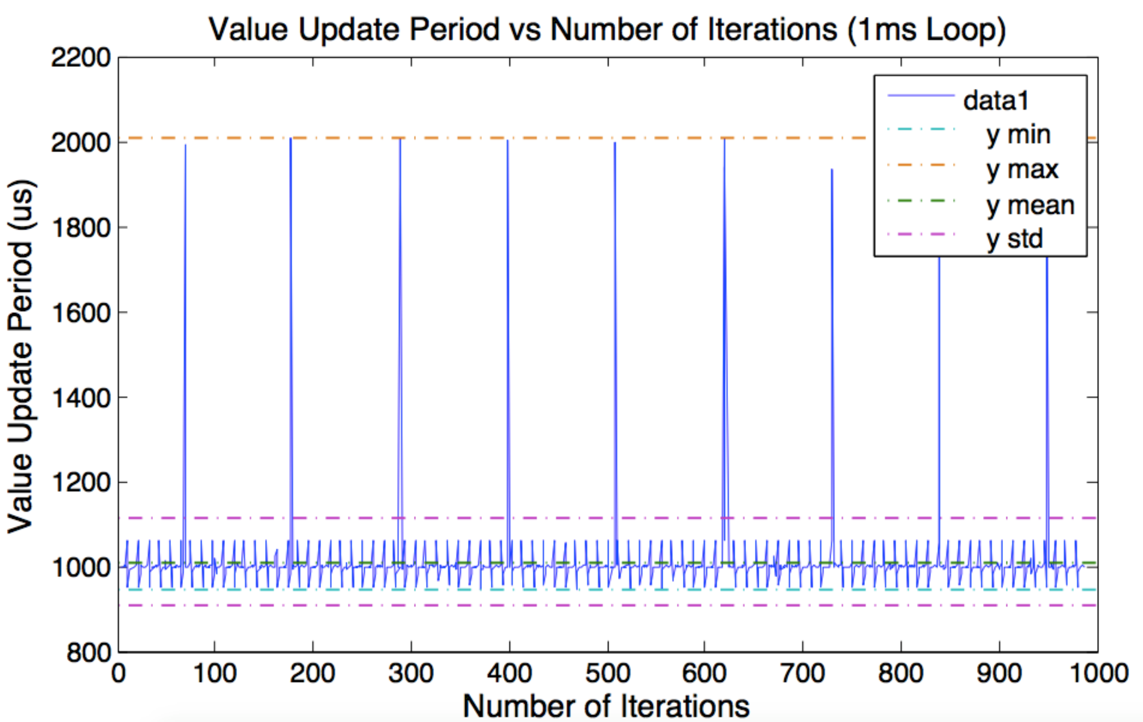

Figure B.6: Value update period vs number of iterations (1ms loop)

Even though the Scan Mode was set at 2 kHz, the control loop still receives an update of the input value from the EtherCAT slave at a frequency of 1 kHz with 6.62%

standard deviation. A plot of the input value update period vs number of iterations is shown in Figure B.7. In the figure jitter is present.

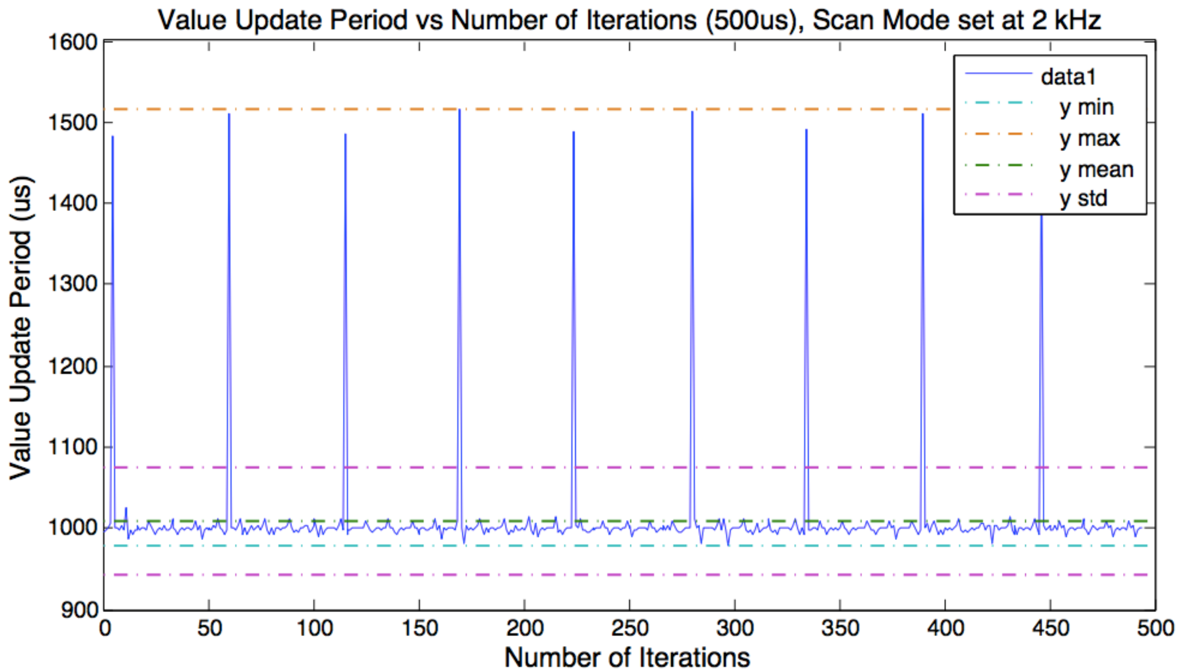

Figure B.7: Value update period vs number of iterations (500us), scan mode set at 2 kHz

B.3 Discussion of Results

The results obtained from the experimental setup show that when the Scan Mode is set at 1 kHz, the presence of jitter is higher when the control loop is set to a faster period. The jitter is lower when the control loop period is set to 5 ms and 10 ms. This suggests that this setup would be suitable for applications that do not require high frequency control loops. When the Scan Mode was set to run at 2 kHz, the LabVIEW software showed a warning stating that stability is not guaranteed for frequencies above 1 kHz. The obtained data demonstrates that the input value from the EtherCAT slave is not updated at 2 kHz, instead it is still updated at 1 kHz with 6.62% of standard deviation.

In conclusion, the setup with an NI master and Beckhoff Automation slaves is not adequate for the exoskeleton. The setup fails to update input values at a frequency above 1 kHz, and the presence of such jitter would cause the exoskeleton to fail. According to NI , for applications with higher–performance requirements such as control loops at more than 1 kHz, LabVIEW FPGA Module should be used with Scan Mode.

In this case, it is necessary to assemble the network with NI EtherCAT slaves (NI–9144), because these devices have on–board FPGA, which allows the use of 40 MHz clock, therefore being able to accomplish faster sampling rates.

B.4 Matlab Code for Statistical Analysis

```
% This piece of code finds the moment in time where
% the Y(amplitude) signal changes its value, to find
% the average sample time of the signal
clear all
clc
load('PV_500us_Scan_500us.mat');
data=PV_500us_Scan_500us;

l=length(data);
n=2;
tvec(1,1)=1;
for i=1:l-1 % find the index where the voltage value changes
        if data(i,2)~=data(i+1,2)
                tvec(n,1)=i+1;% save the index
                n=n+1;
        end
end

for i=1:length(tvec)-1 % add the time from the indices found
        vec(i,1)=sum( data( tvec(i):tvec(i+1)-1 ,1) );
end
vec=vec(2:end); % this vector contains the time between samples

Mean_Sample=mean(vec)% get statistics
Std_Sample=std(vec);
Per_std_Sample=(Std_Sample*100)/Mean_Sample
Min_Sample=min(vec)
Max_Sample=max(vec)
```

```
figure(1)% plot control loop jitter
plot(vec)
title('sample')

load('PL_500us_Scan_500us.mat');
data=PL_500us_Scan_500us;

Mean_Loop=mean(data(:,1))% get statistics
Std_Loop=std(data(:,1));
Per_std_Sample=(Std_Loop*100)/Mean_Loop
Min_Loop=min(data(:,1))
Max_Loop=max(data(:,1))

figure(2)% plot sample frequency jitter
plot(data(:,1))
title('Loop')
```

Appendix C

Experimental Results Figures

C.1 LVDT Sensor – Software Development Figures

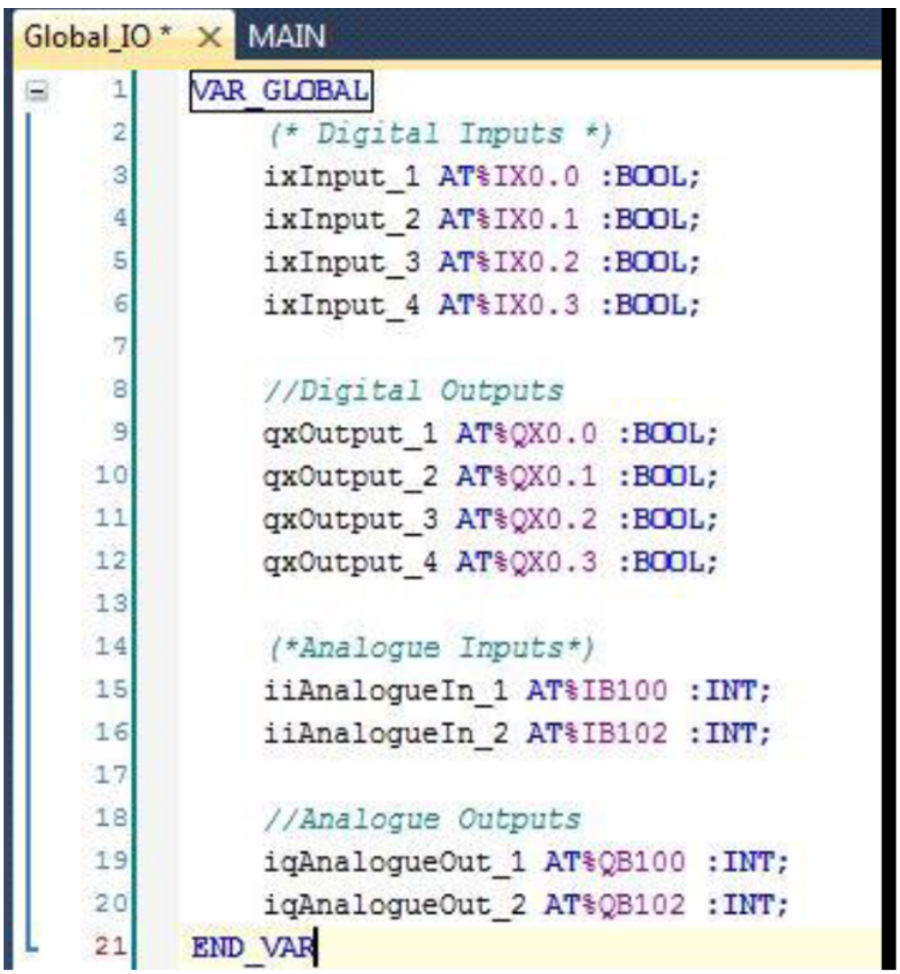


```
VAR_GLOBAL
    (* Digital Inputs *)
    ixInput_1 AT%IX0.0 :BOOL;
    ixInput_2 AT%IX0.1 :BOOL;
    ixInput_3 AT%IX0.2 :BOOL;
    ixInput_4 AT%IX0.3 :BOOL;

    //Digital Outputs
    qxOutput_1 AT%QX0.0 :BOOL;
    qxOutput_2 AT%QX0.1 :BOOL;
    qxOutput_3 AT%QX0.2 :BOOL;
    qxOutput_4 AT%QX0.3 :BOOL;

    (*Analogue Inputs*)
    iiAnalogueIn_1 AT%IB100 :INT;
    iiAnalogueIn_2 AT%IB102 :INT;

    //Analogue Outputs
    iqAnalogueOut_1 AT%QB100 :INT;
    iqAnalogueOut_2 AT%QB102 :INT;
END_VAR
```

Figure C.1: Declaration of global variables

```
FUNCTION F_Scale : REAL
VAR_INPUT
    iRawValue: INT;      // Raw value from the Terminal
    rXHigh: REAL;        // Highest value for the Raw value
    rXLow: REAL;         // Lowest value for the Raw value
    rYHigh: REAL;        // Highest value for the Scaled value
    rYLow: REAL;         // Lowest value for the Scaled value
END_VAR
VAR
    ra: REAL;            // Temp internal variable
    rb: REAL;            // Temp internal variable
END_VAR
```

```
IF (rXHigh - rXLow) < 0.01 AND (rXHigh - rXLow) > -0.01 THEN
    // Check for Overflow
    F_Scale := 0.0;
ELSE
    // Calculate upward gradient
    ra := (rYHigh - rYLow) / (rXHigh - rXLow);
    // Calculate Offset
    rb := rYHigh - ra * rXHigh;
    // Scaled Value
    F_Scale := ra * iRawValue + rb;
END_IF
```

Figure C.2: Algorithm for reading raw values from the sensor

```
IF F_scale > 0 THEN
    F_Length := (10 - F_scale) * 0.5;
END_IF

IF F_scale = 0 THEN
    F_Length := 5;
END_IF

IF F_scale < 0 THEN
    F_Length := (10 - F_scale) * 0.5;
END_IF
```

Figure C.3: 'IF' condition statement for comparing measured voltage against position of the shaft

```
// Scale of the LVDT
rVolt -0.00061 := F_Scale(
iRawValue := Global_IO.iiAnalogueIn_1 -2 ,
rXHigh := 32767,
rXLow := -32767,
rYHigh := 10,
rYLow := -10);
// LVDT length
rLength 5 := F_Length(
iRawValue := Global_IO.iiAnalogueIn_1 -2 ,
rXHigh := 32767,
rXLow := -32767,
rYHigh := 10,
rYLow := -10);
```

Figure C.4: Output results of the LVDT sensor showing the output voltage of the sensor and the position of shaft in cm

C.2 Loadcell Sensor – Software Development Figures

```
FUNCTION F_force : REAL
VAR_INPUT
     iRawValue1: INT;
    rXHigh1: REAL;
    rXLow1: REAL;
    rYHigh1: REAL;
    rYLow1: REAL;
END_VAR
VAR
    ra1: REAL;
    rb1: REAL;
    F_Loadcell : REAL;
END_VAR
```

```
IF (rXHigh1 - rXLow1) < 0.01 AND (rXHigh1 - rXlow1)>-0.01 THEN
    F_Loadcell := 0.0;
    ELSE
        ra1 := (rYHigh1-rYLow1) / (rXHigh1 - rXLow1);
        rb1 := rYHigh1 - ra1 * rXHigh1;
        F_Loadcell := ra1* iRawValue1 + rb1;
    END_IF

F_force :=100 * F_Loadcell;
```

Figure C.5: Algorithm for reading raw values from the loadcell sensor

Appendix D

Ethical Approval

See next page.

Performance, Governance and Operations
Research & Innovation Service
Charles Thackrah Building
101 Clarendon Road
Leeds LS2 9LJ Tel: 0113 343 4873
Email: ResearchEthics@leeds.ac.uk

UNIVERSITY OF LEEDS

Abbas Dehghani-Sanij
School of Mechanical Engineering
University of Leeds
Leeds, LS2 9JT

MaPS and Engineering joint Faculty Research Ethics Committee (MEEC FREC)
University of Leeds

30 October 2018

Dear Abbas

Title of study	**Development of a full-body intelligent modular power enhancing robotic exoskeleton for humans.**
Ethics reference	**MEEC 15-004**

I am pleased to inform you that the application listed above has been reviewed by the MaPS and Engineering joint Faculty Research Ethics Committee (MEEC FREC) and I can confirm a favourable ethical opinion as of the date of this letter. The following documentation was considered:

Document	*Version*	*Date*
MEEC 15-004 Ethical_Application_Exoskeleton_Project_combined.pdf	1	25/09/15

The Chair made the following comments:

- Please ask *all* participants (phase M, 0 and 1) to sign a consent form.

Please notify the committee if you intend to make any amendments to the original research as submitted at date of this approval, including changes to recruitment methodology. All changes must receive ethical approval prior to implementation. The amendment form is available at http://ris.leeds.ac.uk/EthicsAmendment.

Please note: You are expected to keep a record of all your approved documentation, as well as documents such as sample consent forms, and other documents relating to the study. This should be kept in your study file, which should be readily available for audit purposes. You will be given a two week notice period if your project is to be audited. There is a checklist listing examples of documents to be kept which is available at http://ris.leeds.ac.uk/EthicsAudits.

We welcome feedback on your experience of the ethical review process and suggestions for improvement. Please email any comments to ResearchEthics@leeds.ac.uk.

Yours sincerely

Jennifer Blaikie
Senior Research Ethics Administrator, Research & Innovation Service
On behalf of Professor Gary Williamson, Chair, MEEC FREC